AFTER THE FLOW: LANDSCAPE RESPONSE TO THE EMPLACEMENT OF HOLOCENE LAVA FLOWS, CENTRAL OREGON CASCADES, USA

by

NATALIA IRMA DELIGNE

A DISSERTATION

Presented to the Department of Geological Sciences
and the Graduate School of the University of Oregon
in partial fulfillment of the requirements
for the degree of
Doctor of Philosophy

September 2012

DISSERTATION APPROVAL PAGE

Student: Natalia Irma Deligne

Title: After the Flow: Landscape Response to the Emplacement of Holocene Lava Flows, Central Oregon Cascades, USA

This dissertation has been accepted and approved in partial fulfillment of the requirements for the Doctor of Philosophy degree in the Department of Geological Sciences by:

Katharine V. Cashman	Chairperson
Gordon E. Grant	Member
Alan W. Rempel	Member
Joshua J. Roering	Member
Daniel G. Gavin	Outside Member

and

Kimberly Andrews Espy	Vice President for Research & Innovation/Dean of the Graduate School

Original approval signatures are on file with the University of Oregon Graduate School.

Degree awarded September 2012

DISSERTATION ABSTRACT

Natalia Irma Deligne

Doctor of Philosophy

Department of Geological Sciences

September 2012

Title: After the Flow: Landscape Response to the Emplacement of Holocene Lava Flows, Central Oregon Cascades, USA

Effusive volcanic eruptions repave landscapes rapidly with lava flows, resetting the underlying landscape and ecosystem. The unique physical properties of lava pose interesting challenges for recovery, as lava flows can be highly permeable while lava itself is dense, sterile, and generally inhospitable towards life. This dissertation examines two aspects of landscape recovery following lava flow emplacement: (1) hydrologic adaptation of surface and groundwater to recent volcanism and (2) plant colonization of young lava flows. I examine two sites in the central Oregon Cascades: the c. 3 ka Sand Mountain volcanic field (SMVF), located in the headwaters of the McKenzie River, a critical water resource for the state of Oregon, and the c. 1.5 ka Collier Cone lava flow, originating on the north flanks of North Sister volcano.

My investigation of the SMVF and upper McKenzie River watershed reveals a complex volcanic history with profound impacts on the configuration and short-term discharge of the McKenzie River: lava flows from the SMVF and other Holocene vents have buried, dammed, and altered the path of the McKenzie River. Moreover, given the large groundwater contribution from the SMVF to the McKenzie River, I estimate that SMVF activity caused McKenzie River discharge in present-day Eugene, Oregon to

decrease by up to 20% for days to months at a time; future regional mafic volcanic activity could have a similar impact.

The SMVF and the Collier Cone lava flow are notable for the juxtaposition of barren exposed lava and mature forests on the same or similarly aged lava flows. I use a combination of LiDAR analysis, field observations, and soil characterization to examine soil and vegetation at these two sites and find that the presence of an external soil source greatly facilitates plant establishment, growth, and survival. Here, external soil sources are syn- or post-eruptive tephra (SMVF) or flood-borne deposits (Collier Cone lava flow). External soil appears to provide a substrate for plants to grow in along with key nutrients and sufficient moisture; overall, external soil sources are key for the initial recovery following an effusive volcanic disturbance.

This dissertation includes co-authored material submitted for publication.

CURRICULUM VITAE

NAME OF AUTHOR: Natalia Irma Deligne

GRADUATE AND UNDERGRADUATE SCHOOLS ATTENDED:

University of Oregon, Eugene
University of Bristol, Bristol, United Kingdom
California Institute of Technology, Pasadena

DEGREES AWARDED:

Doctor of Philosophy, Geology, 2012, University of Oregon
Master of Science by Research, Natural Hazards, 2006, University of Bristol
Bachelor of Science, Geology, 2004, California Institute of Technology

AREAS OF SPECIAL INTEREST:

Physical volcanology
Landscape evolution

PROFESSIONAL EXPERIENCE:

Graduate Teaching and Research Fellow, Department of Geological Sciences, University of Oregon, 2007 - 2012

Seismic Data Analyst, Seismological Laboratory, California Institute of Technology, 2005 - 2007

Teaching Assistant, Division of Geological and Planetary Sciences, California Institute of Technology, 2004

Laboratory Assistant, Division of Geological and Planetary Sciences, California Institute of Technology, 2001 - 2004

GRANTS, AWARDS, AND HONORS:

Good Citizen Award, Department of Geological Sciences, University of Oregon, 2011 and 2012

Graduate Student Research Grant, Mazamas, 2010

Thayer Scholarship, Department of Geological Sciences, University of Oregon, 2008 and 2009

Kleinman Grant for Volcano Research, US Geological Survey, 2008

Conference Support, IAVCEI General Assembly, 2008

Howard Reynolds Memorial Prize in Geology, Division of Geological and Planetary Sciences, California Institute of Technology, 2004

Summer Undergraduate Research Fellowship, California Institute of Technology, 2001 and 2002

PUBLICATIONS:

Riddick, S., Schmidt, D.A. & Deligne, N.I. in press. An analysis of terrain properties and the location of surface scatterers from persistent scatterer interferometry. *ISPRS Journal of Photogrammetry and Remote Sensing*.

Cashman, K.V., Soule, S.A., Mackey, B.H., Deligne, N.I., Deardorff, N.D. & Dietterich, H.R. in press. How lava flows: New insights from applications of lidar technologies to lava flow studies. *Geosphere*.

Deligne, N.I., Coles, S.G. & Sparks, R.S.J. 2010. Recurrence rates of large explosive volcanic eruptions. *Journal of Geophysical Research – Solid Earth* 115: B06203.

Cashman K.V., Deligne, N.I., Gannett, M.W., Grant, G.E. & Jefferson, A. 2009. Fire and water: Volcanology, geomorphology, and hydrogeology of the Cascades Range, central Oregon. In: O'Connor, J.E., Dorsey, R.I. & Madin, I.P. (eds.) *Volcanoes to Vineyards: Geologic Field Trips through the Dynamic Landscape of the Pacific Northwest: Field Guide 15*, pp. 539-582. Geological Society of America, Boulder, CO, US.

Mosenfelder, J.L., Deligne, N.I., Asimow, P.D. & Rossman, G.R. 2006. Hydrogen incorporation in olivine from 2 – 12 GPa. *American Mineralogist* 91: 285-294.

ACKNOWLEDGMENTS

I thank my advisor, Kathy Cashman, for being incredibly supportive as I followed my curiosity into uncharted territory, and for expecting rigor and clarity in scientific thought, execution, and communication. Kathy has profoundly shaped the scientist I am today. I have also been fortunate to have a fantastic committee – Dan Gavin, Gordon Grant, Josh Roering, and Alan Rempel – who have been very generous with their ideas, energy, resources, and time. Thank you. I also thank Qusheng Jin, Andrew Marcus, and David Schmidt who served on earlier versions of my committee.

Many people went above and beyond what could be reasonably expected to help me over the course of my PhD. I am deeply indebted to Rick Conrey, who taught me how to approach volcanic mapping, freely shared his extensive geochemical database, and analyzed over 100 XRF samples for me on his own dime. I am constantly humbled by his generosity, knowledge, and enthusiasm. I also thank the following people for sharing their data with me: Nick Deardorff (LiDAR data for the Collier Cone lava flow, acquired through a 2006 NCALM graduate student grant), and Duane Champion (paleomagnetic data for the Sand Mountain volcanic field). Karl Morgenstern (Eugene Water and Electric Board) and Ian Madin (Oregon's Department of Geology and Mineral Industries) made acquisition of the upper McKenzie River LiDAR possible.

I am lucky to have had great field assistants: Kathy Cashman (rower extraordinaire!), Jim Cleavenger, Nick Deardorff, Brent Deyo, Ariana Everson, Ali Furmall, Emily Gottesfeld, Kyle House, Daniele Mckay, Win McLaughlin, Leland O'Driscoll, Nick Tanushev, Robin Tuohy, Lucy Walsh, Brian Webb and Josh Roering's river mechanics class. For the days I was alone in the field, Corina Cerovski-Darriau, Scott

Maguffin, Kristin Sweeney, and Nick Tanushev provided me with a safety net – thank you for participating in Operation Staying Alive. Linn County Parks and Recreation provided me with free rowboat rental in exchange for a map. Chad Everson and Brian Cochran from the Eugene Dive Club worked hard to collected a sample from a 40 m deep tree at altitude in frigid water. I have also enjoyed wonderful days in the field exploring, talking with, and learning from the Cashman and Roering groups and associates, Jim O'Connor and the Collier glacier photomatching crew, and the Kleinman grant and Yeehow teams.

In the lab, Willy Amidon guided me through ^{3}He sample preparation from afar and then ran my samples at Caltech the weekend prior to his move to Middlebury College. The Bridgham and Gavin labs provided me with space and resources to conduct my soil analyses; I am particularly grateful to Lorien Reynolds and Erin Herring for always having the time for me despite their packed schedules. The Wallace lab let me monopolize the picking scope for weeks, and Kathryn Watts helped me with sample preparation.

The Cashman lab, in particular Daniele Mckay and Hannah Dietterich, kept me sane and happy. I am grateful to have been part of a great department – many thanks to the faculty, office staff, and grad students who make it the special place that it is.

Finally, I thank my parents for instilling in me a sense of wonder towards the world and determination for figuring things out, and for quietly supporting me over the years.

Financial support was provided by grants from the National Science Foundation to Kathy Cashman (EAR-0738894 and EAR-1019848) and the University of Oregon UCORE program (DUE-0622620), two Thayer scholarships, and a Mazama graduate student research grant; Mazamas support does not imply endorsement of the results and conclusions presented in this dissertation.

For my teachers

TABLE OF CONTENTS

Chapter Page

Chapter Page

Chapter Page

LIST OF FIGURES

Figure Page

CHAPTER II

Figure Page

CHAPTER III

CHAPTER IV

Figure Page

LIST OF TABLES

Table Page

APPENDIX

CHAPTER I

INTRODUCTION

Volcanic eruptions are one of the most awe-inspiring natural phenomena on Earth; they are physical manifestations of the processes that drive plate tectonics and make the Earth the inhabitable world that it is. The raw power they unleash can cause widespread devastation of surrounding areas – effusive eruptions repave adjacent landscapes with lava, and explosive eruptions can cover large areas with tephra. Both lava and tephra can cause great ecologic damage by covering biota with rock, often causing death. In this dissertation, I ask "how do effusive volcanic eruptions impact their environment?" I explore both hydrologic impacts of and processes behind plant establishment and survival on lava flows. I focus on two sites of recent volcanism in the central Oregon Cascades: the Sand Mountain volcanic field (SMVF) in the headwaters of the McKenzie River, and the Collier Cone lava flow situated on the north flanks of North Sister volcano. Below, I provide a brief summary of my dissertation chapters.

Chapter II, CO-EVOLUTION OF THE SAND MOUNTAIN VOLCANIC FIELD AND THE UPPER McKENZIE RIVER, CENTRAL OREGON CASCADES, USA, was co-authored with Rick Conrey (Washington State University – Pullman), my advisor Kathy Cashman, Duane Champion (US Geological Survey – Menlo Park), Willy Amidon (at Caltech at the time of his contribution, now at Middlebury College), and committee member Gordon Grant. This chapter will be submitted to *GSA Bulletin*. Co-authors contributed extensively to data acquisition. In this paper, I investigate the co-evolution of

the Sand Mountain volcanic field (SMVF) and the McKenzie River in the central Oregon Cascades. The SMVF occupies the headwaters of the McKenzie River, the sole source of drinking water for the Eugene metropolitan area. This study was motivated by a desire to evaluate whether and how Eugene's water supply would be impacted if the SMVF were to reactivate. I synthesize numerous datasets, including lava geochemical data, paleomagnetic data, ^{3}He cosmogenic data, bathymetric depth measurements, and extensive field observations to make a geologic map of the SMVF and determine the history of interactions between the SMVF and the McKenzie River. I find that lava flows from the SMVF and other Holocene vents have profoundly impacted the current hydrology of the upper McKenzie River, and that at the time of the SMVF eruptive episode, lava flows could have caused up to a 20% reduction in McKenzie River discharge at present-day Eugene. I conclude that although it is unlikely that the SMVF reactivate, temporary decreases of a similar magnitude in Eugene's water supply are likely to result from future volcanic activity in the central Oregon Cascades.

Chapter III, USING AIRBORNE LIDAR TO QUANTIFY VEGETATION COLONIZATION OF A LATE HOLOCENE LAVA FLOW TRAVERSING A CLIMATIC GRADIENT: THE COLLIER CONE LAVA FLOW, CENTRAL OREGON CASCADES, was co-authored with my advisor Kathy Cashman and committee members Dan Gavin and Josh Roering. Here it is presented as submitted to *Journal of Vegetation Science*; it will be greatly shortened in length and figure and table number and resubmitted to *Geology*. In this study I use Light Detection and Ranging (LiDAR) data to characterize vegetation on and adjacent to the 1.5 ka Collier Cone lava flow from its vent (2150 m) to the lava flow toe (900 m). I use LiDAR data to quantify the concentration

and distribution of trees of varying heights and link them to underlying lava flow morphology. I find that trees growing on young lava flows are shorter and sparser than those immediately off the lava flow. However, where externally-derived sediment has been deposited on the lava flow and provides a rooting medium, the forest resembles the developed forests in adjacent regions. Overall, this works suggests that external soil deposition is critical for rapid establishment of forests on blocky lava flows, and that in the absence of externally-derived soil, plant colonization of lava flows progresses very slowly.

Chapter IV, AFTER THE LAVA FLOW: THE IMPORTANCE OF EXTERNAL SOIL SOURCES FOR PLANT COLONIZATION OF RECENT LAVA FLOWS IN THE CENTRAL OREGON CASCADES, USA, was co-authored with my advisor Kathy Cashman and committee member Josh Roering. This chapter was submitted to a special issue of *Geomorphology* entitled *Process geomorphology and ecosystems: Disturbance regimes and interactions* and is presently in revision. In this chapter, I expand on the foundation provided in Chapters II and III to plant colonization of the young lava flows at both of my field areas, the SMVF and the Collier Cone lava flow, using a combination of LiDAR analysis, field observations, and soil characterization to examine soil and vegetation at these two sites. I confirm that the presence of an external soil source greatly facilitate plant establishment, growth, and survival. External soil sources appears to be syn- or post- eruptive tephra (SMVF) or flood-borne deposits (Collier Cone lava flow). In general, it appears that external soil provides a substrate for plants to grow in along with key nutrients and sufficient moisture. I conclude that external soil sources are key for the initial recovery following an effusive volcanic disturbance.

CHAPTER II

CO-EVOLUTION OF THE SAND MOUNTAIN VOLCANIC FIELD AND THE UPPER McKENZIE RIVER, CENTRAL OREGON CASCADES, USA

This chapter was prepared for submission to *GSA Bulletin*. Co-author Rick Conrey provided ~200 rock samples and their location data, assisted with field work and shared his field notes and insights, and did all the XRF sample preparation and analyses. Co-author Duane Champion provided his paleomagnetic database, co-wrote sections on paleomagnetic methods, results and interpretation, and drafted Figure 9. Co-author Willy Amidon ran the ^{3}He samples at Caltech and determined the cosmogenic scaling factors. Co-authors Kathy Cashman and Gordon Grant provided guidance over the course of the project and editorial assistance. I did much of the field work, synthesized and interpreted all the data, and was the primary author.

INTRODUCTION

The mafic Sand Mountain volcanic field (SMVF) of the central Oregon Cascades, USA, covers 75 km^2 (lava and vents only) and includes the Sand Mountain chain of vents, Nash and Little Nash craters, the Lost Lake chain of vents, and associated lava flows and tephra blankets (Figs. 1 and 2). All activity post-dates the ~7,700 cal yr. BP cataclysmic Mt Mazama eruption (Stuiver et al., 1998), making this one of the youngest fields in the Cascade Range (Sherrod et al., 2004).

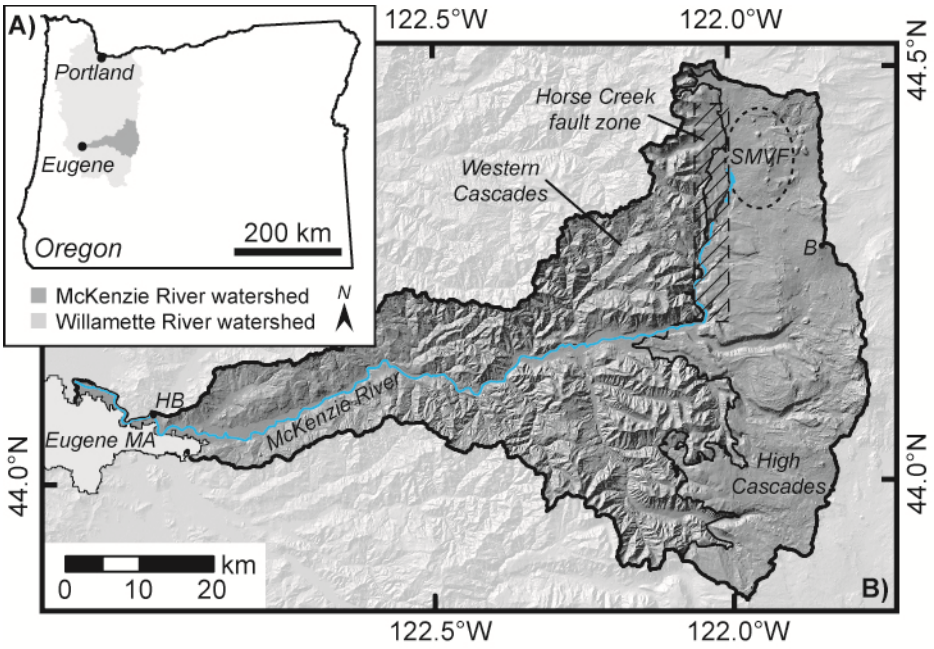

Figure 1. Location map for the McKenzie River watershed and the Sand Mountain volcanic field (SMVF). (A) Map of the state of Oregon showing the greater Willamette River watershed (light grey) and the McKenzie River watershed (dark grey) and the cities of Eugene and Portland (black circles). (B) Shaded relief map of the McKenzie Watershed (bold black line) showing the location of the SMVF (dashed line). Also shown is the McKenzie River (blue line), the contact between the Western and High Cascades (black line), the Horse Creek fault zone (hatching), and the extent of the Eugene metropolitan area (Eugene M.A.; light grey). 'HB' is Haydan Bridge (where the Eugene Water and Electric Board diverts water for treatment), and 'B' indicates Belknap volcano.

In addition to its young age, the SMVF is notable for its location within the headwaters of the McKenzie River (Fig. 1). The McKenzie River is the sole source of drinking water for the Eugene, Oregon, metropolitan area (200,000 residents), and is one of twelve main tributaries of the Willamette River. Roughly 70% of Oregon residents (2.7 million people) live in the Willamette Valley, which contains eight of the state's ten most populous cities (Loy et al., 2001); the valley is also an important agricultural center. The steady flow of High Cascades springs that feed the McKenzie River make it a critical Oregon water resource: in the late summer, McKenzie River water accounts for nearly

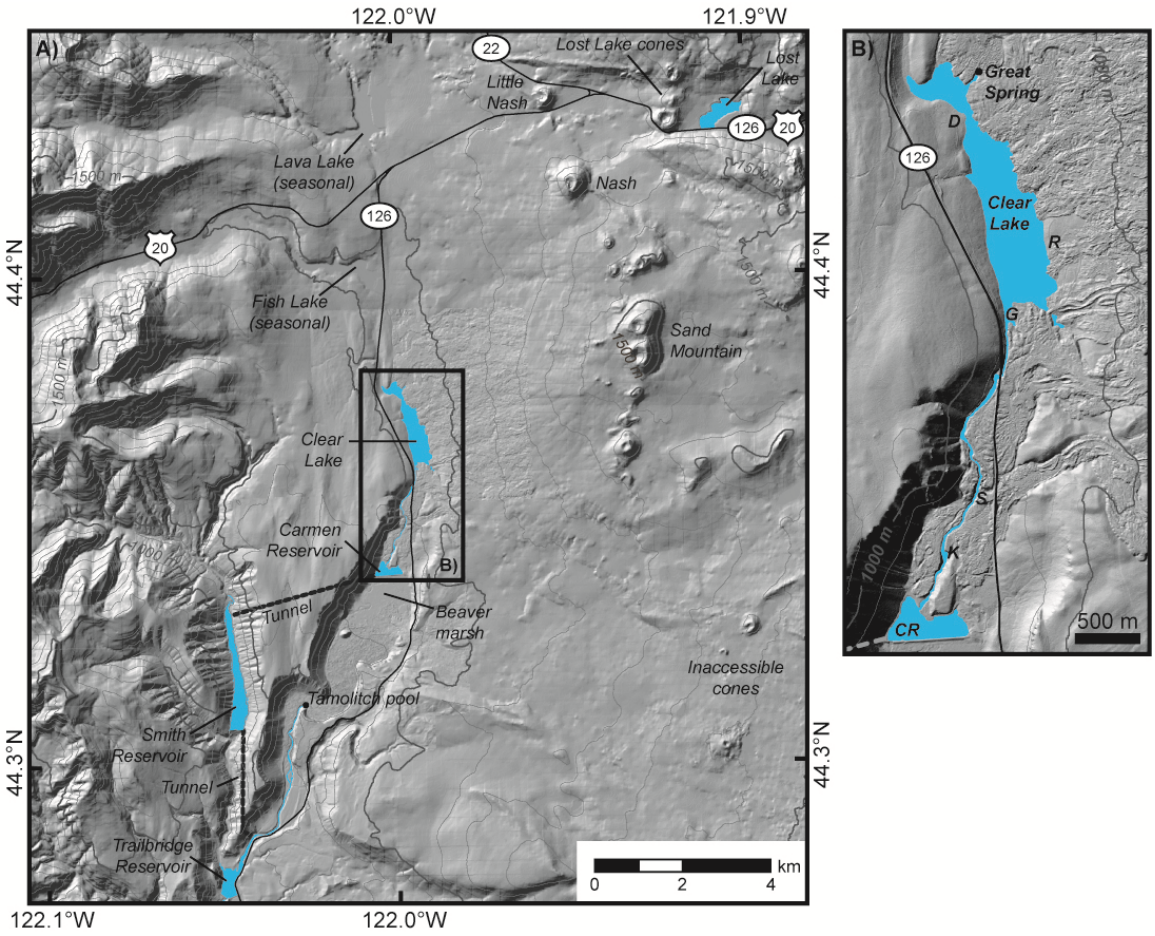

Figure 2. Shaded relief maps of (A) the upper McKenzie River watershed and (B) the region between and including Clear Lake and Carmen Reservoir. The shaded relief map was constructed from LiDAR data where available and a 10 m digital elevation model (DEM) elsewhere. Features referred to in the text are labeled, and also shown are key highways (black lines), surface water (blue), the tunnels of the Carmen-Smith diversion project (dashed bold lines) and 100 m contour intervals (grey, with bold 500 m contour intervals). The extent of (B) shown by a black rectangle. In (B), 'D' is the Clear Lake Resort boat dock, 'R' is the Cold Water Cove campground boat ramp, 'G' is USGS gage 14158500, 'S' is Sahalie Falls, and 'K' is Koosah Falls.

25% of the Willamette River at the latter's confluence with the Columbia River in Portland, Oregon, roughly 300 km downstream of the McKenzie's confluence with the Willamette. Lava flows from the SMVF presently dam the McKenzie River to form Clear Lake, a groundwater-fed lake that is the source of the McKenzie River (Stearns, 1929;

Williams, 1957). The likely effect that SMVF volcanic activity had on the McKenzie River, which we use to evaluate the potential impact of future regional volcanic activity on the river, is the focus of this study.

A recent assessment of volcanic hazards in the Three Sisters region, which includes the SMVF, states that the greatest hazard associated with mafic volcanism in the region are phreatic explosions resulting from the interaction of rising magma with groundwater (Scott et al., 1999). Although this report notes that lava flows can dam rivers, causing inundation upstream, it does not consider downstream ramifications of lava flows entering river drainages. Overall, hazards associated with mafic volcanism in Three Sisters region are predicted to impact only areas within 10 km of the vent, with lava flows affecting a greater proportion of this area than tephra.

In this study we present a detailed investigation of the lava flows and associated vents within the SMVF and their impact on the McKenzie River. We use a combination of geologic mapping and characterization of Clear Lake and the McKenzie River to examine the co-evolution of the SMVF and the McKenzie River during the Holocene. We use our findings to evaluate hazards associated with mafic volcanism in the McKenzie River watershed. Although we do not consider tephra hazards, we note that Mckay (2012) documented > 2 m and 79 cm of SMVF tephra 8 and 13 km northeast of Sand Mountain, respectively, suggesting that tephra hazards associated with mafic volcanism in the central Oregon Cascades are considerably greater than currently accounted for.

BACKGROUND

Geologic setting of the SMVF

The SMVF is situated in the central Oregon Cascades within the High Cascades graben. The Cascades Range extends from northern California, USA, to southern Canada and is a product of subduction of the Juan de Fuca plate underneath the North American plate. The central Oregon Cascades consists of two adjacent volcanic chains: the Western Cascades, which was the center of volcanism from ~35 – 5 Ma, and the High Cascades, which has been the center of volcanism since ~5 Ma (Taylor, 1968; Walker and MacLeod, 1991). The shift in volcanism reflects clockwise rotation of the North American plate over the subduction zone, which produces an apparent eastward migration of volcanism in the central Oregon Cascades and westward migration in the northern Cascades (Wells et al., 1998; McCaffrey et al., 2007). The Western and High Cascades have remarkably different geomorphic expressions: the Western Cascades are highly dissected with a well developed stream network, while the High Cascades are undissected with no to little channel development (Fig. 1). The High Cascades and higher elevation reaches of the Western Cascades were glaciated during the Pleistocene; Pleistocene and older units have large-scale glacial striations and host glacially carved valleys, and there is evidence of syn-eruptive lava-ice interactions in the form of Pleistocene tuyas (Sherrod et al., 2004).

The High Cascade graben is bounded by the Horse Creek fault zone to the west and the Green Ridge fault zone to the east. The graben is 30 km wide, ~2 – 3 km deep and is filled by lava flows (Taylor, 1990; Sherrod et al., 2004). It is related to the Brothers fault zone and consequently to the basin and range extension of the southwest

United States (Sherrod and Smith, 1990). It may also be related to the clockwise rotation of the North American plate. This graben is the focus of considerable mafic volcanism: roughly 60 km^3 of mafic magma has erupted here in the past 15 kyrs; the majority of the mapped 1054 Quaternary vents are cinder cones and mafic vents (Hildreth, 2007). The SMVF is located on the northwest margin of the graben close to the boundary between the High and Western Cascades (Fig. 1).

Hydrology of the High Cascades and the upper McKenzie River

The Oregon Cascades receive between 2000 and 3800 mm of precipitation each year (Taylor and Hannan, 1999), with 80% of precipitation occurring during the winter months ("winter monsoon"; Tague and Grant, 2004). The contrast in geomorphic expression between the Western and High Cascades reflects profound differences in how this precipitation flows through the landscape. The Western Cascades are a dissected landscape with a well-developed stream network. River discharge is strongly linked to precipitation: discharge is high during the winter monsoon and low in the summer following several months of low or no rainfall. In contrast, the High Cascades is a groundwater-dominated system with steady discharge over the course of the year. In the High Cascades, precipitation falls predominately in the form of snow, seeps into the ground following snowmelt, and emerges at springs at the distal end of lava flows abutted against the graben boundary a few to tens of years later; most of the precipitation that falls west of the Cascades crest emerges at the High/Western Cascade graben boundary, with the rest of the precipitation emerging at springs east of the crest (Jefferson et al., 2006). Although the total area-average annual discharge for High and Western Cascades

streams is the same, the difference in seasonal discharge is striking: the peak flow of High Cascade streams during the winter monsoon and spring snowmelt might be 3 – 4 times greater than late summer baseflow, while the peak flow for Western Cascades streams during the winter monsoon is on the order of 1000 times greater than late summer baseflow (Tague and Grant, 2004). For streams with mixed drainage areas, late summer discharge is directly related to the portion of the watershed draining the High Cascades (Tague and Grant, 2004).

The McKenzie River watershed covers 2637 km^2, 61% of which is within the High Cascades (Tague and Grant, 2004). The McKenzie River flows from Clear Lake, a lake dammed by SMVF lava flows, south along the Horse Creek graben-bounding fault zone (Figs. 1 and 2). The McKenzie River enters Carmen Reservoir 2.5 km downstream of Clear Lake; here water is diverted through a 2217 m long tunnel to Smith Reservoir (Fig. 2). From here, the combined water from the McKenzie and Smith Rivers goes through a second tunnel to Trailbridge Reservoir (Fig. 2), generating up to 115 MW. The combined McKenzie and Smith River water is returned to the McKenzie River below Trailbridge Reservoir. Immediately south of Carmen Reservoir the McKenzie River is a dry channel, apart from brief periods during high snowmelt. However, halfway between Carmen and Trailbridge Reservoirs, the McKenzie River reappears at Tamolitch Pool and flows south to Trailbridge Reservoir. Approximately 10 km south of Trailbridge Reservoir, the river makes a sharp turn to the west to flow ~120 km westward to its confluence with the Willamette River just north of Eugene, Oregon.

At Clear Lake, the source of the McKenzie River, roughly 10% of the water (as measured at the lake's outlet) comes from the Great Spring, a single spring situated on

the northeast margin of the lake (Stearns, 1929). The rest of Clear Lake's water comes from springs located on the bottom on the lake. The cold spring water at Clear Lake (~4°C year-round) preserves a forest of drowned Douglas-fir trees, submerged and killed when the lake formed (Stearns, 1929; Fig 3a). The cold water also prevents much from growing in the lake, producing the lake's remarkable namesake clarity. A crude bathymetric map by Johnston et al. (1985) shows that the lake covers 0.6 km^2 (148 acres) and is divided into two regions: a shallow region to the north (< 20% of surface area) and a deep region to the south with a maximum depth of 53.3 m (175 ft).

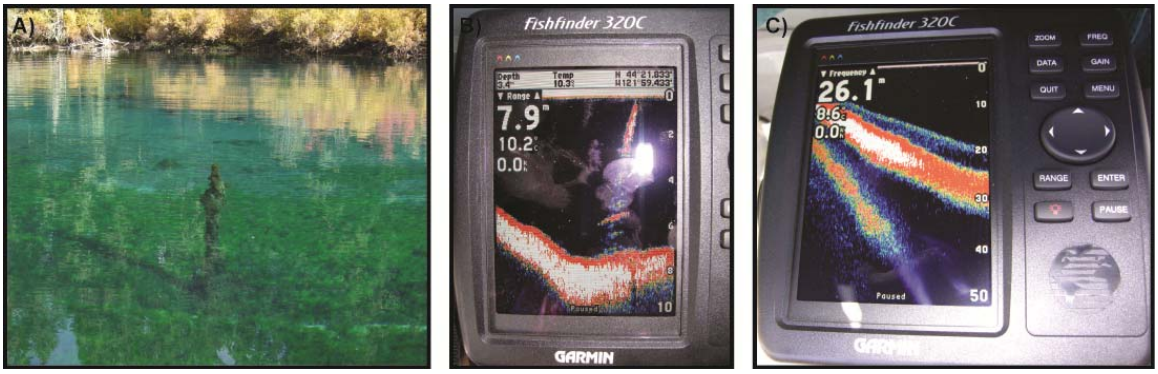

Figure 3. Photographs of (A) a drowned tree immediately east of the Clear Lake Resort boat dock (water depth is 4 – 7 m), (B) detection of a drowned tree with the Fishfinder, and (C) Fishfinder whiteline showing the contact between hard (white line) and soft (no white line) bottom.

Early mapping of the SMVF

The first scientific investigation of the upper McKenzie River valley is presented in Stearns (1929). Stearns was charged with investigating water resources of the upper McKenzie River and evaluating potential dam sites. In his report, he described Clear Lake as being dammed by a lava flow and noted three waterfalls (Upper, Middle, and Lower Falls, presently known as Sahalie and Koosah Falls and Tamolitch Pool,

respectively). At the time of his visit in September 1926, he noted that Lower Falls (Tamolitch Pool) did not have a waterfall – water emerged from surrounding lava flows, but there was no surface water input. Stearns also described a drowned forest at Clear Lake. Here, he observed that all the trees were rotted off at modern lake levels, and concluded that the lake level had therefore been the same since the time the trees were drowned. Finally, Stearns reported evidence of water leakage through the lava dam at the southern end of the lake; this, along with his observation that the McKenzie River discharge increases downstream due to groundwater contributions, led him to recommend against turning Clear Lake into a reservoir for water management.

Reconnaissance mapping by Williams (1957) tied the lava flows around Clear Lake to the Sand Mountain chain of vents. Further mapping by Taylor (1965) identified nine lava flow units emanating from multiple vent systems in the SMVF. Taylor (1965) also mapped a "late-stage" flow from Belknap volcano that entered the McKenzie River valley south of present-day Carmen Reservoir and flowed down the McKenzie drainage to and past Tamolitch Pool. Mapping of the SMVF in the most recent USGS geologic map for the Bend quadrangle (Sherrod et al., 2004) is primarily based on Taylor's work. Notable modifications are that Sherrod et al. (2004) subdivided Taylor's single lava flow from Nash Crater into four units, and mapped several exposures of lava from the Inaccessible line of cones in Taylor's (1965) "late-stage" Belknap lava.

Age of the SMVF

Several ^{14}C ages have been published for the SMVF, including dates for charred roots found at the base of lava flows and submerged drowned trees preserved in Clear

Lake (Table 1). These ages suggest that the field was active c. 3 ka. There are also two ^{14}C dates (of the same sample) associated with the "late-stage" Belknap lava flow south of the SMVF, dating it to c. 1.5 ka (Table 1); these two samples are statistically equivalent at the 95% level (t-test 1.014045 with χ^2 of 3.84). This flow is mapped by both Taylor (1965) and Sherrod et al. (2004) as entering the McKenzie River valley south of Carmen Reservoir and surrounding Tamolitch Pool.

TABLE 1. SUMMARY OF AVAILABLE ^{14}C DATES FOR THE SAND MOUNTAIN VOLCANIC FIELD AND THE BELKNAP LAVA FLOW

Sample name	Lab number	Age*	Description	Reference
TFJ-60A	WSU-370+	1,400 ± 100 yr BP 1,310 ± 96 cal yr BP†	Re-analysis of sample TFJ-60 described below	Champion (1980)
TFJ-60	WSU-292	1,590 ± 160 yr BP 1,526 ± 164 cal yr BP†	Charred roots excavated from base of tree mold within the late-stage Belknap lava flow of Taylor (1965) roughly 0.5 miles east of Highway126	Taylor (1965)
TFJ-204	*WSU-371*	*1,950 ± 150 yr BP* *1,914 ± 183 cal yr BP†*	*Charred wood underneath cinders from cone immediately southwest of Potato Hill, presumably Jack Pine vent*	*Chatters (1968)*
870804-1	*W-6018*	*2,590 ± 150 yr BP* *2,654 ± 190 cal yr BP†*	*Charcoal at contact between soil and tephra attributed to Nash and the northern SMVF*	*Sherrod et al. (2004)*
Sample b	N.R.§	2,705 ± 200 yr BP 2,819 ± 272 cal yr BP†	Outer wood of ~0.3 m (1 ft) diameter stump submerged in Clear Lake at depth of 4 m (13 ft), collected in November 1963	Benson (1965)
CL1964	AA-30522	2.750 ± 45 yr BP 2,848 ± 69 cal yr BP	Part of 0.3 m "rooted snag" submerged in Clear Lake collected by E.M. Taylor in summer 1964 (Liccardi et al., 1999) near the Cold Water Cove campground boat ramp (E.M. Taylor pers. comm. to R.M. Conrey)	Liccardi et al. (1999)
NID10-16MK	N1D10-16MK	2,870 ± 20 yr BP 3,003 ± 35 cal yr BP†	Outer wood of tree submerged in Clear Lake at depth of 40 m (130 ft) near UTM 10N E0580112 N4912933 (WGS1984), collected July 20 2010 and analyzed by NOSAMS Nov 16 2010	This study
TFJ-213	*WSU-449*	*2,990 ± 300 yr BP* *3,178 ± 352 cal yr BP†*	*Charred roots beneath lava flow on east side of Clear Lake*	*Champion (1980)*
Sample a	N.R.§	3,200 ± 220 yr BP 3,415 ± 277 cal yr BP†	Inner wood of sample b described above	Benson (1965)
TFJ-205	*WSU-372*	*3,850 ± 215 yr BP* *4,273 ± 297 cal yr BP†*	*Charred root bark surrounded by soil and roots found near Old Santiam Wagon Road, described as dating the Fish Lake lava flow of Taylor (1968), referred to as the Hackleman Creek lava flow in Champion (1980)*	*Chatters (1968)*

Note: ^{14}C dates inconsistent with stratigraphic relations and/or other dating methods presented in this study are *italicized* and are included for completeness; for more detailed discussion of these ages see Sherrod et al. (2004).

*All ages reported with 1σ error.

†Calibrated age determined with CalPal-2007^{online} (Danzeglocke et al., 2012).

§N.R. = not reported.

As part of a study quantifying cosmogenetic ^{3}He production rates in the central Oregon Cascades, Licciardi et al. (1999) dated a sample of a submerged tree from Clear Lake. Licciardi et al. (1999) assumed the resulting age (2,856 ± 92 cal yr BP, reported to 2σ as with all other ^{14}C dates discussed in this study) to be the age of the youngest-

looking SMVF lava flow located on the eastern margin of Clear Lake and consequently used it to calibrate ^{3}He production rates for the area. Interestingly, this age is roughly 140 years younger than the ^{14}C date of another submerged tree, this one rooted at 40 m depth (3,000 ± 73 cal yr BP; this study).

A note on the submerged Clear Lake tree samples dated in Benson (1965) and Licciardi et al. (1999) is warranted. Licciardi et al. (1999) date a sample provided by Taylor, whose 1965 paper cites Benson (1965)'s submerged tree date for the age of Clear Lake. Despite similarities in sample descriptions, we believe the samples come from different trees. Benson (1965) reports that "several sections of trees were obtained in November, 1963, in what must have been one of the first aqualung operations," whereas Licciardi et al. (1999) states that "Taylor provided [Licciardi et al., 1999] with a wood sample collected by him in the summer of 1964." In the early 1980s, Taylor also told one co-author (RMC) that he collected the sample by tying a cable around the tree, attaching the cable to his truck, and then uprooting and dragging the tree onto land as he drove up the Cold Water Cove campground boat ramp, nearly removing his head in the process! Thus, the differences in reported collection dates and methods suggest that Benson (1965) and Licciardi et al (1999) measured death dates of different trees, although it is likely the trees are from similar sites in the relatively shallow water near the Cold Water Cove campground boat ramp.

METHODS

Our investigation of the Sand Mountain volcanic field (SMVF) and its relation to the evolution of the upper McKenzie River consists of a three-pronged approach: (1)

geologic mapping, with detailed mapping in the southern SMVF in the vicinity of the McKenzie River, (2) bathymetric investigations of Clear Lake, the source of the McKenzie River, and (3) field observations of the hydrology of the upper McKenzie River watershed.

Geologic mapping

Geologic mapping was conducted over a 20 year period. The mapping presented here was started in the mid-1990s by co-author R.M. Conrey and focused on flow unit identification and general SMVF characterization. Acquisition of 1-m resolution research grade Light Detection and Ranging (LiDAR) data in 2008 for the McKenzie River (extended to include the southern SMVF) by the Eugene Water and Electric Board (EWEB) and Oregon's Department of Geology and Mineral Industries (DOGAMI) instigated detailed mapping of the southern SMVF. We use LiDAR data to identify likely flow extents, presumed flow contacts and locations for field checking and sample collection. In 2010 and 2011 we mapped several flow contacts with a handheld GPS device.

Mapped flows were assigned to eruptive units on the basis of field relations and the geochemistry of collected samples. Major and trace element concentrations were measured by X-ray fluorescence spectroscopy (XRF) at Washington State University Pullman (Table A1). Samples include lava (246 samples), vent material (10 samples), and bombs (27 samples); we collected unoxidized unweathered samples when possible. We located samples either on a 7.5 minute quadrant or (starting in 2002) with a hand-held GPS device (Table A2). All sample locations were recorded in UTM Zone 10N

coordinates; device location errors for samples collected in 2009 and later are generally < 10 m. We assigned vents to eruptives units solely on the basis of geochemistry.

A final geologic map was produced in ArcMap 9.3 with contacts drawn at 1:2500 in regions with LiDAR data and 1:10,000 elsewhere. Walked contacts were traced at 1:750 assuming a 6 m possible location error and (where LiDAR data existed) accounting for aspect and flow front consistency. Where LiDAR data were not available (notably in the vent area and in the northern SMVF), we used a combination of a 10-m digital elevation model (DEM)-derived hillshade and 0.5 m pixel georeferenced aerial photography (available from Oregon Image Explorer, http://oregonexplorer.info/) to inform flow contact placement.

For this reason, along with the limited amount of time spent in the northern SMVF, we stress that contacts in areas without LiDAR coverage are located only approximately and thus mapping of the northern SMVF should be treated as reconnaissance.

Relative and quantitative dating

We use relative and quantitative dating techniques to establish the eruption chronology for the SMVF and other units that enter the upper McKenzie River valley. Relative ages are preferentially established at observed field contacts, and are otherwise inferred from flow extents. Specifically, eruptive units with continuous lava coverage are assumed to be younger than adjacent units with discontinuous exposures.

We use three quantitative dating techniques: existing ^{14}C ages for both charred material found at the base of lava flows and of drowned Douglas-fir trees submerged in

Clear Lake (Table 1), analysis of paleomagnetic secular variation and cosmogenic ^{3}He surface exposure dating of individual lava flows.

Paleomagnetic analyses measure the orientation and strength of magnetic grains, which aligned with the ambient magnetic field when lava flows cool. As the geomagnetic field varies with time, it is possible to determine whether different lava flows were emplaced at similar times; when used in conjunction with absolute age dating methods (e.g., ^{14}C or surface age exposure dating), it is possible to attribute a given secular variation to a specific time period. Paleomagnetic samples were collected, processed, and interpreted using the methods described in McElhinny (1973). We cored select lava flows over the course of four field seasons (1973, 1974, 2002, 2011); we only sampled sites with no evidence of post-emplacement slumping, fracturing, or movement. Additionally, we collected samples for XRF analysis at or within 100 m of each site to confirm eruptive unit assignment. Samples were taken in the field using a hand-held, gasoline-powered, 2.5-cm coring drill and oriented using a sun compass. Eight to twelve, 10-cm-long samples were taken at each site. We measured the 2.5-cm-long specimens using a manual and then an automated cryogenic magnetometer and subjected to alternating-field (AF) demagnetization to remove secondary components of magnetization; this work was done at the US Geological Survey Menlo Park Volcano Science Center. These very young mafic volcanic rocks were sometimes found to be free of secondary magnetizations, such that we could use the natural remanent magnetic values (NRM). The characteristic direction of remanent magnetization for each site was calculated using Fisher statistics on data from NRM measurements, a blanket level of AF treatment, and from line fits of data on vector component diagrams.

Cosmogenic ^{3}He surface exposure dating measures the ^{3}He concentration within olivine grains collected within < 4 cm of the surface; the longer the grain has been exposed to cosmogenic radiation, the greater the abundance of cosmogenically produced ^{3}He. Given a ^{3}He production rate and a scaling factor accounting for elevation and latitude, it is possible to determine the length of time that olivine grains have been exposed to cosmogenic radiation. We collected samples for cosmogenic ^{3}He surface exposure dating of olivine grains during the 2009 field season. We collected at exposed sites with no evidence of post-emplacement erosion or coverage by soil or loose material, and also collected samples at each site for XRF analysis to confirm eruptive unit assignment. Only olivine grains from the top 4 cm of the samples were processed. Olivine grains were prepared at the University of Oregon and analyses were conducted at the California Institute of Technology following the procedure in Amidon et al. (2011). To determine flow age based on obtained ^{3}He concentration, we use Licciardi et al.'s (1999) calibrated production rate for the SMVF (114 g^{-1} yr^{-1}) and calculated the scaling factor for each site using Desilets et al. (2006). We do not correct for topographic shielding and cover from vegetation and/or snow, as we expect these to be minimal. The error associated with our results is roughly 10%.

Bathymetric survey

We conducted a bathymetric survey of Clear Lake over the course of four field days by rowing a series of transects across the lake and taking depth measurements with a Garmin Fishfinder 320C (temporarily mounted on the rowboat; no motorized boats are permitted at Clear Lake) connected to a hand-held GPS device; a Fishfinder is a small

sonar device. GPS location accuracy was typically < 6 m, and the Fishfinder hookup required that locations be recorded in latitude / longitude format (all other locations in this study were initially recorded in UTM coordinates). At the start and end of each bathymetric survey we noted lake level relative to the Fishfinder sonar sensor and then calibrated absolute bottom depth based on water level measured that day at USGS gage 14158500 located at the Clear Lake outlet (Fig. 2b).

We combined all the bathymetric measurements (converted to absolute elevation and UTM 10N coordinates) with LiDAR elevation data from within 25 m of the lake margin, as mapped on the LiDAR-derived basemap at 1:2,500. We used these data to construct a 5 m grid bathymetric model using the natural neighbor interpolation method in ArcGIS. This method uses Voronoi polygons to assign a value at a grid point based on area-weighted contribution of the nearest data points (Sibson, 1981). We selected this method because it (1) effectively deals with data that are not uniformly distributed, (2) does not create artificial peaks or lows, and (3) assigns grid values based on the nearest data without having to assign a data input radius.

When we detected drowned trees with the Fishfinder (Fig. 3b), we noted the depth to the top of drowned trees. On two of the four survey days, we also noted the presence or absence of a "whiteline" (Fig. 3c), which when present indicates a hard bottom.

RESULTS

Eruptive units

We identify three main geochemical groups within the SMVF: the Sand, Nash, and Lost Lake groups. The three groups contain a total of thirteen eruptive units,

including three “orphan” lava flows (no presently exposed associated vents) and one line of cones without associated lava flows. We present detailed mapping of the southern SMVF (Sand group) and reconnaissance mapping of the northern SMVF (Nash and Lost Lake groups; Fig. 4).

The Sand group consists of five eruptive units (proto-Clear Lake South, Clear Lake South, Ice Cap, Great Spring, and Clear Lake East) and includes one line of cones without associated lava flows (proto-Clear Lake South vents). Further north, the Nash group consists of four eruptive units (Early Nash I, Early Nash II, Nash, and Little Nash) and includes two orphan lava flows (Early Nash I and II), while the Lost Lake group consists of four eruptive units (Cole Water Cove, Fish Lake, Old Wagon Road, and Lost Lake) with one orphan lava flow (Cold Water Cove). We determined stratigraphic relations on the basis of field contacts for the Sand group.

Within the SMVF near the Lost Lake group we also document an isolated cone without associated lava flows (Jack Pine vent), and in a small area between the Nash and Lost Lake groups, we find a lava flow with limited exposure and no associated vent (SnoPark lava flow). South of the SMVF we find two lava flows (Tamolitch and Belknap) sourced at or near Belknap volcano and Inaccessible chain of cones that entered the McKenzie River valley; we present detailed mapping and stratigraphic relations of these flows where LiDAR data are available.

Lava flow physical characteristics

The SMVF lava flows generally have blocky morphologies with flow fronts up to 15 m thick in the Ice Cap (Sand group) and Cold Water Cove (Lost Lake group) lava

flows. The LiDAR data also highlight a pronounced levee system (with 20 m of relief) within the Cold Water Cove lava flow immediately southeast of Clear Lake (Figs. 2 and 4).

The blocky Clear Lake East lava flow was fed, at least in part, by a lava tube system, which is exposed (as "Lucy's Cavern") at 44.376°N 121.946°W. This tube trends S20°E, extends at least ~150 m and is, in places, ~8 – 10 m deep. This lava tube is remarkable for its drip features and vaulted roof that pinches to a narrow elongated top (Fig. 5). Additionally, we located the two "vertical pipes" documented by Taylor (1965) at 44.378°N 121.939°W and 44.378°N 121.938°W. These are deep circular pits with a ~1 m opening diameter situated at the top of two separate mounds (Fig. 5c). We estimate the pits to be > 20 and > 30 m deep, respectively, based on the time required for a dropped rock to hit something. We note that Clear Lake East lava flows are sourced both from a cinder cone and from vents without associated cones. Additionally, along most of the Clear Lake East lava flow margin with Clear Lake, the lava has cm-scale alternating bands of fresh and oxidized lava (Fig 6). We find these banded oxidation features only within a few meters of the lake, and only north of the Cold Water Cove campground boat ramp.

In contrast to the SMVF lava flows, the Tamolitch and Belknap lava flows have muted flow fronts and Hawaiian flow features, including well defined pahoehoe ropes and pronounced tumuli, particularly in the Tamolitch flow. The Tamolitch lava flow also contains well developed tree molds, some of which were noted by Stearns (1929).

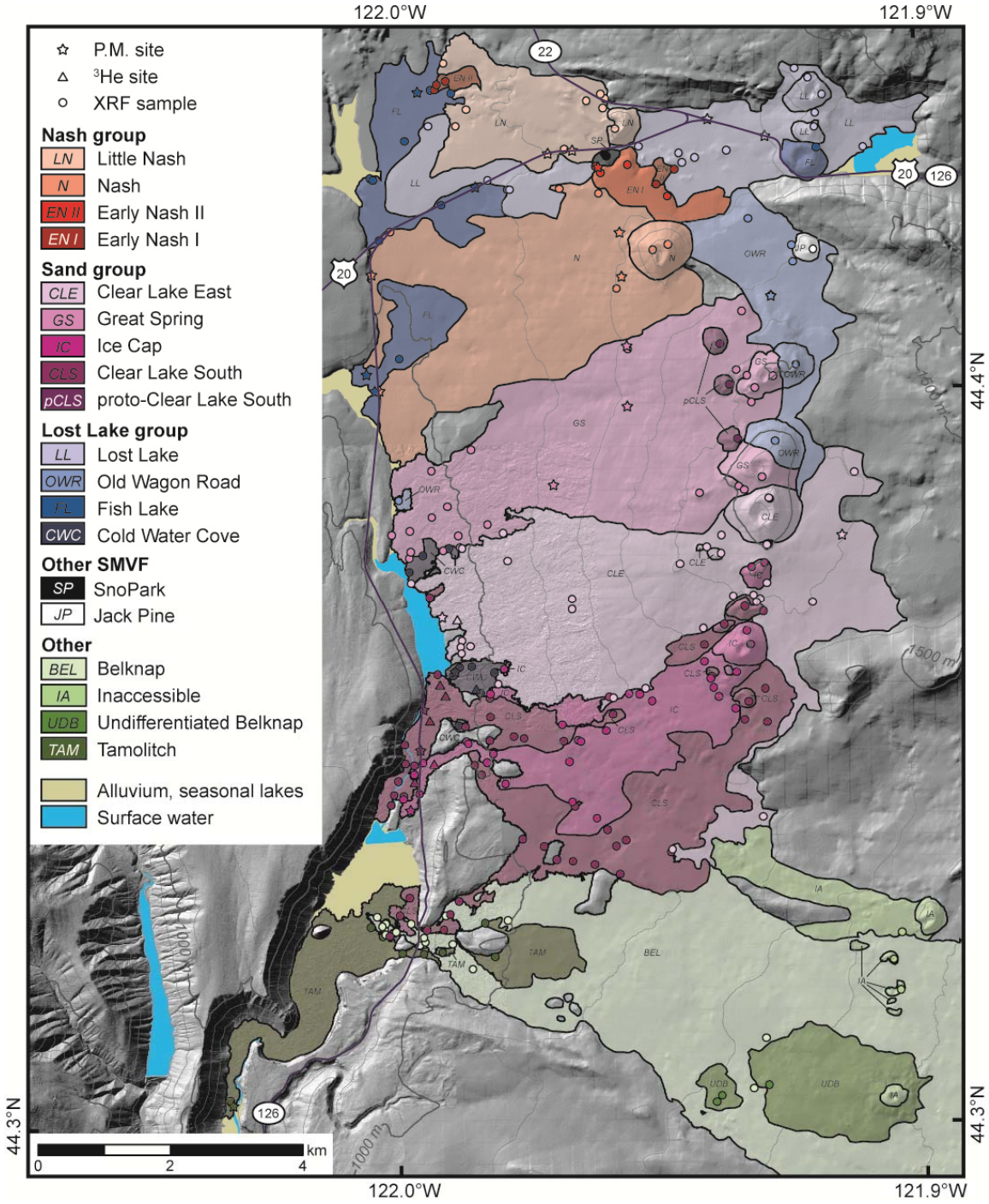

Figure 4. Geologic map of the SMVF and other Holocene lava flows of the upper McKenzie River watershed. Basemap is a shaded relief map constructed from LiDAR data where available and a 10 m DEM elsewhere. Palemagnetic (stars), ^{3}He (triangles), and XRF (circles) sample locations are shown; note that XRF samples also collected at palemagnetic and ^{3}He sites. Also shown are key highways (black lines) and 100 m contour intervals (grey, with bold 500 m contour intervals). Refer to Fig. 2 for geographic names.

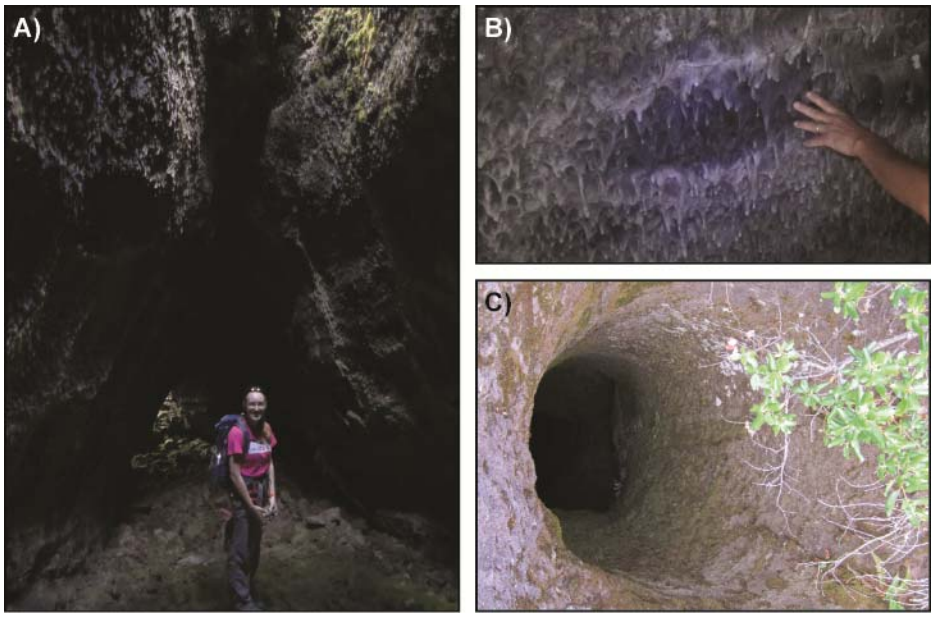

Figure 5. Photographs of (A) a lava tube in Clear Lake East eruptive unit ("Lucy's cavern); note the vaulted ceiling that pinches to a narrow elongated top, (B) drip features on wall of Lucy's cavern with hand for scale, and (C) a deep circular pit at top of a Clear Lake East eruptive unit mound; pit is ~1 m across and estimated to be > 20 m deep.

Geochemistry

Most of the mapped lava flows are calc-alkaline basalt or basaltic andesite (Fig. 7). Unlike some other young lava flows in the region (e.g., Deardorff and Cashman, in revision), individual flows have homogeneous compositions, which we use to identify eruptive units (Fig. 7). Distinguishing elements are SiO_2, TiO_2, MgO, and CaO (major elements, wt %; Table 2), and Ni, Sr, and Ba (trace elements, ppm; Table 3).

The Sand group shows the greatest variation in composition and ranges from basalt to basaltic andesite. Individual Sand group units are distinguishable from each other on the basis of SiO_2, TiO_2, Sr, and Ba concentrations.

The Nash group is entirely basaltic andesite, with individual flow compositions generally showing tight clusters. The Nash group can be distinguished from the other

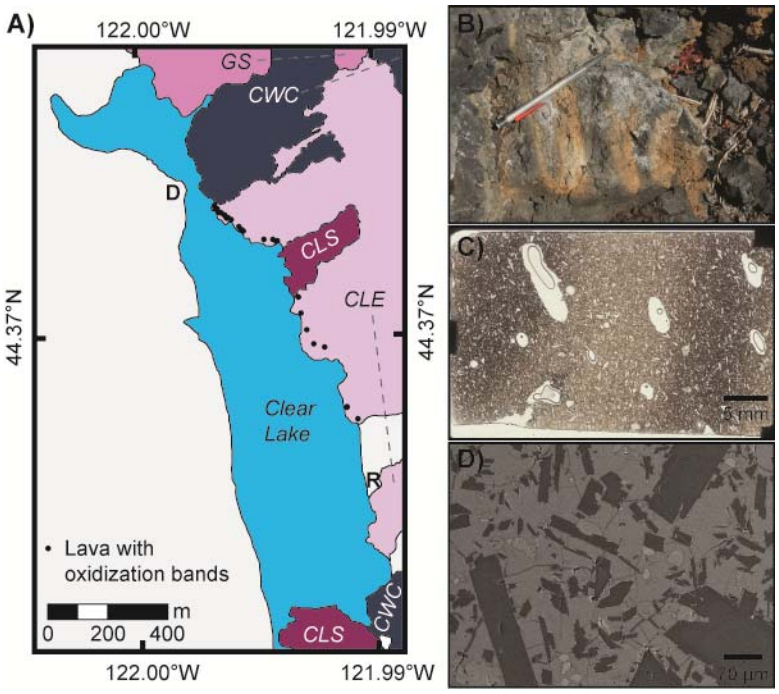

Figure 6. (A) Geologic map of Clear Lake region with black dots showing the location of lava with oxidation bands (see B and C). Lava flows surrounding the lake are, from oldest to youngest, Cold Water Cove (CWC), Clear Lake South (CLS), Great Spring (GS), and Clear Lake East (CLE). 'D' is the Clear Lake Resort boat dock (D) and 'R' is the Cold Water Cove campground boat ramp. (B) Photograph of lava with oxidation bands with pencil for scale. (C) Thin section of Clear Lake East lava with banded oxidation feature (sample NID09-06, co-located with RC09-37). (D) SEM image of NID09-06; note the high glass content (light grey). (C) and (D) are courtesy of Lucy Walsh.

groups by its high SiO_2 content and FeO/MgO ratio, low MgO, TiO_2, CaO, and Cr contents, and atypical Ni vs. MgO trend. Individual units show differences in SiO_2, MgO, Ni, and Sr concentrations.

The Lost Lake group is mostly basalt and individual flows show tight compositional clusters; it differs from the other groups with its high MgO content and relatively low FeO/MgO ratio. Individual units show differences in Ba and Sr concentrations.

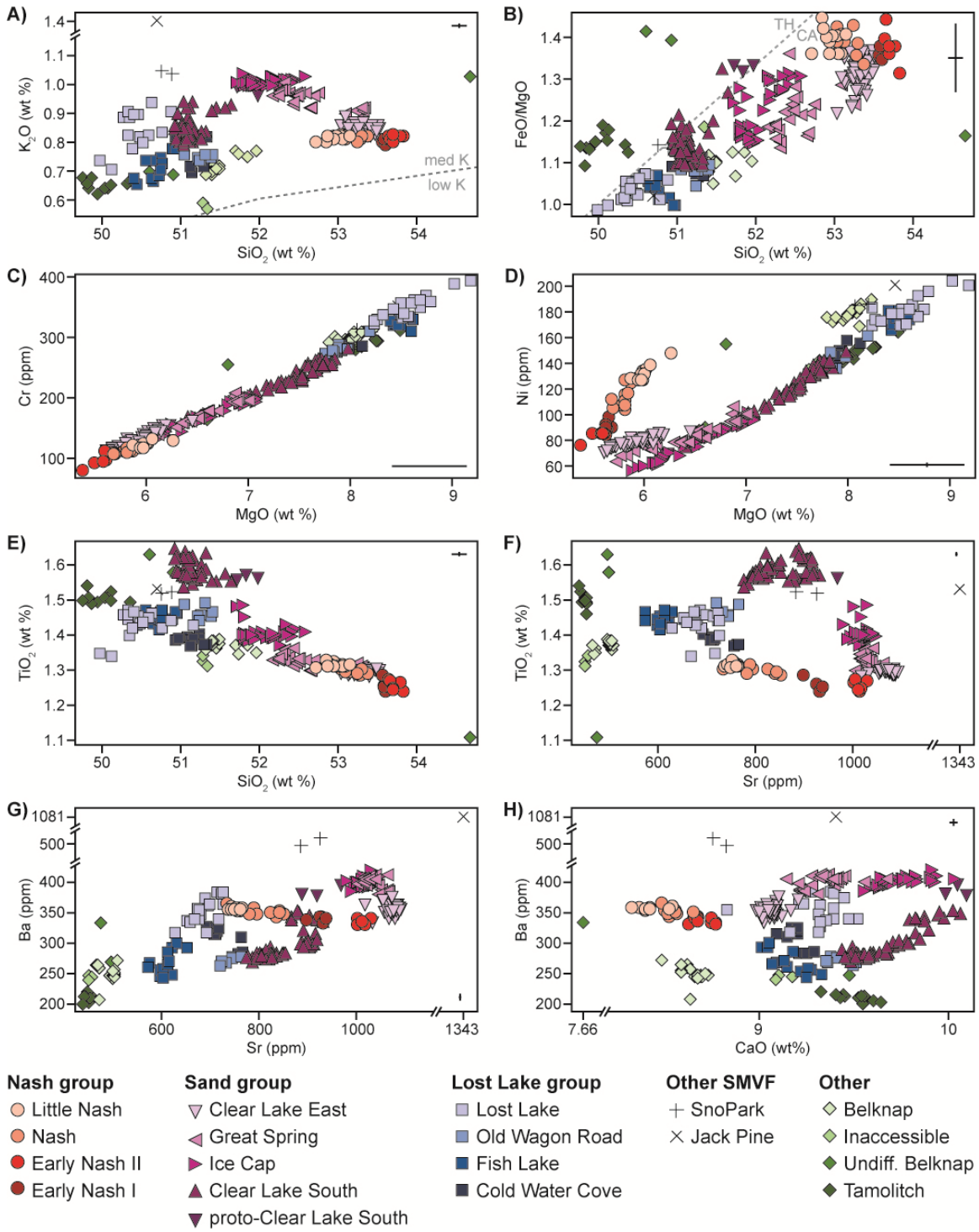

Figure 7. Harker plots for the SMVF and other units mapped in this study; unit colors correspond to Fig. 4. Major and minor elements are in weight percent (wt. %), and trace elements are in parts per million (ppm). XRF instrument error bars (2σ) shown on each plot.(A) K_2O vs. SiO_2, with the low and medium K fields shown following Gill (1981). (B) FeO/MgO vs. SiO_2, with the line separating tholeiitic (TH) and calc-alkaline (CA) lavas shown following Arculus (2003). (C) Cr vs. MgO. (D) Ni vs. MgO. (E) TiO_2 vs. SiO_2. (F) TiO_2 vs. Sr. (G) Ba vs. Sr. (H) Ba vs. CaO.

TABLE 2. ERUPTIVE UNIT RANGE OF NORMALIZED MAJOR ELEMENT WEIGHT % CONCENTRATIONS

Eruptive unit (N)	Metric	SiO_2	TiO_2	Al_2O_3	FeO	MnO	MgO	CaO	Na_2O	K_2O	P_2O_3
NASH GROUP											
Little Nash (11)											
	Min	52.72	1.308	17.61	8.15	0.141	5.88	8.32	3.72	0.80	0.399
	Mean	52.96	1.315	17.79	8.36	0.142	6.01	8.41	3.80	0.81	0.403
	Max	53.15	1.330	17.89	8.61	0.143	6.27	8.53	3.86	0.82	0.410
	Range	0.43	0.021	0.28	0.46	0.002	0.39	0.22	0.14	0.03	0.012
	Stdev	0.13	0.006	0.07	0.14	0.001	0.10	0.06	0.05	0.01	0.004
Nash (10)											
	Min	53.02	1.288	17.87	7.74	0.135	5.68	8.48	3.81	0.80	0.383
	Mean	53.16	1.300	17.94	8.04	0.137	5.80	8.54	3.87	0.82	0.391
	Max	53.37	1.315	18.00	8.30	0.140	5.87	8.64	3.92	0.83	0.401
	Range	0.34	0.028	0.14	0.56	0.005	0.19	0.16	0.11	0.03	0.018
	Stdev	0.13	0.010	0.04	0.16	0.002	0.06	0.04	0.04	0.01	0.007
Early Nash II (6)											
	Min	53.64	1.239	17.82	7.40	0.128	5.38	8.62	3.65	0.80	0.353
	Mean	53.72	1.256	17.96	7.65	0.130	5.55	8.70	3.85	0.82	0.366
	Max	53.83	1.274	18.09	7.81	0.137	5.63	8.76	3.93	0.83	0.395
	Range	0.19	0.035	0.27	0.41	0.010	0.25	0.14	0.28	0.03	0.042
	Stdev	0.07	0.014	0.10	0.15	0.004	0.10	0.06	0.11	0.01	0.015
Early Nash I (5)											
	Min	53.56	1.241	17.90	7.58	0.130	5.63	8.64	3.85	0.79	0.355
	Mean	53.59	1.259	17.97	7.67	0.131	5.65	8.68	3.89	0.80	0.361
	Max	53.61	1.285	18.07	7.77	0.133	5.68	8.76	3.92	0.81	0.370
	Range	0.05	0.044	0.17	0.19	0.003	0.05	0.12	0.07	0.02	0.016
	Stdev	0.02	0.017	0.08	0.07	0.001	0.02	0.05	0.03	0.01	0.006
SAND GROUP											
Clear Lake East (40)											
	Min	53.04	1.284	17.32	7.47	0.131	5.61	8.98	3.55	0.82	0.377
	Mean	53.32	1.295	17.55	7.76	0.134	5.93	9.06	3.71	0.85	0.384
	Max	53.52	1.305	17.77	8.00	0.138	6.46	9.20	3.85	0.89	0.392
	Range	0.47	0.021	0.45	0.52	0.007	0.85	0.23	0.30	0.06	0.014
	Stdev	0.12	0.005	0.12	0.14	0.002	0.18	0.04	0.07	0.01	0.004
Great Spring (27)											
	Min	52.17	1.297	17.00	7.51	0.135	5.73	9.14	3.20	0.88	0.372
	Mean	52.66	1.323	17.30	7.95	0.142	6.47	9.34	3.49	0.95	0.388
	Max	53.34	1.364	17.76	8.28	0.153	7.01	9.67	3.71	1.01	0.416
	Range	1.18	0.068	0.76	0.77	0.018	1.29	0.53	0.51	0.13	0.045
	Stdev	0.39	0.017	0.20	0.23	0.004	0.41	0.11	0.11	0.03	0.010
Ice Cap (36)											
	Min	51.73	1.373	16.96	7.70	0.141	5.89	9.55	3.23	0.97	0.362
	Mean	52.05	1.406	17.20	8.09	0.144	6.62	9.74	3.36	1.01	0.376
	Max	52.58	1.485	17.53	8.32	0.150	7.09	10.03	3.48	1.04	0.411
	Range	0.85	0.112	0.57	0.62	0.009	1.20	0.49	0.25	0.06	0.049
	Stdev	0.24	0.023	0.19	0.16	0.002	0.40	0.12	0.06	0.01	0.008
Clear Lake South (55)											
	Min	50.93	1.537	16.56	8.21	0.145	6.42	9.43	3.20	0.79	0.350
	Mean	51.14	1.588	16.81	8.57	0.148	7.53	9.66	3.34	0.84	0.369
	Max	51.65	1.647	17.27	8.77	0.152	7.99	10.06	3.47	0.94	0.393
	Range	0.73	0.109	0.71	0.57	0.007	1.57	0.63	0.27	0.15	0.043
	Stdev	0.14	0.026	0.12	0.12	0.002	0.29	0.16	0.06	0.04	0.009
Proto - Clear Lake South (3)*											
	RC03-49	51.98	1.561	17.46	8.13	0.146	6.10	10.04	3.24	0.96	0.389
	RC03-50	51.84	1.572	17.32	8.19	0.145	6.21	10.09	3.25	1.00	0.378
	RC04-25	51.73	1.559	17.31	8.32	0.145	6.24	9.98	3.34	0.99	0.382
LOST LAKE GROUP											
Lost Lake (17)											
	Min	49.98	1.340	16.53	8.63	0.151	8.24	8.82	3.10	0.71	0.324
	Mean	50.47	1.433	16.72	8.90	0.154	8.58	9.30	3.24	0.85	0.345
	Max	51.16	1.474	16.83	9.09	0.159	9.18	9.51	3.40	0.94	0.359
	Range	1.18	0.133	0.30	0.46	0.008	0.94	0.69	0.30	0.22	0.035
	Stdev	0.28	0.039	0.07	0.13	0.002	0.26	0.16	0.07	0.06	0.010
Old Wagon Road (7)											
	Min	51.05	1.443	16.70	8.48	0.146	7.75	9.34	3.30	0.74	0.336
	Mean	51.26	1.467	16.79	8.55	0.149	7.91	9.42	3.36	0.75	0.341
	Max	51.41	1.493	16.88	8.65	0.151	8.19	9.51	3.40	0.76	0.344
	Range	0.36	0.050	0.19	0.18	0.005	0.45	0.17	0.10	0.03	0.008
	Stdev	0.12	0.019	0.07	0.06	0.001	0.14	0.07	0.04	0.01	0.003
Fish Lake (14)											
	Min	50.41	1.419	16.72	8.47	0.150	8.40	9.00	3.28	0.66	0.325
	Mean	50.70	1.451	16.82	8.82	0.154	8.49	9.16	3.36	0.72	0.340
	Max	50.96	1.474	16.94	9.08	0.157	8.61	9.32	3.46	0.78	0.360
	Range	0.55	0.055	0.22	0.61	0.007	0.22	0.31	0.18	0.12	0.035
	Stdev	0.16	0.018	0.07	0.20	0.002	0.07	0.10	0.06	0.04	0.013

Cold Water Cove (11)											
	Min	50.93	1.373	16.91	8.51	0.148	7.76	9.08	3.29	0.70	0.343
	Mean	51.15	1.386	17.02	8.69	0.152	7.89	9.20	3.36	0.79	0.361
	Max	51.32	1.403	17.14	8.94	0.157	8.12	9.31	3.46	0.83	0.375
	Range	0.39	0.030	0.23	0.44	0.009	0.36	0.22	0.17	0.13	0.033
	Stdev	0.12	0.011	0.08	0.13	0.003	0.10	0.06	0.05	0.05	0.010
OTHER SMVF											
SnoPark (2)*											
	RC03-57	50.89	1.525	16.36	9.17	0.157	8.08	8.82	3.48	1.04	0.480
	RC11-11	50.76	1.519	16.25	9.38	0.156	8.20	8.75	3.46	1.05	0.483
Jack Pine (1)*											
	RC04-34	50.70	1.531	15.80	8.63	0.145	8.46	9.40	3.30	1.41	0.618
OTHER											
Belknap (17)											
	Min	51.33	1.346	16.80	8.53	0.148	7.79	8.48	3.43	0.69	0.306
	Mean	51.51	1.373	16.94	8.82	0.150	8.02	8.64	3.51	0.72	0.312
	Max	51.96	1.386	17.13	8.94	0.151	8.23	8.72	3.60	0.77	0.332
	Range	0.63	0.040	0.33	0.41	0.004	0.44	0.24	0.16	0.08	0.026
	Stdev	0.18	0.012	0.09	0.11	0.001	0.11	0.06	0.04	0.03	0.007
Inaccessible Cones (3)*											
	SHE95-TFJ23	51.30	1.325	17.39	8.66	0.160	7.84	9.10	3.36	0.59	0.294
	SHE95-TFJ24	51.29	1.340	17.51	8.61	0.161	7.73	9.17	3.29	0.59	0.295
	SHE95-TFJ25	51.35	1.311	17.42	9.04	0.159	7.62	9.08	3.17	0.57	0.277
Undifferentiated Belknap (3)*											
	NID10-26MK	54.67	1.108	16.74	7.93	0.135	6.81	7.66	3.65	1.03	0.280
	NID10-27MK	50.61	1.628	17.52	9.34	0.165	6.61	9.46	3.59	0.70	0.394
	NID10-29MK	50.92	1.581	17.59	9.12	0.160	6.54	9.47	3.55	0.69	0.379
Tamolitch (11)											
	Min	49.77	1.459	16.99	9.07	0.158	7.95	9.32	3.14	0.62	0.324
	Mean	50.03	1.502	17.12	9.32	0.161	8.14	9.49	3.24	0.65	0.336
	Max	50.37	1.541	17.24	9.46	0.163	8.50	9.64	3.36	0.68	0.361
	Range	0.59	0.083	0.25	0.39	0.006	0.55	0.31	0.22	0.06	0.037
	Stdev	0.20	0.021	0.08	0.11	0.002	0.17	0.09	0.07	0.02	0.012
Instrument error		*0.19*	*0.012*	*0.08*	*0.18*	*0.002*	*0.073*	*0.04*	*0.04*	*0.02*	*0.003*

Note: Major elements are normalized on a volatile-free basis, with total Fe expressed as FeO. 'N' indicates the number of rock analysis attributed to the unit, and may include duplicate beads (see Tables DR1 and DR2).

*Results of analyses for units with three or fewer samples are provided in lieu of a summary.

TABLE 3. ERUPTIVE UNIT RANGE OF TRACE ELEMENT CONCENTRATIONS (PPM)

Eruptive unit (N)	Metric	Ni	Cr	Sc	V	Ba	Rb	Sr	Zr	Y	Nb	Ga	Cu	Zn	Pb	La	Ce	Th	Nd	U
NASH GROUP																				
Little Nash (11)																				
	Min	127	116	20	174	353	8	736	161	22	10.8	19	55	90	4	17	39	-1	24	1
	Mean	133	123	21	177	355	9	752	164	24	12.0	20	58	92	5	19	42	1	25	1
	Max	148	131	21	181	360	10	764	167	25	13.2	20	62	94	7	21	45	2	27	2
	Range	21	15	1	7	7	2	27	6	3	2.4	1	7	4	3	4	6	3	3	1
	Stdev	6	5	1	2	2	1	8	2	1	0.8	1	2	1	1	1	2	1	1	1
Nash (10)																				
	Min	104	107	20	168	342	8	733	151	21	9.1	19	52	87	4	16	36	0	21	2
	Mean	113	111	21	176	351	9	806	158	22	10.8	20	56	89	5	18	43	1	25	2
	Max	127	117	22	180	365	10	852	165	24	11.9	22	60	91	7	21	48	2	27	2
	Range	23	10	2	12	22	2	119	14	3	2.8	3	7	4	3	6	12	2	5	0
	Stdev	8	3	1	4	6	1	40	4	1	0.9	1	3	2	1	2	4	1	2	
Early Nash II (6)																				
	Min	77	80	19	165	330	8	1002	148	19	9.2	19	46	82	4	16	37	0	21	1
	Mean	84	97	20	170	335	9	1014	152	21	10.4	20	57	84	5	18	41	2	23	1
	Max	86	111	21	177	340	9	1031	156	22	11.4	21	65	86	6	20	47	3	26	1
	Range	9	31	2	12	10	1	29	8	3	2.2	2	19	4	2	4	10	3	5	0
	Stdev	4	11	1	4	4	0	11	4	1	0.8	1	7	2	1	2	4	1	2	
Early Nash I (5)																				
	Min	89	106	20	174	332	7	898	148	20	8.6	19	57	84	3	16	36	-1	22	2
	Mean	92	108	21	176	339	8	925	149	21	10.1	20	61	85	5	18	40	1	23	2
	Max	99	110	22	177	343	9	939	150	22	11.3	20	63	88	7	20	42	2	25	2
	Range	11	4	3	4	11	2	41	2	2	2.7	1	6	3	4	4	6	3	3	0
	Stdev	4	2	1	1	4	1	16	1	1	1.1	1	2	1	1	2	3	1	1	
SAND GROUP																				
Clear Lake East (40)																				
	Min	71	112	21	168	332	7	1018	147	20	9.2	19	35	80	3	17	41	-1	22	0
	Mean	79	132	23	175	353	9	1075	158	22	11.2	20	59	84	5	21	48	1	26	1
	Max	87	161	24	179	374	11	1093	168	24	12.4	22	64	87	7	25	54	3	30	3
	Range	16	49	3	11	43	3	75	21	4	3.2	3	29	7	4	8	13	4	8	3
	Stdev	4	13	1	3	9	1	15	5	1	0.7	1	4	2	1	2	3	1	2	1
Great Spring (27)																				
	Min	64	121	23	177	380	8	1004	146	21	9.0	18	24	80	4	18	42	0	23	0
	Mean	85	167	26	187	400	10	1035	155	23	11.7	19	60	82	5	21	47	1	26	1
	Max	107	208	27	197	411	12	1069	163	25	13.1	21	81	87	7	24	54	2	30	2
	Range	43	88	4	21	31	4	65	17	4	4.1	4	57	7	4	7	12	2	7	2
	Stdev	12	27	1	6	9	1	17	4	1	1.3	1	10	2	1	2	3	1	1	1
Ice Cap (36)																				
	Min	57	129	26	184	385	8	980	142	22	10.2	17	50	76	3	15	40	0	22	0
	Mean	82	171	28	197	400	10	1024	150	24	12.6	18	62	80	5	20	45	1	26	1
	Max	102	203	29	207	418	12	1048	157	26	14.7	20	68	85	7	24	52	3	29	3
	Range	45	74	3	23	33	4	68	15	4	4.5	4	18	9	4	9	12	3	7	3
	Stdev	15	26	1	4	7	1	16	4	1	1.2	1	3	2	1	2	3	1	2	1
Clear Lake South (55)																				
	Min	76	167	25	182	269	9	775	141	21	12.2	16	43	77	2	14	37	0	21	0
	Mean	126	240	27	200	296	11	850	151	24	14.8	18	60	82	6	18	43	2	24	1
	Max	150	280	28	208	351	12	932	159	26	16.3	21	80	186	154	22	53	3	29	3
	Range	74	113	3	26	82	3	157	18	4	4.1	5	38	110	152	8	16	3	8	3
	Stdev	15	21	1	4	25	1	46	3	1	1.2	1	5	14	20	2	3	1	2	1

Proto - Clear Lake South (3)*																			
	RC03-49	63	139	28	201	394	11	969	156	26	13.6	17	26	83	4	22	48	2	26	
	RC03-50	70	154	29	205	378	11	918	156	26	13.9	20	64	81	31	21	51	2	27	
	RC04-25	70	154	28	205	379	10	888	145	23	13.6	18	63	76	5	21	46	2	27	
LOST LAKE GROUP																			
Lost Lake (17)																			
	Min	170	323	25	181	317	8	626	119	21	7.0	15	43	76	2	12	26	0	20	0
	Mean	183	351	27	199	353	9	686	133	23	10.2	17	63	79	5	15	35	1	22	0
	Max	205	394	28	210	383	10	724	141	26	12.2	18	78	84	12	18	41	2	26	0
	Range	34	71	3	29	66	2	98	21	5	5.2	2	35	8	10	7	15	2	6	0
	Stdev	11	20	1	7	21	1	28	7	1	1.1	1	8	2	2	2	4	1	2	
Old Wagon Road (7)																			
	Min	137	274	25	189	264	8	718	135	21	10.2	17	58	78	3	13	28	0	19	2
	Mean	144	285	26	195	272	9	735	143	23	11.1	18	60	80	4	15	37	1	20	2
	Max	162	310	27	199	279	10	763	146	25	13.0	19	64	82	6	18	43	2	24	2
	Range	25	36	2	10	15	2	45	11	4	2.8	2	6	5	2	5	15	3	5	0
	Stdev	9	12	1	4	5	1	16	4	1	0.9	1	2	2	1	2	5	1	2	
Fish Lake (14)																			
	Min	167	311	24	188	243	8	570	129	22	9.9	17	52	77	2	12	28	-1	19	1
	Mean	178	326	27	198	267	9	606	138	24	11.4	18	61	80	4	15	35	1	21	1
	Max	182	346	28	204	301	10	651	144	25	13.0	19	65	82	7	18	44	2	23	2
	Range	15	35	4	15	58	2	81	15	3	3.1	2	13	6	5	6	16	3	4	1
	Stdev	5	8	1	5	19	1	21	4	1	0.9	1	4	2	1	2	4	1	1	
Cold Water Cove (11)																			
	Min	139	269	26	188	283	8	692	134	24	8.9	16	44	79	2	13	33	0	20	0
	Mean	148	279	27	194	310	9	727	142	25	10.4	18	58	81	3	16	37	1	23	1
	Max	159	288	28	202	328	10	765	149	26	12.0	20	64	84	4	18	41	3	25	3
	Range	20	19	2	14	45	2	73	15	2	3.1	4	20	5	2	5	8	3	5	3
	Stdev	6	6	1	4	18	1	26	4	1	1.1	1	6	1	0	2	3	1	1	1
OTHER SMVF																			
SnoPark (2)*																			
	RC03-57	185	313	25	157	499	10	884	168	28	10.3	18	47	89	5	21	50	3	27	
	RC11-11	187	308	24	183	509	11	925	169	26	12.4	17	59	93	4	20	47	2	28	1
Jack Pine (1)*																			
	RC04-34	201	352	24	191	1081	18	1343	193	22	7.9	19	67	91	6	37	84	4	49	
OTHER																			
Belknap (17)																			
	Min	169	284	24	174	206	10	464	129	24	12.0	17	59	77	1	9	28	0	16	0
	Mean	179	299	25	192	249	11	493	133	24	12.7	18	67	82	3	14	30	1	18	1
	Max	190	313	26	196	270	13	507	139	25	14.9	19	76	84	4	23	36	2	20	2
	Range	21	29	2	22	64	3	43	10	2	2.9	3	17	7	3	14	8	2	4	2
	Stdev	5	7	1	5	14	1	14	3	1	0.7	1	4	2	1	3	2	1	1	0
Inaccessible Cones (3)*																			
	SHE95-TFJ23	141	257	30	205	247	7	448	109	22	9.1	18	54	76	1	0	16	1		
	SHE95-TFJ24	142	253	28	201	244	8	456	113	21	8.3	21	55	80	0	0	34	1		
	SHE95-TFJ25	136	247	28	202	239	6	450	106	21	8.2	21	51	80	1	14	25	0		
Undifferentiated Belknap (3)*																			
	NID10-26MK	155	253	21	161	332	20	474	138	23	11.2	18	59	79	5	16	33	3	17	0
	NID10-27MK	90	164	29	229	268	10	495	154	27	13.8	19	62	84	3	14	33	2	20	1
	NID10-29MK	88	170	29	222	246	9	499	149	27	14.1	19	58	83	2	13	34	1	19	1

Tamolitch (11)																				
	Min	141	278	28	211	199	9	437	126	23	13.4	17	52	76	1	10	25	1	15	0
	Mean	150	290	29	221	210	10	448	131	24	14.8	18	59	80	2	14	30	1	17	1
	Max	164	310	31	229	219	10	453	137	25	15.7	20	64	85	4	17	32	2	20	2
	Range	23	33	3	18	20	1	16	11	2	2.3	3	12	9	3	7	7	1	5	2
	Stdev	6	8	1	5	6	1	5	4	1	0.6	1	4	2	1	2	2	1	1	1
Instrument error (2σ)		4	3	2	5	12	2	5	4	1	1.2	3	7	3	3	6	8	2	4	3

Note: 'N' indicates the number of rock analysis attributed to the unit, and may include duplicate beads (see Tables DR1 and DR2).
*Results of analyses for units with three or fewer samples are provided in lieu of a summary.

The SnoPark lava flow and Jack Pine vent have compositions that are unique in the SMVF. The SnoPark lava flow shares some similarities with the Lost Lake group and the Clear Lake South eruptive unit (Sand group), but is sufficiently different to preclude inclusion in those units. The Jack Pine vent, in contrast, has a composition that is different from the SMVF in that it is an alkali basalt with exceedingly high Ba (1081 ppm) and Sr (1343 ppm) concentrations.

South of the SMVF, Tamolitch and Belknap lava flows are basalts with low Sr values; the two flows are distinguishable on the basis of SiO_2, TiO_2, CaO, and Ba concentrations. Three samples from within mapped Belknap (NID10-26MK) and Tamolitch (NID10-27MK and NID10-29MK) lava flows have similar SiO_2 and Sr values but are otherwise chemically different from these two eruptive units; we refer to these three samples as "undifferentiated Belknap." We have not yet been able to identify the source of the Tamolitch flow. We considered Inaccessible Cones to be the most likely source, but the compositions of samples from these cones match neither the Tamolitch nor Belknap lava flows.

Petrologic observations

Petrologic descriptions of the Sand group lava flows and the Cold Water Cove (Lost Lake group), Tamolitch and Belknap lava flows are provided in Table 4. In hand sample, the Clear Lake East lava flow is easily distinguishable due to its abundance of plagioclase microphenocrysts (absent in the other Sand group lava flows). Differences between the other Sand group lavas are more subtle, although the Clear Lake South lava flow often has larger (< 4 mm) olivine crystals. The Tamolitch and Belknap lava flows

can be distinguished by the abundance of plagioclase and olivine crystals in the Tamolitch lava flow relative to the aphyric Belknap lava flow.

TABLE 4. PETROGRAPHIC DESCRIPTIONS OF LAVA FLOWS MAPPED IN DETAIL

Eruptive unit	Phenocrysts	Groundmass
SAND GROUP		
Clear Lake East	10 – 15% plagioclase, 2% olivine Plagioclase: mostly lathes, up to 2 mm long Olivine: generally 1 mm diameter, some glomerocysts	Microcrystalline plagioclase and olivine
Great Spring	5% olivine, < 1.5% plagioclase Olivine: generally ≤ 1 mm, can be up to 3 mm diameter Plagioclase: mostly lathes, small	Highly microcrystalline plagioclase and olivine
Ice Cap	3 % olivine, < 1% plagioclase Olivine: generally ≤ 2 mm, can be up to 3 mm diameter Plagioclase: generally equant (few lathes) Large glomerocrysts of olivine and plagioclase	Microcrystalline plagioclase and olivine
Clear Lake South	7% olivine, < 0.1% plagioclase Olivine: bimodal size distribution, with sub-mm and 1 – 4 mm diameter grains; larger grains typically > 2 mm	Microcrystalline plagioclase (abundant) and olivine
LOST LAKE GROUP		
Cold Water Cove	5% olivine, trace plagioclase Olivine: bimodal size distribution, with sub-mm and 1 – 2 mm diameter grains	Highly microcrystalline plagioclase and olivine
OTHER		
Belknap	1% olivine, trace plagioclase Olivine: generally ≤ 1 mm, can be up to 4 mm diameter (rare) Overall few phenocrysts Notable for very glassy vesicles	Very glassy
Tamolitch	10% plagioclase, 5% olivine Plagioclase: up to 2 mm diameter Olivine: ≤ 1 mm diameter Glomocrysts of olivine and plagioclase common	Very crystalline, although glass visible

Stratigraphic relations

We established stratigraphic relations for all contacts within the LiDAR-mapped region on the basis of targeted field observations (Fig. 8). Within the Sand group, the Clear Lake East lava flows overlies all other Sand group lava flows. The Cold Water Cove lava flow (Lost Lake group) underlies all the Sand group lava flows and has no exposed contacts with flows from either the Nash or Lost Lake groups. The Clear Lake South lava flow underlies the Ice Cap lava flow. No contacts are exposed between Great Spring lava flow and either the Clear Lake South or Ice Cap lava flows. We note, however, that north of Clear Lake a small exposure of the Old Wagon Road lava flow (Lost Lake group) underlies the Great Springs lava flow. South of the SMVF, the

Tamolitch lava flow underlies the Belknap and Clear Lake South lava flows, while the Belknap lava flow overrides the Clear Lake South lava flow.

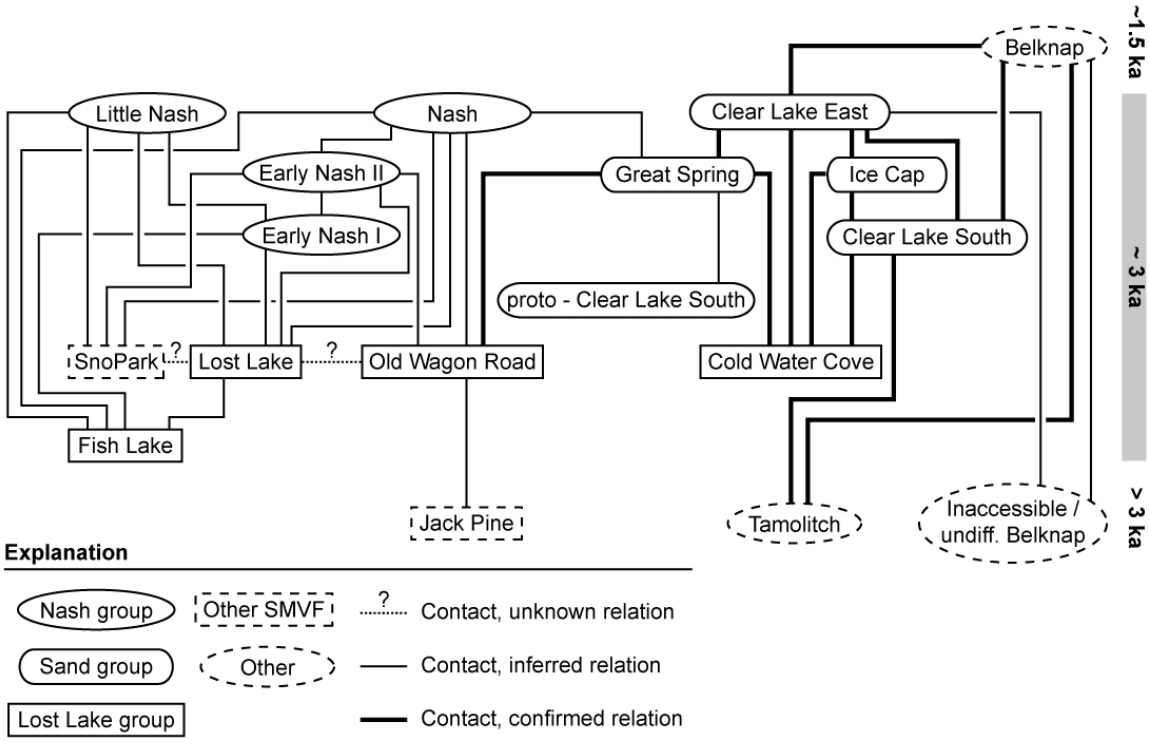

Figure 8. Stratigraphic relations for the SMVF and other units mapped in this study. Younger units overly older units, and units with a field contact are connected by a line. A bold line indicates the nature of the contact (i.e., which unit is younger) has been verified in the field, a regular line indicates the nature of the contact is inferred, and a dashed line indicates not enough information is available to infer the stratigraphic relation.

We infer stratigraphic relations for the Nash and Lost Lake groups on the basis of lava flow extent (Figs. 4 and 8). In the Nash group, Early Nash I appears to be the oldest, covered by the other three eruptive units. It, along with Early Nash II, is an orphan lava flow. Early Nash II appears to be sandwiched between Early Nash I and Nash. No relation is established between Little Nash and Early Nash II / Nash. The Nash lava flow overlies the Great Spring lava flow (Sand group); no other stratigraphic relation is established between two groups. In the Lost Lake group, the Fish Lake lava flow

underlies the Lost Lake lava flow and the Nash group, whereas the Old Wagon Road lava flow underlies the Great Spring flow (Sand group). It is also plausible that the Fish Lake and/or Old Wagon Road lava flows underlies the proto – Clear Lake South vents, although this cannot be confirmed in the field. The Lost Lake lava flow appears to underlie the Nash group. On the basis of flow extent and topography, we cannot determine the relation between the Old Wagon Road and Lost Lake lava flow.

Finally, the SnoPark lava flow appears to underlie the Nash group; its relation with the Lost Lake group is unclear. The Jack Pine vent has no associated lava flows but is surrounded by Old Wagon Road lava. We suspect that it is the oldest of all the units.

South of the SMVF and Carmen Reservoir, Tamolitch lava flows fill the McKenzie River valley; Tamolitch Pool emerges from beneath the Tamolitch lava flow. Tamolitch lava flow underlies Clear Lake South and East lava flows. The Belknap lava flow overrides the Tamolitch and Clear Lake South lava flows, and, according to Sherrod et al. (2004), also overlies Clear Lake East lava flows, consistent with its young age.

Quantitative ages

Paleomagnetic constraints

The scatter of SMVF paleomagnetic site mean directions on an equal-area diagram (Fig. 9a) is remarkably small. Sites within the Sand, Nash, and Lost Lake groups record a normal polarity remanent direction with mean inclination near 50°, and declinations slightly easterly in orientation (Table 5). The close mean directions of the Sand, Nash and Lost Lake eruptive groups strongly indicate that they are of the same eruptive age, and span a time interval no longer than a century. In contrast, results from

the Tamolitch basalt are separate, steeper in inclination, and more westerly in declination. This is clear in the comparison of the three nearly identical eruptive group mean directions with that of the Tamolitch flow (Fig. 9b). The Tamolitch paleomagnetic data shows it is temporally not part of the SMVF event, and due to stratigraphic constraints, must be older.

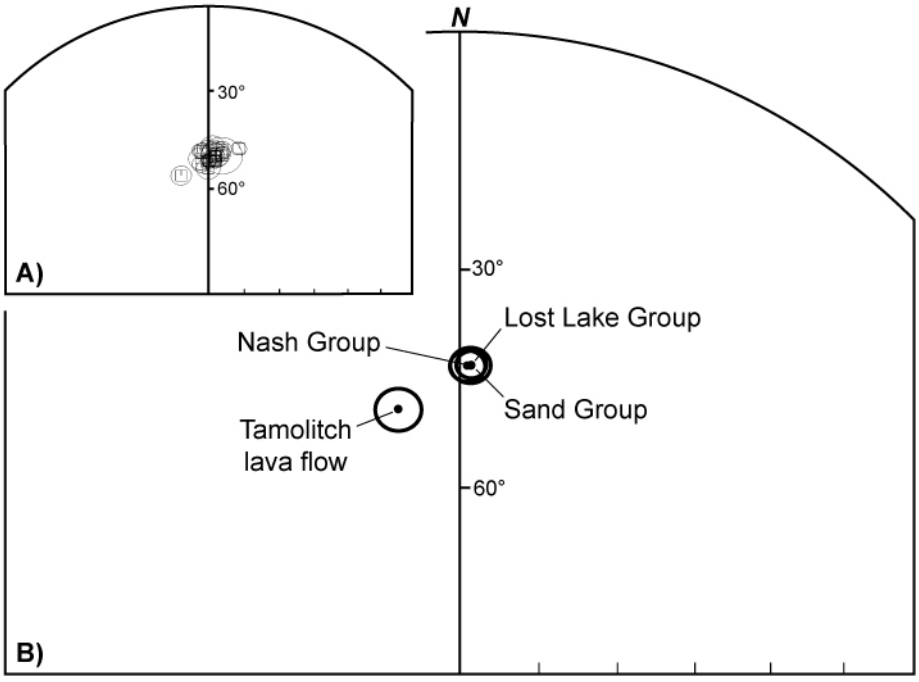

Figure 9. Part of a lower hemisphere equal-area projection showing (A) site mean directions of remanent magnetization and ovals of 95% confidence from paleomagnetic sites taken within the SMVF, and (B) mean remanent directions and ovals of 95% confidence from Sand, Nash and Lost Lake eruptive groups, as they compare to the site mean for the Tamolitch lava flow.

Cosmogenic ^{3}He exposure age dating

We determined cosmogenic ^{3}He exposure ages for seven samples in the vicinity of Clear Lake: one sample each for the Cold Water Cove, Ice Cap, and Great Spring lava flows and four for the Clear Lake South lava flow (Table 6). The ages for six of the

TABLE 5. PALEOMAGNETIC DATA FOR THE SAND MOUNTAIN VOLCANIC FIELD AND THE TAMOLITCH LAVA FLOW

Eruptive unit	Site	XRF Sample	Latitude (°N)	Longitude (°E)	N/No	Exp. (mT)	I (°)	D (°)	α95	k	R	Plat. (°N)	Plong. (°E)
NASH GROUP													
GROUP AVERAGE			44.42°	238.03°	7/7		50.3°	1.4°	2.1°	840	6.99286	76.6°	53.0°
Little Nash													
	LNCO Site 1	RC02-22	44.431°	238.031°	6/6	NRM*	49.6°	3.0°	3.8°	318	5.98428	75.8°	47.6°
	LNCO Sites 2,3,4	RC02-23	44.431°	238.036°	17/17	NRM*	50.5°	2.8°	1.9°	363	16.95587	76.6°	47.6°
			44.431°	238.034°	2/2		50.1°	2.9°	2.0°	15888	1.99994	76.2°	47.5°
Nash													
	221B2	RC95-02	44.401°	237.999°	8/8	10	51.8°	2.7°	1.9°	881	7.99206	77.9°	46.9°
	178B2	RC95-13	44.422°	238.045°	8/8	20+	48.2°	359.2°	2.5°	511	7.98631	74.8°	60.6°
	FsLO 3+4	RC02-20	44.414°	237.998°	1212	NRM*	49.2°	5.5°	2.0°	455	11.97583	75.1°	39.3°
	146B2	RC02-26	44.416°	238.045°	8/8	10	48.7°	356.6°	2.2°	648	7.98919	75.0°	69.6°
			44.41°	238.02°	4/4		49.5°	1.0°	3.4°	725	3.99586	75.9°	54.6°
Early Nash II													
	4371B	RC11-10	44.431°	238.041°	7/9	Li†	54.0°	359.8°	3.2°	360	6.9833	80.1°	59.0°
SAND GROUP													
GROUP AVERAGE			44.38°	238.02°	8/9		50.2°	2.0°	2.4°	521	7.98657	76.5°	50.7°
Clear Lake East													
	170B2§	*RC02-29*	*44.380°*	*238.086°*	*8/8*	*30*	*43.4°*	*0.1°*	*3.9°*	*207*	*7.96624*	*71.0°*	*57.8°*
	210B2	RC02-32	44.370°	238.010°	10/11	20	51.0°	356.7°	3.3°	217	9.95853	77.0°	70.8°
Great Spring													
	194B2	RC95-16	44.398°	238.046°	8/8	10+	48.2°	3.0°	1.9°	816	7.99142	74.6°	48.3°
	186B2	RC95-17	44.387°	238.032°	8/8	20	51.9°	0.4°	2.1°	705	7.99007	78.1°	56.2°
	154B2	RC02-27A	44.406°	238.046°	8/8	20	48.8°	357.5°	2.4°	540	7.98704	75.2°	66.6°
	162B2	RC02-27B	44.406°	238.046°	8/8	10+	50.2°	2.5°	3.7°	226	7.96908	76.4°	49.1°
			44.40°	238.043°	4/4		49.8°	0.9°	2.6°	1224	3.99755	76.2°	55.0°
Ice Cap													
	202B2	RC02-31	44.343°	238.004°	8/8	10	51.7°	3.1°	1.6°	1183	7.99408	77.8°	45.8°
Clear Lake South													
	CrLO 1+2	RC02-30	44.349°	238.006°	12/12	10	51.6°	0.2°	2.0°	464	11.97631	77.9°	57.3°
	CrLO 3+4	RC95-20	44.355°	238.006°	12/12	10+	47.1°	11.8°	2.0°	453	11.97572	71.4°	23.8°
			44.352°	238.006°	2/2		49.5°	6.3°	19.3°	170	1.99413	75.1°	36.5°
LOST LAKE GROUP													
GROUP AVERAGE			44.42°	238.03°	8/8		50.1°	2.1°	1.8°	968	7.99277	76.3°	50.4°
Lost Lake													
	LsLO Site 1	RCNSH-5#	44.432°	238.074°	12/12	NRM*	48.1°	5.4°	2.4°	336	11.96724	74.1°	40.7°
	LsLO Site 2+3	RC02-24	44.435°	238.063°	12/12	NRM*	50.3°	3.0°	1.6°	697	11.98423	76.4°	47.0°
			44.434°	238.069°	2/2		49.2°	4.2°	5.9°	1799	1.99944	75.3°	43.5°
Old Wagon Road													
	137B2	RC02-25	44.413°	238.073°	9/9	20	47.3°	1.6°	3.1°	284	8.97187	74.0°	52.9°
Fish Lake													
	HkmO	RC95-01	44.400°	237.996°	12/12	NRM*	50.3°	2.6°	2.6°	1323	11.99168	76.5°	48.6°
	229B2	RC00-56	44.441°	238.007°	7/8	20	50.0°	5.4°	5.5°	120	6.94985	75.7°	38.9°
	LvLO	RC02-21	44.428°	238.017°	12/12	NRM*	49.7°	2.7°	1.4°	1000	11.98899	75.9°	48.4°
	FsLO 1+2	RC02-42	44.402°	237.998°	12/12	NRM*	52.7°	356.6°	2.4°	327	11.96641	78.6°	72.4°
			44.42°	238.00°	4/4		50.7°	1.9°	3.1°	901	3.99667	76.9°	50.8°
Cold Water Cove													
	4291B	NID11-05MK	44.362°	238.013°	7/8	Li†	51.9°	359.0°	1.6°	1386	6.9957	78.1°	62.1°

OTHER													
Tamolitch													
	4211B	NID11-04MK	44.303°	237.969°	7/8	Li†	55.2°	346.9°	2.8°	474	6.9874	76.8°	111.8°

Note: We use the following abbreviations: 'N/No' is the number of cores used compared to the number of original cores collected at the site, 'Exp.' is the strength of the peak alternating-field used in demagnetization in milliTeslas, 'I' and 'D' are the remanent inclination and declination of the site mean direction, 'α95' is the 95% confidence limit for the mean direction, 'k' is the estimate of the Fisher precision parameter, 'R' is the length of the resulting vector, and 'Plat.' and 'Plong.' are the location in degrees north and east of the virtual geomagnetic pole calculated from the mean direction of the site.

*NRM = no required demagnetization

†Li = a vector component lines analysis was used

§Site data not used to calculate Sand Mountain group mean direction

XRF sample taken within 100 m of paleomagnetic cores

TABLE 6. ^{3}He COSMOGENIC DATA FOR THE SAND GROUP AND THE COLD WATER COVE LAVA FLOW

Sample	Latitude (°N)	Longitude (°E)	Altitude* (km)	Scaling factor†	Sample mass (g)	^{3}He (cps)	^{4}He (mV)	^{3}He corr (cps)	^{4}He corr (mV)	^{3}He (Mat/g)	^{4}He (Ta/g)	^{3}He/^{3}He (Ra§)	Age (ka)
Clear Lake East													
NID09-24	44.369°	238.012°	0.963	2.17	0.4189	2.6 ± 0.10	2.2 ± 0.02	2.5 ± 0.10	1.7 ± 0.16	0.66 ± 0.03	0.021 ± 0.002	136.0	2.7 ± 0.3
Ice Cap													
NID09-31	44.349°	238.007°	0.907	2.07	0.6610	4.0 ± 0.11	2.6 ± 0.02	3.9 ± 0.11	2.0 ± 0.17	0.64 ± 0.02	0.015 ± 0.001	31.1	2.7 ± 0.2
Clear Lake South													
RC09-44	44.347°	238.004°	0.860	1.99	0.4620	2.9 ± 0.09	2.8 ± 0.02	2.8 ± 0.10	2.3 ± 0.16	0.65 ± 0.02	0.025 ± 0.002	19.0	2.9 ± 0.2
NID09-19	44.355°	238.007°	0.917	2.09	0.3088	5.1 ± 0.06	3.4 ± 0.01	5.0 ± 0.06	2.9 ± 0.14	1.76 ± 0.03	0.047 ± 0.003	67.8	7.4 ± 0.5
NID09-29	44.360°	238.009°	0.932	2.11	0.7345	5.1 ± 0.13	3.2 ± 0.02	5.0 ± 0.13	2.4 ± 0.18	0.74 ± 0.02	0.017 ± 0.001	32.1	3.1 ± 0.2
NID09-30	44.359°	238.010°	0.938	2.13	0.8050	5.2 ± 0.06	4.3 ± 0.02	5.1 ± 0.06	2.8 ± 0.14	0.69 ± 0.01	0.017 ± 0.001	28.5	2.8 ± 0.2
Cold Water Cove													
NID09-26	44.359°	238.015°	0.987	2.21	0.5392	3.7 ± 0.05	2.2 ± 0.01	3.6 ± 0.05	1.7 ± 0.14	0.73 ± 0.01	0.016 ± 0.001	33.5	2.9 ± 0.2

Note: Age is determined using Licciardi et al. (1999)'s production rate (114 ± 3 g^{-1} yr^{-1}) calibrated for the Clear Lake East lava flow and a topographic / erosion / shielding factor of 1 (no correction); all errors are 1σ.

*Determined from LiDAR data.

†Determined using Desilets et al. (2006).

§Ratio normalized to blank air sample.

samples lie between 2.7 and 3.1 ka, and the Clear Lake East and Ice Cap lava flow ages are consistently younger than those of the Clear Lake South and Cold Water Cove lava flows. These ages are in agreement with the paleomagnetic data, which show that the lava flows were emplaced over a short period of time. The seventh sample, from the Clear Lake South lava flow, has an age of 7.4 ka, which is inconsistent with both stratigraphic relations established at numerous places across the SMVF and with internal Clear Lake South lava flow lobe stratigraphy (i.e., the 7.4 ka flow lobe overlies a c. 3 ka flow lobe). For this reason, we assume that the date is incorrect.

Clear Lake bathymetry

We use 1087 Fishfinder depth measurements (Table A3) to construct a bathymetric model of Clear Lake (Fig. 10). Our model is generally consistent with Johnson et al. (1985). We find that the lake is divided into three zones: a northern zone (maximum depth: 18 m), a southern zone (majority of the lake; maximum depth: 54 m), and a "pinched" zone separating the northern and southern zones (maximum depth: 7 m). The southern zone is characterized by a deep flat bottom with a shallow platform at the southernmost part of the lake south of the Cold Water Cove campground boat ramp. The Clear Lake Resort boat dock is situated on the western margin of the pinched zone.

Submerged trees

We located 57 submerged trees in Clear Lake, 14 in the northern zone, 11 in the pinched zone, and 32 in the southern region (Fig. 11). In the northern and pinched zones, all the trees were visible from the surface and most tree tops were either at or within 1 – 2

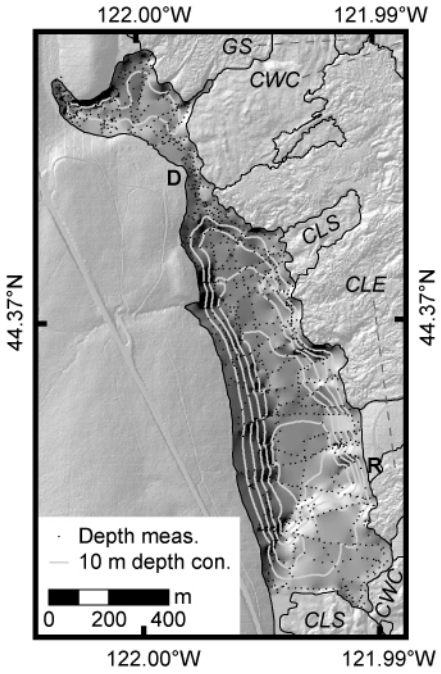

Figure 10. Bathymetric map of Clear Lake, with Fishfinder depth measurements shown (black dots). 10 m bathymetric depth contours are shown in white, and the lake bottom shaded relief map is generated from a 5 m natural neighbor interpolated grid (see text). The land shaded relief map is derived from LiDAR data. Lava flow abbreviations as for Fig. 8, and 'D' is the Clear Lake Resort boat dock (D) and 'R' is the Cold Water Cove campground boat ramp.

m of the water surface. In contrast, most trees in the southern region are not visible at the surface and tree top depths are located at depths up to 27 m below the lake surface. Additionally, divers from the Eugene Dive Club have observed *many* more submerged trees in the deepest part of the lake than we have detected either visually or with the Fishfinder; they have also noted that the tops of many of these trees are at considerable depth (> 20 m).

Lava flow extent into Clear Lake

The Great Spring and Cold Water Cove lava flows are visible on the lake bottom near the lake's northeastern shore. We detected and mapped these lava flows beneath the

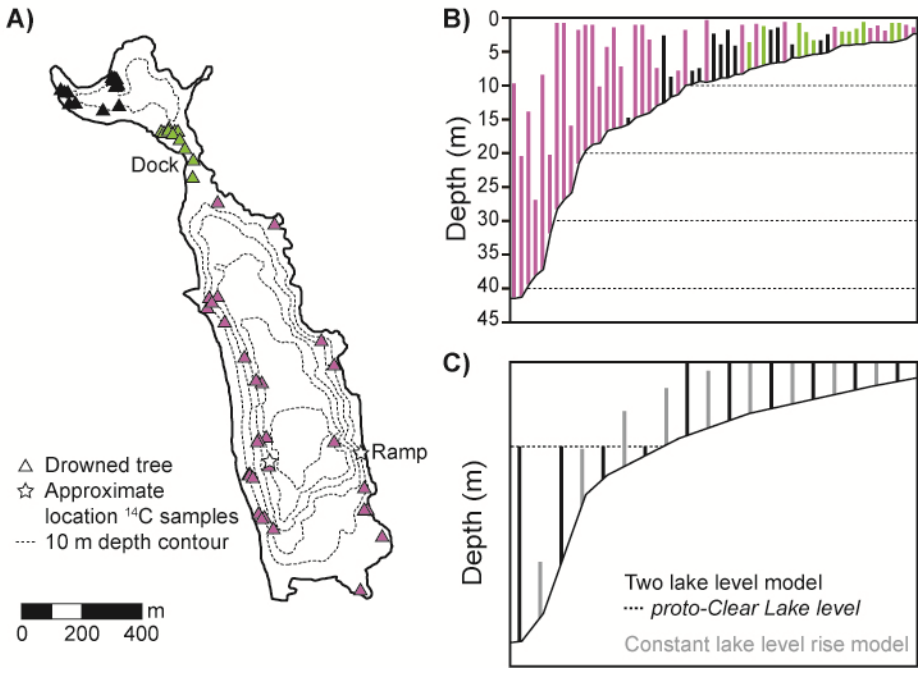

Figure 11. (A) Map of drowned trees (triangles) in Clear Lake located with the Fishfinder (see Fig. 3b). Symbol color indicates whether the tree is in the northern (black), "pinch" (green), or southern (purple) region of the lake. Also shown are 10 m bathymetric contours (dashed lines), the approximate location of this study's and Liccardi et al.'s (1999) ^{14}C samples (stars), the Clear Lake Resort boat dock, and Cold Water Cove campground boat ramp. (B) Tree rooting and top depth of located trees, ordered from deepest to shallowest rooting depth. Colors correspond to lake region following (A). (C) Schematic models of predicted tree rooting and top depth if the lake filled in two stages (black) or with a constant water depth increase rate (grey).

lake using the Fishfinder whiteline (Fig. 3c), which can be used to distinguish a hard from soft lake bottom (Fig. 12). These data show that the southeastern shore of the lake is bordered by Clear Lake East lava flows. Here the boundary between hard and soft lake bottom lies at a maximum depth of 30 m, and is typically found at ~20 m depth. Divers from the Eugene Dive Club confirmed a hard to soft bottom transition at a depth of 24 m (80 ft) in this area.

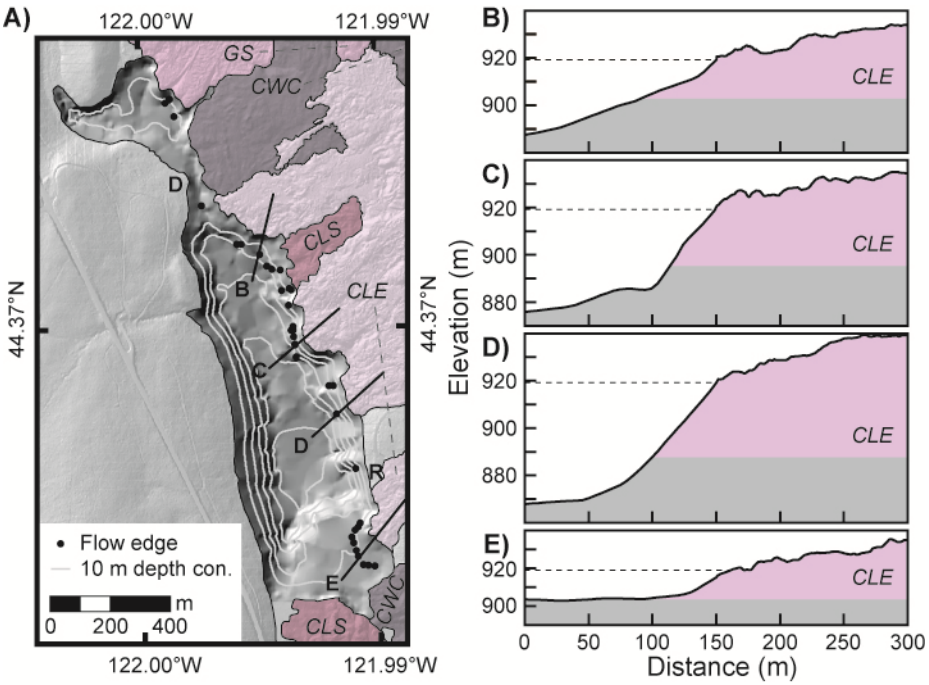

Figure 12. Profiles of Clear Lake East (CLE) lava flow extent into Clear Lake. (A) Hard/soft bottom contact detected with Fishfinder (black circles; see Fig. 3c) and location of profiles (B) – (E) on the bathymetric and geologic maps presented in Figs. 8 and 9. 10 m bathymetric depth contours are shown in grey. (B) – (E) Profiles from the interior of Clear Lake to the Clear Lake East lava flow. The lava flow is light purple, and the underlying (presumably Pleistocene-aged) rock is grey. The modern lake surface (919 m) is indicated with a black dashed line.

Upper McKenzie River observations

To link the history of the SMVF lava flows to the evolution of the McKenzie River, we examined the relationship between the modern river channel and the mapped SMVF units. The McKenzie River flows south from Clear Lake; the outlet itself is relatively shallow (< 5 m). Initially its channel lies between the Clear Lake South lava to the east and Pleistocene-age units to the west (Figs. 2 and 4). The channel jumps onto the Clear Lake South lava flow 1 km downstream of the outlet and follows what appears to be a lava channel, as lava flow levees are observed on both sides of the river. At Sahalie Falls, the river plunges 23 m over a lobe of the Clear Lake South lava flow. Many springs

also emerge from the lava flow where it is exposed at the base of Sahalie Falls. Interestingly, the base of Sahalie Falls is at the same elevation as the bottom of Clear Lake, suggesting a flat valley profile prior to the emplacement of the Clear Lake South lava flow. South of Sahalie Falls, the McKenzie River channel traverses another lobe of the Clear Lake South lava flow, and then plunges 24 m off the flow at Koosah Falls. There are also a number of springs visible at the base of Koosah Falls. South of Koosah Falls, the McKenzie River flows between the Clear Lake South lava flow and a Pleistocene-aged unit to the east until it reaches Carmen Reservoir (Figs. 2 and 4). Between the Clear Lake outlet and Carmen Reservoir, the McKenzie River almost doubles its average discharge going from 8.5 to 14.5 m^3/s (Cashman et al., 2009).

At Carmen Reservoir, the McKenzie River is diverted to Smith Reservoir (Fig. 2). Despite the diversion, ~4 km south of Carmen Reservoir within the upper McKenzie River valley approximately 4.1 m^3/s of water emerges at Tamolitch Pool (Jefferson et al., 2006), ~ 4 km north of where the diverted water is reintroduced into the McKenzie River. These discharge data illustrate the substantial contributions of groundwater flow into the upper McKenzie River in the area of young lava flows.

Another curious feature of the upper McKenzie River channel is the pronounced amphitheatre-like shapes of Sahalie and Koosah Falls. These shapes suggest headwall erosion, although there is very little sediment transported along this stretch of the McKenzie River, which suggests a limited capacity for erosion. However, there are small shallow potholes on top of Sahalie Falls and imbricated bounders on the Tamolitch flow, both of which suggest that rare high discharge events may transport bedloads with large clasts that are capable of eroding the bed.

DISCUSSION AND CONCLUSIONS

In what follows, we discuss the sequence of eruptive events at the SMVF and examine geochemical trends. We show that despite evidence that the three SMVF groups were emplaced over the course of only a few decades to centuries, at least three different magma sources were tapped. We then provide evidence for vent reoccupation and migration, which are contrary to common assumptions regarding behavior at cinder cone fields.

Next, we discuss the formation of Clear Lake, presenting different possible models of lake evolution. We then provide an overview of the co-evolution of the McKenzie River and the SMVF. We end with an assessment of the hydrologic impact of SMVF volcanism on the downstream end of the McKenzie River, and place this discussion within the context of potential hazards posed by future volcanic activity.

Sequence of eruptive activity

On the basis of stratigraphy and paleomagnetic data, the oldest mapped lava flow is the Tamolitch lava flow south of the SMVF, which entered the McKenzie River valley south of present-day Carmen Reservoir. This lava flow was erroneously mapped by Taylor (1965) and Sherrod et al. (2004) as a "late stage" Belknap flow; instead we find that it underlies the young Belknap flow and is considerably older. Using a record of geomagnetic secular variation for the Holocene of the western United States, (Hagstrum and Champion, 2002), we find that while remanent directions from sites at other western US volcanoes compare adequately to Tamolitch at ~4300, ~7400, and ~10,130 ^{14}C yr BP, the best directional comparison is to sites in flows erupted from the northwest rift zone of

Newberry volcano c. 7 ka (Mckay et al., 2009). We thus attribute an age of c. 7 ka to the Tamolitch lava flow.

On the basis of paleomagnetic data, the Lost Lake, Sand, and Nash groups of the SMVF were emplaced over no more than a few decades; cosmogenic and ^{14}C ages indicate that this occurred at c. 3 ka. Stratigraphically, the Lost Lake group (Cold Water Cove, Fish Lake, Old Wagon Road, and Lost Lake units) appear to be the oldest of the SMVF (Fig. 8); this group extends from at least Cold Water Cove to Lost Lake. While we can definitively state that the Fish Lake unit preceded the Lost Lake unit, we are unable to establish other inter-group stratigraphic relationships (Fig. 8). We note however that the Cold Water Cove unit is an "orphan" lava flow, indicating that its source has either been buried or reoccupied. As such we hypothesize that the Cold Water Cove lava flow is the oldest SMVF eruptive unit, followed by the rest of the group.

The SnoPark lava flow has no associated vent but underlies the Nash group. Given its overall similarity to the SMVF lava flows, we hypothesize that it was emplaced during the SMVF episode but prior to the Nash group (perhaps concurrent with the Lost Lake group).

With the possible exception of the proto-Clear Lake South vents, all available evidence suggests that the entire Sand group and the Cold Water Cove lava flow (Lost Lake group) erupted within a few decades to centuries. Cosmogenic dates for the oldest and youngest lava flows (Cold Water Cove and Clear Lake East lava flows, respectively) yield ages of c. 2.9 ka. A short eruptive time scale is confirmed by examination of intermediate units, which have similar cosmogenic dates. We do not consider the

anomalous 7.4 ka Clear Lake South lava flow sample age, as it is geologically implausible.

While both the Nash and Sand groups overlie the Lost Lake eruptive units, there is poor stratigraphic control between the two. To try to improve our stratigraphic constraints we use the observations presented in Chapter IV that mature forests exist on SMVF lava flows covered with tephra from an explosive phase of the Sand Mountain eruption, while flows without tephra are relatively barren. Using these observations, we infer that all currently barren lava flows postdate SMVF explosive activity. As both the Nash and Sand groups have barren (Nash, Little Nash, and Clear Lake East) and vegetated (Early Nash I and II, Clear Lake South, Ice Cap, and Great Spring) lava flows, it appears these two groups were active concurrently. Conversely, these observations constrain the timing of the explosive phase of eruptive activity.

We use observed vent alignments and vegetation cover to infer the chronology of the Sand and Nash eruptive units. Vents associated with Nash and Sand groups are aligned along three different trends (Nash alignment, Sand alignment, and proto-Clear Lake South alignment). The proto-Clear Lake South alignment (N11°W) is closer to the Nash alignment (N18°W) than the Sand alignment (N5°E; Fig. 13). The proto-Clear Lake South vents are surrounded by Great Spring lava and are compositionally similar to the Clear Lake South eruptive unit. We propose that Early Nash I and II erupted from vents (now buried or subsequently reoccupied) along the Nash alignment. The proto-Clear Lake South vents opened up to the south along a similar alignment but tapped a slightly different magma source. These eruptions were followed by the emplacement of the Clear Lake South, Great Spring, and Ice cap units (Sand group). Explosive activity from Sand

Mountain proper then deposited tephra on the existing lava flows before erupting the Clear Lake East lava flows. At about the same time, the Nash group reactivated, emplacing Nash and Little Nash. Charcoal underneath tephra attributed to Nash and Little Nash was dated to 2687 ± 353 cal yr. BP (Table 1; Sherrod et al., 2004), although this is younger than the paleomagnetic age range constraints presented in this study permit.

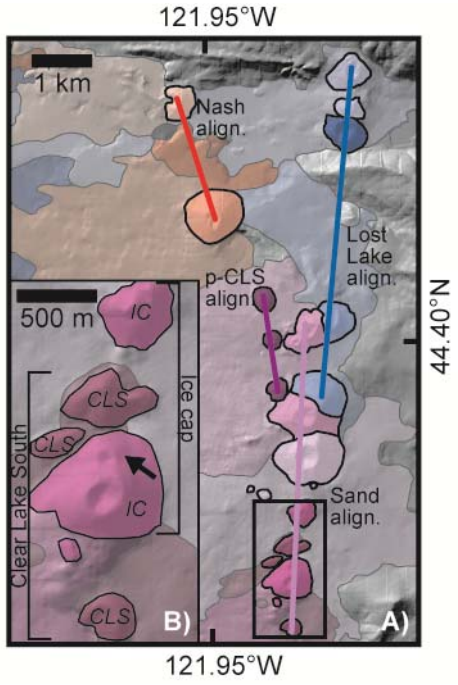

Figure 13. SMVF vents; unit colors are the same as in Fig. 4. (A) Vent area for the entire SMVF, showing the vents and alignment of the Lost Lake group (solid), proto-Clear Lake South vents (dotted), rest of Sand group (big dashes), and Nash group (small dashes). The extent of (B) shown by a black rectangle. (B) Vents of the southern Sand group (Clear Lake South and Ice Cap). The arrow points out a small Ice Cap cone partially buried by the main Ice Cap cone.

The last lava flow to erupt in the McKenzie River headwater region is the Belknap lava flow, which according to ^{14}C dating was emplaced c. 1.5 ka (Table 1). The Belknap lava flow entered the McKenzie River valley but did not reach the river.

We note that results presented in this study along with recent tephrachronology (Mckay, 2012) are inconsistent with many ^{14}C dates collected 30 – 50 years ago (e.g., Chatters, 1968). These dates are often from charcoal mixed in soil collected at the base of a lava flow or tephra layer. In light of the age contradictions, we are skeptical that dates acquired decades ago are valid and/or date what they are thought to date. For example, the Jack Pine vent had been assigned a ^{14}C date of 2,265 ± 79 cal yr BP (Chatters, 1968; see Table 1) based on charcoal found beneath Jack Pine cinders; this would imply that the Jack Pine vent is one of the youngest units in the region. However, our observations and mapping shows that it is post-glacial (i.e., Holocene) and is surrounded by Old Wagon Road lava flows (Lost Lake group). It is also chemically distinct from the SMVF lava flows. We thus suggest that contrary to Chatter's (1968) ^{14}C date, the Jack Pine vent pre-dates the Lost Lake group and consequently the rest of the SMVF. Similar ^{14}C age contradictions exist for the Fish Lake lava flow.

Geochemical trends

Here we use geochemical data primarily as a mapping aid; for this reason, we do not provide a detailed analysis of the geochemical data of the SMVF. We do note, however, that the geochemistry provides interesting insights on the magma bodies tapped to form the SMVF, and has important implications for future episodes of mafic volcanism in the central Oregon Cascades. Most important is the observation that despite the short eruptive time frame established above, there are notable compositional differences between different eruptive groups, which in some cases require different magma sources.

Not surprisingly, the Tamolitch and Belknap lava flows and Inaccessible Cones appear to have a magma source that is distinct from that supplying SMVF. These units have considerably lower Sr concentrations than SMVF lavas (Fig. 7), and have remarkably different lava flow morphologies – the Tamolitch lava flow in particular has beautiful pahoehoe features, whereas the SMVF generally consists of blocky lava.

Within the SMVF, the Nash group is the most distinctive. At 52.5 – 54% SiO_2, the Nash group has, overall, the most silicic compositions in the SMVF. The flows are anomalous in having low CaO and low TiO_2, as well as showing an inverse relationship between TiO_2 and Sr (and also Ba and Sr; Fig. 7). More curious are the Cr and Ni vs. MgO trends, which appear to reflect Ni enrichment relative to Cr. While we have no satisfactory explanation for these trends, we infer that the Nash group must come from a different source than the rest of the SMVF. The Nash group also appears to have a different vent alignment than the rest of the field (Fig. 13).

The Lost Lake and Sand groups appear closely related. That the Lost Lake group, which erupted first, is more primitive than the Sand group suggests a trend of magma evolution with time. Within the Sand group, the Clear Lake South eruptive unit has unusually high TiO_2 and is one of the most heterogeneous flows in the field, which may reflect a more complicated mixing and/or assimilation history than seen in the rest of the group. The two units sandwiched between the Clear Lake South and East eruptive units, Ice Cap and Great Spring, are very similar, with the Great Spring transitional between the Ice Cap and Clear Lake East eruptive units in both TiO_2 and CaO concentration. On this basis, we suggest that the Ice Cap unit erupted before the Great Spring unit. Finally, the presence of plagioclase microphenocrysts in the Clear Lake East lava flow suggests that

the magma stalled at shallow depths prior to erupting. It thus appears the Sand group erupted from a single magma body that evolved over the course of the Sand eruptive episode, and may be related to magma of the Lost Lake group.

The Jack Pine vent in the northern SMVF has a very distinctive geochemical signature in that it is more alkali than any of the other flow units and is an absarokite (rare in the Cascades). Although Taylor (1965) and Sherrod et al. (2004) mapped it as a SMVF vent, its chemistry suggests that it has a very different magma source. Perhaps most unusual are the elevated Sr and Ba concentrations. Additionally, whereas the rest of the field has a Ba/Nb ratio < 21, it is ~137 for the Jack Pine vent, suggesting an arc-like signature (Pearce and Parkinson, 1993). From this we conclude that although the Jack Pine vent is geomorphologically post-glacial, it tapped a very different magma body from the rest of the SMVF.

Vent alignment, migration, and reoccupation

Each of the three SMVF groups erupted along roughly N-S alignments, although each trends in a slightly different direction (Fig. 13): the Lost Lake group vents align N7°E, the Nash vents align N18°W, and the Sand vents align N5°E. The proto – Clear Lake South vents (N11°W) are not aligned with the Sand group but are rather both located and aligned between the Nash and Lost Lake groups. These differences in vent alignment suggest that each group responded to different stress fields. Indeed, it seems likely that earlier eruptive episodes altered stress fields for subsequent episodes.

There is also evidence that one or more vents could have been active at the same time during an eruptive episode, as well as evidence of vent migration through time. For

example, the main cone of the Ice Cap eruptive unit buries a small cone from the same eruption, suggesting that the center of explosive activity shifted over the course of the eruption (Fig. 13b). Finally, in what would traditionally be considered a monogenetic cinder cone field, there is evidence of vent reoccupation. Three vent alignment trends intersect near Sand Mountain, and in close proximity are vents of the Old Wagon Road, proto – Clear Lake South, and Great Spring eruptive units; moreover, the Great Spring vent partially buries the Old Wagon Road vent (Fig. 13a). This suggests that this site was a preferred locale for magma ascent over several decades. Additionally, the presence of numerous orphan flows can be explained if vents were either buried or reoccupied; in the case of the latter the vent would now be covered with cone material from younger eruptive units. The concept of vent reoccupation is contrary to the notion of a cinder cone as both monogenetic and of short duration, and instead suggest that cinder cone fields may also be regions of prolonged magma supply and eruption. Overall, it appears that the field was very active for short amount of time, with multiple eruptive units emplaced over several decades.

Lava flows and the McKenzie River – the formation of Clear Lake

SMVF lava flows greatly impacted the hydrology and geomorphology of the upper McKenzie River watershed. The source of the McKenzie River, Clear Lake, exists only because the upper McKenzie River valley has been inundated with sequential lava flows. The lake has two main sections, a northern shallow zone (maximum depth 18 m), bordered to the east by the Great Spring and Cold Water Cove lava flows, and a southern deep zone (maximum depth 54 m), primarily bordered by Clear Lake East lava flows to

the east and Clear Lake South lava flows to the south (Fig. 10). The McKenzie River outlet is situated at the southwest tip of the lake at the contact between Clear Lake South lava flows and older Pleistocene units, and is relatively shallow (< 5 m deep). The configuration of the lake suggests that it is dammed by Clear Lake South lava flows, which probably blocked the ancestral McKenzie River. Consequently, the age of the Clear Lake South lava flow is the age of the lake.

The Douglas-fir forest preserved in Clear Lake's cold waters must have drowned when the lake formed. Thus, the death date of the trees should correspond to lake formation and the emplacement of the Clear Lake South lava flow. Four submerged drowned tree dates exist (Table 1): Benson's (1965) dates of the outer and inner part of a tree rooted at 4 m depth, likely near Cold Water Cove campground, Licciardi et al.'s (1999) date of the outer part of a tree rooted at a shallow depth near the Cold Water Cove campground, and our date of the outer part of a tree rooted at 40 m depth. Ages for the outer part of a tree are assumed to yield death dates, while Benson's (1965) inner wood approximates the establishment age of the tree. As errors associated with Benson's (1965) ages are large (± 200 yrs) while the dates consistent with Licciardi et al.'s (1999) age, we will use the latter as representative of shallow trees in the southern part of the lake.

Roughly 140 years separate the death date of a tree rooted at 40 m depth (3,000 ± 73 cal yr BP) and a tree rooted at a shallow depth (2,856 ± 92 cal yr BP; Licciardi et al., 1999); these two dates are statistically different at the 95% level (t-test 5.28144 with χ^2 of 3.84, determined with Calib Rev 6.1.0). The 40 m tree most likely died by drowning shortly after the emplacement of the Clear Lake South lava flow. As this tree is rooted 14

m above the maximum depth of the lake, water depth behind the lava dam had to exceed 14 m for the tree to drown; it is possible that this did not occur until a few months to years after dam emplacement. The 4 m tree most likely drowned after the emplacement of the Clear Lake East lava flow, as it appears this lava flow flowed into a proto-Clear Lake that was 10 – 20 m shallower than modern lake levels (discussed later in this section). Given that the water depth at the Clear Lake outlet is < 5 m, the death date of the 4 m tree likely coincided with the establishment of the modern McKenzie River. Overall, the statistically different death dates of the 40 and 4 m deep trees suggest either that lake levels progressively rose over ~140 years or that the lake formed in two or more stages.

Most trees growing on nearby Pleistocene units are > 30 m tall, with a few trees > 50 m (see Chapter IV). Within shallower parts of Clear Lake today, the tops of submerged trees are close to modern lake levels: the part of the tree that was exposed to air has rotted away. Although few, if any, studies have been done on the decay rate of preserved drowned trees exposed to air, in general Douglas-fir trees decay relatively quickly (Harmon et al., 1986); this rate inversely depends on the size of the tree along with whether bark remains on the tree, protecting it. We will now discuss different scenarios for how Clear Lake filled.

The modern volume of the lake is ~1.27 x 10^7 m^3. If fill rates equaled the discharge at the Clear Lake outlet, the lake would fill in 17 days; fill rates equal to the discharge into Carmen Reservoir (that is, the combined water flow out of the lake and through the lava dam) would fill the lake in 10 days. These estimates are orders of

magnitude faster than the ~140 years it apparently took (based on the tree ages) for the lake to fill.

If lake levels rose rapidly to modern levels when the Clear Lake South lava flow was emplaced, we would expect to see preserved trees > 30 m tall with tops rotted off where the tree intersects modern lake levels. If lake levels rose at a constant rate over 140 years (~40 cm/year), we would expect that the preserved portion of the trees would be the same height (relative to the root depth) everywhere for trees of similar decay characteristics (i.e., presence/absence of bark and tree diameter). Conversely, if the volume of the lake increased at a constant rate, we would expect an initial rapid increase in lake levels followed by a decrease in rise rate as the lake surface area increased. Unknown is the permeability evolution of the lava dam, which would also influence the evolution of the fill rate.

We observe that trees of different rooting depths have top depths at modern lake levels, suggesting relatively rapid drowning. However, there are several deeply rooted trees whose rooted tops are also quite deep. Most of these (located) trees lie along the steep western slope of the lake (Fig. 11). Observations by divers indicate that there are many more deeply rooted and topped trees on the deep flat bottom of the lake than detected in our bathymetric study. It is quite possible that these trees are close to their original height – the bottom of the lake is ~50 m, so 30 m trees would have a top at 20 m depth. However, the presence of deeply rooted trees with tops at 10 – 20 m depth contradicts predictions of the steadily filling lake model.

An additional clue to Clear Lake's filling history are the alternating bands of oxidized and fresh lava that are found along the margin of the Clear Lake East lava flow

(youngest Sand group unit) north of the Cold Water Cove campground boat dock (Fig. 6). In thin section, these parts of the flow are quite glassy, which suggest that the flows encountered (and were quenched by) water. Interestingly, quench features are not found south of the Cold Water Cove campground boat ramp where the Clear Lake East lava flows onto a shallow (< 10 m deep) platform. From this we infer that at the time of the Clear Lake East lava flow, the lake level was more than 10 m lower than its current level (below the rooting depth of the shallow dated tree). An alternate explanation would be that this banded feature only occurs when the lava flows into water > 10 m deep. A water level 10 – 20 m lower than the modern level is also consistent with the abundance of tree tops at this level below the lake surface. As lava flows entered the lake, lake levels might have risen due to water displacement.

Another intriguing observation is the oversteepened flow front of the Clear Lake East lava flow where it encounters the lake. If we use the hard/soft bottom contact detected with the Fishfinder (and confirmed by divers) to map the Clear Lake East lava flow margin, we see a pronounced difference in flow front thickness on either side of the Cold Water Cove campground boat ramp (Fig. 12). North of the boat ramp, flow front thickness ranges up to 25 m, while south of the boat dock flow front thicknesses are ~ 10 m, which, while high, are more typical values for this lava flow. Again we suggest that this difference in reflects the presence (north) and absence (south) of ponded water at the time of the Clear Lake East lava flow. Although we do not see classic water interaction features such as pillow basalt or hyloclastite, we suggest that quenching of the flow front at the former lake boundary could have oversteepened the flow front. Another indication that the Clear Lake East lava flow entered an existing lake is the observation that the flow

extends into the current lake only to a depth of 20 – 30 m before stopping abruptly on a very steep slope (~ 20° – 30°) rather than flowing ~60 m farther west to the flat plain at the bottom of the lake (Fig. 12).

Based on these observations, we propose to following sequence of events for the formation of Clear Lake:

before 3,000 ± 72 cal yr BP: The Clear Lake South lava flow dammed the ancestral McKenzie River, forming proto-Clear Lake, which is ~20 meters shallower than modern levels. Water filled only part of southern portion of the lake – the northern portion remained forested.

before 2,856 ± 92 cal yr BP: The Clear Lake East lava flow entered proto-Clear Lake. The flows displaced water, which may have caused lake levels to rise. The lake quenched the Clear Lake East flow front, causing it to oversteepen and the flow to stop on a steep slope. The Clear Lake South lava dam is overtopped c. 2.8 ka.

To test this model, further dating of drowned trees (preferably in both the northern and southern parts of the lake) and a more systematic survey of tree height will be required.

Finally, we address the origin of the Great Spring, which contributes ~10% of Clear Lake's water flowing out of the outlet (Stearns, 1929). The Great Spring emerges from the Great Spring lava flow within a few meters of its contact with the Cold Water Cove lava flow. Stearns (1929) suggested that the Great Spring lava flow buried a pre-existing creek, leading to the formation of the spring. We view this as a plausible explanation; if correct this would suggest that springs are the endpoints of buried surface water pathways.

Evolution of the McKenzie River

The McKenzie River has adapted to the emplacement of lava flows between Clear Lake and Tamolitch Pool in several different ways. As discussed above, it is dammed by the Clear Lake South lava flow. However, as evidenced by the springs at the base of Sahalie and Koosah Falls and the ~75% increase in discharge between Clear Lake and Carmen Reservoir, the Clear Lake South lava flow forms an exceedingly leaky lava dam. If our model for the formation of Clear Lake is correct, then the McKenzie River flowed only through (and not over) its dam for 150 years. We hypothesize that there many have been a decrease in dam permeability with time. In particularly, the extensive tephra sheet that blanketed the older flows of the Sand group would have been deposited within the lake. An influx of fine-grained tephra might be expected to fill permeable pathways. As the base of Sahalie Falls is at the same elevation as the bottom of Clear Lake, perhaps the springs at Sahalie Falls record the river's trajectory at a time when Clear Lake was shallower than it is today.

Another manifestation of lava-river interactions along the McKenzie River can be found south of Clear Lake. Whereas the c. 3 ka Clear Lake South lava flow dammed the McKenzie River, the c. 7 ka Tamolitch lava flow buried it. Apart from periods of high snowmelt, no surface water flows over the Tamolitch lava flow. While it is tempting to attribute the current lack of surface water to the Carmen-Smith diversion project, which removes water from the McKenzie River, the McKenzie River channel was dry in September 1926 when Stearns (1929) made his survey of the area. That the diversion project is affecting some water flow is evident from a comparison of Stearns' estimate of

the discharge at Tamolitch Pool, 9.9 m^3/s, which is more than twice that measured in 2004 (4.1 m^3/s; Jefferson et al., 2006). Interestingly, there is evidence also for a shallow lake formed by water impoundment behind the Tamolitch flow. Beaver Marsh immediately south of Carmen Reservoir borders and in some places covers the Tamolitch flow; this marsh contains accumulated sediment. Given the very small sediment load of the McKenzie, this sediment accumulation reflects the considerable amount of time (7 ka) since the Tamolitch flow was emplaced.

A third type of lava-river interaction can be seen along the stretch of the McKenzie River between Clear Lake and Carmen Reservoir. Where the McKenzie River flows over the Clear Lake South lava flow north of Sahalie Falls, the river has not incised into the lava but has rather adopted a lava channel – a primary lava flow feature – for its own use. Between Sahalie and Koosah Falls it is unclear how the river chose its path over the Clear Lake South lava flow, but we note that this portion has potentially flowed longer – the river segment from Clear Lake to Sahalie was established only once the lava dam was overtopped. Between Koosah Falls and Carmen Reservoir the river reverts back to flowing between the Clear Lake South lava flow and older Pleistocene units.

Finally, it appears that despite a limited sediment supply (and thus available tools), waterfall retreat has been ongoing at both Sahalie and Koosah Falls in late Holocene. Preliminary measurements suggest that the waterfalls have retreated 30 (Sahalie) and 50 m (Koosah). Given a flow age of c. 3 ka, this suggests minimum retreat rates of 1 and 1.6 cm/yr, respectively. If our model for the formation of Clear Lake is correct, Koosah Falls may have existed for ~140 years longer than Sahalie Falls, although

this seems like too short of an age difference to account for the difference in overall retreat.

Co-evolution of the SMVF and the McKenzie River

Based on our findings, we present the following model for the co-evolution of the SMVF and the McKenzie River (Fig. 14):

Early Holocene (Fig. 14a): The ancestral McKenzie River flowed north to south along the High Cascade graben margin.

c. 7 ka – Tamolitch eruptive episode (Fig. 14b): Tamolitch lava flows entered the McKenzie River south of present day Carmen Reservoir and flowed ~4 km down the McKenzie River valley, burying the McKenzie River. After the lava cooled, the McKenzie River flowed as groundwater through the lava flow to emerge at Tamolitch Pool. North of the point of the lava's entrance into the valley a shallow lake formed and accumulated sediment to form Beaver Marsh. South of Tamolitch Pool, the McKenzie River

Figure 14. Model of the co-evolution of the SMVF and the headwaters of the McKenzie River. Unit colors are the same as in Fig. 4, with presumed (i.e., presently buried) lava flow extents indicated with hatched lines. Refer to Fig. 2 for geographic names and Fig. 4 for unit labels. (A) Ancestral McKenzie River in the early Holocene. (B) Configuration of the McKenzie River following emplacement of the Tamolitch lava flow c. 7 ka. Note the lake at present-day Beaver Marsh. (C) Emplacement of the Lost Lake group c. 3 ka, which buries the uppermost McKenzie River. By this time the McKenzie River emerges at Tamolitch Pool. (D) Emplacement of the Clear Lake South lava flow c. 3000 yBP, forming proto-Clear Lake. The McKenzie River flows through the Clear Lake South lava flow and emerges near present day Sahalie Falls. (E) Emplacement of the Ice Cap and Great Spring lava flows. (F) Emplacement of the Clear Lake East lava flow c. 2850 yBP, followed by water levels rising to overtop the Clear Lake South lava dam. Also shown is the later emplacement of the Belknap lava flow c. 1.5 ka, which did not reach the McKenzie River.

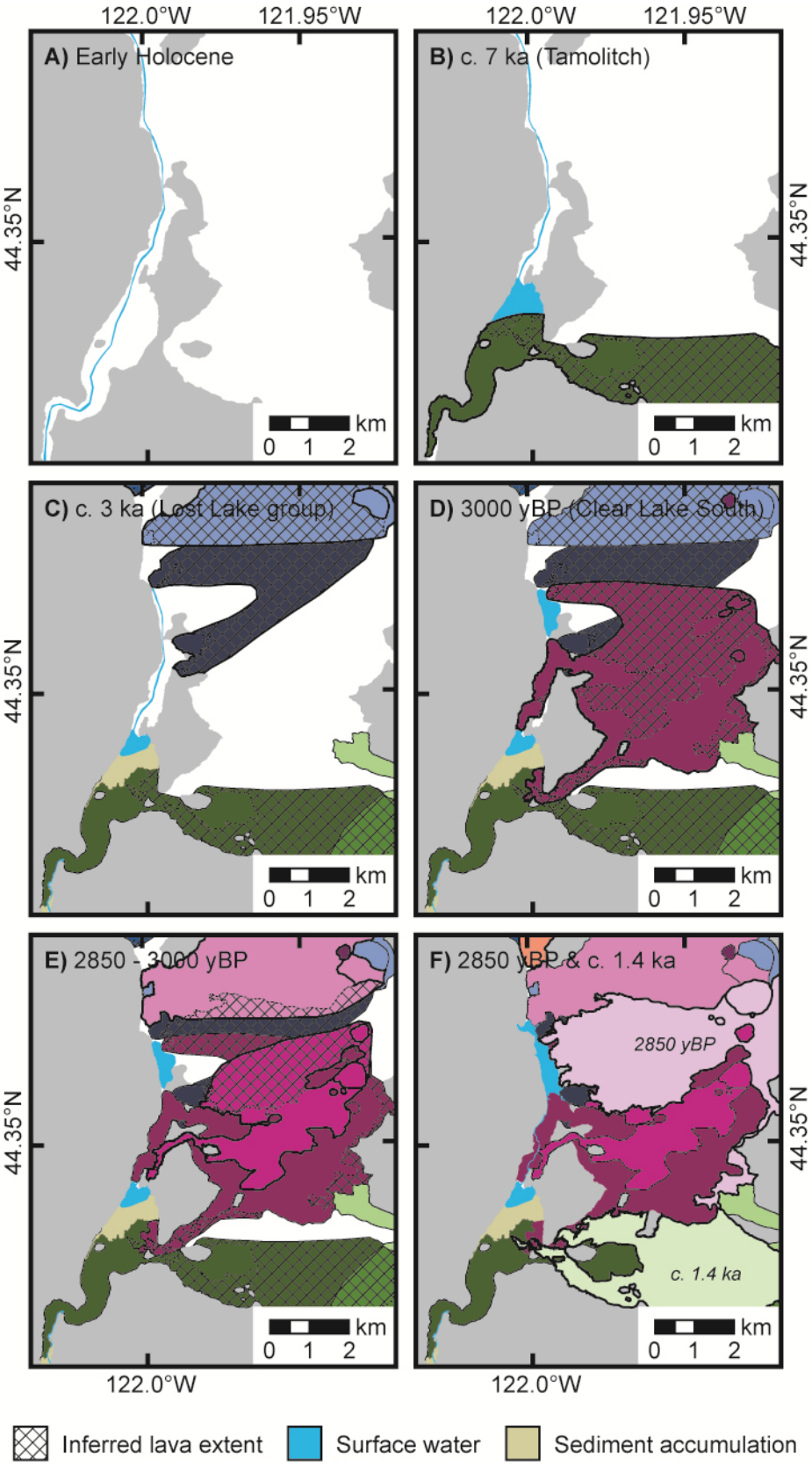
122.0°W
121.95°W
A) Early Holocene
B) c. 7 ka (Tamolitch)
C) c. 3 ka (Lost Lake group)
D) 3000 yBP (Clear Lake South)
E) 2850 - 3000 yBP
F) 2850 yBP & c. 1.4 ka
2850 yBP
c. 1.4 ka
44.35°N
km
0 1 2
Inferred lava extent
Surface water
Sediment accumulation

incised into the Pleistocene bedrock, exposing the margin of the Tamolitch lava flow. Presently, south of Tamolitch Pool the river channel is bound by a cliff of Tamolitch lava flow to the west that can be up to 16 m high.

c. 3 ka – Lost Lake group eruptive episode (Fig. 14c): A system of vents opened up in the northern half of the SMVF; associated lava flows covered the majority of the SMVF. The Fish Lake lava flow dammed Hackleman Creek, a tributary of the McKenzie River, to form Fish Lake, and Crescent Creek, to form Lava Lake. Hackleman Creek re-established itself alongside the Lost Lake group lava flows. Soon after the Lost Lake group eruptive episode, Early Nash I and II (Nash group) and the proto-Clear Lake South vents (Sand group) erupted.

before 3,000 cal yrs BP – Clear Lake South eruptive episode (Fig. 14d): The Clear Lake South lava flows dammed the ancestral McKenzie River, forming proto-Clear Lake, which was ~ 20 m shallower than modern Clear Lake. The lake had no outlet – water seeped through the lava flow and begins to emerge at the base of present-day Sahalie Falls. South of present-day Sahalie Falls, the river flowed over the Clear Lake South lava flow and finally went over a Clear Lake South flow front, forming Koosah Falls. The river was fully established by Beaver Marsh. After Beaver Marsh the river disappeared into Tamolitch lava flow.

Ice Cap and Great Spring eruptive episodes (Fig. 14e): The Great Spring and Ice Cap eruptive episodes occurred; no stratigraphic relation exists between these two. The Ice Cap episode included several vents that may have been

active at the same time, with southern vent migration occurring at the main vent. The Great Spring lava flow may have buried a creek where water now emerges at the Great Spring on the eastern side of Clear Lake.

before 2,856 cal yrs BP – Clear Lake East eruptive episode (Fig. 14f): The Clear Lake East eruptive episode produced several vents, including vents without associated cinder cones. Lava flows entered proto-Clear Lake, which was 10 – 20 m shallower than modern levels. Lake levels may have risen as a consequence of flow emplacement. The lake causes flow front oversteepening, and cooled the flow front sufficiently to cause the flow to stop. Nash and Little Nash (Nash group) were also emplaced close to this time.

2,856 cal yrs BP – McKenzie River established its modern flowpath (Fig. 14f): The McKenzie River overtopped the Clear Lake South lava dam by flowing between the lava flow and an older Pleistocene unit, and then adopting a pre-existing lava channel within the Clear Lake South lava flow. A second waterfall formed at Sahalie Falls, where the river plunges over a flow lobe. Today, the lava dam remains leaky. Waterfall retreat occurs at both Sahalie and Koosah, albeit slowly because of the absence of sediment.

c. 1.5 ka – Belknap eruptive episode (Fig. 14f): The Belknap lava flow entered the McKenzie River Valley between present-day Carmen Reservoir and Tamolitch Pool, but did not reach the river; the McKenzie River was unaffected.

Hazard implications

Although it is unlikely that the Sand Mountain volcanic field will reactivate in the next several thousand years, this study illustrates possible ramifications of future mafic activity within the McKenzie River drainage, which is very likely given its considerable overlap with the High Cascades graben. In particular, we suggest that far-field hazards would likely be the most devastating. As seen elsewhere, tephra could cause air traffic perturbations and pose problems to cities east of the Cascades crest (Mckay, 2012). However, lava flows could also pose significant problems, including severe water shortages if the flows entered and disrupted the McKenzie River system. Given that the McKenzie River is the sole source of drinking water for the Eugene, Oregon metropolitan area (~200,000 residents), and that in the summer months it provides a sizable fraction of the Willamette River water in Portland, Oregon, 450 river-km downstream, any disruption to water flow could have serious consequences.

To assess risks associated with lava flow activity within the McKenzie River watershed, we will first evaluate what impact a repeat of the SMVF eruptive episode would have on the Eugene metropolitian area. Although it is unlikely that activity will resume at the SMVF, this exercise is useful for estimating the magnitude of future mafic volcanism far-field impacts.

Were the SMVF to reactivate, from the perspective of water supply, the time of year of the eruption is an important consideration. Presently, water is diverted by EWEB for treatment at Hayden Bridge 24 km downstream of the McKenzie's confluence with the McKenzie River (Fig. 1). In the late summer, the McKenzie River discharge is ~14 m^3/s at Carmen Reservoir and ~70 m^3/s at Hayden Bridge. Thus, if lava flows temporally

dammed the McKenzie River near Carmen Reservoir during the summer, the water available for the Eugene metropolitan area would drop by at least 20%. If the eruption happened during the winter monsoon, when the McKenzie River discharge is ~20 m^3/s at Carmen Reservoir and ~280 m^3/s at Hayden Bridge, the decrease in flow would be < 10%.

As most of the McKenzie River water comes from High Cascades springs and groundwater seepage, we must also consider the potential impact of an eruption on groundwater flow. Currently, the McKenzie River watershed includes 1609 km^2 in the High Cascades (Fig. 1; Tague and Grant, 2004). The SMVF covers 75 km^2 with an additional ~125 km^2 located between the SMVF and the Cascade crest (presumably the boundary of the McKenzie watershed). Severe perturbation of groundwater flow over ~200 km^2 of the ~1600 km^2 groundwater source area could cause a reduction in summer flow of the McKenzie River of up to 12.5%. This is less than the 20% reduction in flow predicted based on damming of surface water but could last longer than lava dam disruption. If this were to happen, excess groundwater might be diverted to the east side of the Cascade crest or it might "pond" during the course of the eruptive episode, resulting in a slight temporary increase in groundwater flow at the end of the eruptive episode.

Regardless of the season, hydroelectric power generated from the McKenzie River would be reduced. In particular, the Carmen-Smith hydroelectric dam, which is the largest EWEB-owned power source, would likely temporarily cease producing power; presently this hydroelectric dam generates up to 115 MW of power. Lava flows could also cover HWY 126 and HWY 20, which connect the Willamette Valley to central

Oregon (including goods and services). Moreover, the disruption as a whole would likely impact logging and recreation activities in the surrounding Willamette National Forest.

Returning to a broader view of the impact of the mafic volcanism in the McKenzie River watershed, we infer that while the near-field hazards of future activity would likely be minor, eruptive activity could cause economic damage to the Eugene metropolitan area and the greater Willamette Valley, as well as water shortages if an eruption were to occur in the late summer. Additionally, our work suggests that future mafic eruptive activity is likely to include more than one eruption episode, so that the scenario could repeat itself several times over a few decades. Given Tague and Grant's (2004) finding that the summer discharge of streams in the McKenzie River watershed is directly linked to the proportion of the drainage in the High Cascades, *any* future mafic activity in this area will impact water supply for the Eugene metropolitan area; the magnitude of the impact will be related to the area affected.

BRIDGE

In Chapter II, I reconstructed the Holocene history of the Sand Mountain volcanic field (SMVF) and its co-evolution with the McKenzie River. I showed that lava flows from the SMVF and other Holocene vents have profoundly impacted the current hydrology of the upper McKenzie River, and estimate that SMVF activity caused up to a 20% reduction in McKenzie River discharge at its confluence with the Willamette River. However, I also demonstrated that the McKenzie River is resilient and able to adapt to changing conditions presented by the relatively instantaneous influx of lava into its drainage: the McKenzie River flows through and over its lava barriers.

In Chapter III, I begin my investigation of another aspect of landscape recovery following the emplacement of lava flows: plant colonization of lava flows. I use LiDAR data to characterize forests on and adjacent to the c. 1.5 ka Collier Cone lava flow; this lava flow is notable for its traverse across multiple climatic zones, spanning elevations from 2150 to 900 m. I find that regardless of elevation, young lava flows host a sparser and shorter forest than adjacent areas. However, in areas with apparent sediment deposition on the flow, young lava can support forests that are seemingly identical to adjacent areas.

CHAPTER III

USING AIRBORNE LIDAR TO QUANTIFY VEGETATION COLONIZATION OF A LATE HOLOCENE LAVA FLOW TRAVERSING A CLIMATIC GRADIENT: THE COLLIER CONE LAVA FLOW, CENTRAL OREGON CASCADES

This chapter was prepared for submission to *Journal of Vegetation Science*. Co-authors Kathy Cashman, Dan Gavin, and Josh Roering provided guidance over the course of the project, help compiling the existing literature, and editorial assistance. I performed the analysis and was the primary author.

Introduction

Volcanic eruptions re-surface landscapes with lava flows (effusive activity), pyroclastic deposits (explosive activity), or a combination of both. Subsequent plant colonization is dictated by a variety of factors, including eruptive deposit type, seed and nutrient availability, presence of a growth medium (e.g., soil), topographic setting, and climate (Walker & del Moral 2003). Whereas explosive deposits are generally fine-grained and share many characteristics with fertile soil, lava does not – it is massive and fractured rock that is typically inhospitable to plant establishment and growth. Although lava is by far the most common substrate in most regions of active volcanism, there have been many more studies of plant colonization and species succession on explosive volcanic deposits (e.g., Taylor 1957; Clarkson 1990; Whittaker et al. 1992; del Moral &

Wood 1993; Grishin et al. 1996; Tsuyuzaki & Hase 2005; Lindig-Cisnerosa et al. 2006; Marler & del Moral 2011) than on lava flows (Roach 1952; Drake 1992; Drake & Mueller-Dombois 1993; Kitayama et al. 1995; Aplet 1998; Cutler et al. 2008), and post-emplacement environmental studies of lava flows generally focus solely on soil development processes (e.g., Wells et al. 1985; Chadwick et al. 1999; Rasmussen et al. 2010). In this paper, we combine geologic and ecologic perspectives to examine plant colonization of a recent lava flow in the central Oregon Cascades that traversed a climatic and vegetation gradient through subalpine to lowland forests. We assess the role of substrate and of external events (debris flows) in promoting vegetation establishment and growth, and use high resolution Light Detection and Ranging (LiDAR) data to compare mature (off flow) and developing (on flow) forests.

Most studies of soil development on lava flows are from Hawaii, because of the abundance of mapped and dated lava flows that traverse extensive elevation and climatic gradients, which therefore provide excellent climo- and chrono-sequences (e.g., Chadwick et al. 1999, 2003; Kurtz et al. 2001; Porder et al. 2007). At these sites, soil development is positively correlated with age, and soil development rates increase with precipitation and temperature (Chadwick et al. 2003). In the absence of external soil sources, lichens initiate chemical weathering and fix nitrogen, providing key plant nutrients (Jackson & Keller 1970; Brady et al. 1999; Kurina & Vitousek 1999; Gordon 2005). However, external soil and nutrient sources also appear to be important factors in soil formation: Chadwick et al. (1999) found that Asian loess contributes phosphorous and that marine aerosols provide a steady input of calcium, both key soil nutrients. Overall, Asian loess accounts for a substantial fraction of Hawaiian soil mass (up to 25%;

Kurtz et al. 2001; Porder et al. 2007), despite Hawaii's location in one of the least dusty regions of the northern hemisphere (Rea 1994). Studies at Craters of the Moon, Idaho, also emphasize the importance of external biological (debris from nearby trees) and mineral (loess) sources for soil formation (Vaughan & McDaniel 2009; Vaughan et al. 2011), and ash deposition has been found to accelerate soil development on lava flows from Mt. Etna, Italy (Egli et al. 2008). Although some studies discount external factors (e.g., Rasmussen et al. 2010), there is growing recognition among soil scientists that loess and other external soil and nutrient sources play an important role in soil development on lava flows.

Studies of plant colonization and species succession on lava flows are also concentrated in Hawaii using similar climo- and chrono-sequences. These studies emphasize ecological metrics, such as species diversity, individual species density, and individual plant characteristics (e.g., diameter at breast height), and link them to controlling variables, such as substrate age, precipitation, and temperature. A classic study by Aplet et al. (1998) found that precipitation is the dominant control on plant community composition and health; lava flow age and morphology play a lesser role. It has also been recognized that lava flows with volcanic ash cover have bigger trees than lava flows without (Drake & Mueller-Dombois 1993; Kitayama et al. 1995) and that seed availability is not a limiting factor for plant establishment on Hawaiian lava flows (Drake 1992). However, studies of the processes and mechanisms that initiate vegetation colonization of lava flows in non-tropical environments are limited (e.g., Bernhardt 1986; Fridriksson 1987; Bashan 2002) and generally comprise of an inventory of plants present on a specific lava flow or flow field. In this paper, we provide a broader perspective of

vegetation development on lava flows, focusing less on individual plants and species and more on general forest structural characteristics. We focus particularly on the role of substrate (different morphological parts of a lava flow, and areas of external sediment deposition) for vegetation establishment and growth.

As most soil development and plant colonization studies on lava have been based in Hawaii, most examined lava flows either have smooth ropy pāhoehoe or clinkery ʻaʻā lava flow morphologies. Morphology clearly is important: in Hawaii, vegetation colonization rates are faster on pāhoehoe in arid and ʻaʻā' flows in wet environments (Aplet et al. 1998). This difference emphasizes the importance of "safe sites" for seed germination and establishment (e.g., isolated cracks present in pāhoehoe flows) in stressful environments and greater available surface area (ʻaʻā flows) for nutrient uptake in less stressful environments (Aplet et al. 1998). Morphology is also important both for chemical weathering, as rates are generally much slower for pāhoehoe lava flows (Porder et al. 2007), and for soil development on Holocene lava flows in Idaho, where only pāhoehoe lava flows have increased soil cover with age (Vaughan et al. 2011). Here external soil sources (loess) influx rates are the same across the lava flow field, but loess accumulates on the surface of pāhoehoe flows and below the surface (between clinkers) on ʻaʻā flows.

While pāhoehoe and ʻaʻā are common lava flow morphologies, it is important to note that these flow morphologies are exclusive to basaltic (low silica, low viscosity) lava flows. More silicic lava flows (e.g., basaltic andesite, andesite) typically have blocky morphologies, with surfaces formed by submeter to meter scale blocks. These lava flows are also characterized by high (10 – 20 m) levees that form at the active flow front where

rubble is dispersed laterally (Sparks et al. 1976; Griffiths 2000). Our study thus provides insights on vegetation colonization on higher silica lava flows than previously studied (specifically a blocky basaltic andesite to andesite lava flow with levees in the upper portion of the flow), and will also permit assessment of vegetation colonization patterns on different morphological areas of a lava flow (levee vs. channel interior).

We use high resolution (1 m) canopy height and digital elevation models derived from airborne LiDAR measurements. Airborne LiDAR has been used in forest studies to calculate biomass (e.g., Nelson et al. 1988; Boudreau et al. 2008), examine canopy structure (e.g., Lefsky et al. 1999; Zimble et al. 2003), and estimate stand characteristics (e.g., Means et al. 1999; Næsset 2002). LiDAR has also been used by volcanologists to characterize lava flow morphology (e.g., Pyle & Elliot 2006; Deardorff 2011; Cashman et al. in press). This study is the first to combine geological and biological perspectives to use LiDAR to characterize plant colonization of lava flows in a temperate climate.

Study area – Collier Cone lava flow, central Oregon Cascades

We selected the Collier Cone lava flow in the central Oregon Cascades as the subject of our study because of (1) the availability of high resolution (1 m) LiDAR data, (2) the young age of the lava flow, which precludes any glacial influence on the system, and (3) the remarkable range of climatic environments traversed by the lava flow.

Collier Cone erupted 1511 (1354 – 1569) cal yr B.P. (Sherrod et al. 2004) on the north flank of North Sister volcano in the central Oregon Cascades (Fig. 1). It is located within the High Cascades, a region that has been volcanically active since the Pliocene with a high density of Quaternary mafic volcanic centers (Sherrod et al. 2002; Hildreth

2007). The region was extensively glaciated during the Pleistocene (Sherrod et al. 2004), as evidenced by widespread glacial gouges and glacially carved valleys (e.g., the White Branch glacial trough; Fig. 1B).

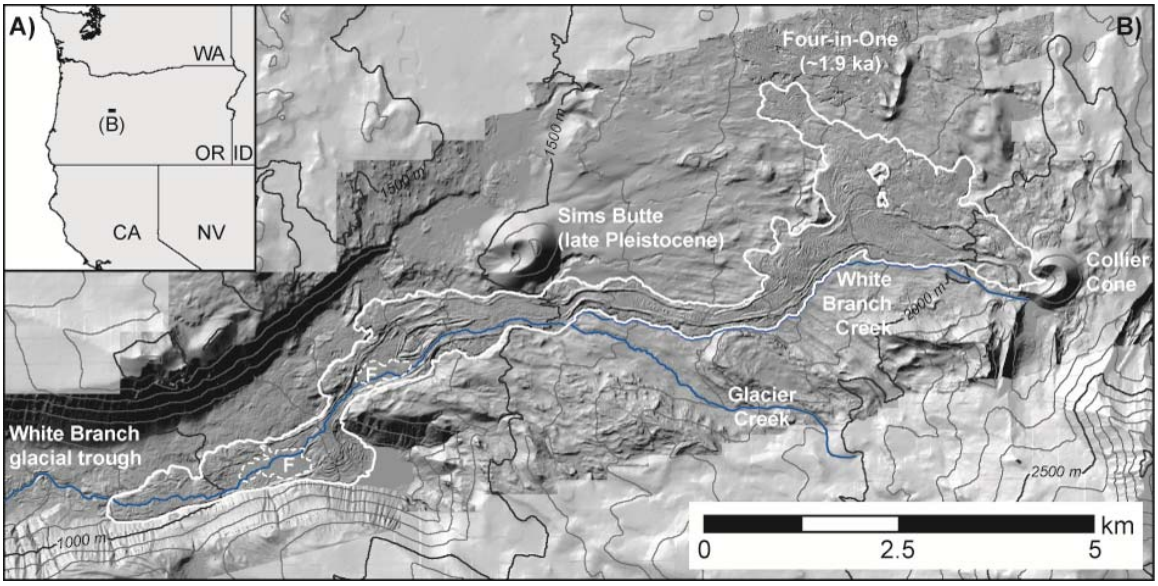

Fig. 1. Location map of study area. (A) Study area in context of Pacific Northwest region of the United States; black box shows extent of (B). (B) Shaded relief map derived from 1-m resolution LiDAR data where available and 10-m digital elevation model (DEM) elsewhere of the area around the Collier Cone lava flow, outlined in white. Creeks (in blue) and other geographic features referred to in the text are labeled; 'F' denotes the flats (outlined with a dashed white line) where the White Branch creek has deposited sediments. 100 m contour intervals derived from 10-m DEM are shown in grey (500 m intervals are bold).

Collier Cone is a scoria cone situated just above tree line, at an elevation of 2150 m. The most extensive lava flow formed during the Collier Cone eruption emerged from the base of the cone and traveled 14 km westward, traversing the High Cascades and then descending into the White Branch glacial trough to an elevation of 900 m, 1250 m below its source elevation. Below 1500 m, the lava flow is either next to or on top of the late Pleistocene basaltic Sims Butte lava flow, which covers most of the White Branch glacial trough valley bottom (Sherrod et al. 2004). The Collier Cone lava flow is blocky and

ranges from basaltic andesite to andesite in composition (Schick 1994), and the entire flow was most likely emplaced in less than a year (Deardorff 2011).

Most precipitation in the area falls in the winter as snow (c. 2500 mm/yr in modern times; Cashman et al. 2009). Melting glaciers on the Three Sisters volcanoes also contribute water, although most percolates into the groundwater system and emerges east of the Cascade crest (Gannett et al. 2001; Gannett & Lite 2004). Along the lava flow, the climate changes with elevation, as expressed by the local vegetation: the lava flow begins above the alpine tree line, flows through subalpine and montane forests, and finally descends into a lowland forest (Fig. 2; Kilsgaard 1999).

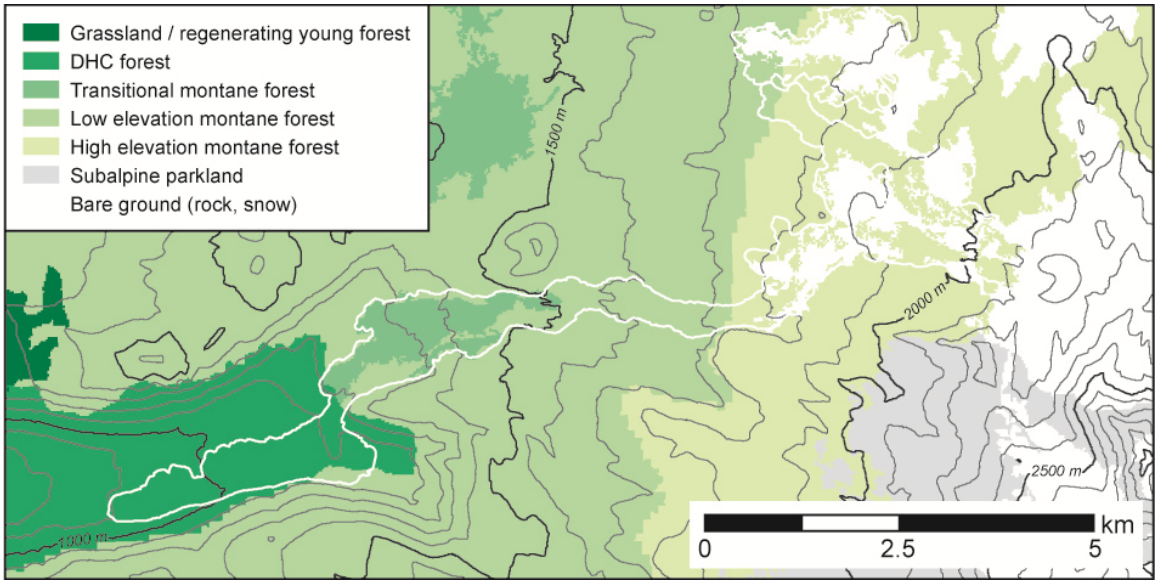

Fig. 2. Vegetation map of area shown in Fig. 1B as mapped by Kilsgaard (1999) at a scale of 1:100,000 using LANDSAT imagery. The outline of the Collier Cone and Four-in-One lava flows (mapped at the 1:2,500 scale) are shown in white and 100 m contour intervals derived from 10-m DEM are shown in grey (500 m intervals are bold).

A peculiarity of the Collier Cone lava flow is that despite its young age, a bedrock channel, the White Branch creek, has incised into the lower part of the lava flow (Fig. 1B). The White Branch channel starts at the glacial lake at the terminus of the retreating

Collier Glacier adjacent to Collier Cone. The channel follows the southern margin of the Collier Cone lava flow until an elevation of ~1500 m, where it migrates onto the flow. The upper portion of the channel is dry; the White Branch is fed by Glacier Creek and snowmelt. Apart from brief periods of high snowmelt and/or rainfall, no water flows on the surface of the lava flow. However, reports of catastrophic glacial outburst floods from Collier Glacier in historic and prehistoric times suggest that for brief episodes, the White Branch carried a heavy sediment load (O'Connor et al. 2001). Accumulations of sediment form flats ("F" on Fig. 1B) on the lower portion of the Collier Cone lava flow. These deposits were probably transported down the channel by outburst floods, which may also have incised the White Branch channel.

Forests adjacent to and on the Collier Cone lava flow range from lowland to subalpine forests common to the Pacific Northwest (Fig. 2; Franklin & Dyrness 1992; Kilsgaard 1999). Lowland forests primarily consist of *Pseudotsuga menziesii* (Douglas-fir), *Tsuga heterophylla* (western hemlock), and *Thuja plicata* (western red cedar); we refer to this forest community as DHC forest. Douglas-fir, a shade intolerant post-fire species, is dominant, with western hemlock and western red cedar in the subcanopy. The DHC forest transitions to a forest co-dominated by *Abies amabilis* (Pacific silver fir) and *A. procera* (noble fir) with *T. heterophylla*, and *T. mertensiana* (mountain hemlock); we refer to this forest community as the low elevation montane forest. The transition from DHC to montane is determined by the elevation of a persistant snow pack (Franklin & Dyrness 1992). In general the Collier Cone lava flow supports the same species assemblage as adjacent mature forests, with the exception of the species assemblage on the lava flow near the DHC-to-montane transition. In this transitional zone, the lava flow

supports *A. lasiocarpa* (subalpine fir) and *Pinus contorta* (lodgepole pine), which are absent from the surrounding mature forest. At elevations higher than the low elevation montane forest, the forest assemblage is dominated by *T. mertensiana* with *A. amabilis*, *P. contorta*, and *P. monticola* (western white pine); we refer to this forest community as the high elevation montane forest. Between the montane forests and the alpine treeline is a subalpine parkland community consisting of *T. mertensiana*, *A. lasiocarpa*, *A. amabilis* and shrubs of *Phyllodoce empetriformis* (red mountain heather), *P. glanduliflora* (green mountain heather), *Cassiope mertensiana* (white mountain heather), and *Empetrum nigrum* (crowberry). Alpine treeline is at 2100 m, a typical value in the broader region (Franklin & Dyrness 1992).

Methods

We use research grade Airborne Laser Mapping LiDAR data of the Collier Cone region collected by the National Center for Airborne Laser Mapping (NCALM) on 28 Jul 2008 (Fig. 1B) to create a high resolution map of canopy heights across the study region. This is generated using both the filtered (bare earth) and unfiltered (first return) LiDAR-derived digital elevation models (DEMs) provided by NCALM and gridded at 1 m point spacing.

The Collier Cone lava flow is situated within the Willamette National Forest and part of it is within the Three Sisters Wilderness Area; as such there has been very little anthropogenic influence on the area. However, the LiDAR data covers a few areas that have been clear-cut, part of Oregon Highway 242, and two small lakes. These areas have all been removed from our analysis to focus solely on the natural canopy and its relation

to the underlying geology. In what follows, "recent lava flows" refers to both the Collier Cone lava flow and the 1910 (1720 – 2123) cal yr B.P. Four-in-One lava flow (Sherrod et al. 2004; Fig. 1B). Areas not covered by recent lava flows are considered representative of mature forest; we note that at the time of the LiDAR data acquisition, no notable fires had disturbed the region in historic time, although in 2010, the Scott Mountain fire affected an area directly north of the study area. We use the LANDSAT-based classification of Kilsgaard (1999) for a general map of the major forest communities in the region; this classification agrees well with our field observations of the dominant tree species on and adjacent to the lava flow.

Substrate mapping and surface roughness quantification

We use bare earth LiDAR-derived hillshade and slopeshade maps to digitally map lava flow and (depositional) flat boundaries at 1:2500 scale. Additionally, we quantify surface roughness for each pixel using a slope-based metric, determined by computing the standard deviation of slope in a 41 m x 41 m window centered on each pixel.

Canopy map

We generate a high resolution (1 m) canopy map by subtracting gridded filtered (bare earth) from unfiltered (first return) LiDAR (Lim et al. 2003). As the Collier Cone lava flow has a surface composed of large blocks, numerous exposed (i.e., unvegetated) lava flow surfaces have different values for the filtered and unfiltered elevation; this occurs because the NCALM algorithm that differentiates between the ground and vegetation misclassifies lava flow rubble as vegetation. To avoid falsely identifying areas

as vegetated, we compare our LiDAR canopy map to color aerial imagery (0.5 m resolution) acquired by the Oregon Orthoimagery Framework Group in summer 2005. Regions where the filtered and unfiltered LiDAR differ by less than 2.0 m often have no vegetation visible in aerial imagery, whereas if the difference is greater than 2.0 m, vegetation is generally visible in the imagery. Thus, in our analysis we designate pixels where the difference between the two LiDAR datasets is less than 2.0 m as bare earth, and everything else as vegetated. Finally, to visualize the canopy structure across the study area, we map the canopy heights using seven classes (bare earth, 2.0 – 5.0 m, 5.1 – 10.0 m, 10.1 – 20.0 m, 20.1 – 30.0 m, 30.1 – 50.0 m and > 50.0 m).

Percent cover

We develop a metric of "percent cover" to quantify the canopy height distribution using the pixel-based concentration of values in each of the seven height classes. To determine percent cover, at each pixel we construct a window extending 20 m in each cardinal direction from the pixel (for a total window size of 41 x 41 m; see Fig. 3). We tally the number of points within this window in each height category and then divide by 1681 (41^2) to calculate percent cover for each category (Fig. 3; Table 1). This is repeated for every pixel in the entire LiDAR dataset. We exclude areas with incomplete surrounding coverage (i.e., pixels within 20 m of the dataset edge or within 20 m of a lake or anthropogenic feature). We select a distance of 20 m as it is large enough to contain numerous trees, and thus is not a metric of tree locations but rather canopy density, yet is small enough to delineate local variations in canopy. We also compute percent cover using a distance of 50 m (101 x 101 m square) for comparison.

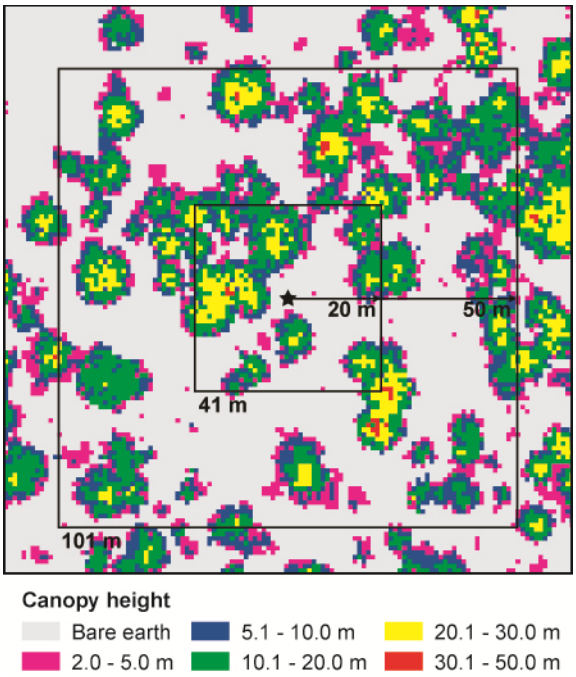

Fig. 3. Example of how a single percent cover value is determined. A box is constructed extending either 20 or 50 m in each cardinal direction from a pixel (star), making a window of 41 or 101 m. The number of pixels in the window within each height class is tallied and converted to percent cover (see Table 1). This example is from the Collier Cone lava flow within the DHC forest reach, and this particular site has no canopy values > 50.0 m.

Table 1. Pixel counts and corresponding percent cover for starred pixel at center of Fig. 3 for a half-window distance of 20 and 50 m (corresponding to windows of 41 and 101 m, respectively). This example contained no pixels > 50.0 m.

Canopy Height	20 m Pixel Count	20 m % Cover	50 m Pixel Count	50 m % Cover
Bare earth (< 2. 0 m)	715	42.53%	5408	53.01%
2.0 – 5.0 m	153	9.10%	1128	11.06%
5.1 – 10.0 m	241	14.34%	1347	13.20%
10.1 – 20.0 m	412	24.51%	1800	17.65%
20.1 – 30.0 m	157	9.34%	495	4.85%
30.1 – 50.0 m	3	0.18%	23	0.23%
Total	1681	100.00%	10201	100.00%

For mapping purposes, we determine classes of percent cover of each height class by visual inspection for natural breaks in the frequency distribution. Bare earth percent cover is used to differentiate areas of sparse, low, moderate, and dense vegetation. Percent cover of bare earth, intermediate (20 – 30 m) and high (> 30 m) canopy is summarized with regard to elevation, vegetation type, substrate, and general landscape morphology.

Results

Surface roughness

Slope-based roughness can be used to distinguish smooth older areas (low values) from recent blocky lava flows (high values; Fig. 4). Lava flow boundaries and the tops of levees have high roughness values due to the abrupt changes in slope in these areas, and the two flats on the lava flow have considerably lower (smoother) values than rest of the lava flow.

Canopy height distribution

Canopy height and vegetation density are inversely related to elevation: at lower elevations, trees are taller and there is more vegetation cover (Fig. 5). Recent lava flows have fewer and shorter trees than adjacent areas. A notable exception to this trend are on the flats where the White Branch creek has delivered sediment onto the lava flow; here, there is little difference between the canopy structure on the intra-lava flats and the forest off the lava flow.

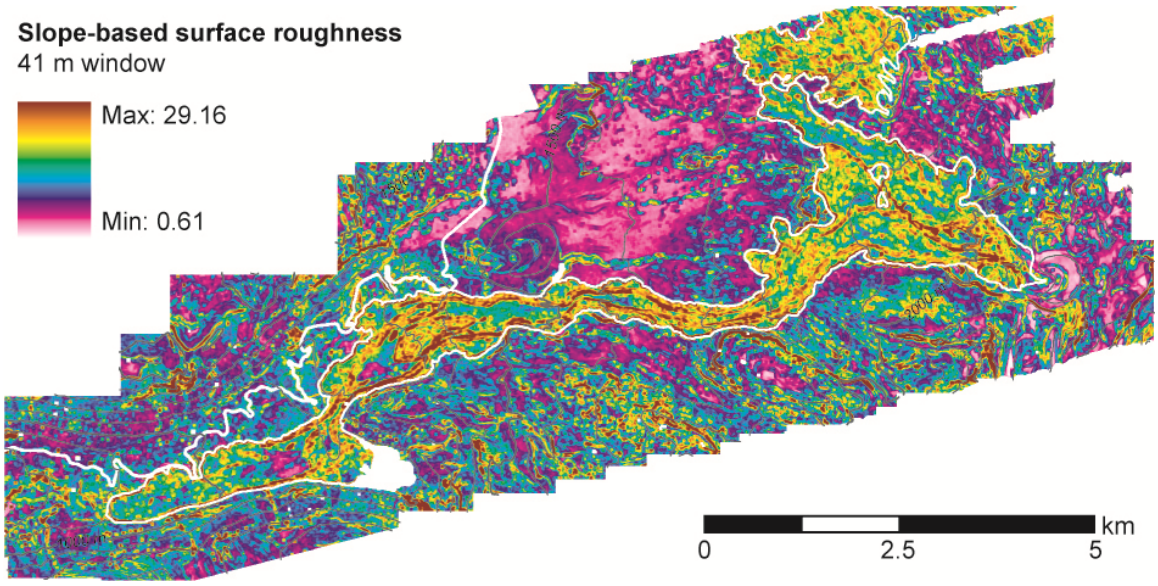

Fig. 4. Slope-based surface roughness map, calculated by taking the standard deviation of slope values within a 41 m window centered about a pixel (thus using the same number of pixels for each measurement as 41 m window percent cover analysis). Recent lava flows are outlined in white, and a highway and two lakes are shown in white. 100 m contour intervals derived from 10-m DEM are shown in grey (500 m intervals are bold).

Forest communities can be clearly identified in the canopy height map (Fig. 5); the spatial extents of these canopy regions are broadly consistent with Kilsgaard's (1999) vegetation map (Fig. 2). The DHC forest is confined to ≤ 1400 m and has a high proportion of trees over 30 m in height. Interestingly, the tallest trees (> 50 m) are found on the north facing slope of the White Branch glacial trough bounding wall, suggesting that here water availability is more important than insolation: north facing slopes have later snowmelt and thus have access to water later in the growing season. The low elevation montane forest spans from 1400 m to 1600 m and is dominated by trees of 5 – 10 m height, with < 15% of trees in the 10 – 30 m height range. The areas mapped by Kilsgaard (1999) as high elevation montane forest and subalpine parkland are indistinguishable in the LiDAR canopy map. Both appear to have taller trees than the low elevation montane forest with a dominant tree height in the 20 – 30 m range. These two

assemblages are found in the 1600 – 2000 m elevation range. The LiDAR canopy map clearly shows the alpine tree line at 2100 m.

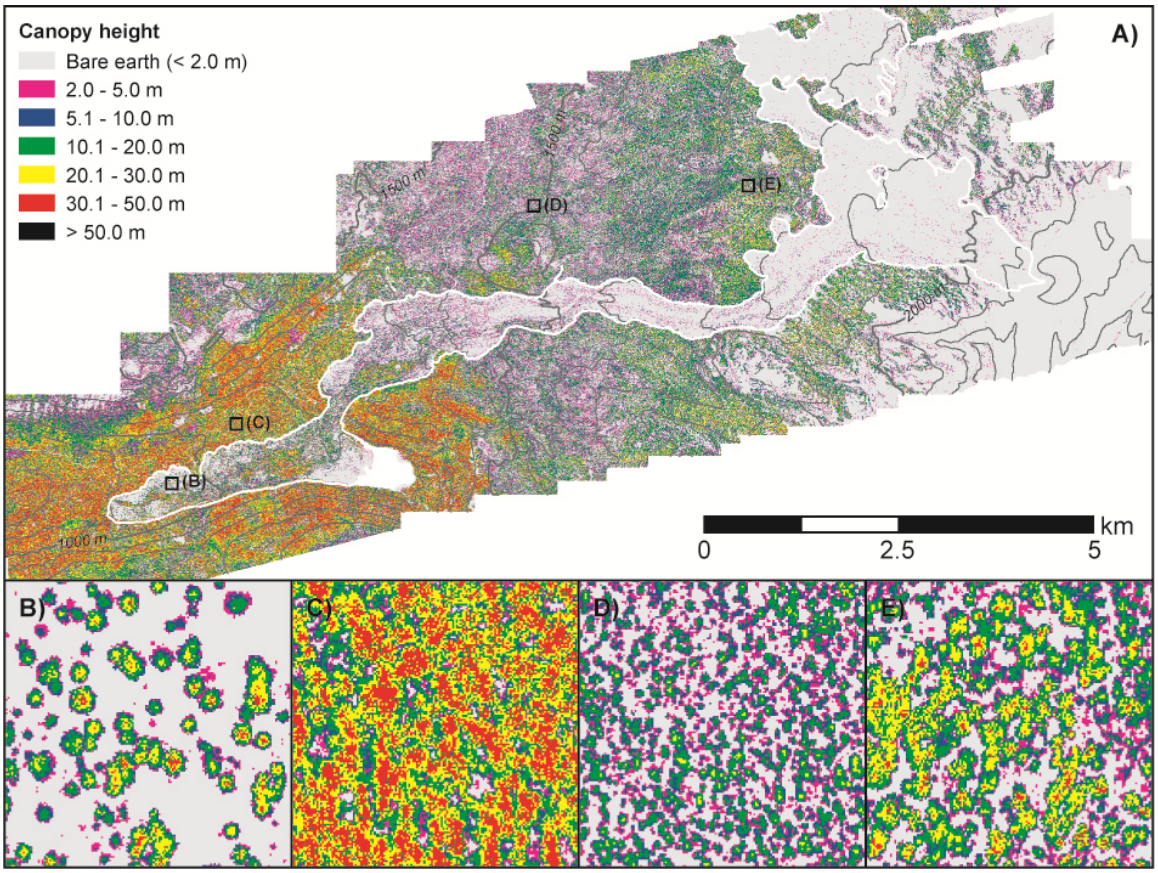

Fig. 5. LiDAR-based canopy maps of the study area. Canopy height is the difference between unfiltered and filtered LiDAR; measurements have been binned into seven height classes. (A) Canopy map of entire study area, and the locations of (B) – (E) are outlined in black and labeled. Recent lava flows outlined in white and 100 m contour intervals derived from 10-m DEM are shown in grey (500 m intervals are bold). (B) DHC forest on the Collier Cone lava flow. (C) DHC forest adjacent to the Collier Cone lava flow. (D) Low elevation montane forest. (E) High elevation montane forest. (B) – (E) are each 150 m by 150 m.

Percent cover

Bare earth percent cover is an effective way of analyzing the importance substrate (i.e., lava flows) on vegetation as it examines the percentage of open space around any

given pixel. Areas with sparse or no vegetation have high bare earth percent cover values, while densely vegetated areas have low values. By examining the presence/absence of vegetation, we can examine what sites and areas are conducive to vegetation establishment and growth. We identify natural breaks in the frequency distribution (Fig. 6) to determine classes of sparse, low, moderate, and dense vegetation. We present results of bare earth percent cover using analysis distances of 20 and 50 m (Fig. 7). These maps show that, as anticipated, calculating percent cover using a larger analysis window (50 m) produces a smoother map (Fig. 7B) than the same calculation with a smaller analysis window (20 m) (Fig. 7A). Results from both distances are consistent with each other; in what follows we focus only on results obtained with a distance of 20 m as this analysis window provides greater detail.

The difference in bare earth percent cover between the DHC and montane forests is striking, with substantially lower bare earth percent cover values in the DHC forest (Fig. 7); the DHC forest has dense vegetation cover (< 8.5% bare earth percent cover) while montane forests have moderate vegetation cover (8.5 – 70% bare earth percent cover). Regardless of elevation, recent lava flows have sparser vegetation cover than adjacent areas. However, there is less open space on the lava flow at lower elevation (moderate vegetation cover in the DHC forest reach compared to sparse cover at higher elevation), suggesting that either conditions are better for forest development at lower elevation or that lower elevation species are better suited for lava flow colonization. Additionally, along the entire flow, lava flow levees have more vegetation cover than adjacent parts of the lava flow, despite being presumably more exposed to harsh weather conditions. Levees have more vegetation than the lava flow even in places where there

are lava flow spillovers separating the levees from the fully developed adjacent forest, indicating that levees are not vegetation hotspots due to proximity to seed sources.

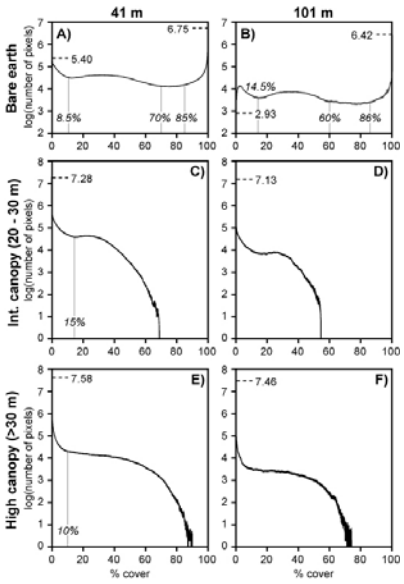

Fig. 6. Log of the total number of pixels for each possible percent cover value for bare earth (A and B), intermediate (C and D), and high canopy (E and F). (A), (C), and (E) are for a 41 m window and (B), (D), and (F) are for a 101 m window. Grey lines show breakdowns used in Figs. 7 and 8; for (C) and (E), an additional break exists at 0.1%.

We can further distinguish between the three main forest types across the study region by examining the density of intermediate (20 – 30 m) and high canopy (> 30 m) (Fig. 8). The DHC forest has the highest percent cover of both intermediate (> 15%) and high canopy (> 10%) anywhere in the study area. The low elevation montane forest has limited intermediate canopy cover (0.1 – 15%) and very few high canopy points. In contrast, the high elevation montane forest has a higher concentration, but patchy distribution, of intermediate and high canopy. The elevation limit of both intermediate and high canopy is lower than alpine tree line identified in Fig. 5 (2100 m) – intermediate canopy values are present up to 2000 m elevation, and high canopy values are present up to 1900 m elevation.

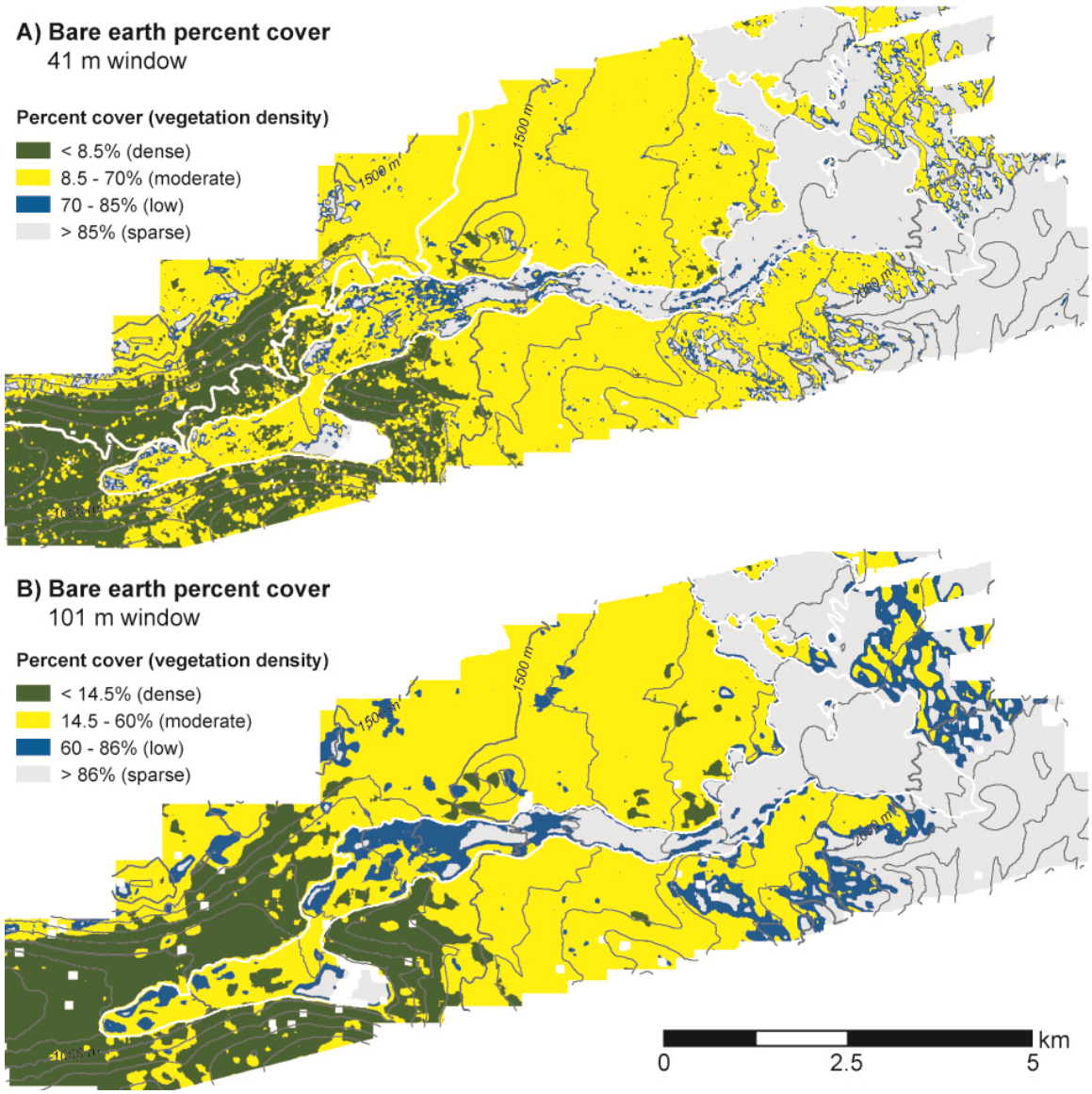

Fig. 7. Bare earth percent cover maps, with windows of (A) 41 m and (B) 101 m. The breakdown between the different categories are as determined in Figs. 6A and B. Recent lava flows outlined in white and 100 m contour intervals derived from 10-m DEM are shown in grey (500 m intervals are bold).

Across all elevations there are fewer canopy values > 20 m on recent lava flows compared to the adjacent forest. In the montane forests, recent lava flows host no trees > 20 m. Within the DHC forest reach, intermediate and high canopy cover accounts for 0.1 – 15% and 0.1 – 10% of the recent lava flow area, respectively (compared with > 15%

and > 10% off the lava flow). An exception is the flat, where intermediate canopy percent cover exceeds 15%, and in patches, high canopy percent cover exceeds 10%.

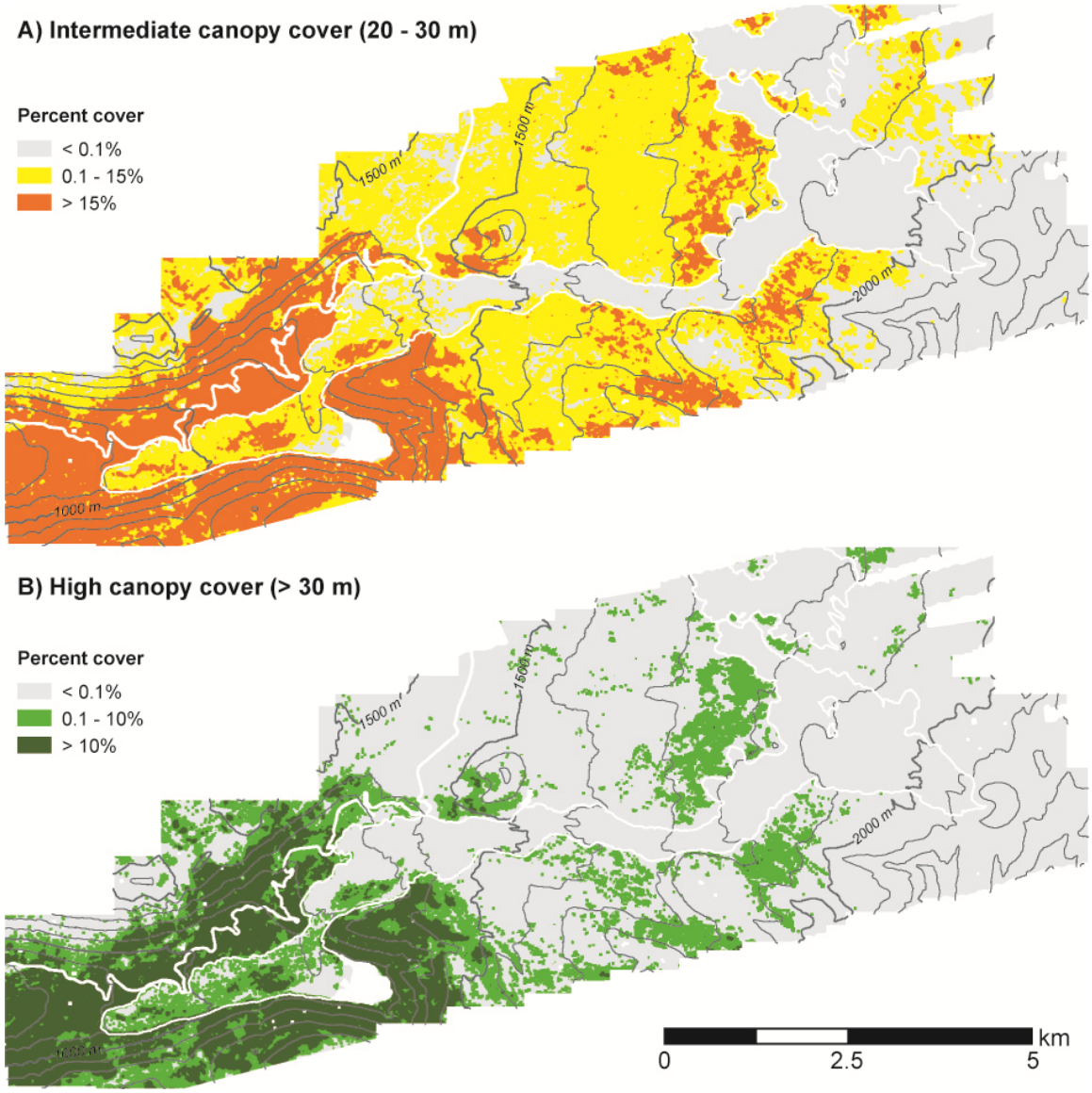

Fig. 8. Percent cover maps with windows of 41 m for (A) intermediate (20 – 30 m) and (B) high (> 30 m) canopy cover. The breakdown between the different categories are as determined in Figs. 6C and E. Recent lava flows outlined in white and 100 m contour intervals derived from 10-m DEM are shown in grey (500 m intervals are bold).

Influence of elevation and substrate on forest characteristics

There are pronounced differences in the canopy height distributions between the DHC and montane forests in areas not covered by recent lava flows. We investigate the relations between canopy height distribution, elevation, and substrate (on/off recent lava flows) by clipping regions of the LiDAR dataset within 25 m elevation of the 1000, 1250, 1500, 1750, and 2000 m elevation contours. Within each elevation band we distinguish between regions on and off recent lava flows. For each elevation band subregion, canopy height measurements are rounded up to the nearest integer and the number of pixels of each canopy height value are tallied and normalized to 100% (Fig. 9). We note that canopy height distribution is not tree height distribution, as individual trees are represented by many pixels.

The DHC forest is dominated by canopy heights of 10 – 30 m. There are fewer canopy height measurements < 10 m than between 10 and 30 m; a possible explanation is that there are few trees < 10 m and canopy height measurements < 10 m are associated with taller trees (Figs. 9B and C). The maximum tree height is 78 m, and there is a relatively small percentage of bare earth pixels (~7 and ~12% of pixels at 1000 and

Fig. 9 (next page). Canopy height as a function of substrate and elevation. (A) Map showing the elevation reaches clipped for analysis shown in parts (B) – (F). Elevation reaches are spaced at 250 m elevation intervals starting at 1000 m and consist of elevations within 25 m of the main elevation (thus, the 1000 m reach covers areas with elevations ranging from 976 to 1025 m). Forest boundaries as mapped by Kilgaard (1999) are roughly indicated on the bottom. Recent lava flows outlined in white and 100 m contour intervals derived from 10-m DEM are shown in grey (500 m intervals are bold). (B) Percentage of pixels within the areas covered by recent lava flows (dashed line) and off the lava flows (solid line) for each canopy height within the 1000 m elevation reach. Stars indicate the number of pixels with no vegetation cover on each substrate, and maximum tree height is indicated. The pie chart shows the proportion of pixels for the elevation reach covering each substrate. (C) – (F) as for (B) for elevation reaches centered at (C) 1250 m, (D) 1500 m, (E) 1750 m, and (F) 2000 m.

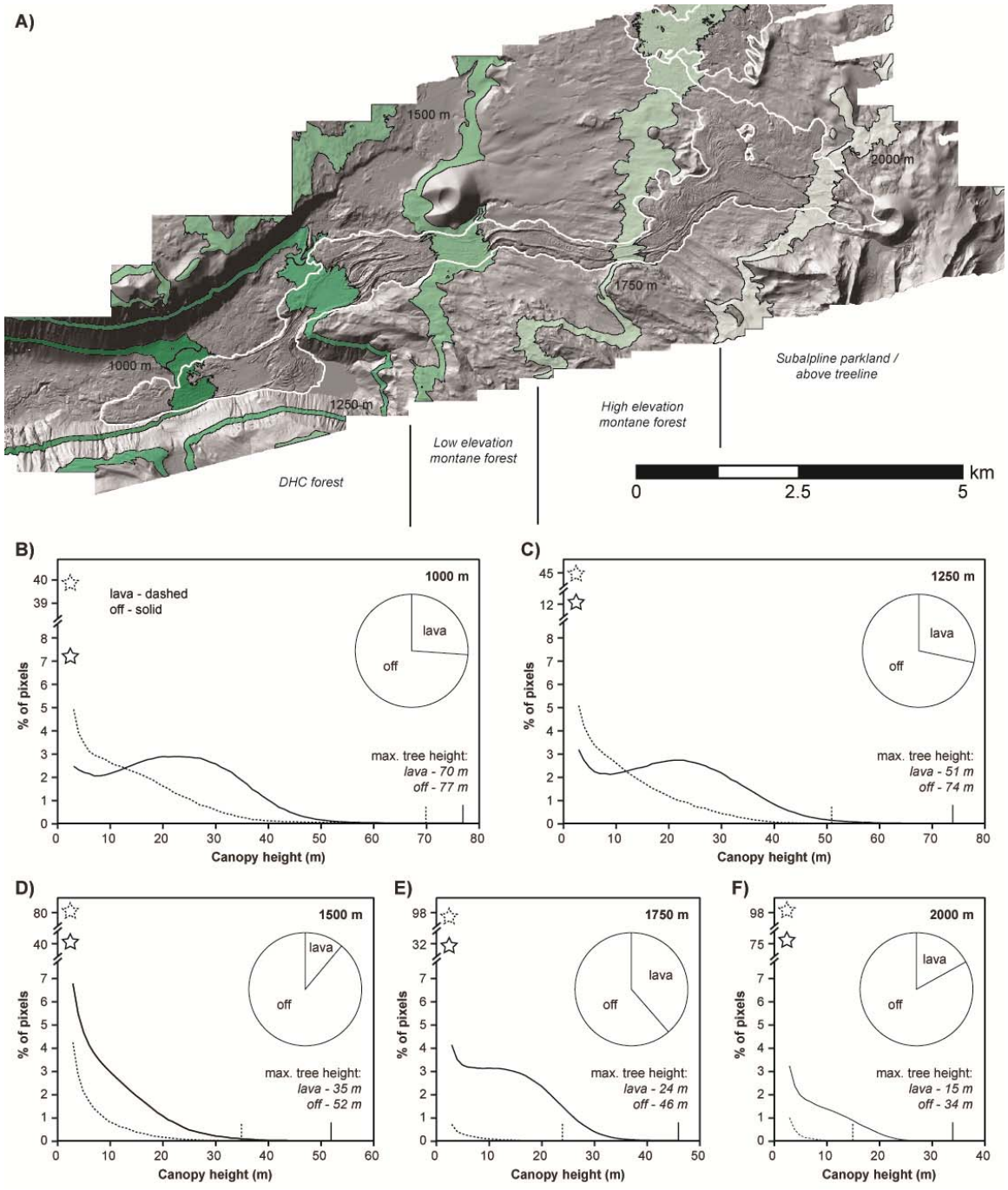
A)
1500 m
2000 m
1750 m
1000 m
1250 m
Subalpine parkland / above treeline
High elevation montane forest
Low elevation montane forest
DHC forest
km
0
2.5
5
B)
1000 m
lava - dashed
off - solid
lava
off
max. tree height:
lava - 70 m
off - 77 m
% of pixels
Canopy height (m)
C)
1250 m
lava
off
max. tree height:
lava - 51 m
off - 74 m
% of pixels
Canopy height (m)
D)
1500 m
lava
off
max. tree height:
lava - 35 m
off - 52 m
% of pixels
Canopy height (m)
E)
1750 m
lava
off
max. tree height:
lava - 24 m
off - 46 m
% of pixels
Canopy height (m)
F)
2000 m
lava
off
max. tree height:
lava - 15 m
off - 34 m
% of pixels
Canopy height (m)

1250 m elevation, respectively). In contrast, both montane forests have a greater percentage of bare earth pixels (~40 and ~32% for the low and high elevation montane forests, respectively) and have shorter maximum tree heights (52 and 46 m, respectively). There is no obvious mode of the canopy height distribution but instead a steady decrease in coverage with increasing height (Figs. 9D and E). This suggests that montane forests have trees with shorter branch lengths and smaller footprints relative to DHC forest trees and that montane forests have a greater range of tree heights. Interestingly, relative to the low elevation montane forest, the high elevation montane forest has more vegetation cover and a greater percentage of canopy height measurements from 10 – 30 m, consistent with general trends observed in Fig. 5.

On recent lava flows maximum tree heights are less than the surrounding forest and the percentage of bare earth pixels is greater (40 – 45% and > 80% of the lava flow within the DHC and montane forest reaches, respectively). No elevation band shows a mode in canopy height; canopy cover decreases with steadily increasing canopy height. The difference in shapes of the canopy distribution curves on and off the lava flows in the DHC forest reach suggests that the distribution of tree heights is more varied on the lava flow, that is, the lava flow does not simply host a sparse version of a DHC forest. In the montane forests, the shape of the canopy distribution curve is similar to the surrounding forest but considerably subdued; here it is possible that the forest on the lava flows is a sparser version of the surrounding forest.

Influence of external soil deposition

We investigate the relation between slope-based surface roughness, substrate, and bare earth percent cover (as a proxy for vegetation development) for the reach from 900 to 1200 m elevation, a portion of the study area within the DHC forest that features a (depositional) flat on the lava flow. Here, there are notable differences in surface roughness between recent lava flows (excluding the flat), the flat on the lava flow, and the adjacent area (Fig. 4). As such, surface roughness can be used as a proxy for external soil deposition within the White Branch glacial trough. We clip the region of interest (900 – 1200 m elevation) from the LiDAR dataset and classify the area according to substrate – lava (no flat), flat, and adjacent areas (Fig. 10A) – and vegetation cover (sparse, low, moderate, and dense) as determined from bare earth percent cover analysis. We round surface roughness values up to the nearest 0.1, and then for each substrate plot surface roughness value frequency (expressed as a percentage) as a function of surface roughness, differentiating between different amounts of vegetation cover.

We find that the lava flow at this elevation is generally rougher and has a broader distribution of roughness values compared to other elevations (Fig. 10B). Both the flat and adjacent off-flow areas have narrower peaks around lower roughness values (Figs. 10C and D). The flat, in particular, is very smooth.

Examining the distribution of bare earth percent cover, we see that the lava flow in the White Branch glacial trough has very little dense vegetation cover (< 8.5%), although areas with dense vegetation exhibit the full range of roughness values. Approximately three quarters of the lava flow has moderate vegetation cover (8.5 – 70% bare earth percent cover), with the remaining area fairly evenly split between low (70 –

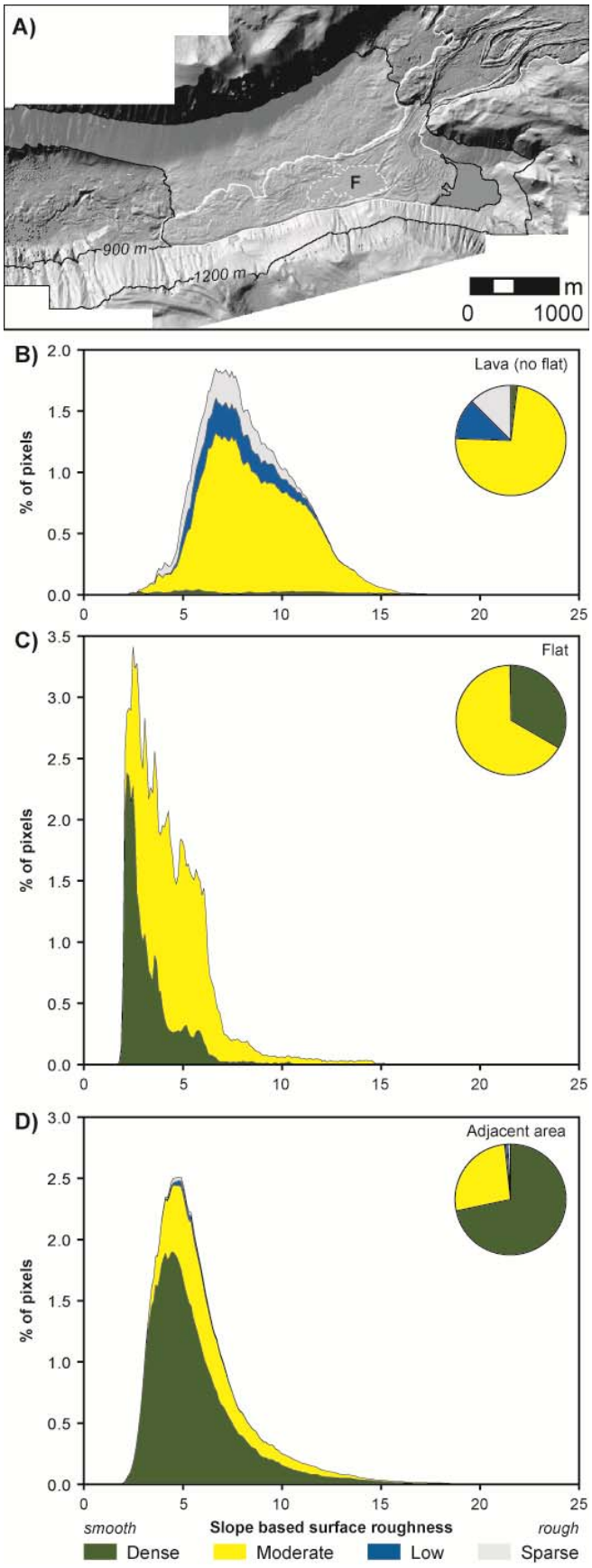

Fig. 10. Slope-based surface roughness as a function of substrate and its relation to bare earth percent cover. (A) Map showing area of interest; analysis shown in parts (B) – (D) from area within 900 – 1200 m elevation (shaded); recent lava flow outlined in white and the flat ("F") outlined with a dashed white line. (B) Percentage of pixels for each surface roughness value (rounded up to the nearest 0.1) on the lava flow (excluding the flat), with the proportion of dense, moderate, low, and sparse vegetation as characterized by bare earth percent cover indicated; colors denoting each type of vegetation density follows Fig. 7A. The overall proportion of each vegetation density class showed in the pie chart. (C) and (D) as for (B) for (C) the flat and (D) adjacent areas off the recent lava flow. The flat has no pixels reporting sparse vegetation cover and only 0.01% of its pixels correspond to low vegetation cover.

85% bare earth percent cover) and sparse (> 85% bare earth percent cover) vegetation cover. In contrast, the flat on the lava flow only has dense (a third of the area) and moderate vegetation cover, with dense vegetation cover predominately in low roughness regions. Adjacent areas also have predominately dense (over two thirds of the area) and moderate vegetation cover, with a few areas of low and sparse vegetation cover.

Discussion

Our analysis of LiDAR-based canopy height measurements on and adjacent to the Collier Cone lava flow provides new ways of both characterizing forest assemblages and examining vegetation development on recent lava flows. In particular, quantification of LiDAR data provides insights into the degree of canopy openness in different forest assemblages, characteristic canopy heights, and the relation between forest structure and underlying substrate. Our results for areas that have not been recently repaved by lava flows permit characterization of three key forest types found in the western central Oregon Cascades and elsewhere: the DHC forest, and low and high elevation montane forests (Table 2). We contrast mature forests with those on recent lava flows to examine how forests develop on lava flows and gain insight into the factors that promote tree establishment and growth.

Mature DHC forest is confined to elevations < 1400 m and has a large proportion of intermediate (20 – 30 m) and high (> 30 m) canopy values. The dominant canopy height is 20 – 30 m while the maximum tree height is 78 m. While roughly a tenth of the pixels in the DHC forest are bare earth pixels (Fig. 9B and C), there are very few contiguous areas with low or sparse bare earth percent cover (Figs. 7 and 10D). This

indicates that bare earth pixels are isolated and scattered throughout the area; close to three quarters of the forest has dense vegetation cover (< 8.5% bare earth percent cover; Figs. 7 and 10D). We suspect that the greater proportion of pixels in the 20 – 30 m range relative to smaller canopy height values indicates that there are few trees < 20 m and that rather, smaller canopy height values come from tree branches. Overall, our analyses show that the DHC forest is populated with trees > 20 m height and is densely vegetated with few open areas.

Table 2. Summary of elevation range and percent cover analysis (20 m distance) results for different forests across study area and on recent lava flows; see Figs. 5, 7, and 8.

		Percent cover		
	Elevation range	Bare earth	Intermediate canopy	High canopy
DHC forest	< 1400 m	< 8.5%	> 15%	> 10%
Low elev. montane forest	1400 – 1600 m	8.5 – 70%	0.1 – 15%	< 0.1%
High elev. montane forest	1600 – 2100 m	8.5 – 70%	> 0.1%	0.1 – 10%
Lava flow: DHC forest	900 – 1400 m	8.5 – 70%	0.1 – 15%	0.1 – 10%
Lava flow: alluvial plain	1000 – 1300 m	< 70%	> 0.1%	> 0.1%
Lava flow: montane forest	1400 – 2100 m	> 70%	< 0.1%	< 0.1%

In contrast, DHC forests on the Collier Cone lava flow are considerably more open, with moderate (not dense) vegetation cover (Fig. 7), and generally shorter trees (Fig. 5). There are considerably more bare earth pixels (~ 40%; Figs. 9B and C), and visual inspection of the canopy map shows that trees tend to be isolated rather than clumped (Fig. 5B). We speculate that the lava flow is not uniformly suitable for tree establishment, and that microsites are very limited in extent where seedlings can survive through the drought-sensitive seedling size classes. As such, vegetation develops only at these microsites, *without* evidence of established vegetation expanding the extent of these microsites by facilitation (e.g., increasing organic matter), generating of tree clumps.

Such limited carrying capacity of small microsites is consistent with the very narrow growth rings observed in cores collected from trees on the Collier Cone lava flow (D.G. Gavin, personal observation). This lack of evidence of succession by facilitation contrasts with evidence of positive interactions between plants in desert environments (e.g., Tewksbury & Lloyd 2001), though we note little similarity, other than dry or thin soils, between our site and desert environments. On the Collier Cone lava flow, it is not clear whether primary succession is progressing on a millennial time scale via autogenic processes or whether the carrying capacity is indeed static and the vegetation has reached a strict "edaphic climax" as suggested by Franklin & Dyrness (1992).

Unlike blocky lava surfaces, areas where external sediment has been brought on to the flow (the flats) exhibit considerably different canopy characteristics; these areas closely resemble mature DHC forests (Fig. 10). Vegetation cover is dense in over a third of the flats, and the percent cover of intermediate and high canopy cover mimics that of mature forests. Thus, it appears that the externally-derived sediment of the flats behaves as a soil substrate and as such promotes tree establishment and growth (allogenic succession). Tree colonization and development is rapid in these areas, and considerably tougher and slower elsewhere on the Collier Cone lava flow within the DHC forest reach (autogenic succession).

Mature low (1400 – 1600 m) and high (1600 – 2100 m) elevation montane forests have little high canopy cover and considerably less intermediate canopy cover relative to the DHC forest (Fig. 8). Surprisingly, it appears that of the two montane forests, the high elevation montane forest has more biomass: the high elevation montane forest has more intermediate and high canopy cover. Furthermore, although both forests

show a steady decrease in pixel frequency with increasing canopy height values (suggesting both heterogeneity in tree heights and more short than tall trees), the high montane elevation forest has a greater proportion of pixels > 10.0 m (Figs. 9D and E). Finally, while vegetation density is low for both forests (Fig. 7), the high elevation montane forest displays an overall lower percentage of bare earth pixels (32 vs 40%; Figs. 9D and E). These observations might be explained with differences in fire history – recent pre-historic fires could have been confined to the low elevation montane forest due to snow and/or cooler and wetter conditions at higher elevation. However, as fire histories have not been reconstructed for the area, this is speculative and requires further investigation. Later snowmelt and fewer fires could also promote tree growth and permit the development of larger, more mature trees at higher elevation.

Vegetation development on lava flows within the montane forest appears quite challenging. Vegetation is sparse, and canopy heights are considerably shorter than in the adjacent mature forests. Suitable tree establishment sites appear scarce, with an exception along lava flow levees, where vegetation density is moderate rather than sparse. Here, trees are present on both the sides of the levees, indicating that there is no establishment preference or enhanced growth conditions related to either cardinal direction or position relative to the exterior of the lava flow. Given that lava flow levees are likely farther above the water table than the flow interior, are more exposed to the elements, and in some cases are farther away from seed sources, this suggests that an intrinsic property of the levees makes them more suitable for vegetation establishment and development. We speculate that block sizes on the levees are smaller than elsewhere on the lava flow, providing a more favorable environment for roots to penetrate to water sources. Smaller

block sizes may also increase moisture retention relative to the flow interior. Thus, it appears that seed or water supply (i.e. later snowmelt) are not limiting factors for vegetation establishment but that instead, the nature of the substrate determines the ease of development. More generally, lava flow morphology (levee vs. channel) dictates the preponderance of feasible establishment sites. Thus, while vegetation development is slow and challenging at high elevations, lava flow levees are more suitable for vegetation establishment and growth than other parts of the flow.

In conclusion, we have developed several new methods utilizing high resolution LiDAR data to characterize forest structure: binned canopy maps for quick visualization of canopy height distribution (Fig. 5), percent cover maps (Figs. 7 and 8), plots of the percentage of pixels of different canopy heights at given elevation (Fig. 9), and the association of vegetation cover and surface roughness (Fig. 10). Our work permits characterization of forest assemblages common in the Pacific Northwest and provides insight on vegetation development on recent lava flows in temperate climates. We find that trees on lava flows are shorter and sparser than those in mature forests, and that tree spacing indicates little facilitative processes occurring that would promote any primary succession process occurring on the lava flow. Vegetation establishment and development is enhanced if the lava flow block size is small enough to increase the density of safe seedling sites, and it is greatly enhanced if external factors deposit a soil growth medium on the lava flow.

Bridge

In Chapter III, I used LiDAR data to characterize vegetation on and adjacent to the 1.5 ka Collier Cone lava flow from its vent (2150 m) to the lava flow toe (900 m), developing methods to examine the concentration and distribution of trees of varying heights and link them to underlying lava flow morphology. I found that trees growing on young lava flows are shorter and sparser than those immediately off the lava flow. However, where externally-derived sediment has been deposited on the lava flow and provides a rooting medium, the forest resembles the developed forests in adjacent regions. I concluded that factors play an important role in forest establishment on the Collier Cone lava flow. This work suggests that external soil deposition is critical for rapid establishment of forests on blocky lava flows in temperate climate regions, and that in the absence of externally-derived soil, plant colonization of lava flows progresses very slowly.

In Chapter IV, I test the conclusions of Chapter III by presenting the results of a field campaign and characterization of soil from both the Collier Cone lava flow and the Sand Mountain volcanic field. As predicted in Chapter III, I find that forests develop on these very young Holocene lava flows where external soil-like material has been deposited on the flows. At Collier, the material appears to be fluvially deposited glacial till sourced from the Three Sisters volcanic area, while for the Sand Mountain volcanic field, the material is tephra from the Sand Mountain volcanic field.

CHAPTER IV

AFTER THE LAVA FLOW: THE IMPORTANCE OF EXTERNAL SOIL SOURCES FOR PLANT COLONIZATION OF RECENT LAVA FLOWS IN THE CENTRAL OREGON CASCADES, USA

This chapter was submitted to *Geomorphology* for a special issue entitled *Process geomorphology and ecosystems: Disturbance regimes and interactions*. Co-authors Kathy Cashman and Josh Roering provided guidance with study design, data interpretation, and editorial assistance. I collected the majority of the data, interpreted it, and was the primary author.

1. Introduction

Effusive volcanic eruptions repave landscapes rapidly with lava flows, covering large regions with massive yet highly permeable rock that is inhospitable to life. These disturbances reset the underlying landscape and ecosystem and pose an interesting challenge for recovery, as fresh lava is sterile and generally quite hard and dense. However, with time, soil, life, and water eventually reclaim the new surface. Traditional pedologic treatment of soil formation assumes that soil is formed in place from the physical and chemical breakdown of rock (e.g., Jenny, 1941), while many plant succession studies examine plant establishment and survival on new surfaces considering nutrient availability but with little consideration of the physical properties of the underlying substrate. Here we will challenge both of these approaches in the context of

young lava flows, and will argue that on very young lava flows, most soil is externally derived and plant colonization occurs predominately in areas with externally derived soil (but not elsewhere on the lava flow).

Most post-emplacement environmental studies of lava flows focus solely on soil development processes (e.g., Wells et al., 1985; Chadwick et al., 1999; Rasmussen et al., 2010). The majority of studies of soil development on lava flows focus on Hawaii due to the abundance of mapped and dated lava flows that traverse extensive elevation and climatic gradients, which therefore provide excellent chrono- and climatic sequences (e.g., Chadwick et al., 1999, 2003; Kurtz et al., 2001; Porder et al., 2007). Here soil development is positively correlated with age, and soil development rates increase with increased precipitation and temperature (Chadwick et al., 2003). External soil and nutrient sources appear to be important factors in soil formation: Chadwick et al. (1999) found that Asian loess is an important source of phosphorous and marine aerosols provide a steady input of calcium, both key soil nutrients. Overall, Asian loess accounts for a substantial fraction of Hawaiian soil (up to 25%; Kurtz et al., 2001; Porder et al., 2007). Elsewhere, loess and debris from nearby trees is a key component of soil at Craters of the Moon in Idaho, USA (Vaughan and McDaniel, 2009; Vaughan et al., 2011). Although some studies discount external factors (e.g., Rasmussen et al., 2010), there is growing recognition among soil scientists that loess and other external soil and nutrient sources play an important role in soil development on lava flows (e.g., Wells et al., 1985; Chadwick et al., 1999; Vaughan and McDaniel, 2009; Ferrier et al., 2011; Vaughan et al., 2011).

Although lava is by far the most common substrate in most regions of active volcanism, there have been many more studies of plant colonization and species succession on explosive volcanic deposits (e.g., Hansen, 1942; Taylor, 1957; Clarkson, 1990; Halpern et al., 1990; Whittaker et al., 1992; del Moral and Wood, 1993; Grishin et al., 1996; Tsuyuzaki and Hase, 2005; Lindig-Cisnerosa et al., 2006; Marler and del Moral, 2011) than on lava flows (Roach, 1952; Drake, 1992; Drake and Mueller-Dombois, 1993; Kitayama et al., 1995; Aplet et al., 1998; Cutler et al., 2008). Similar to soil development studies, we note that the vast majority of studies of plant colonization and species succession on lava flows are also concentrated in Hawaii using similar chrono- and climatic sequences. These studies relate ecological metrics, such as species diversity, individual species density, and individual plant characteristics (e.g., diameter at breast height, DBH), to controlling variables such as substrate age, precipitation, and temperature. Precipitation appears to be the dominant control on plant community composition (Aplet et al., 1998) and seed availability is not a limiting factor for plant establishment on lava flows (Drake, 1992). It has also been recognized that lava flows covered by volcanic ash tend to have bigger trees than lava flows without ash cover (Drake and Mueller-Dombois, 1993; Kitayama et al., 1995). Studies of the processes and mechanisms that initiate vegetation colonization of lava flows in non-tropical environments are limited (Rejmánek et al., 1982; Bernhardt, 1986; Fridriksson, 1987; Bashan, 2002) and generally consist of an inventory of plants present on a specific lava flow or flow field.

Numerous studies have examined basaltic landscape weathering rates by analyzing groundwater and river discharge chemistry (e.g., Louvat and Allègre, 1997;

Aiuppa et al., 2000; Dessert et al., 2003; Das et al., 2005), and by quantifying degree of weathering in both basaltic clasts of known ages (e.g., Eggleton et al., 1987; Navarre-Sitchler and Brantley, 2007) and basaltic clasts artificially weathered in laboratory settings (e.g., Oelkers and Gislason, 2001; Gislason and Oelkers, 2003). As compiled in Navarre-Sitchler and Brantley (2007), inferred watershed-scale weathering rates of basaltic landscapes range from 4 to 152 ton km^{-2} yr^{-1}, and natural weathering front advance rates based on cations range from 0.006 to 362 mm^3 mm^{-2} ky^{-1}. Available surface area drives overall weathering rates as weathering fronts propagate inward (Navarre-Sitchler and Brantley, 2007). These studies investigate the overall rate of basaltic rock dissolution, which we will argue is a less important factor for soil and plant development immediately following lava flow emplacement.

We briefly note ecologic and soil development studies of volcanic material within the Cascade Range, the setting for our research; the majority of these studies concern explosive deposits. Considerable work has focused on plant succession of the explosive 1980 Mount St Helens eruption (e.g., Halpern et al., 1990; del Moral and Wood, 1993; Dale et al., 2005), and some studies have examined plant succession following the cataclysmic early Holocene Mount Mazama eruption that formed Crater Lake (e.g., Hansen, 1942). Other studies have investigated plant succession of and species assemblage on Holocene lahars (volcanic mudflows) and rock avalanches at Lassen Volcanic National Park (e.g., Heath, 1967; Kroh et al., 2000; Kroh et al., 2008). At these reworked volcanic deposits, the nature of the substrate appears to be key for dictating species establishment, with finer grained deposits (e.g., a 1915 Lassen lahar)

demonstrating greater capacity for plant establishment and survival than blocky deposits (e.g., a 1650 AD rock avalanche).

In this study we will identify and examine the factors contributing to soil development and plant establishment and survival on very young lava flows in the temperate climate of the central Oregon Cascades. We will argue that external sediment sources, not *in situ* weathering, form soil, and that while plants can grow on bare lava, plant establishment and growth is greatly promoted in places where external sources have deposited a soil-like substrate on the lava. We will show that disparate processes can deliver soil to lava flows, notably floods and/or debris flows, syn- and post- eruptive explosive volcanic activity, and aeolian processes. As soil development and vegetation cover are commonly used as a geologic mapping tool to determine relative ages, understanding factors that lead to soil development and plant colonization of lava flows will also improve geologic understanding of landscape evolution.

2. Study areas

We examined vegetation and soil development at two sites with young lava flows in the central Oregon Cascades: the Collier Cone lava flow and the southern Sand Mountain Volcanic Field (SMVF; see Chapter II Fig. 1 and Chapter III Fig. 1 for location maps). These sites were selected due to the availability of high resolution (1 m) research grade Light Detection and Ranging (LiDAR) data and the apparent difference in external sediment sources, namely water-transported glacial sediments (Collier), and syn- or post-lava flow emplacement tephra air fall (SMVF). Both are located within the High Cascades, a region that has been volcanically active since the Pliocene and features a

high density of Quaternary mafic volcanic centers (Sherrod et al., 2002; Hildreth, 2007). The region was extensively glaciated during the Pleistocene (Sherrod et al., 2004), and presently the dominant wind direction is to the east and northeast. The selected sites consist of young post-glacial Holocene lava flows, and detailed geologic maps and geochemical data are available for both. Unfortunately, detailed soils maps are unavailable: both sites are within the Willamette National Forest, and the existing Willamette National Forest Soil Inventory Map maps the majority of both sites as "recent volcanic lava flows" (USDA, 2010). We focus on the portion of the study areas below 1300 m, which generally corresponds to a lowland temperate forest typical in the Pacific Northwest primarily consisting of *Pseudotsuga menziesii* (Douglas-fir), *Tsuga heterophylla* (western hemlock), and *Thuja plicata* (western red cedar; Franklin and Dyrness, 1992; Kilsgaard, 1999); we refer to this forest community as the DHC forest. In addition to LiDAR analyses, we conducted field surveys and characterized soil at both field areas.

2.1. Collier Cone lava flow

Collier Cone is located on the north flank of North Sister volcano in the central Oregon Cascades (Fig. 1). The Collier Cone eruption occurred 1511 (1354 – 1569) cal yr B.P. (Sherrod et al., 2004) and produced a scoria cone (elevation 2150 m), a tephra blanket to the northeast, and a ~10 km^2 lava flow comprising of four units (Schick, 1994; Mckay, 2012; Deardorff and Cashman, in revision; Fig. 1a). The entire eruption probably lasted less than one year (Deardorff and Cashman, in revision). The lava flows are blocky basaltic andesite to andesite in composition (Schick, 1994; Deardorff and Cashman, in

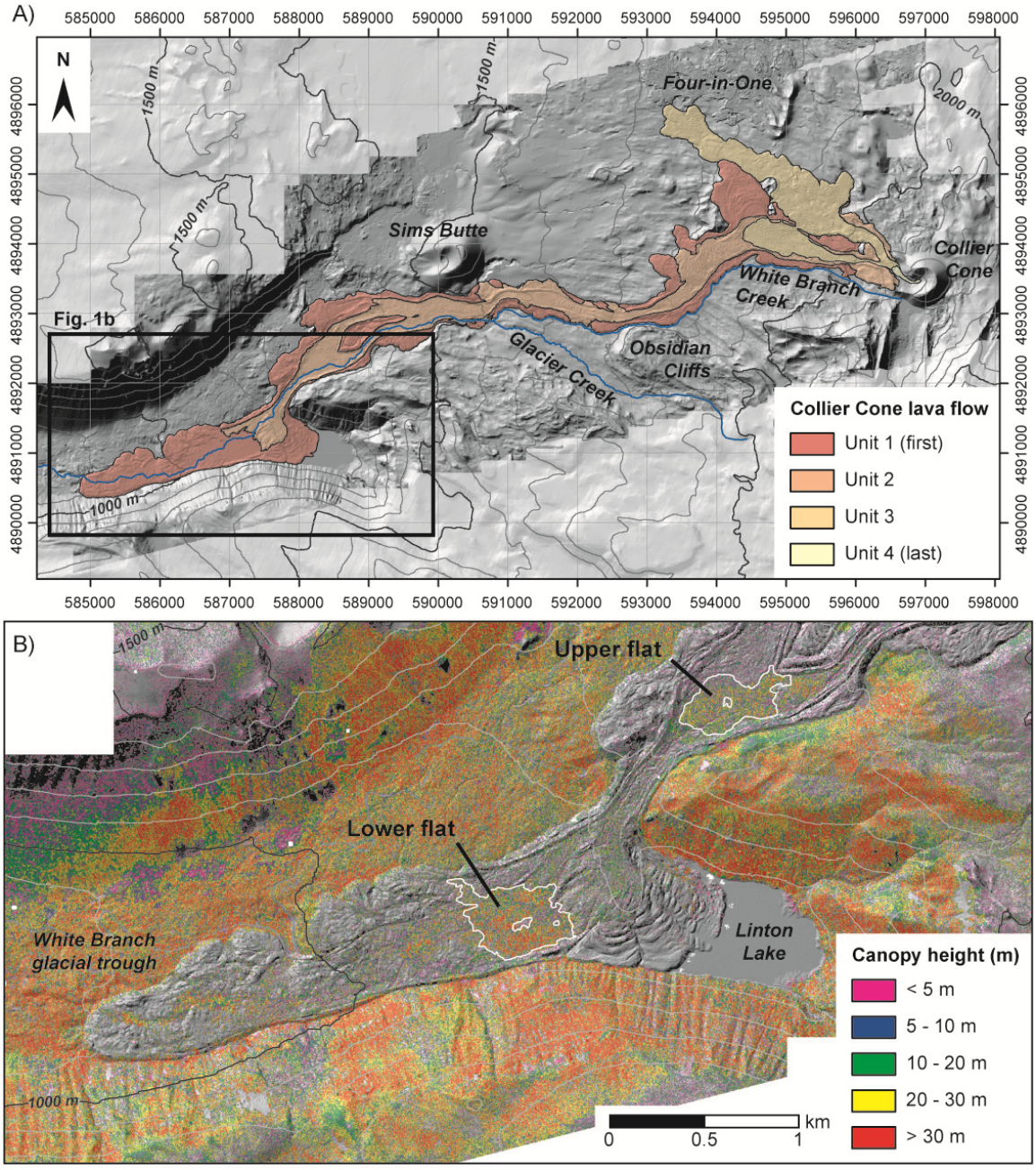

Fig. 1. (A) Overview geologic map of the Collier Cone lava flow showing extent of Units 1 through 4 after Deardroff and Cashman (in revision). Grid spacing is 1 km with labeled UTM zone 10N coordinates. Basemap is a LiDAR-derived shaded relief map where available and a 10 m shaded relief map elsewhere. 100 m contour intervals are show, with bold 500 m contour intervals. White Branch and Glacier creeks are indicted in blue, and geographic features are labeled. Box shows the extent of Fig. 1B. (B) LiDAR-derived shaded relief and canopy map. The upper and lower flats on the Collier Cone lava flow are outlined in white.

revision) and emerged from the base of the scoria cone and traveled westward, traversing the High Cascades. The first lava flow units emplaced, Units 1 and 2, descended into the White Branch glacial trough; the flow toe of the furthest traveled Unit 1 is 1250 m lower than the Collier Cone vent at an elevation of 900 m. Across the majority of the lava flow, the lava appears fresh with little evidence of physical or chemical weathering; primary flow features are obvious with few signs of post-emplacement modifications.

A peculiarity of the Collier Cone lava flow is that despite its young age, a bedrock channel, the White Branch Creek, has incised into the lower part of the lava flow (Fig. 1a). The White Branch channel starts at the glacial lake at the terminus of the retreating Collier Glacier adjacent to Collier Cone. The channel follows the southern margin of the Collier Cone lava flow until an elevation of ~1500 m, where it migrates onto the flow. The upper portion of the channel is dry; the White Branch is presently fed by Glacier Creek and snowmelt. Apart from brief periods of high snowmelt and/or rainfall, no water flows on the surface of the lava flow. However, reports of catastrophic glacial outburst floods from Collier Glacier in historic and prehistoric times (O'Connor et al., 2001) suggest that for brief episodes, the White Branch can carry a heavy sediment load. Two areas within the Collier Cone lava flow appear to be localized areas of sediment deposition, as primary lava flow features are absent and the areas are quite smooth in bare earth (last return) LiDAR derived imagery (Fig. 1b). The higher elevation site (~1250 m) we informally refer to as the upper flat and is situated within lava flow Unit 2, while the lower elevation site (~1050 m) we informally refer to as the lower flat and is situated within lava flow Unit 1. Whereas the lower flat is mapped in the Willamette National Forest Soil Inventory as "recent volcanic lava" (map unit 4), the upper flat coincides with

an area mapped as recent lava flows with shallow, coarse-textured gravelly cobbly stony soil (map unit 62; USDA, 2010).

2.2. Sand Mountain Volcanic Field

The Sand Mountain Volcanic Field (SMVF) is located roughly 25 km northwest of Collier Cone between and west of Mount Jefferson and Mount Washington (Fig. 2). It is part of the upper McKenzie River watershed and borders Clear Lake, the source of the McKenzie River. The SMVF consists of a chain of cinder cones and associated lava flows and tephra blankets; the activity occurred ~3 ka (see Chapter II). The local topography directed lava flows westwards (downhill), while wind deposited tephra to the northeast (downwind; Mckay, 2012).

We examined three lava flows in the southern SMVF, which we informally refer to as the Cold Water Cove, Clear Lake South, and Clear Lake East lava flows (Fig. 2), listed from oldest to youngest based on field relations. As discussed in Chapter II, these lava flows have distinct chemical compositions and are distinguishable from each other in hand sample on the basis of the petrographic texture and the size and concentration of olivine and plagioclase crystals (see Table 4 in Chapter II). Age constraints (see Chapter II) indicate that no more than a few decades separate the Cold Water Cove (oldest) and Clear Lake East (youngest) lava flows of the southern SMVF. The Willamette National Forest Soil Inventory Map maps the majority of the Clear Lake East flow as lava (map unit 4), with a strip within the lava flow as shallow, coarse-textured gravelly cobbly stony soil (map unit 62), and the Clear Lake South and Cold Water Cove lava flows as a mix of map unit 62 and coarse-textured gravelly soil on smooth to somewhat uneven glaciated

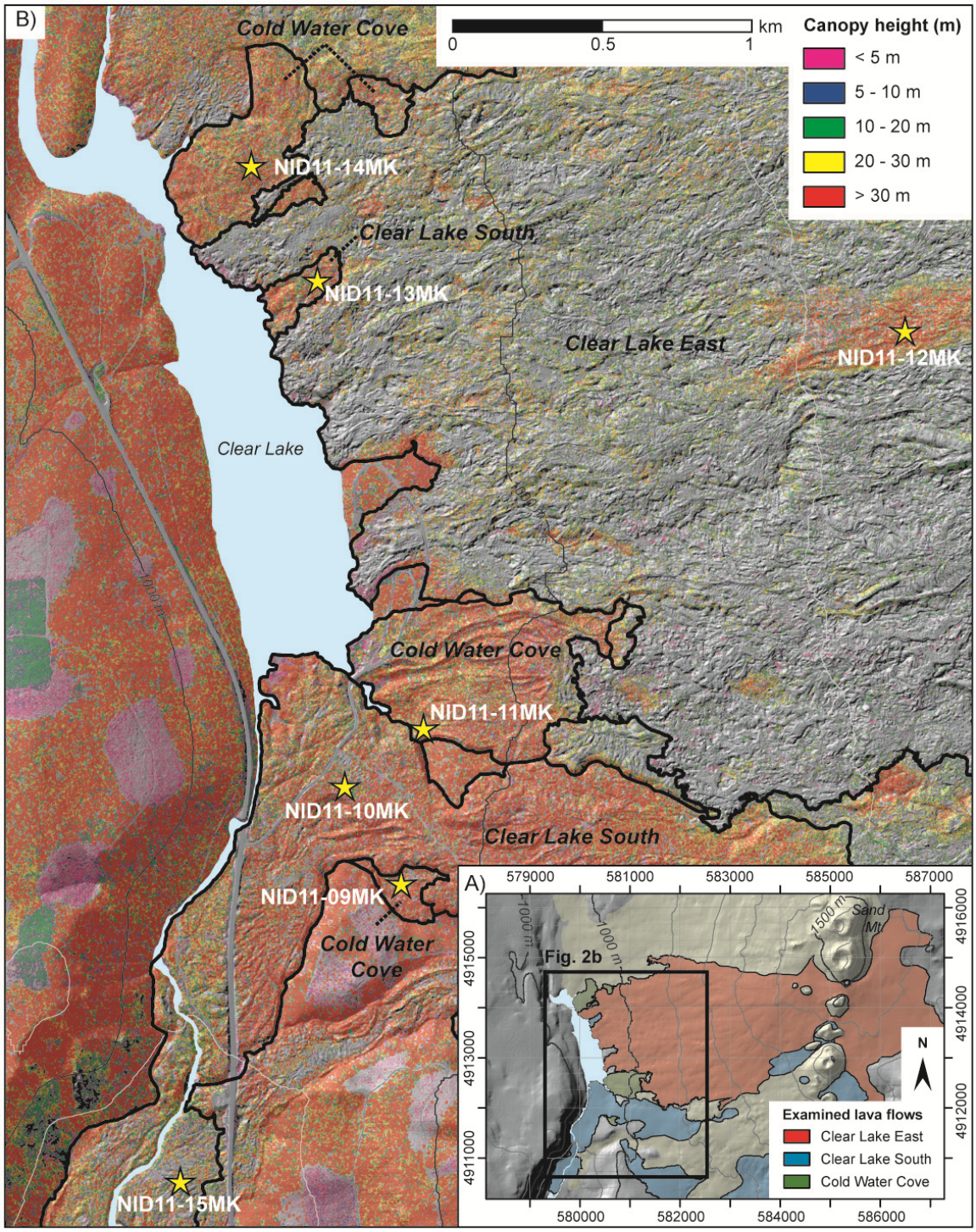

Fig. 2. (A) Overview geologic map of the southern SMVF showing the extent of the Cold Water Cove, Clear Lake South, and Clear Lake East lava flows. Grid spacing is 1 km with labeled UTM zone 10N coordinates. Basemap is a 10 m shaded relief map. 100 m contour intervals are show, with bold 500 m contour intervals. Box shows the extent of Fig. 2B. (B) LiDAR-derived shaded relief and canopy map. Studied lava flows are outlined in black, and soil pit locations are indicated with stars.

lava flows (map unit 66; USDA, 2010); we note that these lava flows are post-glacial and therefore un-glaciated.

3. Methodology

3.1. LiDAR analyses

We use 1 m gridded research grade LiDAR data of the Collier Cone region and the southern SMVF to construct a high resolution canopy map by taking the difference between unfiltered (i.e., first return) and filtered (i.e., bare earth) elevations. We map the canopy heights using six classes (bare earth, ≤ 5.0 m, 5.1 – 10.0 m, 10.1 – 20.0 m, 20.1 – 30.0 m, and > 30.0 m). We examine tree density by quantifying bare earth exposure. We calculate the bare earth exposure value of each pixel by constructing a window extending 20 m in each cardinal direction (total window size 41 x 41 m) and tallying the number of data points within the window where the unfiltered LiDAR value is equal to the filtered LiDAR value (see Chapter III). Areas with high exposure values have sparse vegetation and conversely areas with low exposure values have dense vegetation. We arbitrarily designated dense, moderate, low, and sparse vegetation density as pixels with ≤ 10%, 11 – 50%, 51 – 89%, and ≥ 90% bare earth exposure values, respectively.

At the Collier Cone lava flow, we examine canopy height trends and bare earth exposure to characterize the forest adjacent to the lava flow along with the forest (or lack of) on different parts of the lava flow. At the SMVF, we compare canopy height trends and bare earth exposure at the Cold Water Cove, Clear Lake South, and Clear Lake East lava flow.

3.2. Fieldwork

We conducted field campaigns at the Collier Cone lava flow and in the southern SMVF to map soil depth and characterize soil by hand digging soil pits and describing and sampling soil horizons. We determined soil depth using an auger (maximum augerable clast size ~ 3 cm), and used a handheld GPS to locate auger hole and soil pit locations (location error generally < 10 m). Within soil pits, we identified horizons on the basis of color and textural differences and named horizons according to layer depth, with 'a' referring to the litter layer, 'b' the horizon immediately underneath, and so on; sample names do not reflect whether the horizon is an O, A, B, or C horizon but rather stratigraphic position.

We noted tree species and general observations during fieldwork, although did not undertake a systematic tree survey. We cored and aged several Douglas-fir trees with ~75 cm DBH growing on the lower flat of the Collier Cone lava flow using standard dendrochronologic methods (Phipps, 1985; Grissino-Mayer, 2001).

3.2.1. Collier Cone lava flow

We conducted a systematic survey of soil depth across both the upper and lower flats of the Collier Cone lava flow; away from these two areas there is scant or no soil cover on the lava flow – bare lava is exposed. Where feasible, we augered every 50 to 100 m in a grid pattern. Where it was unclear that the base of the soil (i.e., the top of the underlying lava flow) was reached, a '>' precedes the depth measurement.

We next hand-dug two soil pits in the lower flat. Soil pit NID11-07CC is situated within 20 m of the White Branch at the eastern end of the lower flat just below a notable

break in slope. Time and manpower constraints precluded digging to the basal contact with the underlying lava flow. We sampled each exposed soil horizon, field-sieving samples to obtain the < 2 mm fraction where the horizon included coarser material. Soil pit NID11-08CC is located in the northwest part of the lower flat away from the White Branch in a slightly protected area; a lava flow ridge is visible immediately southwest of the pit. We were able to extend this second pit to the base of the soil column, and sampled representative soil horizons.

We conducted a pebble count in the White Branch channel connecting the two flats. Following standard procedures (Wolman, 1954), we randomly selected 100 pebbles, measured each along their intermediate axis, and categorized each on the basis of rock type and degree of roundness.

3.2.2. Sand Mountain Volcanic Field

At the SMVF, we hand-dug soil pits on each of the three studied lava flows; in every case we reached the base of the soil (i.e., the top of the lava flow) and sampled every horizon below the litter layer. In this portion of the SMVF, the Cold Water Cove lava flow is the oldest lava flow and has been covered by subsequent flows; it is presently only exposed in four areas (Fig. 2). We dug soil pits on three of the Cold Water Cove lava flow exposures, and dug an additional three soil pits on the Clear Lake South lava flow, one at an isolated exposure on the eastern side of Clear Lake and two south of Clear Lake; one of the two southern sites (NID11-15MK) is within a topographically protected area. We dug a final soil pit on the Clear Lake East lava flow in an peculiar area with considerable fine-grained material (mapped as shallow, coarse-textured gravelly cobbly

stony soil in the Willamette National Forest Soil Inventory Map; USDA, 2010); we note that apart from this area there is no soil cover on the Clear Lake East lava flow.

3.3. Estimate of sediment volume in the Collier Cone lava flow flats

We constructed a 10 m grid depth model of soil on both the upper and lower flats on the Collier Cone lava flow using the natural neighbor interpolation method in ArcGIS. We estimated soil volume by integrating the soil depth model and rounding down to the nearest 1000 m^3. Input data consisted of (1) auger measurements and (2) soil "depths" of 0 cm spaced on a 10 m grid in areas of exposed lava both within and surrounding the flats. The natural neighbor method uses Voronoi polygons to assign a value at a grid point based on area-weighted contribution of the nearest data points (Sibson, 1981). We selected this method because it (1) effectively deals with data that are not uniformly distributed, (2) does not create artificial peaks or lows, and (3) assigns grid values based on the nearest data without having to assign a data input radius. Given that a considerable fraction of the depth measurement data was an lower estimate of depth, the volume estimates provide a lower bound for the actual values.

3.4. Soil characterization

We prepared soil samples according to standard procedure (Burt, 2009). We determined soil color for both field moist and dried samples using a Munsell soil color chart, and determined soil texture using the hydrometer method (Burt, 2009). We pre-treated three samples with hydrogen peroxide to remove organic matter, however, due to concerns that the pre-treatment would fragment fragile soil particles, we did not pre-treat

additional samples. We determined organic content with loss on ignition (LOI) using standard procedures (Dean, 1974; Heiri et al., 2001). LOI analyses were conducted both at the University of Oregon (Collier Cone samples; reported values are the average of three measurements) and Washington State University at Pullman (SMVF samples).

We determined sample chemistry using x-ray fluorescence (XRF); we selected this method as geochemical data for the Collier Cone lava flow and the SMVF were acquired using this technique. Additionally, we analyzed two samples of bulk tephra for a known SMVF tephra. We compared soil sample chemistry to available geochemical data for underlying lava flows.

4. Results

4.1. LiDAR analyses

The Collier Cone lava flow LiDAR canopy map and bare earth exposure analysis (Figs. 1b and 3a) reveal that the c. 1.5 ka lava flow has shorter trees and less overall vegetation (i.e., greater bare earth exposure) than its surroundings. This trend is observed in both DHC forest regions that are the subject of this study and in higher elevation montane forests (see Chapter III). Notably, ~95% of the adjacent DHC forest consists of dense or moderate vegetation cover relative to ~51% for the lava flow. The two flats provide notable exceptions to the general trend; here tree height and vegetation density is similar to the adjacent DHC forest (Fig. 3a).

In the southern SMVF the DHC forest density on the c. 3 ka Cold Water Cove and Clear Lake South lava flows is similar to a typical DHC forest. While we did not analyze the adjacent forest due to widespread logging off of Holocene lava flows (visibl

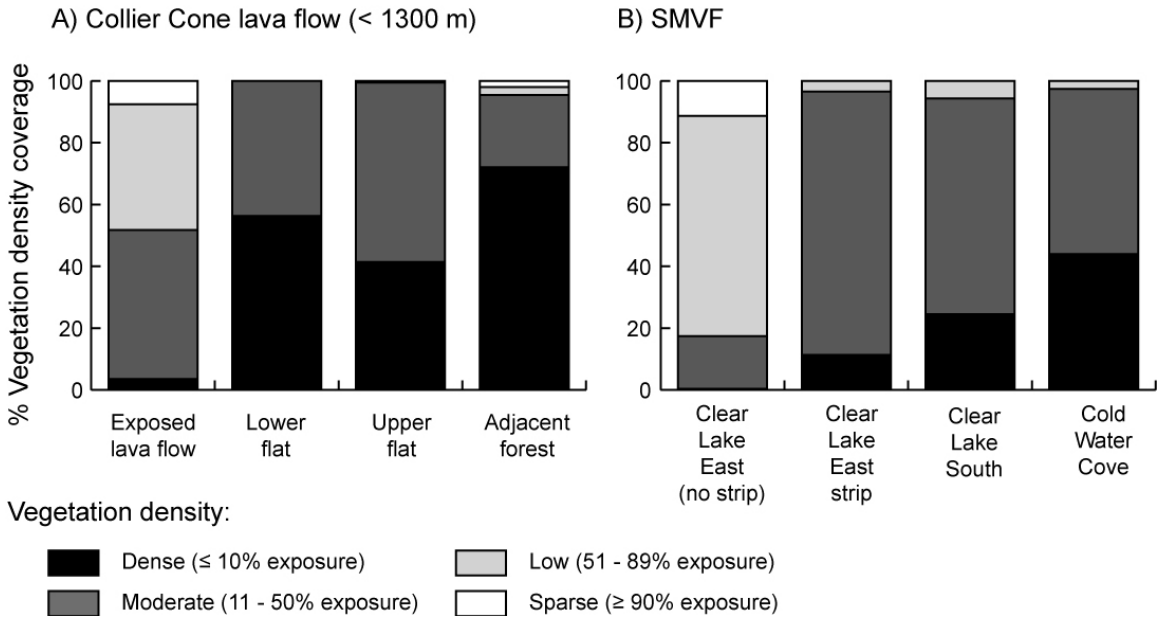

Fig. 3. Stacked histogram plot showing percent of pixels with dense, moderate, low, and sparse vegetation density for regions in the (A) Collier Cone lava flow and (B) SMVF study areas.

in Fig. 2b), the forest on these two lava flows is similar to the adjacent forest at the Collier Cone site, with ~97% (Cold Water Cove) and ~94% (Clear Lake South) dense and moderate vegetation cover (Figs. 2b and Fig. 3b). In contrast, trees on the Clear Lake East lava flows are notably shorter and there is considerably more bare earth exposure, despite an age difference of a few decades with the older southern SMVF lava flows (see Chapter II). Interestingly, a linear strip of increased vegetation density is observable in the center of the Clear Lake East lava flows (Fig. 2b); aerial photographs (not shown) outside the LiDAR coverage shows that this strip extends towards the vent area.

4.2. Collier Cone lava flow

Field observations confirm that the forest assemblage on and adjacent to the Collier Cone lava flow is characteristic of a DHC forest. In general, trees in the upper flat

have smaller DBHs than those in the lower flat. Regions of downed trees, likely related to past windstorms, were found in places in the upper flat. In the lower flat, numerous trees (generally Douglas-fir) have DBH > 1 m; the maximum measured DBH was a 2.4 m diameter Douglas-fir tree (see Fig. 4b). Dendrochronological results yield a maximum age close to 300 years for DBH ~75 cm Douglas-fir trees (Table 1). In the lower flat, western red cedar is common near the surface expression of the White Branch and rare elsewhere. In general, the upper flat is dryer and has less undergrowth than the lower flat. In both locations, the White Branch Creek has clear surface expression, with an active channel bed and well-defined banks. Although the creek was dry at the time of the field campaigns, it carries surface water during times of heavy rain and/or snowmelt.

Table 1
Oldest identified tree ring for trees cored on the Collier Cone lava flow within the lower flat near soil pit NID11-07CC. The pith was not reached in any core, so the cored trees are at least as old as the age provided.

Tree ID	DBH (cm)	Core length (cm)	Youngest possible age
ALE 16	84	23	1923 AD
ALE 17	72.5	27	1909 AD
ALE 18	67.5	26	1905 AD
ALE 19	65	27	1718 AD
ALE 20	68	31	1797 AD
ALE 21	76	29	1718 AD
ALE 22	89.5	32	1734 AD
ALE 23	81.5	32	1762 AD
ALE 24	71	28	1717 AD
ALE 25	63.5	29	1710 AD
ALE 26	70.5	29	1709 AD
ALE 27	73.5	29	1725 AD
ALE 28	72	32	1699 AD
ALE 29	87	29.5	1712 AD
ALE 30	86.5	34	1722 AD

Auger soil depth measurements of the upper (Fig. 4a) and lower (Fig. 4b) flats reveal that a considerable amount of material covers the 1.5 ka lava flow, with maximum soil depths of 188 and 318 cm, respectively. Moreover, it is unlikely that the base of the soil (i.e., the lava flow surface) was reached in numerous sites (indicated with '>' before depth measurement on Fig. 4); at these sites the large grain size (gravel or coarser) and unconsolidated nature of the material made it impossible to auger deeper. Sites near the surface expression of the White Branch were often more gravelly than those further away. Minimum volume estimates for the material covering the upper and lower flats based on the auger soil depth measurements are 56,000 and 138,000 m^3, respectively.

4.2.1. Soil pit NID11-07CC

Soil pit NID11-07CC (dimensions 102 cm x 80 cm x 50 cm) is located close to the White Branch at the eastern end of lower flat (Fig. 4b); field data and physical characteristics are summarized in Tables 2 and 3, respectively. Time and manpower constraints precluded digging to the surface of the Collier Cone lava flow. In addition to the litter layer (NID11-07CCa), we excavated four "soil" horizons. Horizons NID11-07CCb and NID11-07CCe are relatively fine-grained with identifiable soil structures and many or few roots, respectively. Interestingly, the top of NID11-07CCe (88 cm depth) is capped with a thin (< 0.5 cm) light wood-like layer. In contrast, horizons NID11-07CCc and NID11-07CCd have few or no roots, respectively, and by volume are primarily cobbles and gravels with additional occasional boulders in NID11-07CCd. Horizon NID11-7CCc is matrix-supported, while NID11-07CCd is clast supported; both samples were field-sieved to sample the ≤ 2 mm soil fraction. The soil fraction of all the samples

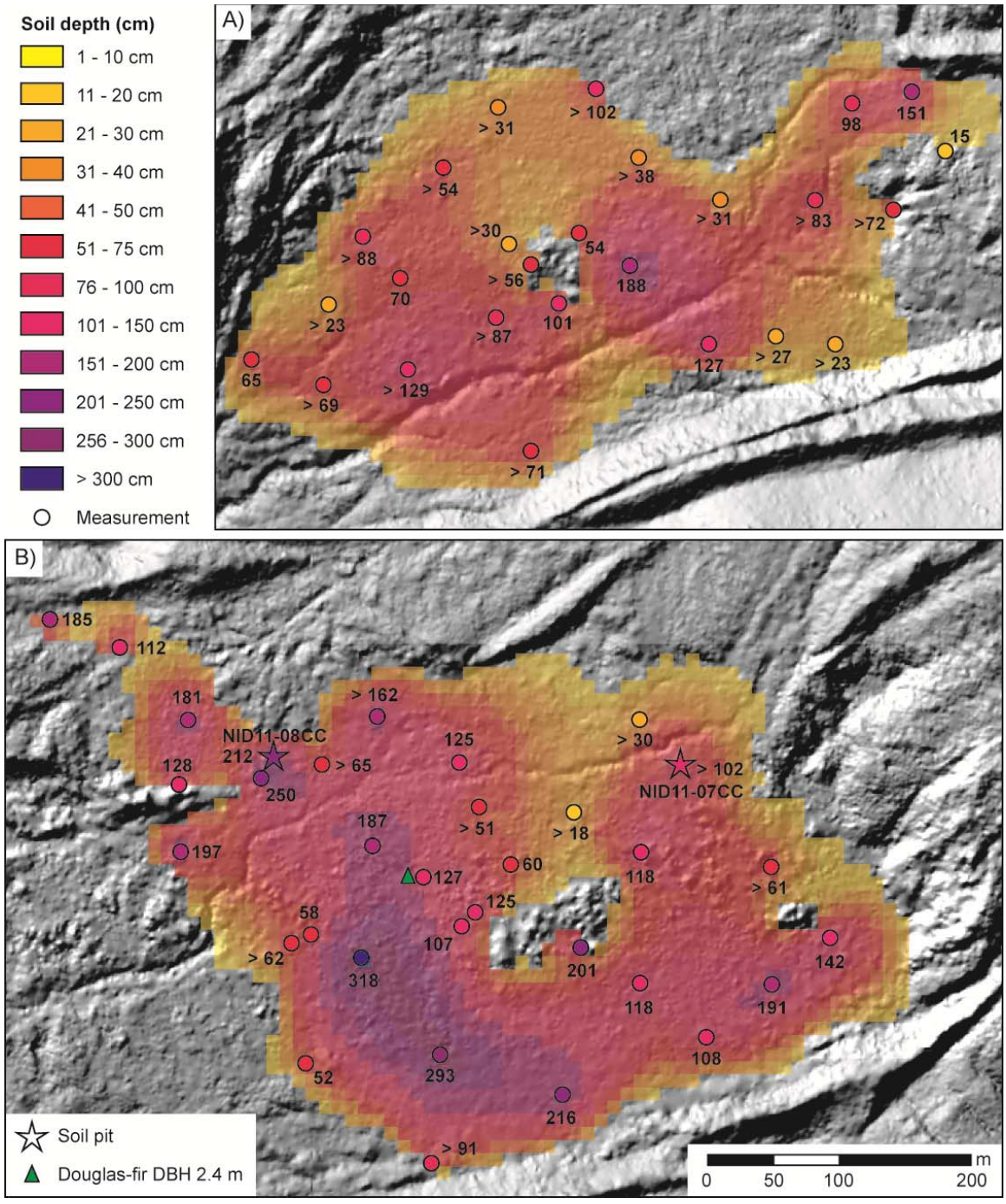

Fig. 4. Map showing augered soil depth measurements in cm for the (A) upper and (B) lower flats of the Collier Cone lava flow, underlain by a soil depth model for both areas; the basemap is a 1 m LiDAR-derived shaded relief map. The color scheme and the scale is the same for both flats. Measurements where it is unlikely that the base of the soil column was reached are indicated with '>'. In (B) the location of the two Collier Cone lava flow soil pits are indicated along with the location of a DBH 2.4 m Douglas-fir tree.

Table 2
Field data for the Collier Cone lower flat and the SMVF soil pits. Location reported in UTM Zone 10N, datum WGS 1984. An asterisk (*) indicates a horizon was sampled, while a double asterisk (**) indicates the sample was field sieved for the soil fraction (< 2 mm). Unless otherwise noted, boundaries between horizons are abrupt and linear.

Soil Pit	Location	Name	Depth	Horizon	Field Notes
NID11-07CC	Collier Cone	A	0 to 5 cm	Oi	Mostly needles, negligible decomposition
	E0587280, N4891217	B*	5 to 19 cm	A or A1	Mostly sand, slightly moist
	Error: ±7m				Granular, weak to moderate structure, friable
					Many very fine, fine, and medium roots
					Distinct wavy boundary between horizons A and C1
		C**	19 to 39 cm	C1	Matrix supported gravel (2 – 40 mm diameter)
					Gravel rounded to subrounded basaltic andesite, obsidian, high silica lava
					Few fine, medium, and coarse roots
					Gradual wavy boundary between horizons C1 and C2
		D**	39 to 88 cm	C2	Clast supported gravel and cobbles (2 – 200 mm diameter), same compositions as horizon C1
					Capped by cobbles
					Cobbles are basaltic andesite and high silica lava; largest clasts high silica lava
					Local void space (no matrix) at ~74 cm depth
					No roots
		E*	88 to 102 cm	A2 or C3	Sand, very similar to horizon A
					Capped by thin beige layer that appears to be wooden
					Few fine roots
					Distinct wavy boundary between horizons A2 and C3
		F	> 102 cm	C3 or C4	Resembles horizon C1

NID11-08CC	Collier Cone E0586972, N4891220 Error: ±7m	A	0 to 5 cm	Oi	Many fine and moderate roots, common very coarse roots
		B*	5 to 22 cm	C1	Many moderate roots and common very coarse roots at boundary with horizon Oi, common moderate and very coarse roots below boundary Well sorted sand, friable Occasional medium gravel (1 cm)
		C*	22 to 36 cm	C2	Well sorted fines, firm Occasional lenses of sand Few fine, medium, and coarse roots
		D	36 to 39 cm	C3	Well sorted sand, friable
		E	39 to 40 cm	C4	Well sorted fines, firm
		F	40 to 42 cm	C5	Well sorted sand, friable
		G	42 to 45 cm	C6	Well sorted fines, firm
		H*	45 to 51 cm	C7	Well sorted sand, friable
		I*	51 to 57 cm	C8	Well sorted fines, firm
		J*	57 to 64 cm	C9	Well sorted sand, friable, few fine roots
		K*	64 to 85 cm	C10	Well sorted fines, firm, few fine roots
		L	85 to 90 cm	C11	Mixture of sand and fines, few fine roots
		M	90 to 100 cm	C12	Well sorted fines, firm
		N	100 to 104 cm	C13	Well sorted sand, friable
		O	104 to 107 cm	C14	Well sorted fines, firm
		P	107 to 108 cm	C15 or A	Resembles buried and compressed O horizon
		Q	108 to 123 cm	C15 or C16	Well sorted fines, firm
		R	123 to 212 cm	C16 or C17	Undifferentiated alternate layers of well sorted friable sand and firm fines
		S	> 212 cm	R	Collier Cone lava flow

NID11-09MK	Cold Water Cove	A	0 to 4 cm	Oi	Litter layer
	E0589612, N4911796	B*	4 to 34 cm	C1	Brown tephra
	Error: ±7m				Slightly indurated at top of horizon but easy to dig through
					Gradual boundary over 5 cm between horizons C1 and C2
		C*	34 to 64 cm	C2	Dark tephra
					Harder to dig through than horizon C1
		D	> 64 cm	R	Cold Water Cove lava flow
NID11-10MK	Clear Lake South	A	0 to 5 cm	Oi	Litter layer
	E0580429, N4912093	B**	5 to 34 cm	C	Tephra between gravel and cobble sized lava clasts
	Error: ±7m				Few very coarse roots
		C	> 34 cm	R	Clear Lake South lava flow
NID11-11MK	Cold Water Cove	A	0 to 5 cm	Oi	Litter layer
	E0580681, N4912272	B*	5 to 40 cm		Brown tephra
	Error: ±14m	C*	40 to 55 cm		Dark tephra
		D	> 55 cm		Cold Water Cove lava flow
NID11-12MK	Clear Lake East	A	0 to 2 cm	Oi	Litter layer with a few thin needles and grass
	E0582315, N4913621	B*	2 to 50 cm	C1	Light brown tephra
	Error: ±7m				Many fine and medium roots, common fine roots
		C*	50 to 184 cm	C2	Dark brown tephra with olivine
					Indurated at top of horizon
					Few coarse roots
		D	> 184 cm	R	Clear Lake East lava flow

NID11-13MK	Clear Lake South	A	0 to 7 cm	Oi	Litter layer with gravel sized lava or scoria clasts
	E0580347, N4913784	B*	7 to 30 cm	C	Brown tephra with some gravel sized clasts
	Error: ±7m				Common moderate roots
		C*	> 30 cm	R	Clear Lake South lava flow
NID11-14MK	Cold Water Cove	A	0 to 5 cm	Oi	Litter layer
	E0580116, N4914170	B*	5 to 40 cm	C	Brown tephra
	Error: ±7m	C	> 40cm	R	Cold Water Cove lava flow
NID11-15MK	Clear Lake South	A	0 to 5 cm	Oi	Litter layer
	E0579896, N4910760	B**	5 to 26 cm	C	Brown tephra with cobbles of lava
	Error: ±7m	C	> 26 cm	R	Clear Lake South lava flow

Table 3
Physical characteristics of samples collected from soil pits on the Collier Cone lower flat and the SMVF. An asterisk (*) denotes the sample was pretreated with H_2O_2 prior to the textural analysis. Carbon LOI analyses were done at the University of Oregon (Collier Cone lava flow) and Washington State University Pullman (SMVF).

	Texture (< 2 mm size fraction)					Munsell soil color	
Sample Name	Texture	% Sand	% Silt	% Clay	% Carbon	Moist	Dry
NID11-07CCb	Sand*	87	12	1	1.34	Dark reddish brown [5YR 2.5/2]	Brown [7.5YR 4/2]
NID11-07CCc	Sand	96	3	1	1.10	Black [10YR 2/1]	Grayish brown [10YR 5/2]
	Sand*	91	8	1			
NID11-07CCd	Sand*	95	4	1	0.60	Black [5YR 2.5/1]	Reddish gray [2.5YR 5/1]
NID11-07CCe	Sand	91	7	2	0.90	Very dark gray [7.5YR 3/1]	Reddish gray [2.5YR 5/1]
NID11-08CCb	Sand	90	9	1	1.22	Very dark gray [10YR 3/1]	Dark reddish gray [2.5YR 4/1]

NID11-08CCc	Silt loam	28	61	11	1.05	Black [7.5YR 2.5/1]	Dark gray [10YR 4/1]
NID11-08CCh	Sand	99	0	1	0.40	Black [10YR 2/1]	Dark reddish gray [2.5YR 4/1]
NID11-08CCi	Silt loam	37	57	6	0.62	Very dark gray [10YR 3/1]	Gray [10YR 5/1]
NID11-08CCj	Sand	98	1	1	0.35	Black [10YR 2/1]	Dark reddish gray [2.5YR 4/1]
NID11-08CCk	Silt loam	27	64	9	0.97	Very dark gray [10YR 3/1]	Grayish brown [10YR 5/2]
NID11-09MKb	Sand	88	8	4	4.72	Very dark grayish brown [10YR 3/2]	Dark yellowish brown [10YR 4/4]
NID11-09MKc	Sand	91	8	1	2.90	Dark reddish brown [5YR2.5/1]	Brown [10YR 4/3]
NID11-10MKb	Sand	94	4	1	6.90	Dark yellowish brown [10YR 3/4]	Yellowish brown [10YR 5/4]
NID11-11MKb	Sand	91	8	1	5.70	Dark brown [10YR 3/3]	Dark yellowish brown [10YR 4/4]
NID11-11MKc	Sand	96	3	1	1.15	Very dark brown [10YR2/2]	Dark gray [10YR 4/1]
NID11-12MKb	Sand	94	4	2	2.77	Very dark brown [10YR2/2]	Dark yellowish brown [10YR 3/4]
NID11-12MKc	Sand	97	2	1	0.95	Black [10YR2/1]	Black [2.5YR 2.5/1]
NID11-13MKb	Loamy sand	78	17	5	7.11	Dark brown [7.5YR 3/3]	Yellowish brown [10YR 5/4]
NID11-14MKb	Sand	88	10	2	4.66	Very dark brown [10YR2/2]	Yellowish brown [10YR 5/4]
NID11-15MKb	Loamy sand	84	11	5	7.70	Dark brown [10YR 3/3]	Brown [7.5YR 3/1]

is in the sand textural class. LOI analyses indicate that every sampled layer has very low (<1.5%) carbon content.

4.2.2. Soil pit NID11-08CC

Soil pit NID11-08CC is located in the northwest portion of the lower flat away from the surface exposure of the White Branch (Fig. 4b); field data and physical characteristics are summarized in Tables 2 and 3, respectively. The pit extended to the top of the Collier lava flow at a depth of 212 cm. In addition to the litter layer (NID11-08CCa), eighteen "soil" horizons were excavated. In contrast to soil pit NID11-07CC, soil pit NID11-08CC contained no horizons containing clasts with diameters exceeding 2 mm. Horizons alternate between coarse- and fine-grained layers (Fig. 5); six representative horizons were sampled. Textural analyses reveal that the coarse horizons are sand and the fine-grained horizons are silt loam (Table 3). A thin apparent buried litter layer was excavated at depth of 107 cm. Pit configuration and time constraints precluded characterizing the lowest portion of the pit (NID11-08CCr), but it appears to resembled the rest of the pit with alternating layers of coarse and fine particles. LOI analyses indicate that every sampled layer has very low (<1.5%) carbon content.

4.2.3. Collier Cone lava flow geochemistry

Major element chemistry of samples from soil pits NID11-07CC and NID11-08CC (Table 4) is the same as typical basaltic andesite to andesite volcanic rocks. Trace element chemistry (Table 4) reveals trends in compatible and incompatible elements that are typical of volcanic rocks. Taking error into consideration, most major element

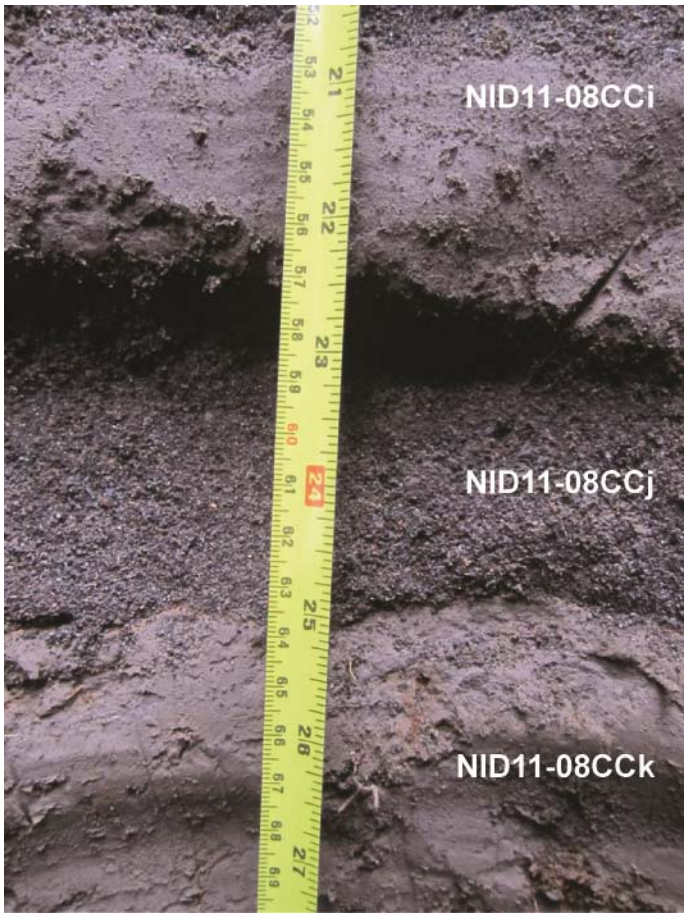

Fig. 5. Photograph of fine and coarse alternating layers present in soil pit NID11-08CC on the lower flat on the Collier Cone lava flow (Fig. 4b). All three layers shown here were sampled (see Tables 2 – 4). The photo spans a depth of 52 to 69 cm, and the measuring tape units are cm on the left and inches on the right.

chemistry (e.g., silica) is similar to the underlying Collier Cone lava flow (Fig. 6a) with a few exceptions (e.g., manganese and phosphorous concentrations are higher in the soil). A plot of two incompatible elements (elements that stay in the melt rather than go into crystals; Fig. 6b) show a similar trend between the soil samples and the underlying lava

Table 4 (next page)
Major and trace element chemistry of samples collected from soil pits on the Collier Cone lower flat and the Sand Mountain Volcanic Field (SMVF), in addition to two bulk tephra samples collected from the Sand Mountain tephra blanket. Chemistry determined by XRF at Washington State University Pullman.

Sample ID	NID11-07CCb	NID11-07CCc	NID11-07CCd	NID11-07CCe	NID11-08CCb	NID11-08CCc	NID11-08CCh	NID11-08CCi
Unnormalized major elements (wt. %)								
SiO_2	55.28	56.05	57.41	55.44	56.81	55.88	58.65	55.43
TiO_2	0.987	1.140	1.143	1.127	1.027	0.954	1.059	0.964
Al_2O_3	17.91	17.24	16.85	17.33	17.58	18.99	17.13	19.28
FeO*	6.58	7.61	7.41	7.51	6.55	6.32	6.74	6.27
MnO	0.123	0.140	0.143	0.138	0.128	0.118	0.133	0.119
MgO	3.92	4.39	4.18	4.56	3.32	3.31	3.16	3.52
CaO	6.84	6.88	6.36	6.90	6.45	7.46	5.95	7.77
Na_2O	4.13	4.15	4.37	4.10	4.45	4.34	4.67	4.23
K_2O	1.04	1.01	1.11	0.97	1.09	0.92	1.23	0.86
P_2O_5	0.238	0.254	0.275	0.240	0.252	0.220	0.267	0.214
Sum	97.05	98.86	99.24	98.32	97.66	98.50	98.99	98.66
Normalized major elements (wt. %)								
SiO_2	56.96	56.70	57.85	56.39	58.17	56.73	59.25	56.18
TiO_2	1.017	1.153	1.151	1.146	1.052	0.969	1.070	0.977
Al_2O_3	18.45	17.43	16.97	17.63	18.00	19.28	17.30	19.54
FeO*	6.78	7.70	7.46	7.64	6.70	6.42	6.81	6.36
MnO	0.127	0.141	0.144	0.141	0.132	0.120	0.135	0.121
MgO	4.04	4.44	4.21	4.64	3.40	3.36	3.20	3.57
CaO	7.05	6.96	6.40	7.01	6.61	7.58	6.01	7.88
Na_2O	4.26	4.20	4.40	4.17	4.56	4.40	4.71	4.28
K_2O	1.07	1.02	1.12	0.99	1.11	0.93	1.24	0.87
P_2O_5	0.245	0.257	0.277	0.245	0.258	0.223	0.270	0.216
Trace elements (ppm)								
Ni	57	65	62	67	40	40	37	43
Cr	66	66	59	66	49	53	44	58
Sc	19	23	20	20	20	19	19	20
V	142	156	148	154	130	132	124	138
Ba	352	373	401	354	392	352	436	339
Rb	17	16	17	14	17	13	19	12
Sr	523	495	463	504	488	569	453	586
Zr	124	146	164	140	155	130	174	121
Y	20	24	27	24	26	23	28	22
Nb	6.9	8.1	8.9	8.1	8.0	6.8	8.6	6.6
Ga	19	19	20	19	20	21	20	20
Cu	73	48	44	55	40	67	36	67
Zn	82	90	92	88	86	80	85	77
Pb	5	8	5	5	5	4	5	4
La	11	11	17	13	14	11	18	10
Ce	27	32	35	27	36	26	37	28
Th	2	2	1	2	2	2	2	1
Nd	17	19	21	19	20	17	20	17
U	1	0	2	1	3	1	1	0

Sample ID	NID11-08CCj	NID11-08CCk	NID11-09MKb	NID11-09MKc	NID11-10MKb	NID11-11MKb	NID11-11MKc	NID11-12MKb
Unnormalized major elements (wt. %)								
SiO_2	59.43	57.97	48.02	49.50	46.13	47.25	50.22	48.83
TiO_2	1.072	0.924	1.422	1.366	1.521	1.491	1.406	1.376
Al_2O_3	16.95	18.36	18.75	18.84	19.03	19.40	17.15	18.36
FeO*	6.57	6.00	8.49	8.36	8.73	8.64	8.92	8.52
MnO	0.135	0.124	0.130	0.129	0.119	0.144	0.157	0.135
MgO	3.01	2.68	5.96	5.49	5.21	5.10	7.96	6.98
CaO	5.70	6.20	8.16	8.24	7.82	8.05	8.89	8.69
Na_2O	4.80	4.75	3.03	3.29	2.90	2.90	3.28	3.00
K_2O	1.29	1.13	0.71	0.70	0.72	0.70	0.79	0.66
P_2O_5	0.280	0.271	0.413	0.358	0.549	0.626	0.351	0.358
Sum	99.26	98.40	95.09	96.27	92.73	94.30	99.11	96.91
Normalized major elements (wt. %)								
SiO_2	59.88	58.91	50.50	51.41	49.75	50.11	50.66	50.39
TiO_2	1.080	0.939	1.495	1.418	1.640	1.581	1.418	1.420
Al_2O_3	17.08	18.65	19.72	19.57	20.52	20.58	17.30	18.94
FeO*	6.62	6.09	8.93	8.68	9.42	9.16	9.00	8.80
MnO	0.136	0.126	0.137	0.134	0.128	0.153	0.158	0.140
MgO	3.04	2.72	6.27	5.70	5.62	5.41	8.03	7.20
CaO	5.75	6.30	8.59	8.56	8.43	8.54	8.97	8.97
Na_2O	4.84	4.83	3.18	3.42	3.13	3.07	3.31	3.10
K_2O	1.30	1.15	0.75	0.73	0.78	0.74	0.80	0.68
P_2O_5	0.282	0.275	0.434	0.371	0.592	0.664	0.354	0.369
Trace elements (ppm)								
Ni	33	30	93	86	78	73	154	122
Cr	40	40	171	128	155	147	292	212
Sc	19	17	25	24	23	26	27	26
V	120	104	195	186	203	205	189	180
Ba	452	427	314	301	302	311	300	285
Rb	20	17	9	8	9	8	9	8
Sr	445	516	842	877	807	859	709	942
Zr	183	160	162	164	170	168	146	155
Y	29	27	21	26	20	22	23	23
Nb	9.4	8.1	12.4	11.8	13.9	13.8	11.3	12.7
Ga	21	23	22	20	21	23	17	20
Cu	33	50	50	62	51	46	79	48
Zn	88	81	78	77	74	77	79	74
Pb	5	6	4	3	5	6	3	3
La	18	15	16	23	17	15	17	21
Ce	40	31	42	53	37	44	37	48
Th	3	2	3	3	2	3	2	2
Nd	24	20	22	28	19	25	21	26
U	0	1	1	0	0	2	1	1

Sample ID	NID11-12MKc	NID11-13MKb	NID11-14MKb	NID11-15MKb	SM10 01B-BK	SM10 01D3-BK	Error (2σ)
Unnormalized major elements (wt. %)							
SiO_2	50.86	46.33	47.65	45.03	50.74	49.80	0.58
TiO_2	1.317	1.477	1.440	1.606	1.273	1.233	0.017
Al_2O_3	17.52	19.73	19.25	18.83	18.35	15.76	0.16
FeO*	8.33	8.82	8.56	8.77	8.10	9.07	0.20
MnO	0.142	0.140	0.131	0.119	0.134	0.150	0.002
MgO	7.59	4.65	5.89	4.90	6.16	10.71	0.08
CaO	8.95	7.46	8.28	7.67	8.59	8.28	0.06
Na_2O	3.15	2.97	2.94	2.74	3.31	2.91	0.04
K_2O	0.74	0.63	0.65	0.69	0.70	0.71	0.03
P_2O_5	0.354	0.661	0.396	0.851	0.368	0.332	0.005
Sum	98.94	92.87	95.20	91.20	97.73	98.95	
Normalized major elements (wt. %)							
SiO_2	51.40	49.89	50.06	49.37	51.92	50.33	0.19
TiO_2	1.331	1.591	1.513	1.761	1.303	1.246	0.012
Al_2O_3	17.71	21.24	20.22	20.65	18.78	15.93	0.08
FeO*	8.42	9.50	8.99	9.62	8.29	9.16	0.18
MnO	0.143	0.151	0.137	0.130	0.137	0.152	0.002
MgO	7.67	5.01	6.19	5.37	6.31	10.83	0.07
CaO	9.04	8.03	8.70	8.41	8.79	8.37	0.04
Na_2O	3.18	3.19	3.09	3.01	3.39	2.94	0.04
K_2O	0.75	0.68	0.69	0.75	0.71	0.71	0.02
P_2O_5	0.358	0.712	0.416	0.933	0.376	0.336	0.003
Trace elements (ppm)							
Ni	136	86	89	68	98	247	4
Cr	224	137	162	166	143	391	3
Sc	24	21	27	24	23	25	2
V	173	197	195	207	168	166	5
Ba	325	321	324	293	304	292	12
Rb	9	9	8	10	8	9	2
Sr	961	788	931	765	964	852	5
Zr	146	175	169	170	154	134	4
Y	23	18	24	20	22	21	1
Nb	11.8	13.9	13.2	14.4	10.9	10.9	1.2
Ga	19	21	21	22	20	17	3
Cu	52	48	58	51	50	80	7
Zn	81	91	75	82	78	87	3
Pb	3	7	7	7	5	6	3
La	16	13	23	16	19	20	6
Ce	44	41	51	35	41	37	8
Th	2	2	3	3	1	0	2
Nd	25	20	30	20	24	22	4
U	2	0	1	1	2	1	3

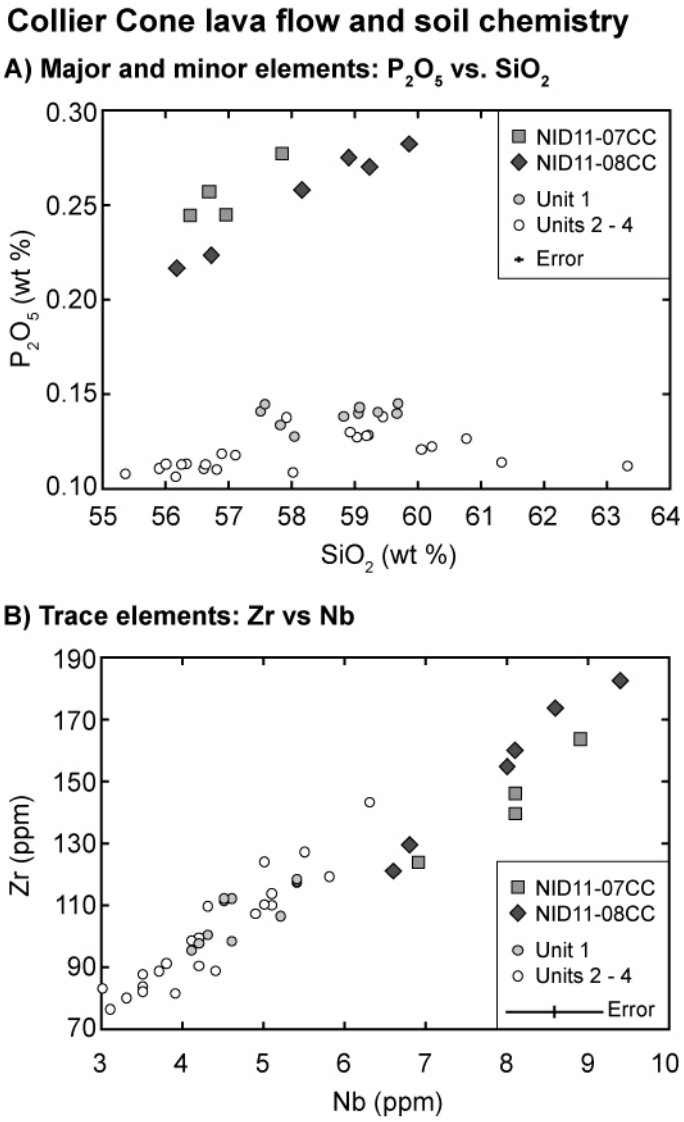

Fig. 6. Chemistry of soil horizons sampled on soil pits NID11-07CC (grey squares) and NID11-08CC (dark grey diamonds) on the lower flat of the Collier Cone lava flow. Lava flow chemistry of the underlying Unit 1 (light grey circles) and Units 2 – 4 (open circles) is shown for comparison; lava flow chemistry from Schick (1994) and Deardorff and Cashman (in revision). Chemistry was determined by XRF at Washington State University Pullman, and instrument errors are shown in the legends (see Table 4). (A) Major element chemistry: P_2O_5 vs. SiO_2. (B) Trace element chemistry: Zr vs. Nb.

flow, although the values are different, with the Collier Cone lava flow having comparatively lower incompatible element concentrations. We note that these two elements, Zr and Nb, are generally considered immobile in volcanic soils (e.g., Kurtz et al., 2000).

4.2.3. Pebble count

A pebble count conducted along the (dry) White Branch creek between the upper and lower flats surveyed 100 randomly selected pebbles (Fig. 7). Compositionally pebbles consist of oxidized scoria, oxidized and non-oxidized basalt and basaltic andesite lava, andesite, and obsidian. Intermediate axis lengths range from 1.1 to 9.6 cm with a median of 2.7 cm and the mode intermediate axis length is between 1.0 and 1.9 cm. Clasts are either subangular or subrounded. Over a quarter of the pebbles are subrounded basalt and basaltic andesite. All andesite and rhyolite clasts (5% each of total) are subrounded.

4.3. Sand Mountain Volcanic Field

Field observations confirm that the forest assemblage on and adjacent to the SMVF is characteristic of a DHC forest, although here western red cedar trees are uncommon. There are fewer large trees (DBH > 1 m) on the SMVF than on the upper and lower flats of the Collier Cone flow. We hand dug a total of seven soil pits on the three examined lava flows (Fig. 2b).

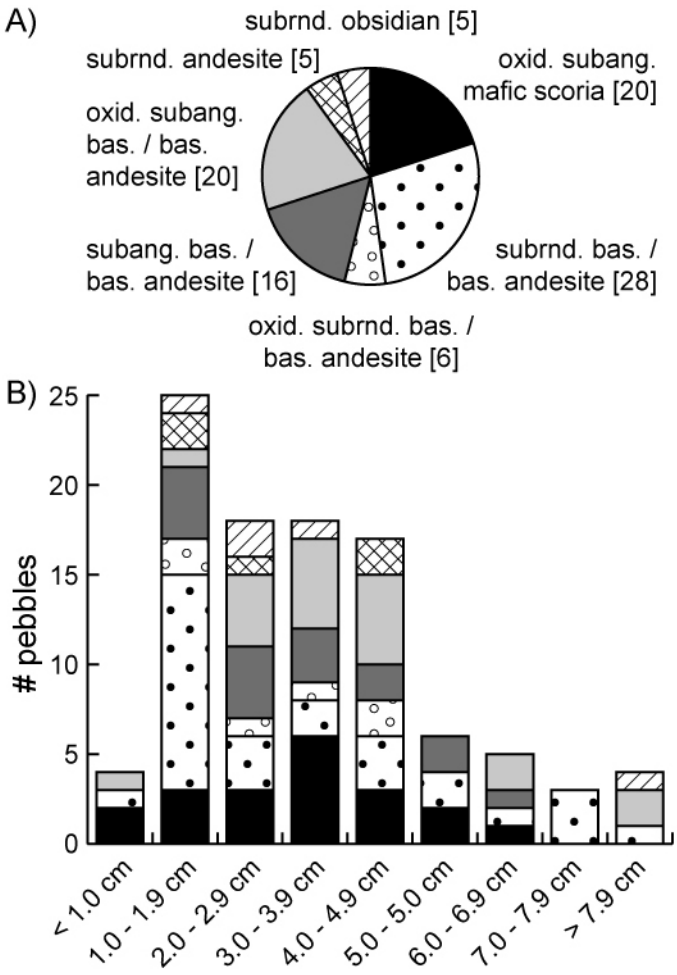

Fig. 7. Results of pebble count conducted in the White Branch Creek between the upper and lower flats on the Collier Cone lava flow. (A) Composition of clasts and legend with the number of clasts in each category in brackets. (B) Grain size distribution based on intermediate axis. Abbreviations: subrnd. = subrounded, subang. = subangular, oxid. = oxidized, bas. = basalt, and bas. andesite = basaltic andesite.

4.3.1. Clear Lake East lava flow

The Clear Lake East lava flow (youngest southern SMVF lava flow; slightly older than 2,856 ± 92 cal yr B.P.) has no soil cover apart from the odd linear feature described in section 3.2.2; this feature is underlain by Clear Lake East lava and has fine-grained material ("soil") that has filled in low topographic points. The vegetation in this strip is

also unusual; in addition to Douglas-fir, there are undifferentiated grasses that are encountered nowhere else in the SMVF.

Soil pit NID11-12MK (169 cm depth) is at the site of the deepest auger measurement (not shown) within this strip; Clear Lake East lava is exposed less than 3 meters from the soil pit. Below the litter layer, soil pit NID11-12MK reveals two tephra layers distinguishable by color (Table 3 and Fig. 8); the lower one contains notable olivine loose crystals. Soil textural analysis shows that these tephra layers can be classified as sand, and the organic content is ~3% (upper tephra) and ~1% (lower tephra).

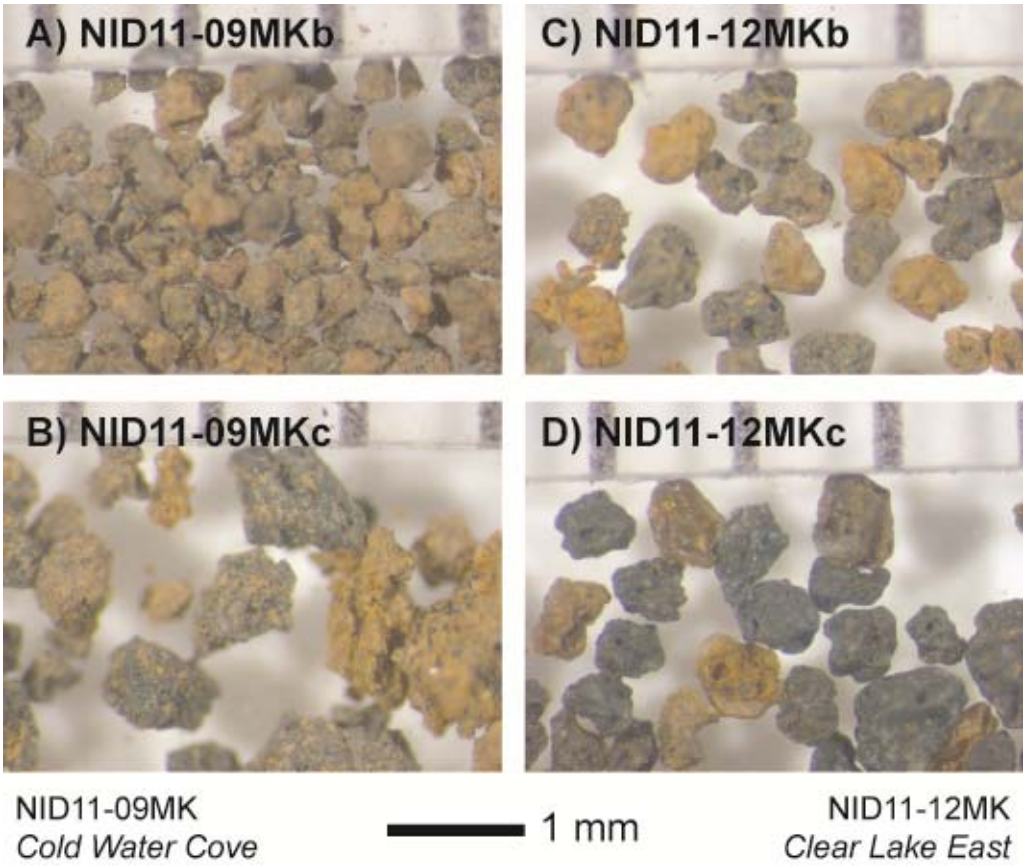

Fig. 8. Photographs of "soil" (tephra) from the SMVF. (A) and (B) are the upper and lower tephra from soil pit NID11-09MK on the Cold Water Cove lava flow, and (C) and (D) are the upper and lower tephra from soil pit NID11-12MK on the Clear Lake East lava flow. The tick marks at the top of the photos show 1 mm intervals.

4.3.2. Clear Lake South lava flow

The Clear Lake South lava flow (slightly older than 3,000 ± 72 cal yr B.P.) hosts a relatively mature DHC forest. Soil covers the majority of the lava flow, although the flow surface has a rough topography and bare rock outcrops that are consistent with its young age. It appears that the soil has accumulated in local topographic lows. The three soil pits (NID11-10MK, NID11-13MK, NID11-15MK) reveal a single yellowish brown or brown tephra deposit of a sand or loamy sand textural class and an organic content around ~7% (Table 3).

4.3.3 .Cold Water Cove lava flow

The Cold Water Cove (oldest southern SMVF lava flow; ~3 ka) and Clear Lake South lava flows are very similar on the basis of forest maturity and assemblage, soil cover and external appearance but are distinguishable in hand sample and with geochemistry (see Chapter II). As with the Clear Lake South lava flow, it appears that the soil on the Cold Water Cove lava flow infills local topographic lows. Two of the soil pits (NID11-09MK and NID11-11MK) contained two tephra layers of a sand textural class distinguishable by color, while one soil pit (NID11-14MK) contains only one tephra of a sand textural class. At all three sites, the top (or sole) tephra is similar in grain size and color to the tephra at the Clear Lake South sites; the lower tephra is darker and has a greater sand fraction. The organic content is ~5% for the top (or sole) tephra and ~2% for the lower tephra.

4.3.4. SMVF soil geochemistry

In hand sample and viewed through a binocular microscope, it is clear that the SMVF "soil" consists of tephra (Fig. 8). The major element chemistry (Table 4; Fig. 9) show that the tephra is mafic and broadly similar to lava from the SMVF (Fig. 9; see Chapter II for SMVF lava chemistry). However, the soil samples tend to have lower SiO_2 contents than the SMVF lava, which is consistent with observations at other basaltic and basaltic andesite volcanic fields where the explosive component (tephra) is more mafic than the effusive (lava) component (e.g., Erlund et al., 2010). Moreover, while individuals SMVF lava flows have quite distinctive chemistry (Fig. 9; see Chapter II), the soil chemistry is considerably more scattered with regard to major and trace elements (Table 4). Importantly, the soil chemistry does not overlap with that of the Clear Lake East (youngest) lava flow, but does broadly overlap with the Clear Lake South and Cold Water Cove lava flows.

The geochemistry of two bulk tephra samples from a < 1 km^3 mafic tephra deposit from Sand Mountain is broadly similar to both the soil samples and the older two lava flows but does not overlap with any group (Fig. 9).

5. Discussion

Both the Collier Cone and SMVF lava flows host relatively mature DHC forests where soil covers lava flows (Figs. 1 and 2). However, field observations and geochemical analyses indicate that at neither site is the soil derived directly from *in situ* weathering of the lava flow. Rather, at both locations, external processes have deposited soil-like sediment onto the lava flows. Where this deposition has occurred, the flows host

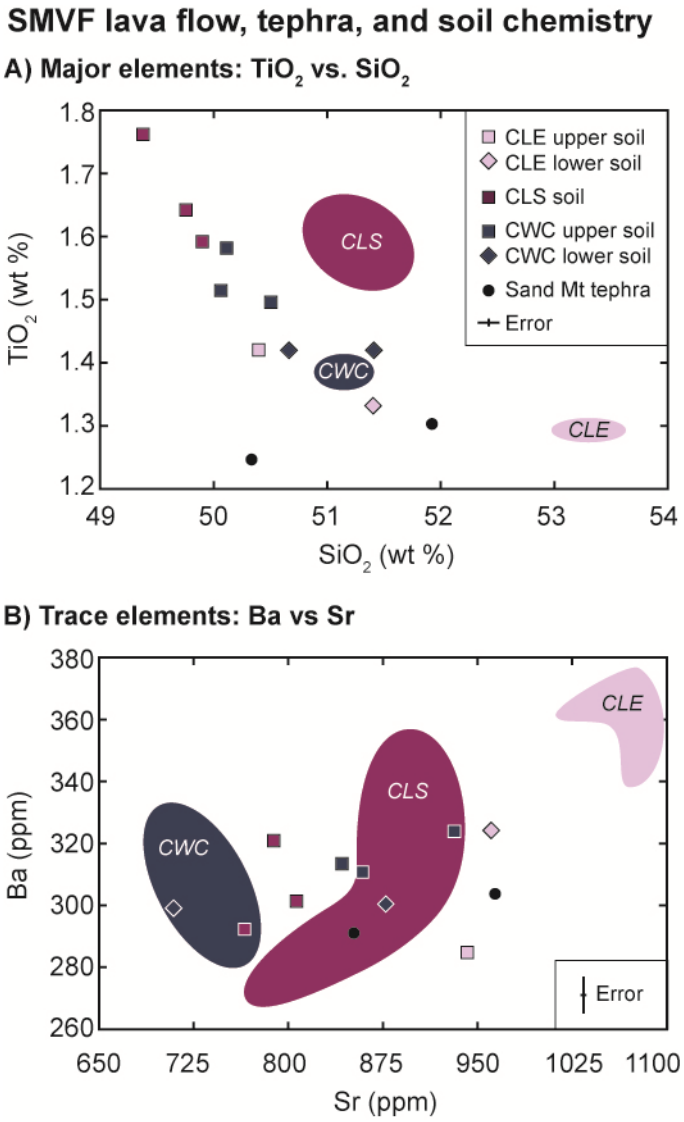

Fig. 9. Chemistry of soil horizons sampled at soil pits dug in the southern SMVF on the Clear Lake East (light purple), Clear Lake South (purple) and Cold Water Cove (dark blue) lava flows along with two samples of bulk Sand Mountain tephra. Upper soil horizons are denoted with squares and in places where there were two tephra layers, the lower horizon is denoted with a diamond. Lava flow chemistry for these three regions are shown as regions based on 29, 51, and 10 samples of bulk lava from the Clear Lake East, Clear Lake South, and Cold Water Cove flows, respectively (see Chapter II), and instrument errors are shown in the legends. (A) Major element chemistry: TiO_2 vs. SiO_2. (B) Trace element chemistry: Ba vs. Sr.

DHC forests that are similar to surrounding DHC forests. However, the source and mode of sediment deposition appears to be different for the two sites: at Collier Cone there is evidence that the sediment was transported onto the lava flow by water (probably as floods or even debris flows), while in the SMVF the soil consists of tephra that must have been deposited as a fall deposit after the underlying lava flow was emplaced. Although isolated trees grow on exposed lava at both sites, the lack of a mature forest in places without soil cover suggests that soil, i.e., an external sediment source, is critical for widespread plant establishment and survival.

In what follows, we will present evidence for external sediment sources for the soil on the lava flow(s) at both sites, consider the chronology of sediment deposition and forest development in both settings, evaluate the suitability of this external soil for hosting DHC forests, and finally discuss other sites of effusive volcanism where external soil sources appear to be important for initial plant colonization and survival on lava flows.

5.1. Floods and the Collier Cone lava flow

Assuming (1) chemical weathering rates similar to those inferred in Hawaii (10 tons km^{-2} yr^{-1}; Dessert et al., 2003) across the entire 10 km^2 Collier Cone lava flow and (2) a lava flow density of 2700 kg/m^3, in 1500 years ~56,000 m^3 of lava would have chemically weathered. As Hawaiian weathering rates are likely greater than those in the Cascades due to increased precipitation and warmer temperatures, ~56,000 m^3 is an upper estimate. Even in the unlikely instance that all the byproducts of weathering from the entire lava flow accumulated at the two flats, the combined volume of "soil" on the upper

and lower flats (138,000 and 56,000 m^3, respectively, for a total volume of 194,000 m^3) is greater than the volume predicted with Hawaiian weathering rates. However, given that exposed lava across the flow field appears fresh with no evidence of weathering, particularly at higher elevations, it is likely that negligible amount of the Collier Cone lava flow has chemically weathered at this stage.

The physical characteristics of the soil further contradict the notion of *in situ* weathering, as the majority of the flow has no soil cover and in places where there is soil (the two flats), the A horizon is a relatively small part of the soil column, with no developed B or E horizons. Near the White Branch Creek and at the base of a notable break in slope on the eastern margin of the lower flat, most of the "soil" consists of gravels and some cobbles; away from the White Branch and slope break, the "soil" consists of well-sorted alternating layers of sand and silt loam (Fig. 5). This alternation of coarse- and fine-grained material is characteristic of flood deposits, while the gravel and cobbles could be related to debris flow activity. We note that the same event can generate both flooding and debris flows. The soil chemistry is sufficiently different from that of the underlying lava to rule out a genetic relationship, although the chemistry indicates a volcanic soil source. As the site is within the glacially active Three Sisters volcanic area, a region with considerable amounts of fine-grained glacially ground volcanic material, there are abundant nearby sediment sources that could have provided sediment to the Collier Cone lava flow flats.

The White Branch Creek is clearly visible in the LiDAR imagery of the upper and lower flats (Fig. 4). At locations near the White Branch Creek, we did not reach the bottom of the deposit by augering in either flat. We find that coarser sediments (gravels

and larger clasts) are located near the creek and finer (augerable) sediments are further away from the creek. Although the location of the White Branch may have changed as sediment was emplaced, the site where the White Branch enters the lower flat is topographically confined to a < 200 m reach between two lava flow levees (Fig. 1a). If we assume that floods followed the White Branch, the input source location of sediment in the lower flat would have been relatively constant over time. Interestingly, there is a small island of exposed lava in the middle of the lower flat. The area shielded from the White Branch's entry point onto the flat by this local high point contains the thickest augerable deposits (Fig. 4b) and has no gravel or cobbles. This is in contrast to the relatively shallow auger depths recorded near the entry point. It seems likely that near the White Branch entry point onto the lower flat, the depth of the deposit is considerably thicker than reported but not measureable given the methods employed. Thus, we hypothesis that the low depth values in the "soil" thickness model in the northeastern part of the lower flat is an artifact of sampling methods and should be in fact considerably greater.

The alternating layers of coarse- (sand) and fine-grained (silt loam) sediment in soil pit NID11-08CC (Fig. 5) are indicative of flood deposits, and suggest that more than one flood event affected the area. If every layer of coarse material (sand) corresponds to a flooding event, there have been at least seven floods that affected the lower flat (and presumably the upper flat) in the last 1,500 years. The apparent buried litter layer at the top of the C3 horizon in soil pit NID11-07CC (88 cm depth) and the A2 or C15 horizon in soil pit NID11-08CC (107 cm depth) would have required sufficient time to develop vegetation when the surface was ~1 m lower than it is today. However, none of the

Douglas-fir trees that were cored on the lower flat show signs of disturbance that could be expected with large floods that carried a lot of sediment. If this interpretation is correct, this observation would suggest that all the flooding events occurred prior to 300 years ago (the age of the oldest aged tree). Moreover, the presence of a DBH 2.4 m Douglas-fir in the lower flat suggests that conditions have permitted tree colonization and growth for several hundred years. Given the young age of the Collier Cone lava flow this indicates that a series of flood events occurred within a few hundred years of the eruption.

The most likely sediment source for the two flats are glacial outburst floods and/or debris flows originating on the west side of the Three Sisters volcanoes. The Three Sisters volcanoes collectively host 17 named glaciers, and are thought to have hosted more prior to the onset of glacial retreat in the last hundred years (O'Connor et al., 2001). These glaciers form lateral and terminal moraines, and their meltwater can provide a source of floodwater. An historic outburst flood in July 1942 in the upper portion of the White Branch creek originated at the moraine-dammed lake at the terminus of Collier Glacier; this flood was caused by a lateral moraine breach (Hopson, 1960). A second smaller outburst flood originating from the same place occurred between 1954 and 1956 (O'Connor et al., 2001). The 1942 event is estimated to have removed 120,000 m^3 of moraine material within 300 m of the breach and generated a debris flow; there is also evidence of downstream incorporation of material into the debris flow (O'Connor et al., 2001). The 1942 event followed the margin of the Collier Cone lava flow; the lowest mapped deposit is at an elevation of 1500 m near the confluence with Glacier Creek where the White Branch channel jumps onto the Collier Cone lava flow.

The volume of material in the upper and lower flats, and their distance from possible outburst flood sources, imply that the floods and/or debris flows that lead to the creation of the two flats were considerably larger than the 1942 event, although the source location may have been identical. Moreover, the observation that the soil on the alluvial plain appears to be sourced from basaltic andesite to andesite lava, while the larger clasts are often obsidian suggests that the flood path went near Obsidian Cliffs, which is located near the terminus of the 1942 debris flow deposit. As there are no robust pre-historic climate records for the area, at this stage we are unable to determine what conditions produce these outburst floods. However, we hypothesize that sufficient warming had to occur to melt glaciers to provide the requisite water for flood generation. A possible source of such warming is the localized effect of the Collier Cone eruption itself, although the absense of quench features or hyaloclastite in the vent area indicative of direct lava – ice contact makes this notion unlikely.

We propose the following model for "soil" development on the lower flat Collier Cone lava flow, and note that presumably flooding events that affected the lower flat also affected the upper flat:

1) 1.5 ka: the Collier Cone lava flow was emplaced rapidly (Deardorff and Cashman, in revision).
2) Between 1.5 and 0.5 ka:
    a. One or likely several large meltwater-generated outburst floods from Collier Glacier transported and deposited enough sediment to create the lower flat (10 km from, and 1100 m lower in elevation than, the current meltwater lake associated with Collier Glacier).

b. Sufficient plant colonization occurred on the lower flat to form a litter layer.

c. One or likely several more large outburst floods from the same source transported and deposited an additional 1 m of sediment on the lower flat.

3) Post-major flood activity: mature forests developed on the flats, with slow and isolated tree establishment and growth away from the flats.

As such, the Collier Cone lava flow showcases the role floods can play in rehabilitating a landscape following an effusive volcanic eruption: they provide a way to transport "soil" onto a lava flow, providing a suitable substrate for plant establishment and survival.

5.2. Importance of tephra as a soil source for the SMVF lava flows

In contrast to the Collier Cone site, there is no surface water activity on the SMVF; instead water moves as groundwater through this highly permeable region (Stearns, 1929; Jefferson et al., 2006). The southern SMVF lava flows were all emplaced within a few decades of each other c. 3 ka, yet the stratigraphically older lava flows have soil and host mature DHC forests while the youngest lava flow is comparatively barren and has little vegetation apart from an odd vegetation strip extending from the vent area. In the SMVF "soil" is deposited as tephra fall deposits, thus providing an interesting case study of the role of eruption chronology on soil development and plant colonization of lava flows.

A general model for mafic volcanic eruptions is that they initiate with explosive activity, and that once the magma is degassed effusive activity dominates (e.g., Luhr and

Simkin, 1993). Explosive activity covers the landscape with tephra. Where soil on lava flows consists of tephra, the tephra source is likely local. This is particularly true in the case of the SMVF, where lava flows are located upwind of major tephra sources. As such, the local eruption chronology could be key for the subsequent plant colonization. Importantly, in areas of repeat volcanism, both wind direction and the order of explosive and effusive activity may dictate where plant colonization occurs on lava flows, with colonization occurring predominately on earlier units that have been covered with tephra from subsequent activity.

5.2.1. Soil on the Cold Water Cove and Clear Lake South lava flows

Lava flows of the southern SMVF cover the area west of the vent system, while SMVF tephra blankets cover a wide region northeast of the vent system. The largest explosive unit of the SMVF is the Sand Mountain tephra, with an estimated volume of <1 km^3 (Mckay, 2012).

There is no obvious genetic relationship between the two lava flows examined and their overlying tephra deposits, although it is clear that these tephra deposits are not related to the Clear Lake East lava flow (Fig. 9). Two of the three soil pits on the Cold Water Cove soil contain two tephras that have similar major element chemistries but different trace element chemistries (Table 4). The upper (or sole) Cold Water Cove tephra is similar to Clear Lake South soil but appears sufficiently different in some of the major and trace element chemistry to indicated that it is a single deposit. Interestingly, the two analyzed samples of bulk Sand Mountain tephra (1) show a considerable spread in

chemistry and (2) are more similar to each other than to the tephra-based soils on the Cold Water Cove and Clear Lake South lava flows.

The Cold Water Cove lava flow is covered by two different tephras; here the lower tephra has half the organic content of the upper tephra. However, the upper tephra on the Cold Water Cove lava flow has a lower organic content than the tephra on the Clear Lake South lava flow. This might suggest that the Clear Lake South "soil" is more mature than the Cold Water Cove "soil", although the stratigraphic relation of the two lava flows and the blanketing nature of tephra ash fall requires that any widespread tephra covering the Clear Lake South lava flow also covered the Cold Water Cove lava flow.

We propose that either syn- or post-effusive explosive activity occurring prior to the emplacement of the Clear Lake East lava flow deposited tephra on the Cold Water Cove and Clear Lake South lava flow, providing the requisite soil base for robust plant colonization.

5.2.3. Clear Lake East lava flow vegetation strip

The origin of the linear strip of soil and vegetation in the middle of the Clear Lake East lava flow that strikes towards the vent area is unclear. Its chemistry indicates that it does not consist of tephra of the same composition as the Clear Lake East eruption; indeed, the composition alone suggests that it is more closely related to the older Cold Water Cove and Clear Lake South eruptions. However, field observations show that the soil is on top of, rather than surrounded by, the Clear Lake East lava flow. The linear nature of the strip resembles a fissure system, but in the field there is no evidence of a fissure system. While we can say that vegetation is present in this area where there is soil,

and that the soil appears to consist of two tephra deposits filling local topographic lows, we have no satisfactory explanation for the origin of the tephra except that it appears to postdate the emplacement of the Clear Lake East lava flow, which is the youngest lava flow in the SMVF.

5.3. Substrate suitability for tree growth

With the exception of the fine (silt loam) sediments in the lower flat, most of the soils sampled on both the Collier Cone lava flow and the SMVF are sand. It is remarkable that mature forests are able to flourish in such soils, as sandy soils are generally nutrient poor from a plant perspective, because of low available surface area. In Linn county, Oregon, which includes the western part of the Three Sisters volcanic area, a survey of areas with the same forest assemblage and elevation as our field sites have mapped soils that consist of gravelly and cobbly silt, clay, and sandy loams (Table 5). This suggests that in the higher elevations of the lowland temperate forest zone, loams provide the best environment for DHC forest. However, the presence of DHC forests on young lava flows with less than optimal soils indicates that substrate alone does not dictate plant survival. On very young surfaces, there will be a lack of competition for light, which could promote growth of shade intolerant Douglas-fir (a key component of DHC forests). Thus, substrate alone may not be the sole factor to consider for plant establishment and growth; competition for resources (including light) may also be key.

Table 6
Textures of mapped soils in Linn county, Oregon, hosting DHC forests above 914 m (3000 ft) elevation. The extent indicates the area in Linn county that meets the selected criteria, and soil horizons are indicated in parentheses.

Soil series	Extent	Subgroup	Texture
Keel gravelly silt loam	42 km^2	Typic Haplocryand	Gravelly silt loam (A1), silt loam (A2, AB), clay loam (Bw), cobbly loam (BC)
Hummington very gravelly loam	13 km^2	Typic Fulvicryand	Gravelly loam (A1, A2), very gravelly loam (Bw1), extremely gravelly loam (Bw2)
Henline very stony sandy loam	11 km^2	Typic Humicryepts	Extremely stoney loam (A), extremely stony sandy loam (C)
Cruiser gravelly loam	11 km^2	Typic Haplocryand	Gravelly loam (A, AB), gravelly heavy loam (Bw1), gravelly clay loam (Bw2, Bw3), very cobbly clay loam (C)

5.4. Role of external soil sources in other sites of effusive volcanism

There are several other sites around the world that illustrate the importance of external soil sources for soil (and vegetation) development on lava flows. Here we will briefly discuss two sites that highlight the importance of (1) loess and (2) tephra as external soil sources.

5.4.1. Loess as an external soil source

Loess appears to be the primary source of soil on the early Holocene lava flows at Craters of the Moon, Idaho, where Vaughan et al. (2011) observed differences in soil development and plant colonization on lava flows with different surface morphologies. ′A′ā lava flows lack soil and show little biologic activity. Vaughan et al. (2011) speculate that any loess input settles through the ′a′ā clinkers, and predict that once the intra-clinkers space has been filled with loess, soil development will initiate. On pahoehoe

flows, loess accumulates in crevices, which also serve to pond water. Larger plants grow in larger crevices, and vegetation shields loess from further erosion. Thus, at Craters of the Moon a positive feedback exists between loess accumulation and biologic activity, with the underlying lava flow morphology providing the initial driver for where loess will accumulate (Vaughan et al., 2011).

Loess is also the primary component of soil in the late Cenozoic Cima Volcanic Field in the Mojave Desert, California, USA (Wells et al., 1985) and on the late Cenozoic Owyhee Basin lava flows, southeastern Oregon, USA. At the latter, over 2 m of loess has accumulated in places since the early Holocene Mount Mazama (Crater Lake) eruption (K. House, pers. comm.). In both of these desert environments there is little vegetation, although the cause is likely due to the environment and not soil suitability.

5.4.2. Tephra as an external soil source

A recent example of tephra as an important source of soil can be found at Volcan Jorullo, Mexico (18.97°N, 101.72°W), which erupted between 1759 and 1774 AD (Gadow, 1930). Over the course the 25 year eruption, eight separate lava flow units were emplaced (A through G; Rowland et al., 2009). Only the last two units, G, and H, erupted after the end of the explosive stage. As a result, units A through F are covered with tephra from the eruption, while units G and H are barren. The difference in vegetation is easily seen in Google Earth, where there is an obvious contrast the surface of flow units G and H relative to the rest of the lava flow field. This difference relates to the presence of vegetation only on flow units A through G. Thus, tephra appears to provide a fertile soil

base on a lava flow that is only 250 years old; moreover plant colonization has occurred where this soil is present.

5.5. Importance of external soil sources

It is not immediately clear why an external soil source is so important for plant establishment and survival. We hypothesize that external soil sources provide a substrate for plant growth, as well as access to key nutrients and water. Although lava flows contain important plant nutrients, they are not readily available, as lava is dense, with low surface area to volume ratios, and is physically hard to break apart. We note that prized volcanically fertile lands (e.g., the Mediterranean, Indonesia) are areas with considerable tephra. We speculate that it is tephra, which is fine grained and has a greater surface area to volume ratio, not lava, that produces fertile volcanic soils. However tephra is not the sole external source: flood deposits (this paper) and loess (e.g., Wells et al., 1985; Vaughan et al., 2011) can also provide plants with both a substrate to establish and extractable key nutrients.

External soil sources may also provide a water source. Young lava flows are among the most permeable surfaces on earth and while they are important groundwater reservoirs (e.g., Jefferson et al., 2006), there is little available surface or near surface water. Fine grained external soil sources may be able store sufficient water within their pore space for plants to survive in the absence of an adequate water supply in the upper portions of a lava flow. This notion is supported by agricultural experiments conducted in tephra from the Sunset Crater eruption, where it was found that when not too thick, tephra acts as a mulch and retains moisture (Ort et al., 2008). Indeed, the Native

American population near Sunset Crater appears to have significantly expanded following the Sunset Crater eruption (sometime between 1040 and 1100 AD; Ort et al., 2002), suggesting an increase in agriculturally viable lands at this time (Ort et al., 2008). Thus, tephra, and likely other fine grained sediments, play an important role in making lava flows a suitable environment for plant colonization.

Once plants have colonized external soil sources on lava flows, mechanical weathering by roots or chemical weathering via biological acids may break down lava. However, it is possible that biological time scales are sufficiently slow that geologic forces prevail in the removal of lava flows from the active landscape, with erosion by glacial or fluvial activity or by burial by later lava flows. Both geologic erosion (rather than biologic weathering) and burial impede the direct transfer of nutrients from the lava to the biosphere. As such, lava may be a relatively biologically inert substrate; fine-grained tephra from explosive volcanic activity could arguably be the driver for delivery of key elements from within the earth to the biosphere.

6. Conclusions

We have presented a detailed study of two sites of recent effusive volcanism in the central Oregon Cascades, USA; these sites are notable for the observed juxtaposition of exposed lava flows and mature forests on a single lava flow or on lava flows of similar ages. At the younger site, the 1.5 ka Collier Cone lava flow, floods and/or debris flows appear to have deposited a total of 194,000 m^3 of sediment at two places on top of the lava flow. These two areas, informally referred to as upper and lower flats, host mature forests indistinguishable from those off the lava flow. At the older ~3 ka Sand Mountain

Volcanic Field, lava flows with tephra cover host mature forests while areas without tephra have no soil cover and limited vegetation.

Based on these two sites, we hypothesize that, at least in temperate areas, soil on lava flows is predominately externally derived and not formed from the *in situ* physical and chemical breakdown of the underlying lava flow. External soil sources can be water-transported, related to syn- or post-eruptive explosive volcanic activity, or derived from aeolian sources. We hypothesize that these external soil sources provide a substrate for vegetation to colonize providing access to key nutrients and water.

Consequently, recovery from an incredibly destructive lava flow disturbance is dictated by external factors, such as floods, other volcanic activity, or a regional source of loess. In the absence of external soil sources in temperate climates, we predict that recovery from the disturbance will be very slow. However, with an external soil source, plant colonization is rapid and can lead to the relatively quick establishment of mature forests. As such, a lava flow may present one of the few environments where floods and explosive volcanic activity serve to rehabilitate the landscape, transforming it into a hospitable environment for life.

CHAPTER V

CONCLUSIONS

In this dissertation I have examined two sites of recent volcanism, the Sand Mountain volcanic field (SMVF) and the Collier Cone lava flow, to answer the question "how do landscapes respond to the rapid emplacement of large quantities of fresh rock?" Below, I summarize the key findings of the three papers presented here, and end with thoughts on the implications of my work and future directions.

In Chapter II, I presented a detailed investigation of the volcanologic and hydrologic history of the Sand Mountain volcanic field (SMVF). I found that the SMVF was emplaced over a relatively short amount of time. Interestingly, despite the compact area and small eruptive volume, SMVF lavas tapped three magma bodies. Additionally, contrary to standard models for monogenetic cinder cone fields, there is evidence for vent migration and reoccupation. Hydrologically, SMVF lavas profoundly impacted the McKenzie River: lava flows from the SMVF and other Holocene vents have dammed, buried, and dictated the path of the river. Although the McKenzie River adapts to changing conditions (i.e., the injection of lava into its watershed), it is likely that lava flows temporarily cause a great reduction in downstream discharge, both by blocking surface water flow and by disrupting groundwater flow. I estimate that, depending on the time of the year, SMVF lava flows could have decreased the discharge of the McKenzie River in Eugene, Oregon by up to 20%. Although it is unlikely that the Sand Mountain volcanic field will reactivate, my work illustrates possible ramifications of future mafic

activity within the McKenzie River drainage, which is very likely given that the McKenzie River's watershed considerably overlaps with the High Cascades graben.

In Chapter III, I began my study of plant colonization of young lava flows. I use LiDAR data to characterize vegetation on and adjacent to the c. 1.5 ka Collier Cone lava flow, which is notable for its traverse across a 1250 m elevational gradient. I developed several ways of characterizing vegetation density and compared forest characteristics to underlying substrates. I found that in general, vegetation on the Collier Cone lava flow is shorter and sparse than adjacent forests, with the exception of two sites with apparent sediment accumulation on the flow surface – these two sites hosted forests that are very similar to nearby forests.

In Chapter IV, I examine soil development and plant colonization of both the SMVF and the Collier Cone lava flow. I find that forests flourish on these young lava flows where external sediment sources have been deposited. At the SMVF, this external soil is tephra from SMVF eruptions, while at Collier, the soil is flood deposits, presumably from glacial outburst floods originating from the upper reaches of the Three Sisters volcanic region. I find that contrary to many models of slow, continuous soil development and progresses plant succession, young lava flows, at least in the central Oregon Cascades, are preferentially colonized after discreet external events.

My results showcase the great disturbance that lava flows cause along with the landscape's remarkable resilience to such events. In the confrontation between the two great geologic floods, lava and water, both can impact the flow and behavior of the other. Lava flows can forces outwardly great changes in the flow of water by burying, damming, and diverting rivers. However, water can cause lava flows to stop and is also

remarkably adaptive to changing conditions. Surface water flow can easily change to groundwater flow through volcanic terrains, and water can adapt lava features to assist with flow. Gravity, not lava, turns out to be the main control on water flow through volcanic landscapes.

Plant colonization of lava flows is greatly accelerated when external "soil" is deposited on lava flows. Thus, the relation between lava flows and biota abides by catastrophism rather than uniformitarianism: lava flows catastrophically destroy biota, and the "catastrophic" events make lava flows easier to colonize.

My dissertation provides a foundation for several avenues of future research. It would be quite interesting to model how the injection of hot magma at depth could affect groundwater flow in the High Cascades, and whether the emplacement of dikes could act as a barrier to flow. Such models could inform predictions for the overall expected length of disruption of water flow associated with mafic volcanism. Another question worth exploring what factors make external soil sources so important for plant establishment and survival on young lava flows – providing a growth medium? holding moisture? nutrient availability? It would also be interesting to examine the role of microbes – what microbes fix nitrogen, how is plant available phosphorous introduced – along with how they are introduced into the system.

Overall, my work highlights the dynamic processes that operate on landscapes following the emplacement of lava flows. With time and fortuitous external events, landscapes recover relatively quickly to widespread comprehensive destruction caused by effusive volcanism!

APPENDIX

SUPPLEMENTARY MATERIAL FOR CHAPTER II

TABLE A1. MAJOR AND MINOR ELEMENT CHEMISTRY FOR SMVF SAMPLES DETERMINED BY XRF

Sample ID	RCEWEB1-1	RCNSH-5	RCSM-1	RCBKP-6	SHE95-TFJ23	SHE95-TFJ24	SHE95-TFJ25	SHE95-TFJ26	RC95-01	RC95-02	RC95-03	RC95-04
Unnormalized major elements (weight %)												
SiO2	52.40	49.37	51.62	50.77	50.60	50.44	50.78	52.62	51.47	53.63	51.21	53.64
TiO2	1.336	1.382	1.249	1.346	1.307	1.318	1.297	1.281	1.463	1.330	1.449	1.296
Al2O3	17.25	16.32	16.97	16.90	17.15	17.22	17.23	17.19	17.00	18.13	17.10	18.05
FeO*	8.05	8.39	7.43	8.42	8.54	8.47	8.94	7.80	8.74	8.21	8.86	7.94
MnO	0.144	0.149	0.129	0.148	0.158	0.158	0.157	0.137	0.155	0.141	0.155	0.137
MgO	6.61	8.28	5.78	8.01	7.73	7.60	7.54	6.41	8.59	5.87	8.52	5.85
CaO	9.46	8.90	8.73	8.51	8.98	9.02	8.98	9.01	9.10	8.62	9.42	8.62
Na2O	3.45	3.31	3.63	3.55	3.31	3.24	3.14	3.52	3.46	3.97	3.39	3.93
K2O	0.97	0.81	0.81	0.70	0.58	0.58	0.56	0.85	0.79	0.83	0.67	0.81
P2O5	0.384	0.337	0.365	0.302	0.290	0.290	0.274	0.377	0.357	0.403	0.329	0.385
Sum	100.05	97.25	96.71	98.66	98.65	98.34	98.90	99.20	101.13	101.13	101.10	100.66
Normalized major elements (weight %)												
SiO2	52.37	50.77	53.37	51.46	51.30	51.29	51.35	53.05	50.90	53.03	50.65	53.29
TiO2	1.335	1.421	1.291	1.364	1.325	1.340	1.311	1.291	1.447	1.315	1.433	1.288
Al2O3	17.24	16.78	17.55	17.13	17.39	17.51	17.42	17.33	16.81	17.93	16.91	17.93
FeO*	8.05	8.63	7.68	8.53	8.66	8.61	9.04	7.86	8.64	8.12	8.76	7.89
MnO	0.144	0.153	0.133	0.150	0.160	0.161	0.159	0.138	0.153	0.139	0.153	0.136
MgO	6.61	8.51	5.98	8.12	7.84	7.73	7.62	6.46	8.49	5.80	8.43	5.81
CaO	9.45	9.15	9.03	8.63	9.10	9.17	9.08	9.08	9.00	8.52	9.32	8.56
Na2O	3.45	3.40	3.75	3.60	3.36	3.29	3.17	3.55	3.42	3.93	3.35	3.90
K2O	0.97	0.83	0.84	0.71	0.59	0.59	0.57	0.86	0.78	0.82	0.66	0.80
P2O5	0.384	0.347	0.377	0.306	0.294	0.295	0.277	0.380	0.353	0.398	0.325	0.382
Unnormalized trace elements (ppm)												
Ni	83	170	81	169	141	142	136	87	182	116	167	104
Cr	177	332	129	284	257	253	247	161	346	111	321	117
Sc	26	25	21	24	30	28	28	23	27	22	28	21
V	187	197	168	174	205	201	202	174	198	178	203	179
Ba	409	317	332	206	247	244	239	366	292	357	249	346
Rb	9	9	8	11	7	8	6	9	9	9	8	8
Sr	1029	689	1034	472	448	456	450	1054	651	788	620	852
Zr	151	131	151	129	109	113	106	151	141	165	138	156
Y	23	21	20	24	22	21	21	21	24	24	23	22
Nb	11.0	10.7	10.8	14.9	9.1	8.3	8.2	9.9	11.5	10.8	9.9	11.0
Ga	19	17	20	17	18	21	21	19	19	22	17	21
Cu	57	61	58	76	54	55	51	60	64	58	64	59
Zn	83	78	80	77	76	80	80	86	82	91	79	89
Pb	7	4	5	2	1	0	1	7	4	6	4	6
La	20	13	19	23	0	0	14	18	15	19	13	17
Ce	42	31	44	31	16	34	25	46	39	46	34	48
Th	1	0	1	1	1	1	0	1	1	0	0	0
Nd	25	20	22					24	22	26	3	27
U												

Note : Major elements are normalized on a volatile-free basis, with total Fe expressed as FeO. 'R' denotes a duplicate bead made from the same rock powder.

TABLE A1. MAJOR AND MINOR ELEMENT CHEMISTRY FOR SMVF SAMPLES DETERMINED BY XRF

Sample ID	RC95-05	RC95-06	RC95-07	RC95-08	RC95-09	RC95-10	RC95-11	RC95-12	RC95-13	RC95-14	RC95-15	RC95-16	RC95-17	RC95-18	RC95-19
Unnormalized major elements (weight %)															
SiO2	50.84	53.62	57.19	51.68	51.45	56.29	53.65	52.91	53.36	52.87	53.54	52.16	52.52	52.72	53.47
TiO2	1.478	1.325	1.098	1.472	1.464	1.043	1.298	1.304	1.291	1.309	1.308	1.356	1.318	1.328	1.305
Al2O3	16.86	18.00	18.80	17.02	16.93	19.60	17.58	17.20	18.00	17.91	17.66	17.06	17.31	17.42	17.71
FeO*	8.95	8.23	6.79	8.60	8.58	6.67	7.73	8.02	7.74	7.98	7.54	7.81	7.75	7.76	7.48
MnO	0.157	0.143	0.117	0.150	0.150	0.115	0.136	0.143	0.137	0.140	0.137	0.144	0.141	0.142	0.135
MgO	8.84	6.05	4.01	7.95	7.93	4.37	6.20	6.90	5.79	5.85	5.93	6.88	6.26	6.37	5.94
CaO	9.41	8.49	7.69	9.45	9.45	7.79	9.15	9.19	8.55	8.46	9.24	9.52	9.37	9.43	9.10
Na2O	3.32	3.89	4.22	3.40	3.42	4.10	3.74	3.51	3.92	3.91	3.70	3.40	3.53	3.55	3.75
K2O	0.90	0.83	0.75	0.75	0.76	0.68	0.87	0.93	0.82	0.83	0.93	1.00	0.96	0.96	0.84
P2O5	0.353	0.405	0.300	0.345	0.343	0.209	0.384	0.385	0.385	0.399	0.389	0.370	0.381	0.385	0.383
Sum	101.11	100.98	100.97	100.82	100.48	100.87	100.74	100.49	99.99	99.66	100.37	99.70	99.54	100.07	100.11
Normalized major elements (weight %)															
SiO2	50.28	53.10	56.64	51.26	51.21	55.81	53.26	52.65	53.36	53.05	53.34	52.32	52.76	52.69	53.41
TiO2	1.462	1.312	1.088	1.460	1.457	1.034	1.288	1.298	1.291	1.313	1.303	1.360	1.324	1.327	1.304
Al2O3	16.68	17.82	18.62	16.88	16.85	19.43	17.45	17.12	18.00	17.97	17.59	17.11	17.39	17.41	17.69
FeO*	8.85	8.15	6.73	8.53	8.54	6.61	7.67	7.98	7.74	8.01	7.51	7.83	7.79	7.75	7.47
MnO	0.155	0.142	0.116	0.149	0.149	0.114	0.135	0.142	0.137	0.140	0.136	0.144	0.142	0.142	0.135
MgO	8.74	5.99	3.97	7.89	7.89	4.33	6.15	6.87	5.79	5.87	5.91	6.90	6.29	6.37	5.93
CaO	9.31	8.41	7.62	9.37	9.41	7.72	9.08	9.15	8.55	8.49	9.21	9.55	9.41	9.42	9.09
Na2O	3.28	3.85	4.18	3.37	3.40	4.06	3.71	3.49	3.92	3.92	3.69	3.41	3.55	3.55	3.75
K2O	0.89	0.82	0.74	0.74	0.76	0.67	0.86	0.93	0.82	0.83	0.93	1.00	0.96	0.96	0.84
P2O5	0.349	0.401	0.297	0.342	0.341	0.207	0.381	0.383	0.385	0.400	0.388	0.371	0.383	0.385	0.383
Unnormalized trace elements (ppm)															
Ni	183	128	31	137	137	54	82	101	108	125	72	94	79	80	80
Cr	369	124	43	289	283	37	153	203	111	111	132	193	151	158	130
Sc	27	21	16	26	27	18	24	25	21	20	23	27	26	26	23
V	210	181	135	199	198	158	178	184	180	180	181	197	188	193	179
Ba	363	356	333	278	275	253	356	405	351	352	384	400	404	406	345
Rb	9	9	7	8	9	5	9	9	9	10	9	9	9	9	7
Sr	695	764	1015	744	743	928	1089	1025	841	763	1069	1023	1031	1036	1084
Zr	139	163	146	145	144	102	154	152	157	162	155	146	151	152	155
Y	23	23	19	23	22	15	22	22	22	22	22	22	23	22	21
Nb	11.3	11.2	8.5	10.8	10.4	4.5	10.4	11.0	10.3	11.4	10.3	11.6	10.7	10.2	10.4
Ga	16	20	20	18	17	21	21	20	20	21	20	20	21	18	20
Cu	68	58	19	63	64	45	62	66	60	55	65	66	63	54	60
Zn	81	94	75	80	82	71	82	82	90	91	81	80	82	82	86
Pb	5	5	4	4	6	4	6	6	5	5	6	6	6	5	7
La	15	20	17	16	14	14	18	23	17	20	23	21	22	18	23
Ce	35	44	43	37	43	27	49	50	41	41	48	49	46	47	49
Th	1	1	1	0	1	1	1	0	0	2	1	2	1	2	1
Nd	21	27	24	20	22	16	28	27	26	21	28	28	26	25	28
U						3									

Note: Major elements are normalized on a volatile-free basis, with total Fe expressed as FeO. 'R' denotes a duplicate bead made from the same rock powder.

TABLE A1. MAJOR AND MINOR ELEMENT CHEMISTRY FOR SMVF SAMPLES DETERMINED BY XRF

Sample ID	RC95-20	RC95-21	RC95-26	RC00-55	RC00-56	RC00-57	RC00-58	RC01-80	RC01-81	RC02-17	RC02-18	RC02-19	RC02-20	RC02-21	RC02-22
Unnormalized major elements (weight %)															
SiO2	51.65	51.44	57.13	49.98	50.31	51.00	53.24	53.05	51.34	53.56	52.74	52.64	52.90	50.47	53.22
TiO2	1.646	1.623	1.048	1.438	1.447	1.471	1.250	1.362	1.474	1.326	1.281	1.330	1.290	1.450	1.330
Al2O3	16.84	16.96	18.94	16.59	16.60	16.87	17.79	16.85	16.35	17.92	17.38	17.27	17.85	16.76	17.86
FeO*	8.41	8.29	5.95	8.88	8.37	8.48	7.66	8.23	8.80	8.48	7.63	7.94	8.04	8.93	8.42
MnO	0.149	0.148	0.114	0.153	0.154	0.156	0.130	0.148	0.158	0.144	0.133	0.143	0.136	0.155	0.144
MgO	7.67	7.55	4.00	8.62	8.39	8.50	5.64	6.41	7.25	6.05	5.98	6.54	5.79	8.47	6.06
CaO	9.55	9.81	7.52	9.24	8.92	9.05	8.61	8.64	8.74	8.44	8.94	9.43	8.48	9.18	8.43
Na2O	3.50	3.45	4.38	3.23	3.41	3.45	3.87	3.50	3.43	3.83	3.61	3.48	3.85	3.27	3.84
K2O	0.85	0.86	0.82	0.83	0.77	0.78	0.79	1.00	1.13	0.83	0.83	0.97	0.81	0.68	0.82
P2O5	0.376	0.367	0.312	0.343	0.348	0.354	0.358	0.336	0.573	0.411	0.376	0.384	0.383	0.328	0.403
Sum	100.64	100.50	100.21	99.30	98.72	100.11	99.34	99.53	99.25	100.99	98.90	100.13	99.53	99.69	100.53
Normalized major elements (weight %)															
SiO2	51.32	51.19	57.01	50.33	50.96	50.94	53.59	53.30	51.73	53.03	53.33	52.57	53.15	50.63	52.94
TiO2	1.636	1.615	1.046	1.448	1.466	1.469	1.258	1.368	1.485	1.313	1.295	1.328	1.296	1.454	1.323
Al2O3	16.73	16.88	18.90	16.71	16.82	16.85	17.91	16.93	16.47	17.74	17.57	17.25	17.93	16.81	17.77
FeO*	8.36	8.25	5.94	8.94	8.48	8.47	7.71	8.27	8.87	8.40	7.71	7.93	8.08	8.96	8.38
MnO	0.148	0.147	0.114	0.154	0.156	0.156	0.131	0.149	0.159	0.143	0.134	0.143	0.137	0.155	0.143
MgO	7.62	7.51	3.99	8.68	8.50	8.49	5.68	6.44	7.31	5.99	6.05	6.53	5.82	8.50	6.03
CaO	9.49	9.76	7.50	9.30	9.04	9.04	8.67	8.68	8.81	8.36	9.04	9.42	8.52	9.21	8.39
Na2O	3.48	3.43	4.37	3.25	3.45	3.45	3.90	3.52	3.46	3.79	3.65	3.48	3.87	3.28	3.82
K2O	0.84	0.86	0.82	0.84	0.78	0.78	0.80	1.00	1.14	0.82	0.84	0.97	0.81	0.68	0.82
P2O5	0.374	0.365	0.311	0.345	0.353	0.354	0.360	0.338	0.577	0.407	0.380	0.384	0.385	0.329	0.401
Unnormalized trace elements (ppm)															
Ni	132	119	30	177	177	176	91	113	145	134	83	88	111	175	136
Cr	251	236	41	350	324	322	109	169	242	123	138	165	116	323	125
Sc	26	28	15	26	27	27	22	25	22	20	23	25	21	26	21
V	208	202	133	203	200	204	177	211	189	179	173	192	176	198	180
Ba	292	302	320	347	293	301	342	360	603	357	350	406	342	254	355
Rb	10	10	10	10	10	9	7	20	13	10	8	9	9	9	9
Sr	822	897	969	677	619	628	929	477	795	758	1058	1025	836	601	754
Zr	156	149	172	134	140	141	148	142	204	164	152	152	157	138	165
Y	22	22	19	23	23	23	20	29	27	23	21	23	21	23	23
Nb	14.4	13.8	11.0	10.9	11.9	11.7	9.5	11.2	14.1	12.4	11.5	12.1	11.3	11.0	13.2
Ga	19	19	20	16	19	18	20	20	19	20	21	19	20	17	20
Cu	60	65	39	64	61	63	62	65	66	56	56	50	53	58	62
Zn	83	79	77	80	81	82	88	84	93	93	86	83	87	77	93
Pb	5	5	2	7	7	6	7	4	4	7	6	6	4	5	7
La	19	21	20	12	12	16	19	0	24	20	22	21	16	13	18
Ce	47	48	46	36	39	44	42	35	60	39	43	50	36	30	40
Th	2	1	4	1	2	1	1	5	2	0	0	1	0	1	0
Nd	25	26		3	23	3	22			24	24	28	27	19	24
U															

Note: Major elements are normalized on a volatile-free basis, with total Fe expressed as FeO. 'R' denotes a duplicate bead made from the same rock powder.

TABLE A1. MAJOR AND MINOR ELEMENT CHEMISTRY FOR SMVF SAMPLES DETERMINED BY XRF

Sample ID	RC02-23	RC02-24	RC02-25	RC02-26	RC02-27A	RC02-27B	RC02-28	RC02-29	RC02-30	RC02-31	RC02-32	RC02-33	RC02-34	RC02-35	RC02-36
Unnormalized major elements (weight %)															
SiO2	53.02	50.59	50.48	52.16	53.19	53.17	53.46	52.69	51.33	51.28	53.00	52.90	53.25	53.20	51.18
TiO2	1.311	1.405	1.430	1.280	1.309	1.310	1.256	1.280	1.592	1.372	1.293	1.284	1.289	1.291	1.466
Al2O3	17.83	16.77	16.55	17.63	17.44	17.55	17.88	17.33	16.85	16.81	17.44	17.55	17.62	17.47	17.13
FeO*	8.34	8.90	8.35	7.99	7.77	7.80	7.62	7.59	8.65	8.09	7.64	7.43	7.50	7.63	8.02
MnO	0.142	0.154	0.146	0.136	0.137	0.138	0.131	0.133	0.149	0.143	0.133	0.131	0.132	0.134	0.144
MgO	5.95	8.82	7.70	5.75	6.00	6.06	5.64	5.96	7.90	6.98	5.85	5.63	5.70	6.17	6.46
CaO	8.39	9.24	9.19	8.37	9.20	9.23	8.65	8.98	9.61	9.53	9.02	9.01	9.03	9.08	9.82
Na2O	3.86	3.34	3.34	3.82	3.59	3.62	3.91	3.70	3.44	3.38	3.75	3.72	3.80	3.72	3.33
K2O	0.82	0.89	0.73	0.81	0.91	0.90	0.81	0.86	0.81	1.00	0.85	0.84	0.85	0.87	1.00
P2O5	0.399	0.346	0.334	0.387	0.383	0.383	0.361	0.378	0.356	0.359	0.379	0.375	0.378	0.378	0.372
Sum	100.06	100.46	98.25	98.33	99.93	100.16	99.72	98.90	100.69	98.94	99.36	98.87	99.55	99.94	98.92
Normalized major elements (weight %)															
SiO2	52.99	50.36	51.38	53.04	53.23	53.08	53.61	53.28	50.98	51.83	53.34	53.50	53.49	53.23	51.74
TiO2	1.310	1.399	1.455	1.302	1.310	1.308	1.260	1.294	1.581	1.387	1.301	1.299	1.295	1.292	1.482
Al2O3	17.82	16.69	16.84	17.93	17.45	17.52	17.93	17.52	16.74	16.99	17.55	17.75	17.70	17.48	17.32
FeO*	8.33	8.86	8.50	8.13	7.78	7.79	7.64	7.67	8.59	8.18	7.69	7.51	7.53	7.63	8.11
MnO	0.142	0.153	0.149	0.138	0.137	0.138	0.131	0.134	0.148	0.145	0.134	0.132	0.133	0.134	0.146
MgO	5.95	8.78	7.84	5.85	6.00	6.05	5.66	6.03	7.85	7.05	5.89	5.69	5.73	6.17	6.53
CaO	8.38	9.20	9.35	8.51	9.21	9.22	8.67	9.08	9.54	9.63	9.08	9.11	9.07	9.09	9.93
Na2O	3.86	3.32	3.40	3.88	3.59	3.61	3.92	3.74	3.42	3.42	3.77	3.76	3.82	3.72	3.37
K2O	0.82	0.89	0.74	0.82	0.91	0.90	0.81	0.87	0.80	1.01	0.86	0.85	0.85	0.87	1.01
P2O5	0.399	0.344	0.340	0.394	0.383	0.382	0.362	0.382	0.354	0.363	0.381	0.379	0.380	0.378	0.376
Unnormalized trace elements (ppm)															
Ni	129	197	137	117	75	77	99	79	137	96	78	74	77	85	76
Cr	121	360	277	111	139	137	110	136	263	203	127	115	120	148	162
Sc	20	27	25	20	24	24	20	22	25	27	22	21	23	23	26
V	179	182	191	175	178	182	177	174	202	184	176	173	174	179	204
Ba	353	364	269	347	386	386	343	360	281	390	352	343	341	362	398
Rb	9	10	9	9	9	8	8	9	10	9	9	8	9	9	8
Sr	756	724	723	796	1053	1063	926	1068	824	1001	1072	1069	1069	1075	1001
Zr	162	134	141	158	156	156	150	153	149	145	156	155	155	152	147
Y	23	22	21	22	22	22	21	21	21	22	21	21	21	21	23
Nb	12.0	12.2	11.2	11.9	12.4	11.9	10.3	11.3	14.9	12.9	11.2	11.7	11.6	11.2	14.7
Ga	20	17	18	20	21	18	20	19	20	18	21	20	20	22	19
Cu	60	78	58	58	63	60	63	61	66	65	61	62	61	57	61
Zn	90	81	79	89	81	84	85	84	82	77	84	85	80	86	79
Pb	5	3	3	6	5	5	5	5	5	5	5	5	6	6	5
La	21	13	15	20	21	24	20	20	18	20	20	21	19	20	18
Ce	41	37	28	44	43	50	36	47	41	40	41	43	42	45	44
Th	0	1	0	1	2	0	1	1	2	1	1	1	1	-1	0
Nd	26	22	19	23	25	30	23	26	25	23	24	25	25	25	24
U															

Note: Major elements are normalized on a volatile-free basis, with total Fe expressed as FeO. 'R' denotes a duplicate bead made from the same rock powder.

TABLE A1. MAJOR AND MINOR ELEMENT CHEMISTRY FOR SMVF SAMPLES DETERMINED BY XRF

Sample ID	RC02-37	RC02-38	RC02-39	RC02-40	RC02-41	RC02-42	RC02-43	RC02-44	RC02-45	RC03-13	RC03-14	RC03-15	RC03-16	RC03-17	RC03-18
Unnormalized major elements (weight %)															
SiO2	51.13	52.80	53.72	53.11	50.66	50.12	50.60	48.42	52.95	52.61	53.47	50.35	52.43	53.04	49.94
TiO2	1.547	1.307	1.237	1.275	1.551	1.420	1.447	1.402	1.299	1.307	1.238	1.460	1.300	1.314	1.462
Al2O3	17.69	17.75	17.89	17.89	16.59	16.83	16.86	16.01	17.47	17.73	18.02	16.74	17.60	17.82	16.61
FeO*	8.93	8.13	7.39	7.60	8.41	8.77	8.83	8.30	7.51	8.32	7.56	8.64	8.17	8.27	8.71
MnO	0.166	0.142	0.127	0.132	0.147	0.154	0.154	0.150	0.134	0.140	0.130	0.154	0.141	0.140	0.155
MgO	6.27	5.98	5.62	5.59	7.68	8.56	8.43	8.20	5.79	5.94	5.61	8.37	6.00	5.87	8.56
CaO	9.20	8.36	8.72	8.57	9.44	9.18	9.25	8.66	9.17	8.49	8.74	9.10	8.44	8.37	9.36
Na2O	3.62	3.83	3.92	3.84	3.40	3.32	3.34	3.22	3.69	3.72	3.84	3.31	3.75	3.75	3.17
K2O	0.84	0.81	0.82	0.80	0.81	0.66	0.68	0.72	0.91	0.81	0.78	0.73	0.80	0.82	0.90
P2O5	0.591	0.398	0.352	0.367	0.352	0.323	0.329	0.329	0.385	0.396	0.354	0.348	0.397	0.403	0.349
Sum	99.98	99.51	99.80	99.17	99.04	99.34	99.92	95.41	99.31	99.46	99.74	99.20	99.03	99.80	99.22
Normalized major elements (weight %)															
SiO2	51.14	53.06	53.83	53.55	51.15	50.45	50.64	50.75	53.32	52.89	53.61	50.76	52.94	53.15	50.33
TiO2	1.547	1.313	1.240	1.286	1.566	1.429	1.448	1.469	1.308	1.314	1.241	1.472	1.313	1.317	1.474
Al2O3	17.69	17.84	17.93	18.04	16.75	16.94	16.87	16.78	17.59	17.83	18.07	16.87	17.77	17.86	16.74
FeO*	8.93	8.17	7.41	7.66	8.49	8.83	8.84	8.70	7.56	8.36	7.58	8.71	8.25	8.29	8.78
MnO	0.166	0.143	0.127	0.133	0.148	0.155	0.154	0.157	0.135	0.141	0.130	0.155	0.142	0.140	0.156
MgO	6.27	6.01	5.63	5.64	7.75	8.62	8.44	8.59	5.83	5.97	5.62	8.44	6.06	5.88	8.63
CaO	9.20	8.40	8.74	8.64	9.53	9.24	9.26	9.08	9.23	8.54	8.76	9.17	8.52	8.39	9.43
Na2O	3.62	3.85	3.93	3.87	3.43	3.34	3.34	3.37	3.72	3.74	3.85	3.34	3.79	3.76	3.20
K2O	0.84	0.81	0.82	0.81	0.82	0.66	0.68	0.75	0.92	0.81	0.78	0.74	0.81	0.82	0.91
P2O5	0.591	0.400	0.353	0.370	0.355	0.325	0.329	0.345	0.388	0.398	0.355	0.351	0.401	0.404	0.352
Unnormalized trace elements (ppm)															
Ni	89	132	85	89	134	178	172	175	68	132	93	182	139	129	186
Cr	137	125	105	107	258	330	322	311	127	124	108	327	131	121	363
Sc	27	21	21	21	25	27	27	24	23	21	21	26	21	21	28
V	199	179	177	177	198	200	201	190	182	175	174	202	174	175	206
Ba	451	354	333	338	275	245	256	267	383	360	332	286	354	354	374
Rb	9	8	9	8	9	9	8	9	9	9	8	9	9	10	10
Sr	585	752	1014	898	787	595	595	572	1064	743	931	611	736	744	686
Zr	207	161	148	150	148	135	136	134	154	165	149	143	163	166	140
Y	30	22	19	20	22	23	23	22	21	25	22	25	24	25	25
Nb	17.2	12.6	10.1	11.3	14.5	11.0	11.5	13.0	11.6	10.8	8.6	11.1	11.2	11.2	10.5
Ga	19	19	21	20	21	18	19	17	21	19	20	18	19	20	18
Cu	62	59	60	57	64	64	63	61	66	57	60	65	60	57	66
Zn	98	92	82	86	78	79	78	77	87	92	84	81	92	91	80
Pb	6	5	6	5	5	3	3	3	5	4	4	3	4	4	4
La	26	18	18	16	19	17	14	14	21	19	17	13	18	21	18
Ce	50	43	38	38	40	28	37	34	48	45	42	38	42	43	39
Th	1	-1	0	-1	1	0	-1	0	0	1	1	1	1	2	1
Nd	28	24	21	23	24	20	23	19	28	25	25	21	25	25	24
U															

Note: Major elements are normalized on a volatile-free basis, with total Fe expressed as FeO. 'R' denotes a duplicate bead made from the same rock powder.

TABLE A1. MAJOR AND MINOR ELEMENT CHEMISTRY FOR SMVF SAMPLES DETERMINED BY XRF

Sample ID	RC03-19	RC03-20	RC03-21	RC03-22	RC03-23	RC03-24R	RC03-25	RC03-26	RC03-27	RC03-28	RC03-29	RC03-30	RC03-31	RC03-32	RC03-33
Unnormalized major elements (weight %)															
SiO2	50.75	51.80	52.09	50.66	51.70	52.26	51.76	52.13	50.76	51.69	50.55	52.31	52.77	50.27	50.65
TiO2	1.551	1.360	1.392	1.610	1.393	1.399	1.399	1.403	1.585	1.380	1.560	1.276	1.290	1.377	1.568
Al2O3	16.79	17.03	17.28	16.68	17.25	17.41	17.29	17.37	16.65	16.97	16.69	17.16	17.39	16.67	16.51
FeO*	8.44	7.83	7.91	8.37	7.76	7.66	7.68	7.85	8.35	8.06	8.44	7.49	7.58	8.35	8.58
MnO	0.147	0.143	0.142	0.145	0.142	0.141	0.142	0.142	0.144	0.142	0.147	0.134	0.132	0.153	0.146
MgO	7.12	6.62	6.23	7.25	6.09	5.86	5.87	5.98	7.39	6.44	7.15	6.08	5.75	7.77	7.53
CaO	9.86	9.69	9.79	9.79	9.80	9.87	9.78	9.84	9.58	9.65	9.86	9.04	9.06	9.13	9.50
Na2O	3.22	3.29	3.34	3.29	3.29	3.40	3.37	3.33	3.34	3.34	3.21	3.54	3.64	3.23	3.34
K2O	0.93	0.99	1.01	0.85	0.98	1.02	1.00	1.02	0.83	1.02	0.91	0.85	0.85	0.81	0.82
P2O5	0.374	0.362	0.369	0.365	0.372	0.375	0.374	0.377	0.358	0.368	0.371	0.374	0.378	0.357	0.356
Sum	99.18	99.12	99.55	99.01	98.78	99.40	98.67	99.44	98.99	99.06	98.89	98.25	98.84	98.12	99.00
Normalized major elements (weight %)															
SiO2	51.17	52.26	52.32	51.17	52.34	52.58	52.46	52.42	51.28	52.18	51.12	53.24	53.39	51.23	51.16
TiO2	1.564	1.372	1.398	1.626	1.410	1.408	1.418	1.411	1.601	1.393	1.578	1.299	1.305	1.403	1.584
Al2O3	16.93	17.18	17.36	16.85	17.46	17.52	17.52	17.47	16.82	17.13	16.88	17.46	17.59	16.99	16.68
FeO*	8.51	7.90	7.95	8.45	7.86	7.71	7.78	7.89	8.44	8.14	8.53	7.62	7.67	8.51	8.67
MnO	0.148	0.144	0.143	0.146	0.144	0.142	0.144	0.143	0.145	0.143	0.149	0.136	0.134	0.156	0.147
MgO	7.18	6.68	6.26	7.32	6.17	5.90	5.95	6.01	7.47	6.50	7.23	6.19	5.82	7.92	7.61
CaO	9.94	9.78	9.83	9.89	9.92	9.93	9.91	9.90	9.68	9.74	9.97	9.20	9.17	9.31	9.60
Na2O	3.25	3.32	3.35	3.32	3.33	3.42	3.42	3.35	3.37	3.37	3.25	3.60	3.68	3.29	3.37
K2O	0.94	1.00	1.01	0.86	0.99	1.03	1.01	1.03	0.84	1.03	0.92	0.87	0.86	0.83	0.83
P2O5	0.377	0.365	0.371	0.369	0.377	0.377	0.379	0.379	0.362	0.371	0.375	0.381	0.382	0.364	0.360
Unnormalized trace elements (ppm)															
Ni	108	85	71	115	66	57	59	61	125	79	108	85	75	151	132
Cr	221	176	155	228	146	129	129	135	245	168	219	153	131	288	256
Sc	28	29	28	27	28	27	28	27	26	27	28	23	23	27	27
V	202	195	196	201	196	198	197	200	199	192	202	175	174	193	198
Ba	344	408	405	319	410	409	418	407	283	404	339	370	353	328	284
Rb	10	10	9	10	10	10	10	10	11	10	10	9	8	9	10
Sr	905	1016	1024	891	1032	1032	1029	1030	835	1011	906	1056	1066	692	802
Zr	151	148	151	153	153	153	153	154	152	149	152	155	159	143	153
Y	25	24	25	24	25	25	25	25	25	24	26	24	23	26	24
Nb	13.5	10.2	10.4	13.7	11.3	10.8	10.8	11.5	13.5	11.4	13.7	9.5	9.8	9.4	13.7
Ga	18	20	19	21	17	19	18	19	18	17	18	19	19	16	18
Cu	66	50	68	62	64	66	64	66	63	61	66	60	62	60	63
Zn	78	78	77	81	80	79	78	79	78	78	79	84	83	84	81
Pb	5	4	6	5	5	5	7	4	3	4	4	5	6	3	5
La	19	17	21	20	18	23	20	21	15	22	22	21	22	15	17
Ce	47	42	44	44	48	44	52	46	43	51	44	48	51	39	42
Th	1	2	1	1	1	1	2	1	2	2	1	1	2	0	2
Nd	28	26	26	25	30	26	29	26	26	26	23	26	28	25	26
U															

Note: Major elements are normalized on a volatile-free basis, with total Fe expressed as FeO. 'R' denotes a duplicate bead made from the same rock powder.

TABLE A1. MAJOR AND MINOR ELEMENT CHEMISTRY FOR SMVF SAMPLES DETERMINED BY XRF

Sample ID	RC03-34	RC03-35	RC03-36	RC03-37	RC03-38	RC03-41	RC03-42	RC03-43	RC03-44	RC03-45	RC03-46	RC03-47	RC03-48	RC03-49	RC03-50
Unnormalized major elements (weight %)															
SiO2	50.18	50.46	50.92	51.10	50.58	54.50	50.43	55.63	50.29	52.65	52.41	51.80	52.66	51.14	51.18
TiO2	1.567	1.559	1.371	1.379	1.536	1.038	1.441	1.035	1.416	1.283	1.299	1.275	1.297	1.535	1.552
Al2O3	16.37	16.50	16.63	16.78	16.54	18.25	16.46	19.39	16.39	17.28	17.48	16.80	17.33	17.17	17.10
FeO*	8.54	8.25	8.14	7.86	8.44	6.96	8.32	6.59	8.41	7.49	7.45	7.93	7.62	8.00	8.09
MnO	0.147	0.149	0.143	0.143	0.149	0.122	0.147	0.114	0.148	0.135	0.136	0.140	0.135	0.143	0.143
MgO	7.51	7.43	6.86	6.85	7.59	4.94	7.60	4.34	8.04	6.05	5.64	6.77	5.71	6.00	6.13
CaO	9.47	9.50	9.49	9.63	9.48	8.02	9.32	7.75	9.17	9.17	9.21	9.04	9.18	9.88	9.96
Na2O	3.22	3.26	3.17	3.23	3.27	3.78	3.30	3.98	3.24	3.53	3.55	3.30	3.57	3.19	3.21
K2O	0.81	0.83	0.99	0.99	0.80	0.75	0.75	0.65	0.72	0.87	0.87	0.91	0.91	0.94	0.99
P2O5	0.349	0.353	0.364	0.362	0.352	0.218	0.335	0.201	0.330	0.377	0.381	0.377	0.385	0.382	0.373
Sum	98.16	98.29	98.08	98.32	98.74	98.58	98.10	99.68	98.15	98.84	98.43	98.34	98.80	98.38	98.73
Normalized major elements (weight %)															
SiO2	51.12	51.34	51.92	51.97	51.23	55.29	51.41	55.81	51.24	53.27	53.25	52.67	53.30	51.98	51.84
TiO2	1.596	1.586	1.398	1.403	1.556	1.053	1.469	1.038	1.443	1.298	1.320	1.296	1.313	1.560	1.572
Al2O3	16.68	16.79	16.96	17.07	16.75	18.51	16.78	19.45	16.70	17.48	17.76	17.08	17.54	17.45	17.32
FeO*	8.70	8.39	8.30	7.99	8.55	7.06	8.48	6.61	8.57	7.58	7.57	8.06	7.71	8.13	8.19
MnO	0.150	0.152	0.146	0.145	0.151	0.124	0.150	0.114	0.151	0.137	0.138	0.142	0.137	0.145	0.145
MgO	7.65	7.56	6.99	6.97	7.69	5.01	7.75	4.35	8.19	6.12	5.73	6.88	5.78	6.10	6.21
CaO	9.65	9.67	9.68	9.79	9.60	8.14	9.50	7.77	9.34	9.28	9.36	9.19	9.29	10.04	10.09
Na2O	3.28	3.32	3.23	3.29	3.31	3.83	3.36	3.99	3.30	3.57	3.61	3.36	3.61	3.24	3.25
K2O	0.83	0.84	1.01	1.01	0.81	0.76	0.76	0.65	0.73	0.88	0.88	0.93	0.92	0.96	1.00
P2O5	0.356	0.359	0.371	0.368	0.357	0.221	0.341	0.202	0.336	0.381	0.387	0.383	0.390	0.388	0.378
Unnormalized trace elements (ppm)															
Ni	131	130	98	93	137	68	138	58	162	78	64	107	68	63	70
Cr	256	251	201	196	264	83	274	41	310	139	121	208	126	139	154
Sc	27	26	27	28	26	20	26	18	26	23	23	25	24	28	29
V	195	198	191	197	196	164	195	152	189	177	179	178	178	201	205
Ba	282	281	395	400	279	267	269	256	271	394	411	396	380	394	378
Rb	10	10	9	10	9	8	9	5	9	10	9	10	9	11	11
Sr	810	807	997	1005	776	605	730	922	720	1047	1063	1004	1046	969	918
Zr	151	151	148	149	150	114	146	100	143	155	158	154	158	156	156
Y	25	24	24	26	25	17	25	15	24	24	24	25	25	26	26
Nb	13.1	12.3	11.1	11.2	12.2	6.5	10.8	4.1	10.2	9.7	9.0	9.3	9.8	13.6	13.9
Ga	19	18	17	19	17	19	19	20	17	18	20	18	18	17	20
Cu	59	58	62	63	52	36	59	59	58	48	64	24	52	26	64
Zn	82	80	84	80	79	76	80	71	81	81	87	83	82	83	81
Pb	4	4	5	4	3	4	4	3	3	5	5	5	6	4	31
La	21	18	20	21	15	8	17	9	13	22	23	23	21	22	21
Ce	41	46	45	45	40	29	38	26	38	49	48	54	50	48	51
Th	1	1	2	0	1	0	2	1	1	2	2	1	1	2	2
Nd	24	26	26	29	21	15	19	17	21	24	26	28	29	26	27
U															

Note: Major elements are normalized on a volatile-free basis, with total Fe expressed as FeO. 'R' denotes a duplicate bead made from the same rock powder.

TABLE A1. MAJOR AND MINOR ELEMENT CHEMISTRY FOR SMVF SAMPLES DETERMINED BY XRF

Sample ID	RC03-51A	RC03-51B	RC03-52	RC03-53	RC03-54	RC03-55	RC03-56	RC03-57	RC03-58	RC03-59	RC03-60	RC04-25	RC04-26	RC04-27	RC04-28
Unnormalized major elements (weight %)															
SiO2	48.81	49.41	49.83	49.57	50.65	52.79	52.46	50.18	49.71	49.84	51.23	50.91	50.62	56.54	50.10
TiO2	1.417	1.427	1.442	1.443	1.438	1.240	1.283	1.503	1.412	1.395	1.387	1.534	1.473	1.116	1.423
Al2O3	16.22	16.42	16.52	16.41	16.68	17.61	17.69	16.13	16.43	16.53	16.79	17.04	16.50	18.52	16.51
FeO*	8.76	8.59	8.68	8.80	8.71	7.44	7.78	9.04	8.66	8.70	7.92	8.18	8.44	6.94	8.89
MnO	0.150	0.153	0.154	0.152	0.158	0.125	0.135	0.154	0.151	0.150	0.143	0.143	0.144	0.117	0.152
MgO	8.31	8.35	8.11	8.35	8.23	5.39	5.61	7.97	8.47	8.33	6.73	6.14	7.73	3.73	8.29
CaO	8.94	9.18	9.23	9.22	9.22	8.58	8.50	8.70	9.24	9.09	9.61	9.82	9.36	7.39	9.03
Na2O	3.13	3.14	3.17	3.16	3.21	3.82	3.77	3.43	3.25	3.22	3.26	3.28	3.29	4.11	3.32
K2O	0.88	0.88	0.92	0.88	0.91	0.81	0.81	1.02	0.81	0.68	1.00	0.98	0.75	0.76	0.70
P2O5	0.340	0.349	0.354	0.336	0.357	0.355	0.381	0.473	0.332	0.327	0.365	0.376	0.334	0.284	0.328
Sum	96.96	97.90	98.41	98.32	99.56	98.16	98.42	98.60	98.47	98.26	98.44	98.40	98.64	99.51	98.74
Normalized major elements (weight %)															
SiO2	50.34	50.47	50.64	50.42	50.87	53.78	53.30	50.89	50.48	50.72	52.04	51.74	51.32	56.82	50.74
TiO2	1.461	1.458	1.465	1.468	1.444	1.263	1.304	1.524	1.434	1.420	1.409	1.559	1.493	1.122	1.441
Al2O3	16.73	16.77	16.79	16.69	16.75	17.94	17.97	16.36	16.69	16.82	17.06	17.32	16.73	18.61	16.72
FeO*	9.03	8.77	8.82	8.95	8.75	7.58	7.90	9.17	8.80	8.85	8.05	8.31	8.56	6.97	9.00
MnO	0.155	0.156	0.156	0.155	0.159	0.127	0.137	0.156	0.153	0.153	0.145	0.145	0.146	0.118	0.154
MgO	8.57	8.53	8.24	8.49	8.27	5.49	5.70	8.08	8.60	8.48	6.84	6.24	7.84	3.75	8.40
CaO	9.22	9.38	9.38	9.38	9.26	8.74	8.64	8.82	9.38	9.25	9.76	9.98	9.49	7.43	9.14
Na2O	3.23	3.21	3.22	3.21	3.22	3.89	3.83	3.48	3.30	3.28	3.31	3.33	3.34	4.13	3.36
K2O	0.91	0.90	0.93	0.90	0.91	0.83	0.82	1.03	0.82	0.69	1.02	1.00	0.76	0.76	0.71
P2O5	0.351	0.356	0.360	0.342	0.359	0.362	0.387	0.480	0.337	0.333	0.371	0.382	0.339	0.285	0.332
Unnormalized trace elements (ppm)															
Ni	171	183	170	179	175	86	106	185	183	182	89	70	150	34	182
Cr	335	341	323	356	331	93	107	313	356	332	192	154	278	44	327
Sc	26	26	26	28	27	21	21	25	28	27	28	28	27	17	26
V	197	200	198	201	200	171	176	157	203	188	194	205	196	134	195
Ba	364	383	381	358	383	340	349	499	341	259	398	379	264	357	261
Rb	9	10	10	10	10	9	9	10	10	9	10	10	10	9	9
Sr	697	713	720	671	724	1002	824	884	676	601	1004	888	718	900	570
Zr	137	140	141	138	140	156	160	168	133	137	149	145	135	120	129
Y	22	25	26	25	25	22	24	28	25	25	25	23	21	17	23
Nb	10.0	10.7	10.8	10.5	10.6	9.2	9.8	10.3	10.2	10.6	10.8	13.6	11.5	6.4	10.1
Ga	16	17	17	17	17	19	21	18	16	17	18	18	17	20	17
Cu	60	67	67	70	59	50	56	47	43	52	63	63	60	39	61
Zn	77	81	80	80	84	83	89	89	78	80	80	76	78	81	79
Pb	3	4	4	4	12	4	4	5	3	3	6	5	5	4	4
La	13	16	17	16	14	20	21	21	15	18	20	21	15	12	16
Ce	35	41	41	38	36	47	48	50	37	33	43	46	41	32	33
Th	2	1	2	1	2	2	1	3	0	2	2	2	2	3	2
Nd	22	23	26	22	21	26	25	27	20	21	27	27	24	19	21
U															

Note: Major elements are normalized on a volatile-free basis, with total Fe expressed as FeO. 'R' denotes a duplicate bead made from the same rock powder.

TABLE A1. MAJOR AND MINOR ELEMENT CHEMISTRY FOR SMVF SAMPLES DETERMINED BY XRF

Sample ID	RC04-29	RC04-30	RC04-31	RC04-32	RC04-33	RC04-34	RC04-35	RC04-36	RC04-66	RC04-67	RC04-68	RC04-69	RC04-70	RC04-71	RC04-72
Unnormalized major elements (weight %)															
SiO2	50.04	49.97	50.08	49.47	48.90	49.86	52.51	52.72	52.95	50.27	50.88	50.98	51.74	50.73	50.58
TiO2	1.398	1.435	1.424	1.395	1.308	1.506	1.291	1.278	1.273	1.548	1.537	1.533	1.414	1.535	1.545
Al2O3	16.46	16.56	16.62	16.43	16.22	15.54	17.72	17.80	17.33	16.91	16.71	17.05	17.20	16.68	16.81
FeO*	8.89	8.84	8.89	8.85	8.79	8.49	8.21	8.03	7.67	8.48	8.34	8.10	7.88	8.32	8.33
MnO	0.149	0.151	0.150	0.151	0.151	0.143	0.137	0.134	0.132	0.146	0.145	0.143	0.139	0.145	0.143
MgO	8.06	8.22	8.35	8.53	8.80	8.32	5.76	5.62	6.03	6.99	6.94	6.39	6.03	7.10	6.30
CaO	8.63	9.23	9.23	9.13	9.28	9.25	8.40	8.47	8.99	9.81	9.76	9.93	9.80	9.70	9.83
Na2O	3.03	3.21	3.25	3.13	3.10	3.25	3.78	3.79	3.56	3.19	3.27	3.29	3.30	3.21	3.27
K2O	0.81	0.82	0.79	0.76	0.70	1.39	0.81	0.79	0.83	0.83	0.91	0.91	0.96	0.90	0.90
P2O5	0.348	0.344	0.335	0.318	0.327	0.608	0.396	0.385	0.379	0.371	0.374	0.374	0.371	0.373	0.373
Sum	97.82	98.78	99.12	98.16	97.58	98.36	99.01	99.02	99.14	98.55	98.87	98.70	98.83	98.69	98.08
Normalized major elements (weight %)															
SiO2	51.16	50.59	50.53	50.40	50.11	50.69	53.03	53.24	53.41	51.01	51.46	51.65	52.35	51.40	51.57
TiO2	1.429	1.453	1.437	1.421	1.340	1.531	1.304	1.291	1.284	1.571	1.555	1.553	1.431	1.555	1.575
Al2O3	16.83	16.76	16.77	16.74	16.62	15.80	17.90	17.98	17.48	17.16	16.90	17.27	17.40	16.90	17.14
FeO*	9.09	8.95	8.97	9.02	9.01	8.63	8.29	8.11	7.74	8.61	8.44	8.21	7.97	8.43	8.49
MnO	0.152	0.153	0.151	0.154	0.155	0.145	0.138	0.135	0.133	0.148	0.147	0.145	0.141	0.147	0.146
MgO	8.24	8.32	8.42	8.69	9.02	8.46	5.82	5.68	6.08	7.09	7.02	6.47	6.10	7.19	6.42
CaO	8.82	9.34	9.31	9.30	9.51	9.40	8.48	8.55	9.07	9.95	9.87	10.06	9.92	9.83	10.02
Na2O	3.10	3.25	3.28	3.19	3.18	3.30	3.82	3.83	3.59	3.24	3.31	3.33	3.34	3.25	3.33
K2O	0.83	0.83	0.80	0.77	0.72	1.41	0.82	0.80	0.84	0.84	0.92	0.92	0.97	0.91	0.92
P2O5	0.356	0.348	0.338	0.324	0.335	0.618	0.400	0.389	0.382	0.376	0.378	0.379	0.375	0.378	0.380
Unnormalized trace elements (ppm)															
Ni	184	174	180	194	205	201	127	112	84	103	102	78	63	106	76
Cr	328	338	348	361	389	352	110	108	148	211	206	167	138	213	168
Sc	27	27	27	27	28	24	21	20	23	27	28	28	28	28	28
V	181	203	201	201	197	191	173	168	173	182	201	204	197	202	202
Ba	354	338	334	318	340	1081	365	348	361	349	342	346	401	338	351
Rb	9	9	9	9	8	18	9	8	8	9	10	10	10	10	10
Sr	676	650	657	626	666	1343	733	781	1018	882	867	880	980	867	878
Zr	129	129	127	121	119	193	156	151	147	143	141	143	142	141	145
Y	22	23	22	22	22	22	23	22	20	22	23	23	22	23	24
Nb	10.2	9.9	9.6	9.3	7.0	7.9	9.1	10.3	9.2	12.6	12.2	12.8	11.2	13.1	12.3
Ga	16	15	18	17	16	19	19	19	20	17	17	19	19	17	18
Cu	52	59	60	62	63	67	52	58	61	60	58	62	63	80	43
Zn	77	78	78	76	79	91	88	87	81	79	78	77	76	186	77
Pb	2	5	6	5	3	6	5	7	5	5	5	5	5	154	4
La	14	16	16	13	14	37	19	18	22	18	20	17	18	18	17
Ce	36	34	26	29	35	84	39	44	46	45	44	44	40	53	44
Th	2	2	1	2	2	4	2	1	2	1	2	2	3	0	2
Nd	22	22	20	2	3	49	22	26	27	28	23	26	25	29	26
U															

Note: Major elements are normalized on a volatile-free basis, with total Fe expressed as FeO. 'R' denotes a duplicate bead made from the same rock powder.

TABLE A1. MAJOR AND MINOR ELEMENT CHEMISTRY FOR SMVF SAMPLES DETERMINED BY XRF

Sample ID	RC09-33	RC09-34	RC09-35	RC09-36	RC09-37	RC09-38	RC09-39	RC09-40	RC09-41	RC09-42	RC09-43	RC09-44	RC09-45	RC09-46	RC09-47
Unnormalized major elements (weight %)															
SiO2	52.37	53.36	51.86	50.93	53.43	51.01	50.54	51.00	50.94	51.14	53.40	51.03	51.32	51.78	50.47
TiO2	1.324	1.306	1.325	1.367	1.293	1.606	1.546	1.581	1.392	1.390	1.296	1.570	1.551	1.391	1.570
Al2O3	17.07	17.51	16.87	17.05	17.62	16.75	16.77	16.62	17.09	17.00	17.67	16.80	16.82	17.06	16.72
FeO*	8.03	7.98	8.04	8.71	7.64	8.47	9.08	8.68	8.62	8.57	7.66	8.62	8.67	8.24	8.62
MnO	0.144	0.145	0.142	0.152	0.132	0.146	0.156	0.146	0.149	0.149	0.131	0.147	0.147	0.143	0.147
MgO	6.99	5.27	6.96	7.81	5.88	7.44	7.61	7.77	7.84	7.85	5.71	7.76	7.75	6.92	7.61
CaO	9.40	8.50	9.34	9.16	9.05	9.80	8.80	9.49	9.16	9.17	9.04	9.53	9.51	9.65	9.47
Na2O	3.41	3.40	3.35	3.35	3.73	3.34	3.41	3.36	3.33	3.35	3.78	3.37	3.38	3.35	3.27
K2O	0.98	1.16	0.97	0.70	0.85	0.89	1.08	0.81	0.81	0.83	0.86	0.79	0.80	1.01	0.80
P2O5	0.375	0.349	0.379	0.358	0.383	0.373	0.593	0.360	0.372	0.357	0.384	0.358	0.357	0.372	0.363
Sum	100.09	98.98	99.24	99.59	100.01	99.83	99.59	99.82	99.70	99.81	99.93	99.98	100.31	99.92	99.04
Normalized major elements (weight %)															
SiO2	52.32	53.91	52.26	51.14	53.43	51.10	50.75	51.09	51.09	51.24	53.44	51.04	51.16	51.82	50.96
TiO2	1.323	1.319	1.335	1.373	1.293	1.609	1.552	1.584	1.396	1.393	1.297	1.570	1.546	1.392	1.585
Al2O3	17.05	17.69	17.00	17.12	17.62	16.78	16.84	16.65	17.14	17.03	17.68	16.80	16.77	17.07	16.88
FeO*	8.02	8.06	8.10	8.75	7.64	8.48	9.12	8.70	8.65	8.59	7.67	8.62	8.64	8.25	8.70
MnO	0.144	0.146	0.143	0.153	0.132	0.146	0.157	0.146	0.149	0.149	0.131	0.147	0.147	0.143	0.148
MgO	6.98	5.32	7.01	7.84	5.88	7.45	7.64	7.78	7.86	7.87	5.71	7.76	7.73	6.93	7.68
CaO	9.39	8.59	9.41	9.20	9.05	9.82	8.84	9.51	9.19	9.19	9.05	9.53	9.48	9.66	9.56
Na2O	3.41	3.44	3.38	3.36	3.73	3.35	3.42	3.37	3.34	3.36	3.78	3.37	3.37	3.35	3.30
K2O	0.98	1.17	0.98	0.70	0.85	0.89	1.08	0.81	0.81	0.83	0.86	0.79	0.80	1.01	0.81
P2O5	0.375	0.353	0.382	0.359	0.383	0.374	0.595	0.361	0.373	0.358	0.384	0.358	0.356	0.372	0.367
Unnormalized trace elements (ppm)															
Ni	101	72	101	145	82	121	174	140	147	148	76	140	142	92	131
Cr	195	112	195	276	123	234	279	256	279	276	116	258	263	191	249
Sc	26	25	27	27	23	26	26	27	26	27	23	26	27	28	26
V	189	194	190	189	178	205	195	200	198	202	176	195	199	198	197
Ba	394	377	398	283	347	316	792	282	316	324	341	275	269	395	274
Rb	12	22	10	8	10	11	13	11	10	10	10	10	10	10	10
Sr	1021	519	1016	754	1084	917	771	826	708	713	1079	813	785	1034	821
Zr	148	149	148	134	155	150	208	149	143	142	158	150	149	148	150
Y	24	32	24	25	23	24	28	24	25	25	23	24	24	25	24
Nb	13.0	10.9	12.7	8.9	10.7	16.2	14.5	14.5	11.4	11.1	12.2	14.9	15.0	13.6	14.9
Ga	19	18	18	17	20	18	18	19	17	18	20	19	19	18	19
Cu	58	62	61	44	61	63	63	63	50	61	59	65	62	64	55
Zn	84	83	81	81	84	78	95	80	81	81	83	79	84	81	80
Pb	4	6	4	3	4	3	5	3	3	3	3	2	4	5	4
La	18	21	22	13	23	19	27	17	15	16	19	17	17	22	19
Ce	45	42	48	36	48	50	68	43	33	40	49	39	42	41	41
Th	2	2	2	1	2	1	3	2	2	3	2	2	2	1	3
Nd	26	25	27	23	28	26	38	24	22	23	25	22	23	25	22
U	2	1	1	0	1	3	3	1	2	0	1	1	0	2	3

Note: Major elements are normalized on a volatile-free basis, with total Fe expressed as FeO. 'R' denotes a duplicate bead made from the same rock powder.

TABLE A1. MAJOR AND MINOR ELEMENT CHEMISTRY FOR SMVF SAMPLES DETERMINED BY XRF

Sample ID	RC09-47R	RC09-48	RC09-49	RC09-50	RC09-51	RC09-52	RC09-53	RC09-54	RC09-55	RC09-56	RC09-57	RC09-58	RC09-59	RC09-60	RC09-61
Unnormalized major elements (weight %)															
SiO2	50.79	51.31	51.82	51.04	51.69	51.92	51.09	51.64	51.18	51.38	51.06	51.05	50.21	51.16	50.83
TiO2	1.577	1.576	1.384	1.579	1.378	1.397	1.560	1.382	1.621	1.630	1.616	1.618	1.623	1.582	1.594
Al2O3	16.70	16.84	17.12	16.87	16.92	17.10	16.71	17.00	16.75	16.82	16.78	16.76	16.53	16.79	16.73
FeO*	8.67	8.60	8.02	8.64	8.20	8.26	8.66	8.08	8.65	8.65	8.63	8.66	8.53	8.61	8.60
MnO	0.148	0.147	0.141	0.147	0.143	0.144	0.146	0.143	0.147	0.146	0.146	0.146	0.146	0.146	0.145
MgO	7.68	7.40	6.35	7.46	6.98	6.95	7.69	6.59	7.57	7.44	7.46	7.45	7.43	7.69	7.49
CaO	9.50	9.91	9.66	9.80	9.62	9.68	9.48	9.58	9.73	9.79	9.73	9.74	9.56	9.60	9.58
Na2O	3.29	3.37	3.40	3.29	3.34	3.37	3.37	3.33	3.40	3.40	3.38	3.40	3.33	3.39	3.36
K2O	0.79	0.92	1.01	0.90	1.00	1.00	0.80	0.99	0.87	0.87	0.85	0.86	0.84	0.83	0.82
P2O5	0.365	0.381	0.374	0.384	0.368	0.376	0.357	0.374	0.372	0.372	0.368	0.373	0.372	0.361	0.364
Sum	99.50	100.45	99.28	100.11	99.64	100.20	99.86	99.11	100.29	100.50	100.02	100.06	98.57	100.16	99.51
Normalized major elements (weight %)															
SiO2	51.04	51.08	52.20	50.98	51.88	51.82	51.16	52.10	51.03	51.13	51.05	51.02	50.94	51.08	51.08
TiO2	1.585	1.569	1.394	1.577	1.383	1.394	1.562	1.394	1.616	1.622	1.616	1.617	1.647	1.579	1.602
Al2O3	16.79	16.76	17.24	16.85	16.98	17.07	16.73	17.15	16.70	16.74	16.78	16.75	16.77	16.76	16.81
FeO*	8.71	8.56	8.08	8.63	8.23	8.24	8.67	8.15	8.62	8.61	8.63	8.66	8.65	8.60	8.64
MnO	0.148	0.146	0.142	0.147	0.144	0.144	0.146	0.144	0.147	0.145	0.146	0.146	0.148	0.146	0.146
MgO	7.72	7.37	6.40	7.45	7.01	6.94	7.70	6.65	7.55	7.40	7.46	7.45	7.54	7.68	7.53
CaO	9.54	9.87	9.73	9.79	9.65	9.66	9.49	9.67	9.70	9.74	9.73	9.73	9.70	9.58	9.63
Na2O	3.30	3.35	3.42	3.29	3.35	3.36	3.37	3.36	3.39	3.38	3.38	3.40	3.38	3.38	3.38
K2O	0.79	0.92	1.02	0.90	1.00	1.00	0.80	1.00	0.87	0.87	0.85	0.86	0.85	0.83	0.82
P2O5	0.367	0.379	0.377	0.384	0.369	0.375	0.357	0.377	0.371	0.370	0.368	0.373	0.377	0.360	0.366
Unnormalized trace elements (ppm)															
Ni	135	116	75	117	96	94	138	83	123	119	121	120	123	132	126
Cr	251	225	157	228	196	190	255	168	237	228	233	228	228	244	236
Sc	26	28	28	28	27	28	28	28	27	27	27	28	27	27	27
V	199	207	196	204	195	199	199	199	202	203	206	204	206	198	201
Ba	275	336	402	337	395	395	275	399	294	299	295	299	301	282	282
Rb	10	12	11	11	11	11	11	10	11	11	11	11	11	12	11
Sr	823	932	1043	920	1030	1036	807	1032	904	914	907	910	888	852	849
Zr	150	150	148	151	145	147	151	148	152	153	152	152	153	150	152
Y	24	24	24	25	24	24	24	24	25	24	24	24	24	24	24
Nb	15.6	16.2	13.1	15.9	13.9	13.3	15.1	13.1	16.0	15.7	15.9	15.8	16.3	15.0	15.4
Ga	17	19	19	20	19	19	19	18	19	20	19	18	17	18	17
Cu	56	65	63	58	64	61	63	64	61	64	62	63	54	62	62
Zn	80	82	78	84	80	82	78	79	81	81	81	80	79	83	81
Pb	3	4	5	3	4	3	3	6	4	4	3	3	3	4	2
La	19	19	19	18	16	20	18	19	16	19	16	20	20	18	18
Ce	42	44	51	48	48	43	43	46	39	43	45	45	43	39	42
Th	2	2	2	2	2	2	1	2	3	2	2	2	1	2	2
Nd	24	24	28	27	26	25	23	24	24	23	23	23	26	25	26
U	2	1	3	3	0	1	2	2	1	2	2	2	0	1	1

Note: Major elements are normalized on a volatile-free basis, with total Fe expressed as FeO. 'R' denotes a duplicate bead made from the same rock powder.

TABLE A1. MAJOR AND MINOR ELEMENT CHEMISTRY FOR SMVF SAMPLES DETERMINED BY XRF

Sample ID	NID09-01	NID09-02	NID09-02R	NID09-03	NID09-04	NID09-05	NID09-07	NID09-08	NID09-09	NID09-10	NID09-11	NID09-12	NID09-13	NID09-13R
Unnormalized major elements (weight %)														
SiO2	51.00	51.02	51.11	51.19	50.96	50.82	49.98	50.94	50.65	50.21	49.97	52.03	51.34	51.73
TiO2	1.572	1.557	1.568	1.590	1.595	1.561	1.603	1.565	1.556	1.489	1.521	1.400	1.393	1.401
Al2O3	16.76	16.70	16.78	16.89	16.79	16.67	16.55	16.71	16.65	17.07	17.04	17.03	16.85	17.04
FeO*	8.51	8.56	8.60	8.62	8.66	8.66	8.51	8.43	8.62	9.04	9.30	8.27	8.20	8.25
MnO	0.149	0.150	0.148	0.150	0.149	0.147	0.143	0.148	0.149	0.158	0.163	0.146	0.145	0.144
MgO	7.62	7.74	7.82	7.54	7.64	7.73	7.15	7.66	7.59	8.05	8.08	6.98	7.02	7.05
CaO	9.44	9.40	9.49	9.59	9.50	9.45	9.58	9.46	9.40	9.49	9.42	9.68	9.54	9.59
Na2O	3.20	3.34	3.34	3.33	3.29	3.32	3.17	3.30	3.23	3.19	3.21	3.29	3.25	3.28
K2O	0.84	0.84	0.80	0.83	0.80	0.81	0.83	0.81	0.79	0.67	0.65	1.01	0.99	1.00
P2O5	0.366	0.371	0.373	0.367	0.372	0.359	0.373	0.367	0.367	0.324	0.346	0.374	0.370	0.373
Sum	99.46	99.68	100.03	100.10	99.76	99.53	97.89	99.39	99.00	99.69	99.70	100.21	99.10	99.85
Normalized major elements (weight %)														
SiO2	51.28	51.18	51.10	51.14	51.08	51.06	51.06	51.25	51.16	50.37	50.12	51.92	51.81	51.81
TiO2	1.581	1.562	1.568	1.588	1.599	1.568	1.638	1.575	1.572	1.494	1.526	1.397	1.406	1.404
Al2O3	16.85	16.75	16.77	16.87	16.83	16.75	16.91	16.81	16.82	17.12	17.09	16.99	17.00	17.07
FeO*	8.56	8.59	8.60	8.61	8.68	8.70	8.69	8.48	8.71	9.07	9.33	8.25	8.27	8.26
MnO	0.150	0.150	0.148	0.150	0.149	0.148	0.146	0.149	0.151	0.158	0.163	0.146	0.146	0.144
MgO	7.66	7.77	7.82	7.53	7.66	7.77	7.30	7.71	7.67	8.07	8.10	6.97	7.08	7.06
CaO	9.49	9.43	9.49	9.58	9.52	9.49	9.79	9.52	9.49	9.52	9.45	9.66	9.63	9.60
Na2O	3.22	3.35	3.34	3.33	3.30	3.34	3.24	3.32	3.26	3.20	3.22	3.28	3.28	3.28
K2O	0.84	0.84	0.80	0.83	0.80	0.81	0.85	0.81	0.80	0.67	0.65	1.01	1.00	1.00
P2O5	0.368	0.372	0.373	0.367	0.373	0.361	0.381	0.369	0.371	0.325	0.347	0.373	0.373	0.373
Unnormalized trace elements (ppm)														
Ni	139	139	141	129	133	142	117	139	136	151	151	97	98	99
Cr	261	255	259	235	252	262	225	258	254	287	287	196	194	195
Sc	26	27	27	26	27	27	27	27	26	28	29	28	27	28
V	200	196	199	200	195	200	199	199	198	217	223	197	196	199
Ba	282	287	284	277	280	272	298	276	272	210	211	395	392	391
Rb	12	12	11	11	11	10	11	10	11	10	10	11	12	11
Sr	796	815	824	835	826	803	884	797	795	451	440	1033	1012	1019
Zr	152	149	149	151	152	149	150	149	148	126	130	149	146	147
Y	24	24	23	24	25	24	24	24	23	24	25	25	23	23
Nb	15.1	15.1	15.5	16.2	15.0	15.2	16.2	15.3	14.9	14.8	14.6	14.0	13.3	13.7
Ga	18	19	18	18	19	18	16	18	18	17	19	19	18	18
Cu	59	58	59	60	48	57	58	57	53	59	57	62	59	62
Zn	82	82	81	81	84	79	80	79	82	79	80	85	80	80
Pb	3	3	2	2	3	4	3	2	4	1	3	4	5	4
La	17	18	18	21	19	18	17	16	16	14	13	19	18	21
Ce	45	45	41	45	40	43	45	43	39	29	25	47	46	48
Th	2	2	1	3	2	2	2	2	2	2	2	1	1	1
Nd	23	23	25	23	21	23	24	24	22	17	15	25	25	27
U	1	2	0	1	2	1	2	1	1	1	2	0	2	2

Note: Major elements are normalized on a volatile-free basis, with total Fe expressed as FeO. 'R' denotes a duplicate bead made from the same rock powder.

TABLE A1. MAJOR AND MINOR ELEMENT CHEMISTRY FOR SMVF SAMPLES DETERMINED BY XRF

Sample ID	NID09-14	NID09-15	NID09-16	NID09-17	NID09-18	NID09-19	NID09-20	NID09-21	NID09-22	NID09-23	NID09-24	NID09-24R	NID09-25	NID09-26
Unnormalized major elements (weight %)														
SiO2	50.76	51.55	51.87	50.44	51.00	50.55	51.58	50.41	49.22	55.10	52.91	53.42	53.68	51.28
TiO2	1.567	1.398	1.393	1.560	1.365	1.589	1.386	1.541	1.523	1.203	1.289	1.301	1.307	1.394
Al2O3	16.77	17.03	17.00	16.49	16.85	16.66	16.99	16.50	16.79	17.94	17.38	17.61	17.75	17.09
FeO*	8.60	8.03	8.09	8.65	8.50	8.51	8.09	8.36	9.18	8.02	7.82	7.72	7.86	8.74
MnO	0.151	0.143	0.143	0.149	0.148	0.150	0.144	0.146	0.159	0.135	0.132	0.132	0.133	0.153
MgO	7.54	6.75	7.01	7.72	7.94	7.55	6.93	7.60	8.40	4.33	5.81	5.87	5.76	7.89
CaO	9.41	9.64	9.55	9.33	9.08	9.45	9.56	9.34	9.43	8.04	8.99	9.05	9.10	9.22
Na2O	3.27	3.31	3.27	3.16	3.33	3.28	3.30	3.25	3.11	3.73	3.68	3.73	3.77	3.34
K2O	0.80	1.01	1.00	0.80	0.81	0.83	0.99	0.80	0.65	0.90	0.84	0.85	0.85	0.82
P2O5	0.363	0.371	0.370	0.364	0.350	0.389	0.373	0.351	0.341	0.393	0.383	0.387	0.387	0.361
Sum	99.23	99.23	99.70	98.66	99.37	98.96	99.34	98.30	98.80	99.79	99.23	100.06	100.60	100.29
Normalized major elements (weight %)														
SiO2	51.15	51.95	52.03	51.12	51.32	51.08	51.92	51.28	49.82	55.22	53.32	53.38	53.36	51.13
TiO2	1.579	1.409	1.397	1.581	1.374	1.606	1.395	1.568	1.541	1.206	1.299	1.300	1.299	1.390
Al2O3	16.90	17.16	17.05	16.71	16.96	16.84	17.10	16.79	16.99	17.98	17.51	17.60	17.64	17.04
FeO*	8.67	8.09	8.11	8.77	8.55	8.60	8.14	8.50	9.29	8.04	7.88	7.71	7.81	8.71
MnO	0.152	0.144	0.143	0.151	0.149	0.152	0.145	0.149	0.161	0.135	0.133	0.132	0.132	0.153
MgO	7.60	6.80	7.03	7.82	7.99	7.63	6.98	7.73	8.50	4.34	5.85	5.87	5.73	7.87
CaO	9.48	9.71	9.58	9.46	9.14	9.55	9.62	9.50	9.54	8.06	9.06	9.04	9.05	9.19
Na2O	3.30	3.34	3.28	3.20	3.35	3.31	3.32	3.31	3.15	3.74	3.71	3.72	3.75	3.33
K2O	0.81	1.02	1.00	0.81	0.82	0.84	1.00	0.81	0.66	0.90	0.85	0.85	0.84	0.82
P2O5	0.366	0.374	0.371	0.369	0.352	0.393	0.375	0.357	0.345	0.394	0.386	0.387	0.385	0.360
Unnormalized trace elements (ppm)														
Ni	134	89	98	143	159	130	95	137	164	37	78	78	76	145
Cr	251	187	200	254	284	243	196	252	310	59	126	125	120	276
Sc	26	29	28	28	26	27	28	27	30	22	24	22	22	28
V	202	198	199	195	194	202	198	199	220	168	171	177	175	196
Ba	281	399	391	273	311	281	393	275	199	390	348	349	348	319
Rb	11	10	10	10	9	11	10	10	10	10	10	9	10	10
Sr	805	1035	1024	815	761	847	1025	795	437	694	1078	1082	1085	713
Zr	151	147	147	149	141	151	147	147	130	160	161	160	161	144
Y	24	24	25	24	24	24	24	23	24	28	23	24	23	25
Nb	15.9	13.6	13.3	15.1	10.9	15.4	13.6	13.8	15.7	11.4	11.6	11.5	11.2	11.0
Ga	19	18	19	19	17	18	18	18	18	19	20	19	20	18
Cu	58	62	61	61	63	51	59	60	52	58	58	60	58	61
Zn	81	79	81	80	81	80	81	82	79	97	86	85	84	79
Pb	3	5	4	3	4	3	4	4	2	3	4	4	3	3
La	20	21	21	20	16	20	20	16	10	19	23	21	20	14
Ce	39	46	44	47	38	44	45	39	27	45	51	53	49	38
Th	1	2	2	2	2	3	2	2	2	2	1	2	2	2
Nd	21	26	24	26	21	24	26	24	18	23	26	26	28	22
U	1	0	0	1	0	2	1	1	2	1	1	0	3	3

Note: Major elements are normalized on a volatile-free basis, with total Fe expressed as FeO. 'R' denotes a duplicate bead made from the same rock powder.

TABLE A1. MAJOR AND MINOR ELEMENT CHEMISTRY FOR SMVF SAMPLES DETERMINED BY XRF

Sample ID	NID09-27	NID09-28	NID09-29	NID09-30	NID09-31	NID09-32	NID09-33	RC10-18	RC10-19	RC10-19R	RC10-20	RC10-21	RC10-22	RC10-23	RC10-24
Unnormalized major elements (weight %)															
SiO2	51.37	52.19	50.76	51.03	51.03	51.20	52.10	51.37	51.66	51.66	51.47	50.57	51.69	51.47	53.16
TiO2	1.398	1.389	1.586	1.611	1.366	1.626	1.354	1.439	1.395	1.395	1.389	1.558	1.383	1.382	1.292
Al2O3	17.14	17.39	16.70	16.85	16.76	16.85	16.85	16.84	17.01	17.02	17.05	16.56	17.17	17.21	17.58
FeO*	8.67	7.86	8.41	8.42	8.00	8.49	8.70	8.23	8.21	8.12	8.25	8.45	8.02	7.82	7.54
MnO	0.158	0.142	0.147	0.146	0.142	0.147	0.148	0.145	0.144	0.144	0.143	0.147	0.140	0.141	0.130
MgO	7.93	6.11	7.70	7.52	6.97	7.51	7.90	6.72	6.94	6.91	6.57	7.36	6.14	6.03	5.58
CaO	9.20	9.73	9.50	9.64	9.38	9.75	8.63	9.62	9.62	9.64	9.58	9.73	9.73	9.69	9.01
Na2O	3.34	3.36	3.34	3.40	3.25	3.38	3.51	3.40	3.38	3.40	3.36	3.37	3.44	3.43	3.82
K2O	0.83	1.01	0.79	0.82	0.98	0.85	0.77	1.02	1.00	1.01	1.01	0.93	1.02	1.01	0.84
P2O5	0.377	0.377	0.368	0.366	0.371	0.375	0.310	0.376	0.373	0.372	0.376	0.380	0.374	0.377	0.384
Sum	100.41	99.56	99.30	99.80	98.25	100.18	100.27	99.16	99.74	99.67	99.19	99.07	99.11	98.56	99.34
Normalized major elements (weight %)															
SiO2	51.16	52.42	51.12	51.13	51.94	51.11	51.96	51.81	51.80	51.83	51.89	51.05	52.16	52.22	53.52
TiO2	1.392	1.395	1.597	1.614	1.390	1.623	1.350	1.452	1.399	1.399	1.400	1.572	1.395	1.402	1.301
Al2O3	17.07	17.47	16.82	16.88	17.06	16.82	16.80	16.98	17.06	17.08	17.19	16.71	17.33	17.46	17.70
FeO*	8.63	7.89	8.47	8.44	8.14	8.47	8.68	8.30	8.23	8.15	8.32	8.53	8.09	7.93	7.59
MnO	0.157	0.143	0.148	0.146	0.145	0.147	0.148	0.146	0.144	0.144	0.144	0.148	0.141	0.143	0.131
MgO	7.90	6.14	7.75	7.53	7.09	7.50	7.88	6.78	6.96	6.93	6.62	7.43	6.19	6.12	5.61
CaO	9.16	9.77	9.57	9.66	9.55	9.73	8.61	9.70	9.65	9.68	9.66	9.82	9.82	9.83	9.07
Na2O	3.33	3.37	3.36	3.41	3.31	3.37	3.50	3.43	3.39	3.41	3.39	3.41	3.47	3.48	3.85
K2O	0.83	1.01	0.80	0.82	1.00	0.85	0.77	1.03	1.01	1.01	1.02	0.94	1.03	1.02	0.85
P2O5	0.375	0.379	0.371	0.367	0.378	0.374	0.309	0.380	0.374	0.373	0.379	0.383	0.377	0.382	0.386
Unnormalized trace elements (ppm)															
Ni	148	62	133	123	96	121	176	87	92	92	82	115	67	63	71
Cr	279	136	251	234	197	230	295	179	189	190	173	225	145	135	112
Sc	28	27	26	27	26	26	25	28	28	28	28	28	27	28	23
V	194	193	197	201	192	204	192	207	201	199	198	205	195	200	171
Ba	324	401	276	282	385	303	259	396	401	402	403	341	408	400	347
Rb	10	11	11	10	10	10	12	12	10	11	12	11	11	10	10
Sr	710	1036	825	854	991	900	470	1018	1030	1032	1029	917	1048	1040	1073
Zr	145	150	152	152	145	154	135	156	154	155	157	156	157	156	165
Y	26	25	24	25	24	25	25	24	24	25	24	24	24	24	23
Nb	12.0	13.0	15.2	15.1	13.3	16.1	12.9	14.5	13.2	13.2	13.0	15.9	13.7	12.9	11.2
Ga	16	18	19	19	17	19	17	18	18	19	18	18	19	18	20
Cu	59	59	59	63	61	62	65	63	64	64	64	63	62	60	59
Zn	82	78	80	80	78	80	82	82	80	80	78	80	80	79	83
Pb	2	4	3	3	5	4	3	5	3	4	4	3	3	5	4
La	15	19	16	19	15	20	15	20	20	19	20	22	24	20	22
Ce	36	48	40	41	43	47	29	46	46	44	47	46	45	47	50
Th	2	2	2	2	2	2	2	2	2	1	1	2	0	1	1
Nd	24	27	24	24	24	26	17	26	24	25	26	26	24	24	24
U	2	2	3	2	1	1	1	2	0	2	2	0	1	2	1

Note: Major elements are normalized on a volatile-free basis, with total Fe expressed as FeO. 'R' denotes a duplicate bead made from the same rock powder.

TABLE A1. MAJOR AND MINOR ELEMENT CHEMISTRY FOR SMVF SAMPLES DETERMINED BY XRF

Sample ID	RC10-25	RC10-26	RC10-27	RC10-28	RC10-29	RC10-30	RC10-31R	RC10-32R	RC10-33	RC10-34	RC10-35	RC10-36	RC10-37	RC10-38	NID10-01MK
Unnormalized major elements (weight %)															
SiO2	51.98	53.16	51.47	51.31	51.49	49.40	51.36	50.58	50.59	50.49	51.59	52.17	52.98	50.69	51.39
TiO2	1.389	1.290	1.386	1.360	1.339	1.478	1.371	1.523	1.555	1.606	1.312	1.303	1.289	1.380	1.372
Al2O3	17.25	17.58	17.26	16.94	16.72	17.02	16.88	16.41	16.62	16.59	16.98	17.07	17.46	16.83	17.08
FeO*	7.83	7.58	7.88	8.78	8.62	9.14	8.82	8.69	8.41	8.38	8.08	8.03	7.66	8.84	8.77
MnO	0.142	0.131	0.142	0.150	0.148	0.158	0.150	0.147	0.147	0.145	0.141	0.141	0.130	0.151	0.150
MgO	6.13	5.67	6.09	8.23	8.07	7.97	8.03	7.92	7.67	7.46	6.82	6.68	5.63	8.08	8.13
CaO	9.69	9.03	9.66	8.65	8.57	9.45	8.61	9.36	9.48	9.67	9.28	9.31	8.99	9.04	8.58
Na2O	3.45	3.78	3.35	3.55	3.51	3.32	3.50	3.30	3.40	3.38	3.37	3.49	3.80	3.35	3.49
K2O	1.01	0.82	0.99	0.69	0.75	0.61	0.71	0.80	0.80	0.84	0.95	0.93	0.85	0.82	0.70
P2O5	0.381	0.385	0.406	0.306	0.306	0.324	0.306	0.347	0.357	0.369	0.383	0.382	0.383	0.361	0.320
Sum	99.26	99.43	98.64	99.98	99.52	98.87	99.73	99.08	99.01	98.93	98.90	99.51	99.17	99.53	99.98
Normalized major elements (weight %)															
SiO2	52.36	53.47	52.18	51.33	51.74	49.96	51.50	51.05	51.09	51.04	52.17	52.43	53.42	50.93	51.40
TiO2	1.400	1.297	1.405	1.360	1.346	1.495	1.375	1.537	1.570	1.623	1.327	1.310	1.299	1.387	1.372
Al2O3	17.38	17.68	17.50	16.94	16.80	17.21	16.93	16.56	16.78	16.77	17.17	17.16	17.61	16.91	17.08
FeO*	7.89	7.63	7.99	8.79	8.66	9.25	8.84	8.77	8.49	8.47	8.17	8.07	7.73	8.88	8.77
MnO	0.143	0.131	0.144	0.150	0.149	0.160	0.151	0.149	0.148	0.147	0.142	0.141	0.131	0.152	0.150
MgO	6.18	5.70	6.17	8.23	8.11	8.06	8.05	7.99	7.74	7.54	6.89	6.71	5.67	8.12	8.13
CaO	9.76	9.08	9.79	8.65	8.61	9.55	8.63	9.45	9.57	9.78	9.38	9.36	9.07	9.08	8.58
Na2O	3.48	3.80	3.40	3.55	3.52	3.36	3.51	3.34	3.43	3.42	3.40	3.50	3.84	3.36	3.49
K2O	1.02	0.83	1.00	0.69	0.76	0.62	0.71	0.80	0.81	0.85	0.96	0.93	0.85	0.82	0.70
P2O5	0.383	0.387	0.411	0.306	0.307	0.328	0.307	0.350	0.360	0.373	0.387	0.383	0.386	0.362	0.320
Unnormalized trace elements (ppm)															
Ni	65	76	64	190	183	144	182	150	134	121	94	89	75	157	186
Cr	138	116	136	313	307	278	307	280	255	230	193	177	117	287	308
Sc	28	22	28	24	26	29	26	27	26	27	26	27	23	27	25
V	202	178	197	193	195	223	191	198	202	206	189	189	174	194	193
Ba	404	347	405	243	262	211	255	276	279	298	405	401	345	315	254
Rb	11	10	10	11	12	9	10	10	11	10	9	10	10	9	10
Sr	1043	1075	1042	503	469	444	501	775	806	899	1025	1030	1079	707	498
Zr	157	164	157	133	137	130	133	150	157	159	157	157	166	149	136
Y	24	23	24	24	25	24	24	23	23	24	24	24	23	25	25
Nb	12.3	11.2	13.1	12.7	12.6	13.4	13.0	13.6	15.1	15.8	13.1	12.0	11.9	10.9	13.4
Ga	20	19	19	17	17	17	18	17	17	20	18	19	20	19	17
Cu	63	60	57	67	67	63	70	62	64	64	60	61	60	62	64
Zn	78	86	79	82	81	81	84	81	82	79	82	82	85	83	83
Pb	4	4	4	3	3	4	4	3	4	4	5	4	5	4	3
La	23	20	20	9	13	12	13	14	19	19	18	19	21	17	14
Ce	47	49	45	32	36	32	31	37	37	51	42	50	45	35	32
Th	1	1	2	1	1	1	1	2	1	2	0	1	2	0	1
Nd	27	25	27	16	18	16	17	21	21	27	25	26	24	23	20
U	2	2	0	1	2	1	0	0	3	0	1	1	0	1	1

Note: Major elements are normalized on a volatile-free basis, with total Fe expressed as FeO. 'R' denotes a duplicate bead made from the same rock powder.

TABLE A1. MAJOR AND MINOR ELEMENT CHEMISTRY FOR SMVF SAMPLES DETERMINED BY XRF

Sample ID	NID10-02MK	NID10-02MKR	NID10-03MK	NID10-04MK	NID10-05MK	NID10-06MK	NID10-07MK	NID10-08MK	NID10-09MK	NID10-10MK	NID10-11MK
Unnormalized major elements (weight %)											
SiO2	50.14	50.02	51.48	50.48	50.07	52.90	53.13	53.38	53.07	52.42	52.21
TiO2	1.510	1.505	1.372	1.463	1.497	1.283	1.287	1.286	1.288	1.318	1.313
Al2O3	17.26	17.19	17.05	17.16	17.13	17.54	17.68	17.68	17.54	17.31	17.10
FeO*	9.34	9.46	8.88	9.25	9.41	7.74	7.71	7.69	7.77	8.06	8.06
MnO	0.163	0.163	0.151	0.158	0.163	0.131	0.130	0.131	0.131	0.145	0.145
MgO	7.97	7.94	8.07	8.08	7.99	5.80	5.64	5.63	5.83	6.50	6.59
CaO	9.45	9.41	8.59	9.43	9.31	8.97	8.93	8.98	8.98	9.31	9.22
Na2O	3.28	3.28	3.53	3.28	3.29	3.74	3.77	3.76	3.74	3.47	3.48
K2O	0.64	0.64	0.69	0.66	0.65	0.84	0.82	0.85	0.83	0.97	0.96
P2O5	0.342	0.340	0.315	0.325	0.361	0.386	0.388	0.387	0.385	0.393	0.410
Sum	100.10	99.94	100.13	100.29	99.87	99.33	99.49	99.77	99.56	99.90	99.49
Normalized major elements (weight %)											
SiO2	50.09	50.05	51.41	50.34	50.13	53.26	53.41	53.50	53.30	52.47	52.48
TiO2	1.509	1.506	1.370	1.459	1.499	1.292	1.294	1.289	1.294	1.319	1.320
Al2O3	17.24	17.20	17.03	17.11	17.15	17.66	17.77	17.72	17.62	17.33	17.19
FeO*	9.33	9.46	8.87	9.22	9.42	7.79	7.75	7.71	7.80	8.07	8.10
MnO	0.163	0.163	0.151	0.158	0.163	0.132	0.131	0.131	0.132	0.145	0.146
MgO	7.96	7.95	8.06	8.06	8.00	5.84	5.67	5.64	5.86	6.51	6.62
CaO	9.44	9.42	8.58	9.40	9.32	9.03	8.98	9.00	9.02	9.32	9.27
Na2O	3.28	3.28	3.53	3.27	3.29	3.77	3.79	3.77	3.76	3.47	3.50
K2O	0.64	0.64	0.69	0.66	0.65	0.85	0.82	0.85	0.83	0.97	0.96
P2O5	0.342	0.341	0.315	0.324	0.361	0.389	0.390	0.388	0.387	0.393	0.412
Unnormalized trace elements (ppm)											
Ni	141	144	182	147	145	78	74	72	79	84	89
Cr	285	285	301	288	291	124	114	113	128	171	177
Sc	31	29	26	28	30	23	23	22	24	26	25
V	229	226	196	222	226	177	176	176	176	195	191
Ba	213	210	251	213	219	355	351	356	354	410	410
Rb	10	9	11	9	10	10	10	10	10	10	11
Sr	449	450	502	453	446	1087	1082	1083	1093	1040	1028
Zr	136	135	136	132	137	167	168	168	166	162	162
Y	25	25	24	24	25	23	23	23	23	24	24
Nb	14.9	14.9	12.9	14.9	15.0	12.4	12.1	11.8	11.8	12.9	13.1
Ga	20	17	19	18	19	20	21	20	20	20	19
Cu	64	63	68	59	55	61	60	59	62	62	72
Zn	83	81	83	81	85	84	85	83	86	85	82
Pb	4	2	4	3	2	5	5	4	5	4	5
La	13	15	15	15	17	25	23	21	21	21	18
Ce	31	32	29	29	32	49	54	54	48	51	47
Th	1	1	1	1	1	3	1	0	1	1	2
Nd	20	18	17	17	18	27	29	30	27	27	27
U	1	0	1	0	1	1	1	0	2	0	1

Note: Major elements are normalized on a volatile-free basis, with total Fe expressed as FeO. 'R' denotes a duplicate bead made from the same rock powder.

TABLE A1. MAJOR AND MINOR ELEMENT CHEMISTRY FOR SMVF SAMPLES DETERMINED BY XRF

Sample ID	NID10-12MK	NID10-13MK	NID10-14MK	NID10-15MK	NID10-18MK	NID10-19MK 2012	NID10-19MK 2012R	NID10-20MK	NID10-21MK	NID10-22MK
Unnormalized major elements (weight %)										
SiO2	52.35	51.88	52.17	52.03	51.92	51.37	51.44	51.34	53.39	53.04
TiO2	1.322	1.334	1.326	1.325	1.400	1.380	1.384	1.360	1.293	1.288
Al2O3	17.29	16.95	17.12	17.03	17.00	16.91	16.94	16.82	17.39	17.36
FeO*	8.11	8.09	8.16	8.18	8.12	8.88	8.95	8.79	7.91	7.87
MnO	0.143	0.152	0.146	0.143	0.150	0.151	0.150	0.150	0.132	0.134
MgO	6.33	6.86	6.84	6.87	7.03	8.01	8.01	7.80	6.03	6.11
CaO	9.29	9.24	9.33	9.29	9.64	8.67	8.68	8.52	9.05	9.04
Na2O	3.48	3.32	3.39	3.37	3.39	3.49	3.49	3.41	3.71	3.70
K2O	0.97	0.97	0.97	0.96	1.01	0.70	0.71	0.76	0.87	0.87
P2O5	0.403	0.413	0.397	0.383	0.370	0.309	0.310	0.330	0.386	0.387
Sum	99.69	99.21	99.85	99.58	100.03	99.88	100.07	99.28	100.16	99.79
Normalized major elements (weight %)										
SiO2	52.51	52.29	52.25	52.25	51.91	51.43	51.41	51.71	53.31	53.15
TiO2	1.326	1.345	1.328	1.331	1.400	1.382	1.383	1.370	1.291	1.291
Al2O3	17.34	17.09	17.15	17.10	16.99	16.93	16.93	16.94	17.36	17.40
FeO*	8.14	8.15	8.17	8.21	8.12	8.89	8.94	8.85	7.90	7.89
MnO	0.143	0.153	0.146	0.144	0.150	0.151	0.150	0.151	0.132	0.135
MgO	6.35	6.91	6.85	6.90	7.03	8.02	8.00	7.86	6.02	6.12
CaO	9.32	9.31	9.34	9.33	9.64	8.68	8.68	8.58	9.03	9.06
Na2O	3.49	3.35	3.40	3.38	3.39	3.50	3.49	3.43	3.70	3.70
K2O	0.97	0.98	0.97	0.96	1.01	0.70	0.70	0.77	0.87	0.87
P2O5	0.404	0.416	0.398	0.385	0.370	0.310	0.310	0.332	0.385	0.387
Unnormalized trace elements (ppm)										
Ni	79	95	95	95	102	178	178	173	83	84
Cr	159	197	193	194	198	292	293	301	144	146
Sc	27	27	27	27	26	26	24	25	24	23
V	192	194	194	193	201	194	191	194	177	173
Ba	411	406	407	410	406	247	244	262	361	361
Rb	11	11	12	10	10	10	10	13	10	10
Sr	1040	1015	1032	1026	1025	503	503	464	1086	1085
Zr	163	159	160	159	155	132	132	139	160	159
Y	24	23	24	24	23	25	25	25	23	23
Nb	12.4	12.7	12.5	12.9	13.0	12.8	12.1	12.0	11.3	11.2
Ga	20	20	19	20	19	18	18	18	20	19
Cu	63	56	61	59	65	68	69	62	50	60
Zn	83	85	82	83	83	83	82	83	85	86
Pb	5	5	6	5	4	4	2	3	5	4
La	19	23	20	22	18	11	13	15	22	20
Ce	48	47	45	48	44	28	31	28	48	48
Th	1	1	1	1	1	2	1	1	0	1
Nd	27	27	26	26	22	17	19	17	23	25
U	1	1	1	1	2	1	1	0	1	1

Note: Major elements are normalized on a volatile-free basis, with total Fe expressed as FeO. 'R' denotes a duplicate bead made from the same rock powder.

TABLE A1. MAJOR AND MINOR ELEMENT CHEMISTRY FOR SMVF SAMPLES DETERMINED BY XRF

Sample ID	NID10-22MKR	NID10-23MK	NID10-24MK	NID10-25MK	NID10-26MK	NID10-27MK	NID10-28MK	NID10-29MK	NID10-30MK	NID10-31MK	NID10-32MK
Unnormalized major elements (weight %)											
SiO2	53.12	52.88	53.11	53.04	54.45	50.61	51.67	50.93	51.43	50.77	53.06
TiO2	1.285	1.280	1.290	1.286	1.103	1.628	1.365	1.581	1.384	1.621	1.294
Al2O3	17.32	17.30	17.37	17.35	16.67	17.52	16.90	17.60	16.89	16.69	17.35
FeO*	7.96	7.84	7.91	7.70	7.90	9.34	8.72	9.13	8.78	8.71	7.96
MnO	0.135	0.135	0.135	0.134	0.134	0.165	0.149	0.160	0.150	0.148	0.136
MgO	6.15	6.01	6.05	5.95	6.78	6.61	7.76	6.54	7.98	7.50	6.10
CaO	9.04	9.02	9.02	9.05	7.63	9.46	8.45	9.47	8.71	9.63	9.10
Na2O	3.71	3.69	3.65	3.72	3.63	3.59	3.57	3.55	3.51	3.34	3.68
K2O	0.86	0.86	0.86	0.87	1.02	0.70	0.75	0.69	0.72	0.86	0.89
P2O5	0.386	0.383	0.391	0.386	0.279	0.394	0.322	0.379	0.312	0.372	0.389
Sum	99.97	99.40	99.80	99.47	99.60	100.01	99.65	100.02	99.86	99.64	99.95
Normalized major elements (weight %)											
SiO2	53.13	53.20	53.22	53.32	54.67	50.61	51.85	50.92	51.50	50.95	53.09
TiO2	1.285	1.288	1.293	1.292	1.108	1.628	1.370	1.581	1.386	1.627	1.294
Al2O3	17.32	17.41	17.41	17.44	16.74	17.52	16.96	17.59	16.91	16.75	17.36
FeO*	7.96	7.89	7.93	7.74	7.93	9.34	8.75	9.12	8.80	8.74	7.96
MnO	0.135	0.135	0.135	0.135	0.135	0.165	0.150	0.160	0.150	0.149	0.136
MgO	6.15	6.04	6.07	5.98	6.81	6.61	7.79	6.54	7.99	7.53	6.10
CaO	9.04	9.07	9.03	9.09	7.66	9.46	8.48	9.47	8.72	9.67	9.10
Na2O	3.72	3.71	3.66	3.74	3.65	3.59	3.58	3.55	3.51	3.35	3.68
K2O	0.86	0.87	0.86	0.87	1.03	0.70	0.75	0.69	0.72	0.86	0.89
P2O5	0.386	0.385	0.392	0.388	0.280	0.394	0.323	0.379	0.313	0.373	0.389
Unnormalized trace elements (ppm)											
Ni	86	81	81	79	155	90	176	88	176	123	78
Cr	145	139	144	138	253	164	292	170	295	235	142
Sc	22	24	24	22	21	29	25	29	25	26	24
V	178	176	177	176	161	229	191	222	191	203	178
Ba	358	362	362	359	332	268	270	246	247	293	374
Rb	11	10	10	10	20	10	12	9	11	11	10
Sr	1086	1083	1079	1083	474	495	507	499	494	890	1075
Zr	158	159	159	158	138	154	139	149	133	156	158
Y	23	23	23	23	23	27	24	27	24	24	23
Nb	11.2	12.0	12.2	12.1	11.2	13.8	12.5	14.1	13.1	15.7	11.2
Ga	20	19	20	20	18	19	18	19	19	19	21
Cu	59	58	57	59	59	62	67	58	66	58	62
Zn	84	84	84	83	79	84	83	83	83	80	84
Pb	6	4	5	5	5	3	3	2	4	2	4
La	20	19	24	18	16	14	18	13	17	20	17
Ce	48	49	49	50	33	33	33	34	29	46	46
Th	2	1	2	1	3	2	1	1	2	1	1
Nd	24	27	26	28	17	20	18	19	19	26	26
U	1	0	2	2	0	1	2	1	1	0	1

Note: Major elements are normalized on a volatile-free basis, with total Fe expressed as FeO. 'R' denotes a duplicate bead made from the same rock powder.

TABLE A1. MAJOR AND MINOR ELEMENT CHEMISTRY FOR SMVF SAMPLES DETERMINED BY XRF

Sample ID	NID10-33MK	NID10-34MK	NID10-35MK	NID10-36MK	NID10-37MK	RC11-01	RC11-02	RC11-03	RC11-04	RC11-05	RC11-06	RC11-07	RC11-08A	RC11-08B
Unnormalized major elements (weight %)														
SiO2	50.73	51.70	52.02	53.00	50.95	51.65	49.86	51.28	51.46	49.74	51.38	51.46	53.08	53.37
TiO2	1.610	1.310	1.319	1.293	1.368	1.388	1.488	1.377	1.379	1.503	1.382	1.384	1.261	1.262
Al2O3	16.71	16.94	17.00	17.51	17.04	16.95	17.09	16.83	17.00	17.09	16.90	17.00	17.88	17.99
FeO*	8.71	7.97	8.08	7.88	8.70	8.98	9.34	8.91	8.90	9.37	8.91	8.90	7.73	7.72
MnO	0.145	0.140	0.141	0.133	0.155	0.152	0.160	0.149	0.150	0.160	0.150	0.150	0.136	0.128
MgO	7.30	6.34	6.45	5.78	7.73	8.07	8.25	8.07	8.01	8.26	8.04	7.97	5.53	5.35
CaO	9.80	9.25	9.30	9.02	9.20	8.71	9.53	8.65	8.70	9.58	8.67	8.72	8.53	8.60
Na2O	3.38	3.45	3.46	3.76	3.42	3.49	3.23	3.47	3.52	3.13	3.49	3.52	3.61	3.87
K2O	0.86	0.96	0.95	0.85	0.71	0.72	0.68	0.70	0.70	0.64	0.71	0.70	0.81	0.81
P2O5	0.369	0.384	0.386	0.384	0.369	0.319	0.329	0.309	0.308	0.331	0.311	0.308	0.391	0.368
Sum	99.60	98.43	99.10	99.60	99.65	100.43	99.96	99.75	100.13	99.80	99.94	100.11	98.96	99.47
Normalized major elements (weight %)														
SiO2	50.93	52.52	52.49	53.21	51.13	51.43	49.88	51.41	51.39	49.84	51.41	51.40	53.64	53.66
TiO2	1.616	1.331	1.331	1.298	1.373	1.382	1.489	1.381	1.377	1.506	1.383	1.382	1.274	1.269
Al2O3	16.78	17.21	17.15	17.58	17.10	16.88	17.10	16.87	16.98	17.12	16.91	16.98	18.07	18.09
FeO*	8.74	8.09	8.15	7.91	8.73	8.94	9.34	8.93	8.89	9.39	8.92	8.89	7.81	7.76
MnO	0.146	0.142	0.143	0.133	0.156	0.151	0.160	0.149	0.150	0.160	0.150	0.150	0.137	0.129
MgO	7.33	6.44	6.51	5.80	7.76	8.04	8.25	8.09	8.00	8.28	8.04	7.96	5.59	5.38
CaO	9.84	9.40	9.38	9.06	9.24	8.67	9.53	8.67	8.69	9.60	8.67	8.71	8.62	8.65
Na2O	3.39	3.51	3.49	3.77	3.43	3.48	3.23	3.48	3.52	3.14	3.49	3.52	3.65	3.89
K2O	0.86	0.97	0.96	0.85	0.72	0.72	0.68	0.70	0.70	0.64	0.71	0.70	0.82	0.81
P2O5	0.370	0.390	0.389	0.386	0.371	0.318	0.329	0.310	0.308	0.332	0.311	0.308	0.395	0.370
Unnormalized trace elements (ppm)														
Ni	112	79	85	77	139	179	152	179	177	153	180	174	86	77
Cr	218	162	167	124	269	300	296	301	295	293	300	295	95	80
Sc	27	26	26	21	26	25	28	25	25	28	25	25	19	20
V	203	188	191	175	188	195	218	192	188	211	192	195	169	169
Ba	306	404	404	348	283	244	212	247	244	205	242	249	330	340
Rb	11	10	10	10	8	10	10	10	11	10	11	10	9	9
Sr	918	1018	1027	1086	755	502	453	498	502	452	499	503	1004	1031
Zr	153	153	155	161	139	131	127	130	130	128	131	131	153	156
Y	24	25	24	23	25	25	23	24	24	24	24	24	21	21
Nb	15.9	12.1	12.0	11.2	9.1	12.6	14.6	12.8	12.0	15.1	12.0	12.4	11.4	10.4
Ga	19	19	20	21	20	18	17	17	18	17	17	19	21	21
Cu	64	62	64	59	53	59	59	69	68	60	59	69	46	58
Zn	80	80	81	84	80	84	79	83	81	79	83	81	86	85
Pb	3	6	4	4	3	3	2	3	1	2	2	2	5	5
La	19	18	18	24	18	13	15	12	13	11	14	13	18	16
Ce	45	48	42	50	36	29	29	30	31	28	29	29	37	43
Th	1	1	1	1	0	0	2	2	2	2	1	1	2	3
Nd	24	26	23	24	22	18	16	18	18	17	16	18	21	24
U	2	0	0	1	1	1	2	1	1	2	1	1	1	1

Note: Major elements are normalized on a volatile-free basis, with total Fe expressed as FeO. 'R' denotes a duplicate bead made from the same rock powder.

TABLE A1. MAJOR AND MINOR ELEMENT CHEMISTRY FOR SMVF SAMPLES DETERMINED BY XRF

Sample ID	RC11-09	RC11-10	RC11-11	RC11-12	RC11-13	RC11-14	RC11-15	RC11-16	RC11-17	RC11-18	RC11-19A	RC11-19B	RC11-19C	RC11-19D	RC11-20	RC11-21
Unnormalized major elements (weight %)																
SiO2	53.33	53.49	50.33	52.42	52.71	52.71	50.05	50.84	52.88	51.48	53.09	53.00	52.95	53.19	51.61	53.24
TiO2	1.238	1.240	1.506	1.319	1.308	1.309	1.351	1.485	1.288	1.380	1.295	1.286	1.293	1.286	1.343	1.293
Al2O3	17.81	17.75	16.11	17.75	17.61	17.72	16.55	16.70	17.79	17.03	17.60	17.45	17.51	17.38	17.23	17.44
FeO*	7.58	7.69	9.30	8.54	8.54	8.46	9.08	8.62	8.15	8.68	7.89	7.85	7.89	7.92	8.15	7.87
MnO	0.127	0.130	0.155	0.142	0.142	0.141	0.153	0.148	0.135	0.149	0.137	0.133	0.135	0.134	0.139	0.134
MgO	5.57	5.58	8.13	5.90	6.27	5.95	9.19	7.94	5.79	7.79	5.94	5.97	5.96	6.09	5.99	5.99
CaO	8.70	8.64	8.68	8.25	8.41	8.39	9.47	9.47	8.51	9.31	8.98	9.03	8.94	9.03	9.52	9.06
Na2O	3.81	3.91	3.43	3.69	3.78	3.82	3.23	3.29	3.84	3.47	3.56	3.62	3.54	3.65	3.15	3.69
K2O	0.79	0.82	1.04	0.79	0.80	0.82	0.74	0.76	0.81	0.72	0.84	0.84	0.83	0.84	0.93	0.85
P2O5	0.354	0.360	0.479	0.407	0.404	0.405	0.329	0.343	0.386	0.344	0.379	0.379	0.377	0.377	0.382	0.382
Sum	99.31	99.61	99.16	99.21	99.97	99.73	100.14	99.60	99.58	100.35	99.71	99.56	99.43	99.90	98.44	99.95
Normalized major elements (weight %)																
SiO2	53.70	53.70	50.76	52.84	52.72	52.86	49.98	51.05	53.10	51.30	53.24	53.24	53.26	53.24	52.43	53.27
TiO2	1.247	1.245	1.519	1.330	1.308	1.313	1.349	1.491	1.293	1.375	1.299	1.292	1.300	1.287	1.364	1.294
Al2O3	17.93	17.82	16.25	17.89	17.61	17.77	16.53	16.77	17.87	16.97	17.65	17.53	17.61	17.40	17.50	17.45
FeO*	7.63	7.72	9.38	8.61	8.54	8.48	9.07	8.65	8.18	8.65	7.91	7.88	7.94	7.93	8.28	7.87
MnO	0.128	0.131	0.156	0.143	0.142	0.141	0.153	0.149	0.136	0.148	0.137	0.134	0.136	0.134	0.141	0.134
MgO	5.61	5.60	8.20	5.95	6.27	5.97	9.18	7.97	5.81	7.76	5.96	6.00	5.99	6.10	6.08	5.99
CaO	8.76	8.67	8.75	8.32	8.41	8.41	9.46	9.51	8.55	9.28	9.01	9.07	8.99	9.04	9.67	9.06
Na2O	3.84	3.93	3.46	3.72	3.78	3.83	3.23	3.30	3.86	3.46	3.57	3.64	3.56	3.65	3.20	3.69
K2O	0.80	0.83	1.05	0.80	0.80	0.82	0.74	0.76	0.81	0.72	0.84	0.84	0.83	0.84	0.94	0.85
P2O5	0.356	0.361	0.483	0.410	0.404	0.406	0.329	0.344	0.388	0.343	0.380	0.381	0.379	0.377	0.388	0.382
Unnormalized trace elements (ppm)																
Ni	86	86	187	127	148	128	201	146	108	139	80	82	78	85	73	81
Cr	96	111	308	117	130	116	394	281	109	272	133	137	133	141	149	131
Sc	20	21	24	21	20	21	27	27	20	27	22	23	22	22	27	23
V	171	165	183	175	175	178	201	195	178	195	168	172	172	170	185	176
Ba	331	335	509	356	354	355	339	279	349	286	340	353	350	358	403	351
Rb	8	9	11	10	10	10	9	10	10	8	10	10	10	9	10	9
Sr	1019	1012	925	752	748	762	714	763	843	765	1080	1083	1078	1085	1041	1088
Zr	149	151	169	167	165	165	125	146	159	136	155	154	156	155	150	156
Y	21	21	26	24	24	24	23	22	23	24	23	23	23	23	25	23
Nb	11.0	10.2	12.4	12.8	12.9	12.1	9.2	13.0	11.6	9.2	11.0	10.5	11.0	11.4	12.8	11.0
Ga	19	20	17	20	19	19	17	17	20	17	20	20	20	19	18	20
Cu	61	65	59	55	60	59	65	61	54	64	58	35	58	60	81	64
Zn	83	84	93	94	94	90	79	79	89	82	84	84	84	84	81	84
Pb	4	5	4	5	4	4	2	4	4	3	5	6	4	4	4	4
La	19	20	20	19	17	19	16	18	18	16	19	22	22	20	20	19
Ce	40	41	47	41	45	45	32	35	42	34	52	44	53	49	45	44
Th	2	2	2	1	2	2	2	2	1	2	3	2	2	2	2	3
Nd	24	24	28	25	24	26	21	19	25	20	26	26	26	26	25	27
U	1	1	1	1	1	2	0	2	2	1	1	0	3	2	0	1

Note: Major elements are normalized on a volatile-free basis, with total Fe expressed as FeO. 'R' denotes a duplicate bead made from the same rock powder.

TABLE A1. MAJOR AND MINOR ELEMENT CHEMISTRY FOR SMVF SAMPLES DETERMINED BY XRF

Sample ID	RC11-22	RC11-23	RC11-24	RC11-25	RC11-26	RC11-27	RC11-28	NID11-04MK	NID11-05MK
Unnormalized major elements (weight %)									
SiO2	53.38	52.75	51.52	53.55	50.69	50.30	50.70	49.53	50.84
TiO2	1.301	1.289	1.477	1.250	1.460	1.431	1.478	1.492	1.391
Al2O3	17.62	17.47	17.21	17.89	16.74	16.76	16.78	16.94	16.87
FeO*	7.70	7.94	8.10	7.76	9.06	9.06	9.07	9.38	8.92
MnO	0.132	0.134	0.143	0.130	0.150	0.153	0.156	0.159	0.151
MgO	5.77	5.89	6.33	5.63	8.51	8.57	8.48	8.23	7.90
CaO	9.03	8.98	9.98	8.67	9.07	9.22	9.15	9.59	9.16
Na2O	3.66	3.61	3.30	3.90	3.33	3.28	3.37	3.18	3.34
K2O	0.84	0.84	1.03	0.81	0.74	0.68	0.74	0.68	0.81
P2O5	0.385	0.383	0.378	0.360	0.360	0.326	0.350	0.324	0.349
Sum	99.82	99.29	99.47	99.95	100.11	99.78	100.27	99.50	99.74
Normalized major elements (weight %)									
SiO2	53.48	53.13	51.80	53.58	50.63	50.41	50.56	49.77	50.97
TiO2	1.303	1.298	1.485	1.251	1.458	1.434	1.474	1.500	1.394
Al2O3	17.65	17.60	17.30	17.90	16.72	16.80	16.73	17.02	16.92
FeO*	7.71	8.00	8.14	7.77	9.05	9.08	9.05	9.43	8.94
MnO	0.132	0.135	0.144	0.130	0.150	0.153	0.156	0.159	0.151
MgO	5.78	5.93	6.36	5.63	8.50	8.59	8.46	8.27	7.92
CaO	9.05	9.04	10.03	8.67	9.06	9.24	9.12	9.64	9.19
Na2O	3.67	3.64	3.32	3.90	3.33	3.29	3.36	3.19	3.35
K2O	0.84	0.85	1.04	0.81	0.74	0.68	0.74	0.68	0.81
P2O5	0.386	0.386	0.380	0.360	0.360	0.327	0.349	0.326	0.350
Unnormalized trace elements (ppm)									
Ni	78	79	69	90	182	180	176	153	147
Cr	118	126	144	106	320	332	320	293	278
Sc	22	22	29	21	27	28	26	28	27
V	172	170	201	175	201	196	201	215	190
Ba	349	351	403	341	266	243	271	201	324
Rb	10	10	10	9	10	9	10	10	9
Sr	1071	1077	1030	939	611	602	612	450	716
Zr	157	155	149	150	144	137	144	130	144
Y	23	22	23	21	25	24	25	23	25
Nb	11.3	11.3	13.4	11.0	12.1	11.6	12.7	15.2	10.1
Ga	20	20	19	19	17	18	17	18	18
Cu	58	60	61	60	58	58	64	58	63
Zn	87	85	77	85	80	79	82	76	81
Pb	5	4	4	3	4	3	2	1	3
La	21	21	19	17	16	17	16	16	18
Ce	48	50	46	42	34	35	37	30	41
Th	3	2	2	2	2	2	2	1	2
Nd	28	26	26	23	19	20	22	18	23
U	1	2	1	2	1	1	2	0	0

Note: Major elements are normalized on a volatile-free basis, with total Fe expressed as FeO. 'R' denotes a duplicate bead made from the same rock powder.

TABLE A2. XRF, PALEOMAGNETIC, AND ^{3}HE SAMPLE LOCATIONS FOR THE SMVF

Sample ID	Assigned Unit	Material	Collection Date	Datum: WGS1984 Easting	Datum: WGS1984 Northing	Datum: NAD1927 Easting	Datum: NAD1927 Northing	Location method	Error (m)	Co-located paleomagnetic or ^{3}He sample site
RCEWEB1-1	Great Spring	Lava		580236	4915598			Estimated from map		
RCNSH-5	Lost Lake	Lava		585280	4920675			Estimated from map		LsLO Site 1
RCSM-1	Clear Lake East	Lava		580700	4913015			Estimated from map		
RCBKP-6	Belknap	Lava		580069	4908414			Estimated from map		
SHE95-TFJ23	Inaccessible Cones	Lava		587237	4908215	587317	4908023	RC GPS; NAD1927		
SHE95-TFJ24	Inaccessible Cones	Lava		587349	4907753	587429	4907561	RC GPS; NAD1927		
SHE95-TFJ25	Inaccessible Cones	Lava		587364	4908624	587444	4908432	RC GPS; NAD1927		
SHE95-TFJ26	Clear Lake East	Lava		585257	4910364			Estimated from map		
RC95-01	Fish Lake	Lava		579380	4916806			Estimated from map		HkmO
RC95-02	Nash	Lava		579450	4916812	579530	4916620	RC GPS; NAD1927		221B2
RC95-03	Fish Lake	Lava		579443	4919084			Estimated from map		
RC95-04	Nash	Lava		579610	4919219			Estimated from map		
RC95-05	Lost Lake	Lava		581090	4919999			Estimated from map		
RC95-06	Little Nash	Lava		582248	4920472			Estimated from map		
RC95-07	Pleistocene	Lava		582828	4921133			Estimated from map		
RC95-08	Old Wagon Road	Lava		585702	4918769			Estimated from map		
RC95-09	Old Wagon Road	Lava		585683	4919026			Estimated from map		
RC95-10	Pleistocene	Lava		585492	4919763			Estimated from map		
RC95-11	Clear Lake East	Lava		586637	4915596			Estimated from map		
RC95-12	Great Spring	Lava		585080	4916650			Estimated from map		
RC95-13	Nash	Lava		583078	4919217	583158	4919025	RC GPS; NAD1927		178B2
RC95-14	Nash	Lava		583041	4918358			Estimated from map		
RC95-15	Great Spring	Lava		583213	4917443			Estimated from map		
RC95-16	Great Spring	Lava		583207	4916589	583287	4916397	RC GPS; NAD1927		194B2
RC95-17	Great Spring	Lava		582085	4915391	582165	4915199	RC GPS; NAD1927		186B2
RC95-18	Great Spring	Lava		580830	4915923			Estimated from map		
RC95-19	Clear Lake East	Lava		580685	4912923			Estimated from map		
RC95-20	Clear Lake South	Lava		580121	4911972	580201	4911780	RC GPS; NAD1927		CrLO 3+4
RC95-21	Clear Lake South	Lava		580171	4908644			Estimated from map		
RC95-26	Pleistocene	Lava		580491	4922337			Estimated from map		
RC00-55	Lost Lake	Lava	7/31/2000	586765	4920511			Estimated from map		
RC00-56	Fish Lake	Lava	7/31/2000	580021	4921338	580101	4921146	RC GPS; NAD1927		229B2
RC00-57	Fish Lake	Lava	7/31/2000	580214	4921359			Estimated from map		
RC00-58	Early Nash I	Lava	7/31/2000	580277	4921366			Estimated from map		
RC01-80	Pleistocene	Lava	7/8/2001	580022	4912501			Estimated from map		
RC01-81	Pleistocene	Lava	7/8/2001	580088	4910499			Estimated from map		
RC02-17	Little Nash	Bomb	6/16/2002	583010	4920779	583090	4920587	RC GPS; NAD1927		
RC02-18	Clear Lake East	Bomb	6/16/2002	585365	4915180	585445	4914988	RC GPS; NAD1927		
RC02-19	Great Spring	Cone	6/16/2002	585238	4915520	585318	4915328	RC GPS; NAD1927		
RC02-20	Nash	Lava	6/20/2002	579337	4918591	579417	4918399	RC GPS; NAD1927		FsLO 3+4
RC02-21	Fish Lake	Lava	6/20/2002	580899	4919898	580979	4919706	RC GPS; NAD1927		LvLO
RC02-22	Little Nash	Lava	6/20/2002	581996	4920412	582076	4920220	RC GPS; NAD1927		LNCO Site 1
RC02-23	Little Nash	Lava	6/20/2002	582370	4920457	582450	4920265	RC GPS; NAD1927		LNCO Sites 2, 3, 4
RC02-24	Lost Lake	Lava	6/20/2002	584407	4920931	584487	4920739	RC GPS; NAD1927		LSLO Site 2+3
RC02-25	Old Wagon Road	Lava	6/20/2002	585376	4918256	585456	4918064	RC GPS; NAD1927		137B2
RC02-26	Nash	Lava	6/20/2002	583118	4918544	583198	4918352	RC GPS; NAD1927		146B2

TABLE A2. XRF, PALEOMAGNETIC, AND ^{3}HE SAMPLE LOCATIONS FOR THE SMVF

				Datum: WGS1984		Datum: NAD1927				Co-located paleomagnetic or
Sample ID	Assigned Unit	Material	Collection Date	Easting	Northing	Easting	Northing	Location method	Error (m)	^{3}He sample site
RC02-27A	Great Spring	Lava	6/20/2002	583187	4917496	583267	4917304	RC GPS; NAD1927		154B2
RC02-27B	Great Spring	Lava	6/20/2002	583187	4917496	583267	4917304	RC GPS; NAD1927		162B2
RC02-28	Early Nash I	Lava	6/21/2002	583909	4920167	583989	4919975	RC GPS; NAD1927		
RC02-29	Clear Lake East	Lava	6/21/2002	586450	4914648	586530	4914456	RC GPS; NAD1927		170B2
RC02-30	Clear Lake South	Lava	6/22/2002	580072	4911367	580151	4911175	RC GPS; NAD1927		CrLO 1+2
RC02-31	Ice Cap	Lava	6/22/2002	579923	4910453	580003	4910261	RC GPS; NAD1927		202B2
RC02-32	Clear Lake East	Lava	6/22/2002	580399	4913382	580479	4913190	RC GPS; NAD1927		210B2
RC02-33	Clear Lake East	Lava	6/24/2002	584400	4914455	584480	4914263	RC GPS; NAD1927		
RC02-34	Clear Lake East	Lava	6/24/2002	584400	4914455	584480	4914263	RC GPS; NAD1927		
RC02-35	Clear Lake East	Lava	6/24/2002	585329	4914490	585409	4914298	RC GPS; NAD1927		
RC02-36	Ice Cap	Bomb	6/24/2002	585277	4914215	585357	4914023	RC GPS; NAD1927		
RC02-37	Pleistocene	Lava	6/24/2002	587254	4914202	587334	4914010	RC GPS; NAD1927		
RC02-38	Little Nash	Scoria	6/24/2002	582583	4921204	582663	4921012	RC GPS; NAD1927		
RC02-39	Early Nash II	Lava	6/24/2002	582792	4920117	582872	4919925	RC GPS; NAD1927		
RC02-40	Early Nash I	Lava	6/24/2002	583638	4919947	583718	4919755	RC GPS; NAD1927		
RC02-41	Clear Lake South	Lava	6/25/2002	579624	4910527	579704	4910335	RC GPS; NAD1927		
RC02-42	Fish Lake	Lava	6/25/2002	579249	4917058	579329	4916866	RC GPS; NAD1927		
RC02-43	Fish Lake	Lava	6/25/2002	579753	4917290	579833	4917098	RC GPS; NAD1927		
RC02-44	Fish Lake	Lava	6/25/2002	580380	4919623	580460	4919431	RC GPS; NAD1927		
RC02-45	Great Spring	Lava	6/25/2002	584933	4918023	585013	4917831	RC GPS; NAD1927		
RC03-13	Little Nash	Lava	7/15/2003	580417	4921769			Estimated from map		
RC03-14	Early Nash I	Lava	7/15/2003	580441	4921499			Estimated from map		
RC03-15	Fish Lake	Lava	7/15/2003	580532	4921311	580612	4921119	RC GPS; NAD1927		
RC03-16	Little Nash	Lava	7/15/2003	580755	4921068	580835	4920876	RC GPS; NAD1927		
RC03-17	Little Nash	Lava	7/15/2003	580597	4920815	580677	4920623	RC GPS; NAD1927		
RC03-18	Lost Lake	Lava	7/15/2003	580179	4920817	580259	4920625	RC GPS; NAD1927		
RC03-19	Clear Lake South	Bomb	7/16/2003	584976	4913554	585056	4913362	RC GPS; NAD1927		
RC03-20	Ice Cap	Bomb	7/16/2003	585068	4912969	585148	4912777	RC GPS; NAD1927		
RC03-21	Ice Cap	Lava	7/16/2003	584857	4912548	584937	4912356	RC GPS; NAD1927		
RC03-22	Clear Lake South	Bomb	7/16/2003	585042	4912104	585122	4911912	RC GPS; NAD1927		
RC03-23	Ice Cap	Lava	7/16/2003	584843	4912004	584923	4911812	RC GPS; NAD1927		
RC03-24R	Ice Cap	Lava	7/16/2003	584590	4912184	584670	4911992	RC GPS; NAD1927		
RC03-25	Ice Cap	Lava	7/16/2003	584514	4912319	584594	4912127	RC GPS; NAD1927		
RC03-26	Ice Cap	Lava	7/16/2003	584468	4912457	584548	4912265	RC GPS; NAD1927		
RC03-27	Clear Lake South	Lava	7/16/2003	584480	4912489	584560	4912297	RC GPS; NAD1927		
RC03-28	Ice Cap	Lava	7/16/2003	584371	4912706	584451	4912514	RC GPS; NAD1927		
RC03-29	Clear Lake South	Lava	7/16/2003	584371	4912962	584451	4912770	RC GPS; NAD1927		
RC03-30	Clear Lake East	Lava	7/16/2003	584352	4913218	584432	4913026	RC GPS; NAD1927		
RC03-31	Clear Lake East	Lava	7/16/2003	584810	4913712	584890	4913520	RC GPS; NAD1927		
RC03-32	Cold Water Cove	Lava	7/17/2003	580849	4912627	580929	4912435	RC GPS; NAD1927		
RC03-33	Clear Lake South	Lava	7/17/2003	581119	4912153	581199	4911961	RC GPS; NAD1927		
RC03-34	Clear Lake South	Lava	7/17/2003	581126	4911866	581206	4911674	RC GPS; NAD1927		
RC03-35	Clear Lake South	Lava	7/17/2003	581121	4911506	581201	4911314	RC GPS; NAD1927		
RC03-36	Ice Cap	Lava	7/17/2003	581178	4911313	581258	4911121	RC GPS; NAD1927		
RC03-37	Ice Cap	Lava	7/17/2003	581361	4910859	581441	4910667	RC GPS; NAD1927		
RC03-38	Clear Lake South	Lava	7/17/2003	581619	4910021	581699	4909829	RC GPS; NAD1927		

TABLE A2. XRF, PALEOMAGNETIC, AND ^{3}HE SAMPLE LOCATIONS FOR THE SMVF

				Datum: WGS1984		Datum: NAD1927				
Sample ID	Assigned Unit	Material	Collection Date	Easting	Northing	Easting	Northing	Location method	Error (m)	Co-located paleomagnetic or ^{3}He sample site
RC03-41	Pleistocene	Lava	7/19/2003	586655	4918082	586735	4917890	RC GPS; NAD1927		
RC03-42	Old Wagon Road	Lava	7/19/2003	585027	4919421	585107	4919229	RC GPS; NAD1927		
RC03-43	Pleistocene	Lava	7/19/2003	587261	4919079	587341	4918887	RC GPS; NAD1927		
RC03-44	Old Wagon Road	Bomb	7/20/2003	585752	4917220	585832	4917028	RC GPS; NAD1927		
RC03-45	Great Spring	Bomb	7/20/2003	585402	4917046	585482	4916854	RC GPS; NAD1927		
RC03-46	Great Spring	Bomb	7/20/2003	585127	4916866	585207	4916674	RC GPS; NAD1927		
RC03-47	Great Spring	Bomb	7/20/2003	585015	4917049	585095	4916857	RC GPS; NAD1927		
RC03-48	Great Spring	Lava	7/20/2003	584846	4917134	584926	4916942	RC GPS; NAD1927		
RC03-49	Proto - Clear Lake South	Bomb	7/20/2003	584599	4917522	584679	4917330	RC GPS; NAD1927		
RC03-50	Proto - Clear Lake South	Bomb	7/20/2003	584743	4916917	584823	4916725	RC GPS; NAD1927		
RC03-51	Lost Lake	Lava	7/21/2003	584024	4920273	584104	4920081	RC GPS; NAD1927		
RC03-52	Lost Lake	Lava	7/21/2003	583977	4920418	584057	4920226	RC GPS; NAD1927		
RC03-53	Lost Lake	Lava	7/21/2003	584695	4920459	584775	4920267	RC GPS; NAD1927		
RC03-54	Lost Lake	Lava	7/21/2003	584215	4920351	584295	4920159	RC GPS; NAD1927		
RC03-55	Early Nash II	Bomb	7/21/2003	583807	4919761	583887	4919569	RC GPS; NAD1927		
RC03-56	Nash	Lava	7/21/2003	582765	4919803	582845	4919611	RC GPS; NAD1927		
RC03-57	SnoPark	Lava	7/22/2003	582857	4920411	582937	4920219	RC GPS; NAD1927		
RC03-58	Lost Lake	Lava	7/22/2003	581417	4919857	581497	4919665	RC GPS; NAD1927		
RC03-59	Fish Lake	Lava	7/22/2003	581379	4919852	581459	4919660	RC GPS; NAD1927		
RC03-60	Ice Cap	Lava	7/22/2003	580062	4910701	580142	4910509	RC GPS; NAD1927		
RC04-25	Proto - Clear Lake South	Bomb	6/17/2004	584870	4916093	584950	4915901	RC GPS; NAD1927		
RC04-26	Old Wagon Road	Bomb	6/17/2004	585437	4916059	585517	4915867	RC GPS; NAD1927		
RC04-27	Pleistocene	Lava	6/19/2004	581876	4922078			Estimated from map		
RC04-28	Fish Lake	Bomb	6/19/2004	586057	4920506	586137	4920314	RC GPS; NAD1927		
RC04-29	Lost Lake	Bomb	6/19/2004	586029	4920816	586109	4920624	RC GPS; NAD1927		
RC04-30	Lost Lake	Lava	6/19/2004	586040	4921024	586120	4920832	RC GPS; NAD1927		
RC04-31	Lost Lake	Bomb	6/19/2004	586141	4921307	586221	4921115	RC GPS; NAD1927		
RC04-32	Lost Lake	Bomb	6/19/2004	585928	4921563			Estimated from map		
RC04-33	Lost Lake	Cone	6/19/2004	585724	4921701			Estimated from map		
RC04-34	Jack Pine	Cone	6/20/2004	586013	4918966	586093	4918774	RC GPS; NAD1927		
RC04-35	Nash	Bomb	6/20/2004	583815	4919030	583895	4918838	RC GPS; NAD1927		
RC04-36	Nash	Agglutinate	6/20/2004	583589	4918953	583669	4918761	RC GPS; NAD1927		
RC04-66	Clear Lake East	Lava	6/24/2004	586005	4913621	586085	4913429	RC GPS; NAD1927		
RC04-67	Clear Lake South	Lava	6/24/2004	585294	4912306			Estimated from map		
RC04-68	Clear Lake South	Lava	6/24/2004	584976	4911829	585056	4911637	RC GPS; NAD1927		
RC04-69	Clear Lake South	Lava	6/24/2004	585322	4911797	585402	4911605	RC GPS; NAD1927		
RC04-70	Ice Cap	Agglutinate	6/24/2004	585011	4913182	585091	4912990	RC GPS; NAD1927		
RC04-71	Clear Lake South	Bomb	6/24/2004	584672	4913278	584752	4913086	RC GPS; NAD1927		
RC04-72	Clear Lake South	Bomb	6/24/2004	585264	4913474	585344	4913282	RC GPS; NAD1927		
RC09-33	Great Spring	Lava	8/2/2009	579631	4914630			NID GPS; WGS1984		
RC09-34	Pleistocene	Lava	8/2/2009	579658	4914655	579538	4914463	RC GPS; NAD1927		
RC09-35	Great Spring	Lava	8/2/2009	579903	4914274			NID GPS; WGS1984		
RC09-36	Cold Water Cove	Lava	8/2/2009	579899	4914066			NID GPS; WGS1984		
RC09-37	Clear Lake East	Lava	8/2/2009	579929	4913893			NID GPS; WGS1984		
RC09-38	Clear Lake South	Lava	8/2/2009	580207	4913678			NID GPS; WGS1984		
RC09-39	Pleistocene	Lava	8/2/2009	580435	4913085	580514	4912893	RC GPS; NAD1927		

TABLE A2. XRF, PALEOMAGNETIC, AND ^{3}HE SAMPLE LOCATIONS FOR THE SMVF

				Datum: WGS1984		Datum: NAD1927				
Sample ID	Assigned Unit	Material	Collection Date	Easting	Northing	Easting	Northing	Location method	Error (m)	Co-located paleomagnetic or ^{3}He sample site
RC09-40	Clear Lake South	Lava	8/2/2009	580333	4912512			NID GPS; WGS1984		
RC09-41	Cold Water Cove	Lava	8/2/2009	580568	4912491			NID GPS; WGS1984		
RC09-42	Cold Water Cove	Lava	8/2/2009	580659	4912613			NID GPS; WGS1984		
RC09-43	Clear Lake East	Lava	8/2/2009	580699	4912823			NID GPS; WGS1984		
RC09-44	Clear Lake South	Lava	8/2/2009	579985	4910881			NID GPS; WGS1984		^{3}He site
RC09-45	Clear Lake South	Lava	8/3/2009	580897	4911137	580977	4910945	RC GPS; NAD1927		
RC09-46	Ice Cap	Lava	8/3/2009	581078	4911182	581158	4910990	RC GPS; NAD1927		
RC09-47	Clear Lake South	Lava	8/3/2009	581487	4911572	581567	4911380	RC GPS; NAD1927		
RC09-48	Clear Lake South	Lava	8/3/2009	581645	4911546	581725	4911354	RC GPS; NAD1927		
RC09-49	Ice Cap	Lava	8/3/2009	582218	4911751	582298	4911559	RC GPS; NAD1927		
RC09-50	Clear Lake South	Lava	8/3/2009	582236	4911503	582316	4911311	RC GPS; NAD1927		
RC09-51	Ice Cap	Lava	8/3/2009	582326	4911193	582406	4911001	RC GPS; NAD1927		
RC09-52	Ice Cap	Lava	8/3/2009	582375	4910585	582455	4910393	RC GPS; NAD1927		
RC09-53	Clear Lake South	Lava	8/3/2009	582406	4910518	582486	4910326	RC GPS; NAD1927		
RC09-54	Ice Cap	Lava	8/3/2009	582748	4910338	582828	4910146	RC GPS; NAD1927		
RC09-55	Clear Lake South	Lava	8/3/2009	582902	4910167	582982	4909975	RC GPS; NAD1927		
RC09-56	Clear Lake South	Lava	8/3/2009	583184	4910010	583264	4909818	RC GPS; NAD1927		
RC09-57	Clear Lake South	Lava	8/3/2009	583042	4909921	583122	4909729	RC GPS; NAD1927		
RC09-58	Clear Lake South	Lava	8/3/2009	582714	4909641	582794	4909449	RC GPS; NAD1927		
RC09-59	Clear Lake South	Lava	8/3/2009	582379	4909688	582459	4909496	RC GPS; NAD1927		
RC09-60	Clear Lake South	Lava	8/3/2009	582138	4909716	582218	4909524	RC GPS; NAD1927		
RC09-61	Clear Lake South	Lava	8/3/2009	581945	4909910	582025	4909718	RC GPS; NAD1927		
NID09-01	Clear Lake South	Lava	8/7/2009	579675	4910679			NID GPS; WGS1984	10	
NID09-02	Clear Lake South	Lava	8/7/2009	579975	4911134			NID GPS; WGS1984	6	
NID09-03	Clear Lake South	Lava	8/7/2009	579831	4911444			NID GPS; WGS1984	6	
NID09-04	Clear Lake South	Lava	8/7/2009	579846	4911162			NID GPS; WGS1984	6	
NID09-05	Clear Lake South	Lava	8/7/2009	579738	4910891			NID GPS; WGS1984	10	
NID09-07	Clear Lake South	Lava	8/7/2009	579907	4909129			NID GPS; WGS1984	4	
NID09-08	Clear Lake South	Lava	8/7/2009	579766	4908862			NID GPS; WGS1984	6	
NID09-09	Clear Lake South	Lava	8/7/2009	579608	4908548			NID GPS; WGS1984	6	
NID09-10	Tamolitch	Lava	8/7/2009	579506	4908543			NID GPS; WGS1984	6	
NID09-11	Tamolitch	Lava	8/7/2009	579800	4908288			NID GPS; WGS1984	7	
NID09-12	Ice Cap	Lava	9/21/2009	580105	4911175			NID GPS; WGS1984	5	
NID09-13	Ice Cap	Lava	9/21/2009	579975	4910998			NID GPS; WGS1984	4	
NID09-14	Clear Lake South	Lava	9/21/2009	579972	4910978			NID GPS; WGS1984	5	
NID09-15	Ice Cap	Lava	9/21/2009	580774	4911498			NID GPS; WGS1984	8	
NID09-16	Ice Cap	Lava	9/21/2009	580802	4911460			NID GPS; WGS1984	6	
NID09-17	Clear Lake South	Lava	9/21/2009	580753	4911718			NID GPS; WGS1984	6	
NID09-18	Cold Water Cove	Lava	9/21/2009	580649	4911738			NID GPS; WGS1984	7	
NID09-19	Clear Lake South	Lava	9/21/2009	580216	4911804			NID GPS; WGS1984	6	^{3}He site
NID09-20	Ice Cap	Lava	9/21/2009	579812	4910617			NID GPS; WGS1984	6	
NID09-21	Clear Lake South	Lava	9/21/2009	579817	4910666			NID GPS; WGS1984	5	
NID09-22	Tamolitch	Lava	9/21/2009	577193	4906060			NID GPS; WGS1984	5	
NID09-23	Pleistocene	Lava	10/22/2009	578514	4908612			Estimated from map		
NID09-24	Clear Lake East	Lava	11/1/2009	580626	4913341			NID GPS; WGS1984		^{3}He site
NID09-25	Clear Lake East	Lava	11/1/2009	580824	4912936			NID GPS; WGS1984		

TABLE A2. XRF, PALEOMAGNETIC, AND ^{3}HE SAMPLE LOCATIONS FOR THE SMVF

				Datum: WGS1984		Datum: NAD1927				Co-located paleomagnetic or
Sample ID	Assigned Unit	Material	Collection Date	Easting	Northing	Easting	Northing	Location method	Error (m)	^{3}He sample site
NID09-26	Cold Water Cove	Lava	11/2/2009	580914	4912291			NID GPS; WGS1984	8	^{3}He site
NID09-27	Cold Water Cove	Lava	11/2/2009	580981	4912230			NID GPS; WGS1984	8	
NID09-28	Ice Cap	Lava	11/2/2009	581128	4912216			NID GPS; WGS1984	8	
NID09-29	Clear Lake South	Lava	11/2/2009	580370	4912354			NID GPS; WGS1984	4	^{3}He site
NID09-30	Clear Lake South	Lava	11/2/2009	580449	4912190			NID GPS; WGS1984	9	^{3}He site
NID09-31	Ice Cap	Lava	11/2/2009	580280	4911150			NID GPS; WGS1984	8	^{3}He site
NID09-32	Clear Lake South	Lava	11/2/2009	580431	4908651			NID GPS; WGS1984	6	
NID09-33	Belknap	Lava	11/2/2009	580457	4908866			NID GPS; WGS1984	4	
RC10-18	Ice Cap	Lava	8/27/2010	582460	4911515	582540	4911323	RC GPS; NAD1927		
RC10-19	Ice Cap	Lava	8/27/2010	582498	4911495	582578	4911303	RC GPS; NAD1927		
RC10-20	Ice Cap	Lava	8/27/2010	582882	4911663	582962	4911471	RC GPS; NAD1927		
RC10-21	Clear Lake South	Lava	8/27/2010	582987	4911907	583067	4911715	RC GPS; NAD1927		
RC10-22	Ice Cap	Lava	8/27/2010	583584	4912115	583664	4911923	RC GPS; NAD1927		
RC10-23	Ice Cap	Lava	8/27/2010	583387	4912214	583467	4912022	RC GPS; NAD1927		
RC10-24	Clear Lake East	Lava	8/27/2010	583478	4912307	583558	4912115	RC GPS; NAD1927		
RC10-25	Ice Cap	Lava	8/27/2010	583230	4912223	583310	4912031	RC GPS; NAD1927		
RC10-26	Clear Lake East	Lava	8/27/2010	582992	4912160	583072	4911968	RC GPS; NAD1927		
RC10-27	Ice Cap	Lava	8/27/2010	582928	4912172	583008	4911980	RC GPS; NAD1927		
RC10-28	Belknap	Lava	8/28/2010	580151	4908457			NID GPS; WGS1984	5	
RC10-29	Belknap	Lava	8/28/2010	580126	4908526			NID GPS; WGS1984	3	
RC10-30	Tamolitch	Lava	8/28/2010	581054	4908758			NID GPS; WGS1984	6	
RC10-31	Belknap	Lava	8/28/2010	581393	4908794			NID GPS; WGS1984	4	
RC10-32	Clear Lake South	Lava	8/29/2010	581001	4910995			NID GPS; WGS1984	6	
RC10-33	Clear Lake South	Lava	8/30/2010	580654	4909085			NID GPS; WGS1984	5	
RC10-34	Clear Lake South	Scoria	8/30/2010	580526	4908884			NID GPS; WGS1984	4	
RC10-35	Great Spring	Lava	8/30/2010	584888	4915373			NID GPS; WGS1984	4	
RC10-36	Great Spring	Lava	8/30/2010	584293	4915270			NID GPS; WGS1984	5	
RC10-37	Clear Lake East	Lava	8/31/2010	581248	4912366			NID GPS; WGS1984	6	
RC10-38	Cold Water Cove	Lava	8/31/2010	581192	4912538			NID GPS; WGS1984	4	
NID10-01MK	Belknap	Lava	7/16/2010	580557	4908431			NID GPS; WGS1984	4	
NID10-02MK	Tamolitch	Lava	7/16/2010	581202	4908239			NID GPS; WGS1984	7	
NID10-03MK	Belknap	Lava	7/16/2010	580865	4908057			NID GPS; WGS1984	4	
NID10-04MK	Tamolitch	Lava	7/16/2010	580408	4908312			NID GPS; WGS1984	5	
NID10-05MK	Tamolitch	Lava	7/16/2010	580129	4908280			NID GPS; WGS1984	5	
NID10-06MK	Clear Lake East	Lava	7/17/2010	582366	4913658			NID GPS; WGS1984	5	
NID10-07MK	Clear Lake East	Lava	7/17/2010	582366	4913505			NID GPS; WGS1984	5	
NID10-08MK	Clear Lake East	Lava	7/17/2010	581391	4914233			NID GPS; WGS1984	3	
NID10-09MK	Clear Lake East	Lava	7/17/2010	581319	4914664			NID GPS; WGS1984	6	
NID10-10MK	Great Spring	Lava	7/17/2010	581084	4914789			NID GPS; WGS1984	9	
NID10-11MK	Great Spring	Lava	7/17/2010	580640	4914620			NID GPS; WGS1984	5	
NID10-12MK	Great Spring	Lava	7/17/2010	580475	4915061			NID GPS; WGS1984	5	
NID10-13MK	Great Spring	Lava	7/17/2010	580245	4914891			NID GPS; WGS1984	6	
NID10-14MK	Great Spring	Lava	7/17/2010	579909	4914685			NID GPS; WGS1984	8	
NID10-15MK	Great Spring	Lava	7/17/2010	579925	4914370			NID GPS; WGS1984	5	
NID10-18MK	Ice Cap	Lava	9/21/2010	581341	4912593			NID GPS; WGS1984	6	
NID10-19MK	Belknap	Lava	9/22/2010	579524	4908663			NID GPS; WGS1984	5	

TABLE A2. XRF, PALEOMAGNETIC, AND ^{3}HE SAMPLE LOCATIONS FOR THE SMVF

				Datum: WGS1984		Datum: NAD1927				
Sample ID	Assigned Unit	Material	Collection Date	Easting	Northing	Easting	Northing	Location method	Error (m)	Co-located paleomagnetic or ^{3}He sample site
NID10-20MK	Belknap	Lava	9/22/2010	579927	4908741			NID GPS; WGS1984	5	
NID10-21MK	Clear Lake East	Lava	10/16/2010	585313	4914492			NID GPS; WGS1984	5	
NID10-22MK	Clear Lake East	Lava	10/16/2010	585313	4913908			NID GPS; WGS1984	6	
NID10-23MK	Clear Lake East	Lava	10/16/2010	585116	4913721			NID GPS; WGS1984	6	
NID10-24MK	Clear Lake East	Lava	10/16/2010	585209	4913667			NID GPS; WGS1984	3	
NID10-25MK	Clear Lake East	Lava	10/16/2010	585157	4913618			NID GPS; WGS1984	4	
NID10-26MK	Undifferentiated Belknap	Lava	10/18/2010	584558	4906055			NID GPS; WGS1984	4	
NID10-27MK	Undifferentiated Belknap	Lava	10/18/2010	584640	4906153			NID GPS; WGS1984	5	
NID10-28MK	Belknap	Lava	10/18/2010	585122	4906261			NID GPS; WGS1984	5	
NID10-29MK	Undifferentiated Belknap	Lava	10/18/2010	585357	4906315			NID GPS; WGS1984	4	
NID10-30MK	Belknap	Lava	10/18/2010	585305	4907024			NID GPS; WGS1984	4	
NID10-31MK	Clear Lake South	Lava	10/22/2010	583092	4909492			NID GPS; WGS1984	5	
NID10-32MK	Clear Lake East	Lava	10/22/2010	583892	4909870			NID GPS; WGS1984	3	
NID10-33MK	Clear Lake South	Lava	10/22/2010	583868	4909831			NID GPS; WGS1984	4	
NID10-34MK	Great Spring	Lava	11/12/2010	580412	4914393			NID GPS; WGS1984	6	
NID10-35MK	Great Spring	Lava	11/12/2010	580670	4914442			Adjusted based on LiDAR from UTM 10N WGS 1984 580670 4914437. error 5 m (NID GPS)		
NID10-36MK	Clear Lake East	Lava	11/12/2010	580700	4914427			Adjusted based on LiDAR from UTM 10N WGS 1983 580700 4914432. error 5 m (NID GPS)		
NID10-37MK	Cold Water Cove	Lava	11/17/2010	580504	4914430			NID GPS; WGS1984	6	
RC11-01	Belknap	Lava	8/27/2011	579548	4908738			NID GPS; WGS1984	4	
RC11-02	Tamolitch	Lava	8/27/2011	579550	4908762			NID GPS; WGS1984	4	
RC11-03	Belknap	Lava	8/27/2011	579494	4908699			NID GPS; WGS1984	3	
RC11-04	Belknap	Lava	8/27/2011	579416	4908843			NID GPS; WGS1984	5	
RC11-05	Tamolitch	Lava	8/27/2011	579321	4908689			NID GPS; WGS1984	6	
RC11-06	Belknap	Lava	8/27/2011	579545	4908577			NID GPS; WGS1984	5	
RC11-07	Belknap	Lava	8/27/2011	579701	4908620			NID GPS; WGS1984	6	
RC11-08	Early Nash II	Cinder	8/28/2011	583207	4920239			NID GPS; WGS1984	4	
RC11-09	Early Nash II	Lava	8/28/2011	582717	4920212			NID GPS; WGS1984	4	
RC11-10	Early Nash II	Lava	8/28/2011	582758	4920204			NID GPS; WGS1984	6	437 1B
RC11-11	SnoPark	Lava	8/28/2011	582884	4920368			NID GPS; WGS1984	7	
RC11-12	Little Nash	Lava	8/28/2011	582830	4921094			NID GPS; WGS1984	6	
RC11-13	Little Nash	Lava	8/28/2011	582862	4921239			NID GPS; WGS1984	6	
RC11-14	Little Nash	Lava	8/28/2011	582795	4921310			NID GPS; WGS1984	5	
RC11-15	Lost Lake	Lava	8/28/2011	583371	4920510			NID GPS; WGS1984	6	
RC11-16	Old Wagon Road	Lava	8/28/2011	579747	4915145			NID GPS; WGS1984	5	
RC11-17	Nash	Lava	8/28/2011	582172	4919870			NID GPS; WGS1984	4	
RC11-18	Cold Water Cove	Lava	8/29/2011	580108	4914319			NID GPS; WGS1984	8	
RC11-19	Clear Lake East	Bombs	8/30/2011	585342	4915194			NID GPS; WGS1984	5	
RC11-20	Great Spring	Lava	8/30/2011	584975	4915317			NID GPS; WGS1984	7	
RC11-21	Clear Lake East	Lava	8/30/2011	584630	4914636			NID GPS; WGS1984	4	
RC11-22	Clear Lake East	Lava	8/30/2011	583998	4914197			NID GPS; WGS1984	4	
RC11-23	Clear Lake East	Scoria	8/30/2011	584623	4914357			NID GPS; WGS1984	5	
RC11-24	Ice Cap	Bomb	8/30/2011	585091	4914146			NID GPS; WGS1984	5	

TABLE A2. XRF, PALEOMAGNETIC, AND ^{3}HE SAMPLE LOCATIONS FOR THE SMVF

				Datum: WGS1984		Datum: NAD1927				Co-located paleomagnetic or
Sample ID	Assigned Unit	Material	Collection Date	Easting	Northing	Easting	Northing	Location method	Error (m)	^{3}He sample site
RC11-25	Early Nash I	Lava	8/31/2011	580310	4921442			NID GPS; WGS1984	5	
RC11-26	Fish Lake	Lava	8/31/2011	579308	4920029			NID GPS; WGS1984	4	
RC11-27	Fish Lake	Lava	8/31/2011	579349	4919998			NID GPS; WGS1984	7	
RC11-28	Fish Lake	Lava	8/31/2011	579828	4920585			NID GPS; WGS1984	4	
NID11-04MK	Tamolitch	Lava	9/13/2011	577241	4905989			NID GPS; WGS1984	9	421 1B
NID11-05MK	Cold Water Cove	Lava	9/13/2011	580599	4912552			NID GPS; WGS1984	6	429 1B

TABLE A3. BATHYMETRIC DATA AND OBSERVATIONS FOR CLEAR LAKE

Waypoint	Collection date	Latitude	Longitude	USGS gage elevation (ft)	USGS gage elevation (m)	Depth (m)	Elevation (m)	Tree top depth (m)	Tree height (m)	Whiteline	Water temperature (°C)
1	7/23/2008	44.376367	-122.002617	3018.0	919.9	14.7	905.2			Present	7.2
455	7/23/2008	44.377383	-122.003467	3018.0	919.9	0.5	919.4			Absent	7.7
456	7/23/2008	44.377500	-122.003250	3018.0	919.9	1.0	918.9			Present	7.9
457	7/23/2008	44.377200	-122.003450	3018.0	919.9	1.9	918.0			Present	7.9
458	7/23/2008	44.377167	-122.003267	3018.0	919.9	3.6	916.3			Present	7.8
459	7/23/2008	44.377150	-122.003333	3018.0	919.9	6.3	913.6			Present	7.8
461	7/23/2008	44.376883	-122.003433	3018.0	919.9	0.9	919.0			Present	7.6
463	7/23/2008	44.376983	-122.003283	3018.0	919.9	7.9	912.0			Present	7.5
464	7/23/2008	44.377083	-122.003050	3018.0	919.9	3.2	916.7			Present	6.4
465	7/23/2008	44.377050	-122.003167	3018.0	919.9	8.1	911.8			Present	7.1
466	7/23/2008	44.376900	-122.003267	3018.0	919.9	1.5	918.4			Present	7.3
467	7/23/2008	44.376800	-122.003133	3018.0	919.9	9.6	910.3			Present	7.3
468	7/23/2008	44.376850	-122.002850	3018.0	919.9	4.4	915.5			Present	7.3
469	7/23/2008	44.376683	-122.002900	3018.0	919.9	12.7	907.2			Present	7.1
470	7/23/2008	44.376583	-122.003067	3018.0	919.9	6.8	913.1			Present	7.0
471	7/23/2008	44.376417	-122.003167	3018.0	919.9	2.1	917.8			Present	7.1
472	7/23/2008	44.376383	-122.002983	3018.0	919.9	13.1	906.8			Present	7.1
473	7/23/2008	44.376383	-122.002750	3018.0	919.9	14.6	905.3			Present	7.1
474	7/23/2008	44.376417	-122.002633	3018.0	919.9	7.9	912.0			Present	7.1
475	7/23/2008	44.376583	-122.002517	3018.0	919.9	3.6	916.3			Present	7.0
476	7/23/2008	44.376667	-122.002467	3018.0	919.9	8.1	911.8			Present	7.0
477	7/23/2008	44.376600	-122.002567	3018.0	919.9	15.4	904.5			Present	6.9
478	7/23/2008	44.376317	-122.002717	3018.0	919.9	6.4	913.5			Present	6.9
479	7/23/2008	44.376267	-122.002867	3018.0	919.9	2.0	917.9			Present	6.9
481	7/23/2008	44.376233	-122.002867	3018.0	919.9	8.5	911.4			Present	7.0
482	7/23/2008	44.376333	-122.002583	3018.0	919.9	15.2	904.7			Present	7.0
483	7/23/2008	44.376383	-122.002600	3018.0	919.9	15.6	904.3	14.6	1.0	Present	6.9
484	7/23/2008	44.376633	-122.002333	3018.0	919.9	7.5	912.4			Present	6.8
485	7/23/2008	44.376733	-122.002333	3018.0	919.9	2.2	917.7			Present	6.8
486	7/23/2008	44.376633	-122.002350	3018.0	919.9	11.3	908.6			Present	6.8
487	7/23/2008	44.376483	-122.002417	3018.0	919.9	16.1	903.8			Present	6.8
488	7/23/2008	44.376250	-122.002483	3018.0	919.9	7.6	912.3			Present	6.8
489	7/23/2008	44.376017	-122.002483	3018.0	919.9	2.0	917.9			Present	6.9
490	7/23/2008	44.376167	-122.002300	3018.0	919.9	7.3	912.6			Present	6.9
491	7/23/2008	44.376217	-122.002167	3018.0	919.9	10.8	909.1			Present	6.9
492	7/23/2008	44.376367	-122.002000	3018.0	919.9	14.2	905.7			Present	6.9
493	7/23/2008	44.376550	-122.001883	3018.0	919.9	13.3	906.6			Present	6.9
494	7/23/2008	44.376783	-122.001867	3018.0	919.9	2.5	917.4			Present	6.9
495	7/23/2008	44.376633	-122.001800	3018.0	919.9	11.4	908.5			Present	6.8
496	7/23/2008	44.376533	-122.001767	3018.0	919.9	15.4	904.5			Present	6.8
497	7/23/2008	44.376267	-122.001667	3018.0	919.9	12.5	907.4			Present	6.8
498	7/23/2008	44.376050	-122.001583	3018.0	919.9	7.9	912.0			Present	6.8
499	7/23/2008	44.375900	-122.001567	3018.0	919.9	3.7	916.2			Present	6.8

Note: USGS gage 14158500 is located at the Clear Lake outlet (see Fig. 2b); USGS gage elevation determined by taking averaging gage height over the period out on the lake (maximum range: 0.02 ft) and adding this value to the gage datum (3015.32 ft above sea level). The water temperature is of the top 30 cm of the lake.

TABLE A3. BATHYMETRIC DATA AND OBSERVATIONS FOR CLEAR LAKE

Waypoint	Collection date	Latitude	Longitude	USGS gage elevation (ft)	USGS gage elevation (m)	Depth (m)	Elevation (m)	Tree top depth (m)	Tree height (m)	Whiteline	Water temperature (°C)
500	7/23/2008	44.375950	-122.001450	3018.0	919.9	6.7	913.2			Present	6.9
501	7/23/2008	44.376033	-122.001450	3018.0	919.9	9.5	910.4			Present	6.9
502	7/23/2008	44.376167	-122.001450	3018.0	919.9	12.4	907.5	2.4	10.0	Present	6.9
503	7/23/2008	44.376600	-122.001533	3018.0	919.9	15.4	904.5			Present	6.9
504	7/23/2008	44.376767	-122.001583	3018.0	919.9	7.3	912.6			Present	6.9
505	7/23/2008	44.376883	-122.001600	3018.0	919.9	2.8	917.1			Present	6.9
506	7/23/2008	44.376700	-122.001500	3018.0	919.9	14.9	905.0			Present	6.9
507	7/23/2008	44.376533	-122.001417	3018.0	919.9	13.2	906.7			Present	6.9
508	7/23/2008	44.376300	-122.001317	3018.0	919.9	15.4	904.5			Present	6.9
509	7/23/2008	44.376200	-122.001150	3018.0	919.9	12.3	907.6			Present	6.9
510	7/23/2008	44.376050	-122.001300	3018.0	919.9	9.6	910.3			Present	6.8
511	7/23/2008	44.375817	-122.001183	3018.0	919.9	2.7	917.2			Present	6.8
512	7/23/2008	44.375967	-122.001117	3018.0	919.9	7.8	912.1			Present	6.9
513	7/23/2008	44.376167	-122.001083	3018.0	919.9	13.9	906.0			Present	6.9
514	7/23/2008	44.376200	-122.001083	3018.0	919.9	15.3	904.6			Present	6.9
515	7/23/2008	44.376450	-122.001083	3018.0	919.9	13.1	906.8			Present	6.8
516	7/23/2008	44.376750	-122.001117	3018.0	919.9	15.6	904.3			Present	6.8
517	7/23/2008	44.376883	-122.001167	3018.0	919.9	10.9	909.0			Present	6.8
518	7/23/2008	44.377033	-122.001250	3018.0	919.9	2.9	917.0			Present	6.8
519	7/23/2008	44.376783	-122.000983	3018.0	919.9	12.8	907.1			Present	6.8
520	7/23/2008	44.376600	-122.000817	3018.0	919.9	11.3	908.6			Present	6.7
521	7/23/2008	44.376333	-122.000750	3018.0	919.9	11.8	908.1			Present	6.7
522	7/23/2008	44.376283	-122.000750	3018.0	919.9	11.5	908.4	8.5	3.0	Present	6.7
523	7/23/2008	44.375900	-122.000917	3018.0	919.9	5.3	914.6			Barely present	6.8
524	7/23/2008	44.375950	-122.000950	3018.0	919.9	7.4	912.5			Present	6.8
525	7/23/2008	44.376133	-122.000950	3018.0	919.9	12.8	907.1			Present	6.8
526	7/23/2008	44.376483	-122.000900	3018.0	919.9	11.5	908.4			Present	6.8
527	7/23/2008	44.376917	-122.000867	3018.0	919.9	9.0	910.9			Present	6.7
528	7/23/2008	44.376950	-122.000817	3018.0	919.9	9.1	910.8	2.1	7.0	Present	6.6
529	7/23/2008	44.376933	-122.000817	3018.0	919.9	9.5	910.4			Present	6.5
530	7/23/2008	44.377200	-122.001083	3018.0	919.9	0.8	919.1			Present	6.5
531	7/23/2008	44.377150	-122.001033	3018.0	919.9	5.1	914.8	3.1	2.0	Present	6.6
532	7/23/2008	44.377117	-122.000850	3018.0	919.9	6.5	913.4	1.5	5.0	Present	6.6
533	7/23/2008	44.377000	-122.000817	3018.0	919.9	8.9	911.0			Present	6.6
534	7/23/2008	44.377267	-122.000617	3018.0	919.9	8.8	911.1			Present	6.6
535	7/23/2008	44.377483	-122.000783	3018.0	919.9	3.9	916.0			Present	6.6
536	7/23/2008	44.377567	-122.000533	3018.0	919.9	8.1	911.8			Present	6.8
537	7/23/2008	44.377617	-122.000300	3018.0	919.9	9.6	910.3			Present	7.0
538	7/23/2008	44.377783	-122.000117	3018.0	919.9	9.6	910.3			Present	7.1
539	7/23/2008	44.378117	-122.000383	3018.0	919.9	0.8	919.1			Absent	7.6
540	7/23/2008	44.378033	-122.000367	3018.0	919.9	3.1	916.8			Present	8.0
541	7/23/2008	44.377917	-122.000267	3018.0	919.9	7.6	912.3			Present	8.1
542	7/23/2008	44.377900	-121.999883	3018.0	919.9	8.3	911.6			Present	8.1

Note: USGS gage 14158500 is located at the Clear Lake outlet (see Fig. 2b); USGS gage elevation determined by taking averaging gage height over the period out on the lake (maximum range: 0.02 ft) and adding this value to the gage datum (3015.32 ft above sea level). The water temperature is of the top 30 cm of the lake.

TABLE A3. BATHYMETRIC DATA AND OBSERVATIONS FOR CLEAR LAKE

Waypoint	Collection date	Latitude	Longitude	USGS gage elevation (ft)	USGS gage elevation (m)	Depth (m)	Elevation (m)	Tree top depth (m)	Tree height (m)	Whiteline	Water temperature (°C)
543	7/23/2008	44.377967	-121.999550	3018.0	919.9	10.5	909.4			Present	8.0
544	7/23/2008	44.378167	-121.999367	3018.0	919.9	0.5	919.4			Absent	6.6
545	7/23/2008	44.378133	-121.999417	3018.0	919.9	1.7	918.2			Absent	6.5
546	7/23/2008	44.377867	-121.999617	3018.0	919.9	7.6	912.3			Present	6.2
547	7/23/2008	44.377733	-121.999767	3018.0	919.9	9.0	910.9			Present	6.0
548	7/23/2008	44.377600	-121.999800	3018.0	919.9	11.3	908.6			Present	6.2
549	7/23/2008	44.377467	-121.999800	3018.0	919.9	13.7	906.2			Present	6.3
550	7/23/2008	44.377317	-121.999800	3018.0	919.9	15.2	904.7			Present	6.4
551	7/23/2008	44.377083	-121.999817	3018.0	919.9	18.8	901.1			Present	6.6
552	7/23/2008	44.376950	-121.999900	3018.0	919.9	17.5	902.4			Present	6.6
547	7/23/2008	44.377733	-121.999767	3018.0	919.9	9.0	910.9			Present	6.0
548	7/23/2008	44.377600	-121.999800	3018.0	919.9	11.3	908.6			Present	6.2
549	7/23/2008	44.377467	-121.999800	3018.0	919.9	13.7	906.2			Present	6.3
550	7/23/2008	44.377317	-121.999800	3018.0	919.9	15.2	904.7			Present	6.4
551	7/23/2008	44.377083	-121.999817	3018.0	919.9	18.8	901.1			Present	6.6
552	7/23/2008	44.376950	-121.999900	3018.0	919.9	17.5	902.4			Present	6.6
553	7/23/2008	44.376833	-121.999950	3018.0	919.9	16.5	903.4			Absent	6.6
554	7/23/2008	44.376817	-121.999950	3018.0	919.9	18.0	901.9			Present	6.7
555	7/23/2008	44.376750	-121.999983	3018.0	919.9	15.6	904.3			Present	6.7
556	7/23/2008	44.376683	-122.000233	3018.0	919.9	11.2	908.7			Present	6.6
557	7/23/2008	44.376583	-122.000333	3018.0	919.9	11.2	908.7			Present	6.6
558	7/23/2008	44.376433	-122.000300	3018.0	919.9	11.7	908.2			Present	6.7
559	7/23/2008	44.376283	-122.000267	3018.0	919.9	11.2	908.7			Present	6.7
560	7/23/2008	44.376117	-122.000233	3018.0	919.9	11.5	908.4			Present	6.7
561	7/23/2008	44.375800	-122.000300	3018.0	919.9	4.7	915.2			Barely present	6.7
562	7/23/2008	44.375950	-122.000233	3018.0	919.9	10.9	909.0			Patchy	6.7
563	7/23/2008	44.376167	-122.000033	3018.0	919.9	11.9	908.0			Present	6.6
564	7/23/2008	44.376317	-121.999867	3018.0	919.9	13.0	906.9			Present	6.6
565	7/23/2008	44.376467	-121.999733	3018.0	919.9	12.2	907.7			Present	6.6
566	7/23/2008	44.376583	-121.999550	3018.0	919.9	12.9	907.0			Present	6.6
567	7/23/2008	44.376783	-121.999133	3018.0	919.9	16.5	903.4			Present	6.6
568	7/23/2008	44.376867	-121.998900	3018.0	919.9	15.8	904.1			Flow edge	6.5
569	7/23/2008	44.376983	-121.998717	3018.0	919.9	8.9	911.0			Flow edge	6.6
570	7/23/2008	44.377067	-121.998633	3018.0	919.9	5.5	914.4			Present	6.4
571	7/23/2008	44.376950	-121.998750	3018.0	919.9	15.2	904.7			Flow edge	6.2
572	7/23/2008	44.376783	-121.998767	3018.0	919.9	15.1	904.8			Present	6.2
573	7/23/2008	44.376683	-121.998567	3018.0	919.9	14.7	905.2			Present	6.3
574	7/23/2008	44.376633	-121.998400	3018.0	919.9	8.0	911.9			Present (definitively lava flow)	6.1
575	7/23/2008	44.376617	-121.998283	3018.0	919.9	5.1	914.8			Present	5.5
576	7/23/2008	44.376583	-121.998133	3018.0	919.9	4.0	915.9			Present (thin)	5.2
577	7/23/2008	44.376583	-121.998000	3018.0	919.9	6.1	913.8			Present	4.9
578	7/23/2008	44.376633	-121.997850	3018.0	919.9	2.9	917.0			Present	4.6
579	7/23/2008	44.376683	-121.997783	3018.0	919.9	2.7	917.2			Barely present	4.4

Note: USGS gage 14158500 is located at the Clear Lake outlet (see Fig. 2b); USGS gage elevation determined by taking averaging gage height over the period out on the lake (maximum range: 0.02 ft) and adding this value to the gage datum (3015.32 ft above sea level). The water temperature is of the top 30 cm of the lake.

TABLE A3. BATHYMETRIC DATA AND OBSERVATIONS FOR CLEAR LAKE

Waypoint	Collection date	Latitude	Longitude	USGS gage elevation (ft)	USGS gage elevation (m)	Depth (m)	Elevation (m)	Tree top depth (m)	Tree height (m)	Whiteline	Water temperature (°C)
580	7/23/2008	44.376533	-121.997867	3018.0	919.9	6.6	913.3			Absent	4.3
581	7/23/2008	44.376383	-121.997917	3018.0	919.9	7.8	912.1			Barely present	4.3
582	7/23/2008	44.376233	-121.998050	3018.0	919.9	8.4	911.5			Barely present	4.3
583	7/23/2008	44.376100	-121.998167	3018.0	919.9	9.5	910.4			Absent	4.3
584	7/23/2008	44.376033	-121.998267	3018.0	919.9	12.6	907.3			Absent	4.3
585	7/23/2008	44.375917	-121.998467	3018.0	919.9	13.7	906.2			Present	4.3
586	7/23/2008	44.375800	-121.998667	3018.0	919.9	11.5	908.4			Present	4.4
587	7/23/2008	44.375717	-121.998817	3018.0	919.9	7.2	912.7			Present	4.4
588	7/23/2008	44.375633	-121.998950	3018.0	919.9	4.4	915.5			Present	4.4
589	7/23/2008	44.375383	-121.999250	3018.0	919.9	2.1	917.8			Absent	4.8
590	7/23/2008	44.375433	-121.998967	3018.0	919.9	3.3	916.6			Absent	5.2
591	7/23/2008	44.375517	-121.998700	3018.0	919.9	4.4	915.5			Present	5.2
592	7/23/2008	44.375567	-121.998450	3018.0	919.9	8.8	911.1			Barely present	5.1
593	7/23/2008	44.375600	-121.998217	3018.0	919.9	9.6	910.3			Absent	5.0
594	7/23/2008	44.375633	-121.997967	3018.0	919.9	5.3	914.6			Absent	5.0
595	7/23/2008	44.375550	-121.998067	3018.0	919.9	8.1	911.8			Absent	5.0
596	7/23/2008	44.375400	-121.998167	3018.0	919.9	6.6	913.3			Absent	5.1
597	7/23/2008	44.375267	-121.998317	3018.0	919.9	2.7	917.2			Barely present	5.1
598	7/23/2008	44.375233	-121.998183	3018.0	919.9	3.8	916.1	1.8	2.0	Present	5.1
599	7/23/2008	44.375233	-121.997817	3018.0	919.9	6.6	913.3			Barely present	5.1
600	7/23/2008	44.375200	-121.997633	3018.0	919.9	6.2	913.7			Present	5.1
601	7/23/2008	44.375100	-121.997867	3018.0	919.9	5.8	914.1			Absent	5.2
602	7/23/2008	44.375000	-121.998083	3018.0	919.9	2.3	917.6			Absent	5.1
603	7/23/2008	44.374967	-121.997983	3018.0	919.9	3.8	916.1	1.8	2.0	Absent	4.9
604	7/23/2008	44.375000	-121.997683	3018.0	919.9	7.4	912.5			Barely present	4.9
605	7/23/2008	44.375033	-121.997533	3018.0	919.9	1.5	918.4			Barely present	4.9
606	7/23/2008	44.374883	-121.997667	3018.0	919.9	6.8	913.1			Absent	4.9
607	7/23/2008	44.374683	-121.997833	3018.0	919.9	4.8	915.1			Barely present	5.0
608	7/23/2008	44.374650	-121.997467	3018.0	919.9	3.3	916.6			Present	5.1
609	7/23/2008	44.374617	-121.997600	3018.0	919.9	7.4	912.5			Barely present	5.1
610	7/23/2008	44.374550	-121.997783	3018.0	919.9	4.7	915.2			Barely present	5.1
611	7/23/2008	44.374600	-121.997633	3018.0	919.9	7.4	912.5	3.4	4.0	Present	5.2
612	7/23/2008	44.374467	-121.997667	3018.0	919.9	7.0	912.9			Absent	5.2
613	7/23/2008	44.374300	-121.997617	3018.0	919.9	7.1	912.8			Absent	5.1
614	7/23/2008	44.374183	-121.997617	3018.0	919.9	6.8	913.1			Absent	5.3
615	7/23/2008	44.374067	-121.997633	3018.0	919.9	6.2	913.7			Absent	5.4
616	7/23/2008	44.373917	-121.997600	3018.0	919.9	5.8	914.1			Absent	5.6
617	7/23/2008	44.373900	-121.997467	3018.0	919.9	8.1	911.8			Present	6.3
618	7/23/2008	44.374100	-121.997067	3018.0	919.9	1.0	918.9			Barely present	6.1
619	7/23/2008	44.374117	-121.997267	3018.0	919.9	6.6	913.3			Barely present	6.0
620	7/23/2008	44.374133	-121.997417	3018.0	919.9	9.8	910.1			Present	6.0
621	7/23/2008	44.374150	-121.997733	3018.0	919.9	4.2	915.7			Present	5.9
622	7/23/2008	44.374150	-121.997883	3018.0	919.9	0.6	919.3			Absent	5.9

Note: USGS gage 14158500 is located at the Clear Lake outlet (see Fig. 2b); USGS gage elevation determined by taking averaging gage height over the period out on the lake (maximum range: 0.02 ft) and adding this value to the gage datum (3015.32 ft above sea level). The water temperature is of the top 30 cm of the lake.

TABLE A3. BATHYMETRIC DATA AND OBSERVATIONS FOR CLEAR LAKE

Waypoint	Collection date	Latitude	Longitude	USGS gage elevation (ft)	USGS gage elevation (m)	Depth (m)	Elevation (m)	Tree top depth (m)	Tree height (m)	Whiteline	Water temperature (°C)
623	7/23/2008	44.374050	-121.997783	3018.0	919.9	1.9	918.0			Present	6.3
624	7/23/2008	44.373833	-121.997600	3018.0	919.9	5.9	914.0			Absent	6.9
625	7/23/2008	44.373717	-121.997517	3018.0	919.9	7.7	912.2			Absent	7.0
626	7/23/2008	44.373717	-121.997417	3018.0	919.9	8.9	911.0			Flow edge	7.0
627	7/23/2008	44.373650	-121.997183	3018.0	919.9	3.3	916.6			Present	7.2
628	7/23/2008	44.373700	-121.996817	3018.0	919.9	0.6	919.3			Absent?	7.3
629	7/23/2008	44.373550	-121.997117	3018.0	919.9	6.8	913.1			Present	7.6
630	7/23/2008	44.373533	-121.997250	3018.0	919.9	11.5	908.4			Present	7.6
631	7/23/2008	44.373433	-121.997483	3018.0	919.9	6.3	913.6			Present	7.6
632	7/23/2008	44.373317	-121.997650	3018.0	919.9	4.8	915.1			Present	7.7
633	7/23/2008	44.373217	-121.997900	3018.0	919.9	1.2	918.7			Barely present	7.8
634	7/23/2008	44.373133	-121.997683	3018.0	919.9	4.3	915.6			Present	8.0
635	7/23/2008	44.373083	-121.997467	3018.0	919.9	5.3	914.6			Present	8.1
636	7/23/2008	44.373083	-121.997233	3018.0	919.9	13.8	906.1			Present	8.1
637	7/23/2008	44.373083	-121.997050	3018.0	919.9	13.0	906.9			Present	8.1
638	7/23/2008	44.373117	-121.996850	3018.0	919.9	8.3	911.6			Present	8.1
639	7/23/2008	44.373200	-121.996617	3018.0	919.9	4.3	915.6			Present	8.1
640	7/23/2008	44.373350	-121.996183	3018.0	919.9	2.6	917.3			Present	8.0
641	7/23/2008	44.373183	-121.996317	3018.0	919.9	3.9	916.0			Present	8.1
642	7/23/2008	44.373083	-121.996483	3018.0	919.9	5.7	914.2			Present	8.1
643	7/23/2008	44.373000	-121.996600	3018.0	919.9	7.9	912.0			Present	8.1
644	7/23/2008	44.372883	-121.996833	3018.0	919.9	19.5	900.4			Present	8.1
645	7/23/2008	44.372800	-121.997017	3018.0	919.9	21.5	898.4			Present	8.1
646	7/23/2008	44.372700	-121.997233	3018.0	919.9	22.4	897.5			Patchy	8.1
647	7/23/2008	44.372583	-121.997467	3018.0	919.9	17.7	902.2			Present	8.1
648	7/23/2008	44.372533	-121.997667	3018.0	919.9	12.7	907.2			Present	8.1
649	7/23/2008	44.372400	-121.997933	3018.0	919.9	7.8	912.1			Absent	8.1
650	7/23/2008	44.372333	-121.998067	3018.0	919.9	4.2	915.7			Absent	8.2
651	7/23/2008	44.372300	-121.997733	3018.0	919.9	13.4	906.5			Absent	8.2
652	7/23/2008	44.372267	-121.997433	3018.0	919.9	22.0	897.9			Absent	8.2
653	7/23/2008	44.372283	-121.997150	3018.0	919.9	24.9	895.0			Present	8.3
654	7/23/2008	44.372317	-121.996867	3018.0	919.9	25.4	894.5			Patchy	8.4
655	7/23/2008	44.372383	-121.996550	3018.0	919.9	25.4	894.5			Patchy	8.3
656	7/23/2008	44.372533	-121.996233	3018.0	919.9	24.3	895.6			Patchy	8.3
657	7/23/2008	44.372633	-121.996000	3018.0	919.9	17.9	902.0			Absent	8.2
658	7/23/2008	44.372683	-121.995667	3018.0	919.9	10.6	909.3			Present	8.1
659	7/23/2008	44.372733	-121.995350	3018.0	919.9	5.1	914.8			Present	8.1
660	7/23/2008	44.372767	-121.995283	3018.0	919.9	3.0	916.9			Present	8.1
661	7/23/2008	44.372600	-121.995483	3018.0	919.9	8.7	911.2			Present	8.3
662	7/23/2008	44.372483	-121.995650	3018.0	919.9	15.6	904.3			Absent	8.2
663	7/23/2008	44.372367	-121.995817	3018.0	919.9	25.4	894.5			Absent	8.2
664	7/23/2008	44.372200	-121.996000	3018.0	919.9	26.2	893.7			Absent	8.2
665	7/23/2008	44.372033	-121.996150	3018.0	919.9	26.2	893.7			Absent	8.1

Note: USGS gage 14158500 is located at the Clear Lake outlet (see Fig. 2b); USGS gage elevation determined by taking averaging gage height over the period out on the lake (maximum range: 0.02 ft) and adding this value to the gage datum (3015.32 ft above sea level). The water temperature is of the top 30 cm of the lake.

TABLE A3. BATHYMETRIC DATA AND OBSERVATIONS FOR CLEAR LAKE

Waypoint	Collection date	Latitude	Longitude	USGS gage elevation (ft)	USGS gage elevation (m)	Depth (m)	Elevation (m)	Tree top depth (m)	Tree height (m)	Whiteline	Water temperature (°C)
666	7/23/2008	44.371850	-121.996283	3018.0	919.9	27.7	892.2			Absent	8.1
667	7/23/2008	44.371717	-121.996483	3018.0	919.9	28.3	891.6			Absent	8.2
668	7/23/2008	44.371583	-121.996750	3018.0	919.9	29.8	890.1			Absent	8.3
669	7/23/2008	44.371467	-121.996967	3018.0	919.9	25.0	894.9			Absent	8.3
670	7/23/2008	44.371367	-121.997183	3018.0	919.9	14.7	905.2			Present (thin)	8.4
671	7/23/2008	44.371233	-121.997450	3018.0	919.9	3.0	916.9			Present (thin)	8.6
672	7/23/2008	44.371200	-121.997283	3018.0	919.9	10.6	909.3			Absent	8.7
673	7/23/2008	44.371183	-121.997083	3018.0	919.9	20.8	899.1			Absent	8.9
674	7/23/2008	44.371200	-121.996867	3018.0	919.9	30.4	889.5			Absent	9.0
675	7/23/2008	44.371217	-121.996700	3018.0	919.9	32.8	887.1			Absent	9.0
676	7/23/2008	44.371217	-121.996333	3018.0	919.9	30.7	889.2			Absent	9.0
677	7/23/2008	44.371250	-121.996000	3018.0	919.9	31.8	888.1			Absent	8.9
678	7/23/2008	44.371350	-121.995633	3018.0	919.9	30.9	889.0			Absent	8.9
679	7/23/2008	44.371367	-121.995300	3018.0	919.9	31.8	888.1			Absent	8.8
680	7/23/2008	44.371433	-121.995000	3018.0	919.9	31.1	888.8			Absent	8.7
681	7/23/2008	44.371517	-121.994667	3018.0	919.9	29.2	890.7			Very patchy	8.7
682	7/23/2008	44.371567	-121.994450	3018.0	919.9	22.9	897.0			Present	8.7
683	7/23/2008	44.371650	-121.994217	3018.0	919.9	13.8	906.1			Patchy	8.7
684	7/23/2008	44.371800	-121.993967	3018.0	919.9	2.0	917.9			Present (thin)	8.7
685	7/23/2008	44.371750	-121.994083	3018.0	919.9	7.2	912.7			Flow edge	8.7
686	7/23/2008	44.371467	-121.994533	3018.0	919.9	29.9	890.0			Absent	8.7
687	7/23/2008	44.371300	-121.994767	3018.0	919.9	31.5	888.4			Absent	8.7
688	7/23/2008	44.371167	-121.994900	3018.0	919.9	33.0	886.9			Absent	8.7
689	7/23/2008	44.371017	-121.995133	3018.0	919.9	32.4	887.5			Absent	8.7
690	7/23/2008	44.370883	-121.995367	3018.0	919.9	33.2	886.7			Absent	8.7
691	7/23/2008	44.370750	-121.995600	3018.0	919.9	33.9	886.0			Absent	8.7
692	7/23/2008	44.370617	-121.995850	3018.0	919.9	33.0	886.9			Absent	8.7
693	7/23/2008	44.370433	-121.996017	3018.0	919.9	33.9	886.0			Absent	8.8
694	7/23/2008	44.370300	-121.996167	3018.0	919.9	36.6	883.3			Absent	8.8
695	7/23/2008	44.370167	-121.996300	3018.0	919.9	34.5	885.4			Patchy	8.8
696	7/23/2008	44.370033	-121.996483	3018.0	919.9	25.1	894.8			Patchy	8.9
697	7/23/2008	44.369900	-121.996650	3018.0	919.9	15.7	904.2			Absent	8.9
698	7/23/2008	44.369650	-121.996967	3018.0	919.9	2.0	917.9			Present	9.1
699	7/23/2008	44.369600	-121.996383	3018.0	919.9	15.7	904.2			Present?	9.5
700	7/23/2008	44.369667	-121.996400	3018.0	919.9	16.2	903.7	1.2	15.0	Absent	9.5
701	7/23/2008	44.369850	-121.996067	3018.0	919.9	36.7	883.2			Absent	9.4
702	7/23/2008	44.369883	-121.995800	3018.0	919.9	37.5	882.4			Absent	9.4
703	7/23/2008	44.369900	-121.995533	3018.0	919.9	39.9	880.0			Absent	9.4
704	7/23/2008	44.369900	-121.995200	3018.0	919.9	40.1	879.8			Very patchy	9.4
705	7/23/2008	44.369900	-121.994933	3018.0	919.9	40.6	879.3			Patchy	9.4
706	7/23/2008	44.369933	-121.994650	3018.0	919.9	38.4	881.5			Patchy	9.3
707	7/23/2008	44.369933	-121.994367	3018.0	919.9	34.1	885.8			Patchy	9.3
708	7/23/2008	44.369950	-121.994050	3018.0	919.9	33.8	886.1			Absent	9.2

Note: USGS gage 14158500 is located at the Clear Lake outlet (see Fig. 2b); USGS gage elevation determined by taking averaging gage height over the period out on the lake (maximum range: 0.02 ft) and adding this value to the gage datum (3015.32 ft above sea level). The water temperature is of the top 30 cm of the lake.

TABLE A3. BATHYMETRIC DATA AND OBSERVATIONS FOR CLEAR LAKE

Waypoint	Collection date	Latitude	Longitude	USGS gage elevation (ft)	USGS gage elevation (m)	Depth (m)	Elevation (m)	Tree top depth (m)	Tree height (m)	Whiteline	Water temperature (°C)
709	7/23/2008	44.369983	-121.993750	3018.0	919.9	25.1	894.8			Patchy	9.2
710	7/23/2008	44.369983	-121.993583	3018.0	919.9	16.6	903.3			Present (definitively lava flow)	9.2
711	7/23/2008	44.370017	-121.993350	3018.0	919.9	7.8	912.1			Present (definitively lava flow)	9.2
712	7/23/2008	44.369900	-121.993583	3018.0	919.9	20.1	899.8			Flow edge	9.2
713	7/23/2008	44.369817	-121.993833	3018.0	919.9	27.5	892.4			Absent	9.2
714	7/23/2008	44.369717	-121.994000	3018.0	919.9	32.9	887.0			Patchy	9.2
715	7/23/2008	44.369600	-121.994300	3018.0	919.9	36.3	883.6			Absent	9.1
716	7/23/2008	44.369450	-121.994600	3018.0	919.9	41.6	878.3			Absent	9.0
717	7/23/2008	44.369317	-121.994833	3018.0	919.9	43.7	876.2			Absent	8.9
718	7/23/2008	44.369233	-121.994983	3018.0	919.9	43.9	876.0			Absent	8.9
719	7/23/2008	44.369117	-121.995167	3018.0	919.9	42.7	877.2			Absent	8.9
720	7/23/2008	44.369033	-121.995333	3018.0	919.9	42.3	877.6			Absent	8.9
721	7/23/2008	44.369417	-121.995683	3018.0	919.9	41.8	878.1			Barely present	9.0
722	7/23/2008	44.369700	-121.995767	3018.0	919.9	41.3	878.6			Barely present	9.0
723	7/23/2008	44.370117	-121.995833	3018.0	919.9	35.7	884.2			Absent	9.0
724	7/23/2008	44.370433	-121.995867	3018.0	919.9	34.1	885.8			Barely present	9.1
725	7/23/2008	44.371150	-121.995900	3018.0	919.9	32.5	887.4			Barely present	8.9
726	7/23/2008	44.371117	-121.995567	3018.0	919.9	32.8	887.1			Barely present	9.0
727	7/23/2008	44.371033	-121.995400	3018.0	919.9	33.1	886.8			Barely present	9.0
728	7/23/2008	44.370883	-121.995000	3018.0	919.9	33.4	886.5			Absent	9.1
729	7/23/2008	44.370817	-121.994783	3018.0	919.9	30.7	889.2			Absent	9.1
730	7/23/2008	44.370817	-121.994567	3018.0	919.9	24.1	895.8			Absent	9.1
731	7/23/2008	44.370850	-121.994150	3018.0	919.9	18.4	901.5			Absent	9.1
732	7/23/2008	44.370883	-121.993900	3018.0	919.9	16.0	903.9			Absent	9.1
734	7/23/2008	44.370800	-121.993767	3018.0	919.9	9.0	910.9			Present (definitively lava flow)	9.2
735	7/23/2008	44.370667	-121.993767	3018.0	919.9	10.6	909.3			Flow edge?	9.4
736	7/23/2008	44.370583	-121.993783	3018.0	919.9	14.7	905.2			Present (definitively lava flow)	9.4
737	7/23/2008	44.370533	-121.993800	3018.0	919.9	19.1	900.8			Absent	9.4
738	7/23/2008	44.370483	-121.993800	3018.0	919.9	18.6	901.3			Present (definitively lava flow)	9.5
739	7/23/2008	44.370467	-121.993717	3018.0	919.9	19.1	900.8			Absent	9.4
740	7/23/2008	44.370333	-121.993583	3018.0	919.9	21.2	898.7			Absent	9.5
741	7/23/2008	44.370267	-121.993517	3018.0	919.9	17.4	902.5			Present (definitively lava flow)	9.5
742	7/23/2008	44.370033	-121.993583	3018.0	919.9	21.2	898.7			Flow edge	9.7
743	7/23/2008	44.369917	-121.993667	3018.0	919.9	21.0	898.9			Flow edge	9.7
744	7/23/2008	44.369767	-121.993467	3018.0	919.9	12.6	907.3			Present (definitively lava flow)	9.7
745	7/23/2008	44.369633	-121.993400	3018.0	919.9	12.6	907.3			Present (definitively lava flow)	9.7
746	7/23/2008	44.369483	-121.993500	3018.0	919.9	23.2	896.7			Flow edge	9.7
747	7/23/2008	44.369367	-121.993683	3018.0	919.9	36.5	883.4			Absent	9.7
748	7/23/2008	44.369267	-121.993917	3018.0	919.9	33.3	886.6			Absent	9.7
749	7/23/2008	44.369200	-121.994133	3018.0	919.9	32.9	887.0			Absent	9.7
750	7/23/2008	44.369133	-121.994317	3018.0	919.9	39.9	880.0			Absent	9.7
751	7/23/2008	44.369050	-121.994500	3018.0	919.9	42.7	877.2			Barely present	9.6
752	7/23/2008	44.368800	-121.995117	3018.0	919.9	44.9	875.0			Barely present	9.4

Note: USGS gage 14158500 is located at the Clear Lake outlet (see Fig. 2b); USGS gage elevation determined by taking averaging gage height over the period out on the lake (maximum range: 0.02 ft) and adding this value to the gage datum (3015.32 ft above sea level). The water temperature is of the top 30 cm of the lake.

TABLE A3. BATHYMETRIC DATA AND OBSERVATIONS FOR CLEAR LAKE

Waypoint	Collection date	Latitude	Longitude	USGS gage elevation (ft)	USGS gage elevation (m)	Depth (m)	Elevation (m)	Tree top depth (m)	Tree height (m)	Whiteline	Water temperature (°C)
753	7/23/2008	44.368717	-121.995267	3018.0	919.9	37.2	882.7			Barely present	9.4
754	7/23/2008	44.368583	-121.995567	3018.0	919.9	25.8	894.1	15.8	10.0	Barely present	9.4
755	7/23/2008	44.368417	-121.995900	3018.0	919.9	12.6	907.3			Present	9.6
756	7/23/2008	44.368283	-121.996200	3018.0	919.9	3.9	916.0			Absent	9.9
757	7/23/2008	44.368183	-121.996033	3018.0	919.9	7.3	912.6			Absent	10.3
758	7/23/2008	44.368133	-121.995883	3018.0	919.9	10.2	909.7			Present	10.4
759	7/23/2008	44.368000	-121.995683	3018.0	919.9	15.4	904.5			Present	10.5
760	7/23/2008	44.367900	-121.995317	3018.0	919.9	29.0	890.9			Present	10.5
761	7/23/2008	44.367867	-121.995083	3018.0	919.9	37.2	882.7	8.2	29.0	Absent	10.5
762	7/23/2008	44.367867	-121.994883	3018.0	919.9	45.6	874.3			Present	10.1
763	7/23/2008	44.367917	-121.994567	3018.0	919.9	47.9	872.0			Present	10.0
764	7/23/2008	44.367933	-121.994233	3018.0	919.9	43.0	876.9			Barely present	9.9
765	7/23/2008	44.367967	-121.993917	3018.0	919.9	42.4	877.5			Present	9.9
766	7/23/2008	44.368033	-121.993583	3018.0	919.9	43.8	876.1			Barely present	9.9
767	7/23/2008	44.368083	-121.993250	3018.0	919.9	43.2	876.7			Barely present	9.9
768	7/23/2008	44.368133	-121.992950	3018.0	919.9	38.1	881.8			Absent	9.7
769	7/23/2008	44.368133	-121.992633	3018.0	919.9	33.8	886.1			Absent	9.6
770	7/23/2008	44.368183	-121.992417	3018.0	919.9	31.1	888.8			Absent	9.5
771	7/23/2008	44.368217	-121.992083	3018.0	919.9	19.8	900.1			Flow edge	9.4
772	7/23/2008	44.368333	-121.991783	3018.0	919.9	10.8	909.1			Present	9.4
773	7/23/2008	44.368217	-121.991900	3018.0	919.9	21.5	898.4			Flow edge	9.5
774	7/23/2008	44.368117	-121.992167	3018.0	919.9	22.5	897.4			Absent	9.4
775	7/23/2008	44.367983	-121.992383	3018.0	919.9	23.0	896.9			Absent	9.3
776	7/23/2008	44.367883	-121.992550	3018.0	919.9	29.2	890.7			Absent	9.2
777	7/23/2008	44.367800	-121.992700	3018.0	919.9	41.0	878.9			Barely present	9.2
778	7/23/2008	44.367717	-121.992933	3018.0	919.9	45.5	874.4			Barely present	9.1
779	7/23/2008	44.367617	-121.993167	3018.0	919.9	46.9	873.0			Barely present	9.0
780	7/23/2008	44.367550	-121.993567	3018.0	919.9	44.2	875.7			Barely present	8.9
781	7/23/2008	44.367500	-121.993850	3018.0	919.9	44.8	875.1			Barely present	8.9
782	7/23/2008	44.367433	-121.994083	3018.0	919.9	46.7	873.2			Barely present	9.0
783	7/23/2008	44.367317	-121.994283	3018.0	919.9	48.5	871.4			Barely present	8.9
784	7/23/2008	44.367233	-121.994450	3018.0	919.9	49.1	870.8			Present	9.0
785	7/23/2008	44.367183	-121.994617	3018.0	919.9	43.4	876.5			Absent	9.0
786	7/23/2008	44.367117	-121.994783	3018.0	919.9	37.1	882.8			Barely present	9.0
787	7/23/2008	44.367017	-121.995017	3018.0	919.9	27.0	892.9			Absent	9.1
788	7/23/2008	44.366933	-121.995317	3018.0	919.9	17.4	902.5			Present	9.2
789	7/23/2008	44.366850	-121.995533	3018.0	919.9	13.1	906.8			Present	9.3
790	7/23/2008	44.366650	-121.995867	3018.0	919.9	4.7	915.2			Absent	9.7
791	7/23/2008	44.366517	-121.995717	3018.0	919.9	10.9	909.0			Present	10.0
792	7/23/2008	44.366383	-121.995267	3018.0	919.9	24.9	895.0			Present	10.2
793	7/23/2008	44.366317	-121.995017	3018.0	919.9	31.6	888.3			Present	10.2
794	7/23/2008	44.366267	-121.994900	3018.0	919.9	40.3	879.6			Present	10.2
795	7/23/2008	44.366133	-121.994583	3018.0	919.9	50.0	869.9			Present	10.1

Note: USGS gage 14158500 is located at the Clear Lake outlet (see Fig. 2b); USGS gage elevation determined by taking averaging gage height over the period out on the lake (maximum range: 0.02 ft) and adding this value to the gage datum (3015.32 ft above sea level). The water temperature is of the top 30 cm of the lake.

TABLE A3. BATHYMETRIC DATA AND OBSERVATIONS FOR CLEAR LAKE

Waypoint	Collection date	Latitude	Longitude	USGS gage elevation (ft)	USGS gage elevation (m)	Depth (m)	Elevation (m)	Tree top depth (m)	Tree height (m)	Whiteline	Water temperature (°C)
796	7/23/2008	44.366083	-121.994317	3018.0	919.9	53.4	866.5			Present	10.0
797	7/23/2008	44.366017	-121.993950	3018.0	919.9	52.4	867.5			Present	9.9
798	7/23/2008	44.365933	-121.993683	3018.0	919.9	53.0	866.9			Present	9.9
799	7/23/2008	44.365900	-121.993400	3018.0	919.9	53.7	866.2			Present	9.8
800	7/23/2008	44.365867	-121.993100	3018.0	919.9	53.7	866.2			Present	9.7
801	7/23/2008	44.365917	-121.992767	3018.0	919.9	53.7	866.2			Present	9.5
802	7/23/2008	44.366067	-121.992333	3018.0	919.9	53.2	866.7			Present	9.4
803	7/23/2008	44.366167	-121.992067	3018.0	919.9	52.4	867.5			Present	9.3
804	7/23/2008	44.366233	-121.991833	3018.0	919.9	44.8	875.1			Present	9.3
805	7/23/2008	44.366267	-121.991550	3018.0	919.9	31.4	888.5			Absent	9.2
806	7/23/2008	44.366283	-121.991317	3018.0	919.9	23.4	896.5			Absent	9.2
807	7/23/2008	44.366283	-121.990800	3018.0	919.9	4.9	915.0			Absent	9.1
808	7/23/2008	44.366200	-121.990833	3018.0	919.9	7.2	912.7			Barely present	9.8
809	7/23/2008	44.366217	-121.991050	3018.0	919.9	16.0	903.9			Absent	9.9
810	7/23/2008	44.366217	-121.991417	3018.0	919.9	34.6	885.3			Absent	9.7
811	7/23/2008	44.366200	-121.991817	3018.0	919.9	51.8	868.1			Present	9.5
812	7/23/2008	44.366100	-121.991650	3018.0	919.9	35.8	884.1			Absent	9.3
813	7/23/2008	44.366017	-121.991400	3018.0	919.9	22.5	897.4			Barely present	9.2
814	7/23/2008	44.365917	-121.991183	3018.0	919.9	12.9	907.0			Absent	9.2
815	7/23/2008	44.365833	-121.990950	3018.0	919.9	9.4	910.5			Present but off flow	9.1
816	7/23/2008	44.365800	-121.990817	3018.0	919.9	6.6	913.3			Present (definitively lava flow)	9.1
817	7/23/2008	44.365683	-121.991000	3018.0	919.9	21.5	898.4			Flow edge	9.1
818	7/23/2008	44.365583	-121.991233	3018.0	919.9	39.1	880.8			Absent	9.1
819	7/23/2008	44.365517	-121.991400	3018.0	919.9	45.3	874.6			Barely present	9.0
820	7/23/2008	44.365333	-121.991683	3018.0	919.9	48.1	871.8			Present	9.0
821	7/23/2008	44.365233	-121.991950	3018.0	919.9	50.0	869.9			Present	9.0
822	7/23/2008	44.365100	-121.991867	3018.0	919.9	48.3	871.6			Present	9.0
823	7/23/2008	44.364983	-121.991667	3018.0	919.9	46.5	873.4			Barely present	9.0
824	7/23/2008	44.364917	-121.991533	3018.0	919.9	46.1	873.8			Present	9.0
825	7/23/2008	44.364717	-121.991200	3018.0	919.9	30.7	889.2			Absent	9.0
826	7/23/2008	44.364633	-121.990867	3018.0	919.9	26.0	893.9			Absent	9.0
827	7/23/2008	44.364550	-121.990550	3018.0	919.9	16.0	903.9	7.0	9.0	Absent	8.9
828	7/23/2008	44.364367	-121.990217	3018.0	919.9	6.3	913.6			Barely present (flow?)	9.0
829	7/23/2008	44.364400	-121.990483	3018.0	919.9	13.3	906.6			Absent	9.3
830	7/23/2008	44.364217	-121.990650	3018.0	919.9	13.9	906.0			Present (definitively lava flow)	9.3
831	7/23/2008	44.364033	-121.990833	3018.0	919.9	14.7	905.2			Present; lava flow	9.2
832	7/23/2008	44.363917	-121.990900	3018.0	919.9	12.5	907.4			Present; lava flow	9.2
833	7/23/2008	44.363817	-121.991050	3018.0	919.9	12.9	907.0			Present; lava flow	9.3
834	7/23/2008	44.363617	-121.991183	3018.0	919.9	12.9	907.0			Present; lava flow	9.2
835	7/23/2008	44.363433	-121.991117	3018.0	919.9	12.5	907.4			Present; lava flow	9.2
836	7/23/2008	44.363200	-121.991017	3018.0	919.9	11.1	908.8			Present; lava flow	9.2
837	7/23/2008	44.363017	-121.990933	3018.0	919.9	9.0	910.9			Present; lava flow	9.2
838	7/23/2008	44.362767	-121.990717	3018.0	919.9	6.8	913.1			Present; lava flow	9.2

Note: USGS gage 14158500 is located at the Clear Lake outlet (see Fig. 2b); USGS gage elevation determined by taking averaging gage height over the period out on the lake (maximum range: 0.02 ft) and adding this value to the gage datum (3015.32 ft above sea level). The water temperature is of the top 30 cm of the lake.

TABLE A3. BATHYMETRIC DATA AND OBSERVATIONS FOR CLEAR LAKE

Waypoint	Collection date	Latitude	Longitude	USGS gage elevation (ft)	USGS gage elevation (m)	Depth (m)	Elevation (m)	Tree top depth (m)	Tree height (m)	Whiteline	Water temperature (°C)
839	7/23/2008	44.362750	-121.990500	3018.0	919.9	6.7	913.2			Present; lava flow	9.2
840	7/23/2008	44.362717	-121.990233	3018.0	919.9	6.3	913.6			Present; lava flow	9.2
841	7/23/2008	44.362683	-121.990000	3018.0	919.9	5.5	914.4			Barely present	9.2
842	7/23/2008	44.362650	-121.989667	3018.0	919.9	1.9	918.0			Absent	9.6
843	7/23/2008	44.362550	-121.989783	3018.0	919.9	1.7	918.2			Absent	10.2
844	7/23/2008	44.362467	-121.989983	3018.0	919.9	3.6	916.3			Absent	10.4
845	7/23/2008	44.362333	-121.990233	3018.0	919.9	3.6	916.3			Absent	10.4
846	7/23/2008	44.362200	-121.990483	3018.0	919.9	3.1	916.8			Absent	10.2
847	7/23/2008	44.361917	-121.990767	3018.0	919.9	3.5	916.4			Absent	10.1
848	7/23/2008	44.361783	-121.990783	3018.0	919.9	5.6	914.3			Absent	10.3
849	7/23/2008	44.361617	-121.990733	3018.0	919.9	4.4	915.5			Absent	10.6
850	7/23/2008	44.361383	-121.990650	3018.0	919.9	1.8	918.1			Absent	10.8
851	7/23/2008	44.361450	-121.990850	3018.0	919.9	5.4	914.5			Absent	10.9
852	7/23/2008	44.361567	-121.991150	3018.0	919.9	8.7	911.2			Absent	11.1
853	7/23/2008	44.361583	-121.991383	3018.0	919.9	5.9	914.0			Absent	11.4
854	7/23/2008	44.361783	-121.991417	3018.0	919.9	11.7	908.2			Absent	11.5
855	7/23/2008	44.361917	-121.991433	3018.0	919.9	8.9	911.0			Absent	11.5
856	7/23/2008	44.362133	-121.991533	3018.0	919.9	8.4	911.5			Absent	11.4
857	7/23/2008	44.362367	-121.991733	3018.0	919.9	9.1	910.8			Absent	11.0
859	7/23/2008	44.362517	-121.991867	3018.0	919.9	11.2	908.7			Barely present	10.7
860	7/23/2008	44.362867	-121.992167	3018.0	919.9	13.4	906.5			Present	10.2
861	7/23/2008	44.363100	-121.992350	3018.0	919.9	14.3	905.6			Present	10.0
862	7/23/2008	44.363367	-121.992533	3018.0	919.9	15.5	904.4			Barely present	9.8
863	7/23/2008	44.363583	-121.992617	3018.0	919.9	17.5	902.4			Barely present	9.7
864	7/23/2008	44.363767	-121.992667	3018.0	919.9	20.5	899.4			Barely present	9.6
865	7/23/2008	44.364033	-121.992783	3018.0	919.9	22.0	897.9			Absent	9.5
866	7/23/2008	44.364217	-121.992883	3018.0	919.9	30.6	889.3			Absent	9.5
867	7/23/2008	44.364367	-121.992967	3018.0	919.9	39.7	880.2			Absent	9.4
868	7/23/2008	44.364533	-121.993100	3018.0	919.9	50.0	869.9			Present	9.4
869	7/23/2008	44.364333	-121.993250	3018.0	919.9	40.3	879.6			Absent	9.4
870	7/23/2008	44.364167	-121.993317	3018.0	919.9	41.2	878.7			Absent	9.4
871	7/23/2008	44.364017	-121.993333	3018.0	919.9	37.5	882.4			Absent	9.4
872	7/23/2008	44.363850	-121.993400	3018.0	919.9	35.7	884.2			Absent	9.4
873	7/23/2008	44.363650	-121.993467	3018.0	919.9	32.9	887.0			Absent	9.5
874	7/23/2008	44.363417	-121.993567	3018.0	919.9	34.5	885.4			Absent	9.4
875	7/23/2008	44.363217	-121.993617	3018.0	919.9	25.9	894.0			Absent	9.3
876	7/23/2008	44.362983	-121.993633	3018.0	919.9	21.8	898.1			Absent	9.3
877	7/23/2008	44.362783	-121.993633	3018.0	919.9	20.9	899.0			Absent	9.3
878	7/23/2008	44.362550	-121.993650	3018.0	919.9	21.8	898.1			Absent	9.3
879	7/23/2008	44.362317	-121.993783	3018.0	919.9	15.6	904.3			Absent	9.4
881	7/23/2008	44.362017	-121.993933	3018.0	919.9	7.4	912.5			Absent	9.6
882	7/23/2008	44.361933	-121.994083	3018.0	919.9	4.4	915.5			Absent	9.7
883	7/23/2008	44.361850	-121.994333	3018.0	919.9	1.1	918.8			Absent	9.8

Note: USGS gage 14158500 is located at the Clear Lake outlet (see Fig. 2b); USGS gage elevation determined by taking averaging gage height over the period out on the lake (maximum range: 0.02 ft) and adding this value to the gage datum (3015.32 ft above sea level). The water temperature is of the top 30 cm of the lake.

TABLE A3. BATHYMETRIC DATA AND OBSERVATIONS FOR CLEAR LAKE

Waypoint	Collection date	Latitude	Longitude	USGS gage elevation (ft)	USGS gage elevation (m)	Depth (m)	Elevation (m)	Tree top depth (m)	Tree height (m)	Whiteline	Water temperature (°C)
884	7/23/2008	44.361967	-121.994417	3018.0	919.9	8.3	911.6			Absent	9.8
885	7/23/2008	44.362117	-121.994517	3018.0	919.9	9.1	910.8			Absent	9.7
886	7/23/2008	44.362317	-121.994683	3018.0	919.9	5.9	914.0			Absent	9.8
887	7/23/2008	44.362550	-121.994617	3018.0	919.9	8.5	911.4			Absent	9.8
888	7/23/2008	44.362700	-121.994500	3018.0	919.9	14.0	905.9			Absent	9.8
889	7/23/2008	44.362900	-121.994450	3018.0	919.9	17.8	902.1			Absent	9.8
890	7/23/2008	44.363150	-121.994433	3018.0	919.9	22.4	897.5			Absent	9.8
891	7/23/2008	44.363417	-121.994433	3018.0	919.9	23.9	896.0			Absent	9.8
892	7/23/2008	44.363600	-121.994450	3018.0	919.9	27.4	892.5			Absent	9.8
893	7/23/2008	44.363733	-121.994433	3018.0	919.9	28.8	891.1			Absent	9.8
894	7/23/2008	44.364217	-121.994483	3018.0	919.9	33.4	886.5			Absent	9.8
895	7/23/2008	44.364583	-121.994583	3018.0	919.9	34.5	885.4			Absent	9.8
896	7/23/2008	44.364800	-121.994717	3018.0	919.9	30.4	889.5			Absent	9.8
899	7/23/2008	44.365267	-121.994567	3018.0	919.9	41.5	878.4			Absent	9.9
900	7/23/2008	44.365250	-121.994583	3018.0	919.9	41.5	878.4	9.5	32.0	Absent	9.9
901	7/23/2008	44.365167	-121.994317	3018.0	919.9	50.0	869.9			Absent	9.9
902	7/23/2008	44.365367	-121.994300	3018.0	919.9	49.1	870.8			Absent	9.9
903	7/23/2008	44.365650	-121.994450	3018.0	919.9	52.0	867.9			Absent	9.9
904	7/23/2008	44.365767	-121.994317	3018.0	919.9	53.9	866.0			Absent	9.9
905	7/23/2008	44.366067	-121.994183	3018.0	919.9	52.8	867.1			Absent	10.0
906	7/23/2008	44.366350	-121.994217	3018.0	919.9	52.2	867.7			Absent	10.0
907	7/23/2008	44.366650	-121.994117	3018.0	919.9	51.6	868.3			Absent	9.9
908	7/23/2008	44.366933	-121.994217	3018.0	919.9	49.8	870.1			Absent	9.7
909	7/23/2008	44.367133	-121.994167	3018.0	919.9	48.7	871.2			Absent	9.6
910	7/23/2008	44.367250	-121.994233	3018.0	919.9	47.1	872.8			Absent	9.6
911	7/23/2008	44.367450	-121.994167	3018.0	919.9	48.9	871.0			Absent	9.6
912	7/23/2008	44.367683	-121.994200	3018.0	919.9	47.9	872.0			Absent	9.5
913	7/23/2008	44.367883	-121.994283	3018.0	919.9	45.1	874.8			Absent	9.5
914	7/23/2008	44.368050	-121.994550	3018.0	919.9	48.3	871.6			Absent	9.5
915	7/23/2008	44.367867	-121.994700	3018.0	919.9	44.2	875.7			Absent	9.6
916	7/23/2008	44.367833	-121.994633	3018.0	919.9	48.7	871.2			Absent	9.7
917	7/23/2008	44.368017	-121.994767	3018.0	919.9	48.7	871.2			Absent	9.5
918	7/23/2008	44.368283	-121.994617	3018.0	919.9	48.3	871.6			Absent	9.4
919	7/23/2008	44.368400	-121.994650	3018.0	919.9	46.3	873.6			Absent	9.4
920	7/23/2008	44.368517	-121.994700	3018.0	919.9	47.1	872.8			Absent	9.4
921	7/23/2008	44.368683	-121.994833	3018.0	919.9	45.1	874.8			Absent	9.4
922	7/23/2008	44.368817	-121.994883	3018.0	919.9	44.2	875.7			Absent	9.3
923	7/23/2008	44.368950	-121.995050	3018.0	919.9	43.2	876.7			Absent	9.3
924	7/23/2008	44.369017	-121.995400	3018.0	919.9	38.5	881.4			Absent	9.3
926	7/23/2008	44.368967	-121.995650	3018.0	919.9	29.5	890.4			Absent	9.3
927	7/23/2008	44.368850	-121.995917	3018.0	919.9	17.8	902.1			Absent	9.2
928	7/23/2008	44.368717	-121.996117	3018.0	919.9	10.6	909.3			Absent	9.3
929	7/23/2008	44.368583	-121.995950	3018.0	919.9	12.5	907.4			Absent	9.7

Note: USGS gage 14158500 is located at the Clear Lake outlet (see Fig. 2b); USGS gage elevation determined by taking averaging gage height over the period out on the lake (maximum range: 0.02 ft) and adding this value to the gage datum (3015.32 ft above sea level). The water temperature is of the top 30 cm of the lake.

TABLE A3. BATHYMETRIC DATA AND OBSERVATIONS FOR CLEAR LAKE

Waypoint	Collection date	Latitude	Longitude	USGS gage elevation (ft)	USGS gage elevation (m)	Depth (m)	Elevation (m)	Tree top depth (m)	Tree height (m)	Whiteline	Water temperature (°C)
930	7/23/2008	44.368667	-121.996050	3018.0	919.9	10.9	909.0			Absent	9.7
931	7/23/2008	44.368833	-121.996117	3018.0	919.9	11.5	908.4			Absent	9.8
932	7/23/2008	44.368983	-121.995917	3018.0	919.9	18.4	901.5			Absent	9.6
933	7/23/2008	44.369217	-121.995900	3018.0	919.9	28.2	891.7			Absent	9.4
934	7/23/2008	44.369317	-121.995767	3018.0	919.9	34.1	885.8			Absent	9.4
935	7/23/2008	44.369433	-121.995733	3018.0	919.9	39.2	880.7			Absent	9.3
936	7/23/2008	44.369633	-121.995667	3018.0	919.9	41.3	878.6			Absent	9.2
937	7/23/2008	44.369783	-121.995767	3018.0	919.9	39.7	880.2			Absent	9.3
938	7/23/2008	44.369933	-121.995933	3018.0	919.9	38.1	881.8			Absent	9.3
939	7/23/2008	44.370083	-121.995967	3018.0	919.9	36.2	883.7			Absent	9.3
940	7/23/2008	44.370200	-121.995950	3018.0	919.9	35.0	884.9			Absent	9.3
941	7/23/2008	44.370317	-121.995950	3018.0	919.9	34.4	885.5			Absent	9.4
942	7/23/2008	44.370433	-121.996183	3018.0	919.9	35.6	884.3			Absent	9.3
943	7/23/2008	44.370517	-121.996367	3018.0	919.9	35.8	884.1			Absent	9.4
944	7/23/2008	44.370683	-121.996483	3018.0	919.9	34.6	885.3			Absent	9.3
945	7/23/2008	44.370733	-121.996633	3018.0	919.9	30.9	889.0			Absent	9.3
946	7/23/2008	44.370800	-121.996833	3018.0	919.9	23.8	896.1			Absent	9.3
947	7/23/2008	44.370883	-121.996867	3018.0	919.9	22.1	897.8			Absent	9.2
948	7/23/2008	44.371017	-121.996867	3018.0	919.9	25.6	894.3			Absent	9.2
949	7/23/2008	44.371100	-121.996817	3018.0	919.9	28.3	891.6			Absent	9.2
950	7/23/2008	44.371200	-121.996800	3018.0	919.9	29.5	890.4			Absent	9.2
951	7/23/2008	44.371383	-121.996850	3018.0	919.9	29.0	890.9			Absent	9.2
952	7/23/2008	44.371600	-121.996883	3018.0	919.9	27.5	892.4			Absent	9.2
953	7/23/2008	44.371833	-121.996750	3018.0	919.9	28.3	891.6			Absent	9.2
954	7/23/2008	44.372033	-121.996850	3018.0	919.9	27.3	892.6			Absent	9.2
955	7/23/2008	44.372150	-121.996867	3018.0	919.9	25.4	894.5			Absent	9.2
956	7/23/2008	44.372250	-121.996933	3018.0	919.9	26.3	893.6			Absent	9.2
957	7/23/2008	44.372400	-121.996967	3018.0	919.9	24.9	895.0			Absent	9.2
958	7/23/2008	44.372650	-121.997000	3018.0	919.9	22.5	897.4			Absent	9.2
959	7/23/2008	44.372833	-121.996983	3018.0	919.9	19.8	900.1			Absent	9.2
960	7/23/2008	44.372933	-121.996983	3018.0	919.9	17.7	902.2			Absent	9.2
961	7/23/2008	44.372933	-121.996983	3018.0	919.9	17.9	902.0			Absent	9.2
962	7/23/2008	44.373267	-121.997083	3018.0	919.9	10.3	909.6			Absent	8.9
963	7/23/2008	44.373400	-121.997133	3018.0	919.9	10.3	909.6			Absent	8.8
964	7/23/2008	44.373517	-121.997183	3018.0	919.9	11.2	908.7			Absent	8.7
965	7/23/2008	44.374050	-121.997517	3018.0	919.9	7.8	912.1			Barely present	7.7
966	7/23/2008	44.374283	-121.997550	3018.0	919.9	7.5	912.4			Barely present	7.3
967	7/23/2008	44.374450	-121.997567	3018.0	919.9	7.8	912.1			Barely present	7.0
977	9/23/2008	44.377267	-122.003333	3017.3	919.7	1.4	918.3			Present	4.4
978	9/23/2008	44.377183	-122.003300	3017.3	919.7	2.5	917.2			Present	4.3
979	9/23/2008	44.377117	-122.003333	3017.3	919.7	5.3	914.4			Present	4.3
980	9/23/2008	44.377000	-122.003433	3017.3	919.7	1.2	918.5			Present	4.3
981	9/23/2008	44.377050	-122.003283	3017.3	919.7	7.0	912.7			Present	4.4

Note: USGS gage 14158500 is located at the Clear Lake outlet (see Fig. 2b); USGS gage elevation determined by taking averaging gage height over the period out on the lake (maximum range: 0.02 ft) and adding this value to the gage datum (3015.32 ft above sea level). The water temperature is of the top 30 cm of the lake.

TABLE A3. BATHYMETRIC DATA AND OBSERVATIONS FOR CLEAR LAKE

Waypoint	Collection date	Latitude	Longitude	USGS gage elevation (ft)	USGS gage elevation (m)	Depth (m)	Elevation (m)	Tree top depth (m)	Tree height (m)	Whiteline	Water temperature (°C)
982	9/23/2008	44.377067	-122.003117	3017.3	919.7	2.1	917.6			Present	4.4
983	9/23/2008	44.376933	-122.003117	3017.3	919.7	5.6	914.1			Present	4.4
984	9/23/2008	44.376900	-122.003183	3017.3	919.7	8.3	911.4			Present	4.4
985	9/23/2008	44.376833	-122.003333	3017.3	919.7	1.3	918.4			Present	4.4
986	9/23/2008	44.376800	-122.003217	3017.3	919.7	5.7	914.0	3.7	2.0	Present	4.4
987	9/23/2008	44.376933	-122.002950	3017.3	919.7	1.8	917.9			Present	4.5
988	9/23/2008	44.376717	-122.002933	3017.3	919.7	9.6	910.1	7.6	2.0	Present	4.7
989	9/23/2008	44.376717	-122.003067	3017.3	919.7	8.7	911.0	3.7	5.0	Present	4.9
990	9/23/2008	44.376733	-122.003100	3017.3	919.7	8.8	910.9			Present	5.1
991	9/23/2008	44.376617	-122.003233	3017.3	919.7	2.3	917.4			Present	5.1
992	9/23/2008	44.376667	-122.002967	3017.3	919.7	10.6	909.1			Present	5.1
993	9/23/2008	44.376783	-122.002767	3017.3	919.7	1.8	917.9			Present	5.4
994	9/23/2008	44.376600	-122.002883	3017.3	919.7	12.7	907.0			Present	5.4
995	9/23/2008	44.376383	-122.003167	3017.3	919.7	1.3	918.4			Present	5.4
996	9/23/2008	44.376367	-122.002883	3017.3	919.7	9.2	910.5	7.2	2.0	Present	5.4
997	9/23/2008	44.376467	-122.002750	3017.3	919.7	13.7	906.0			Present	5.3
998	9/23/2008	44.376683	-122.002483	3017.3	919.7	2.7	917.0			Present	5.4
999	9/23/2008	44.376467	-122.002583	3017.3	919.7	15.5	904.2			Present	5.7
1000	9/23/2008	44.376317	-122.002683	3017.3	919.7	12.2	907.5			Present	5.7
1001	9/23/2008	44.376267	-122.002700	3017.3	919.7	8.5	911.2			Present	5.6
1002	9/23/2008	44.376133	-122.002817	3017.3	919.7	1.9	917.8			Present	5.2
1003	9/23/2008	44.376117	-122.002600	3017.3	919.7	4.0	915.7			Present	5.0
1004	9/23/2008	44.376350	-122.002183	3017.3	919.7	13.4	906.3			Present	5.0
1005	9/23/2008	44.376467	-122.002033	3017.3	919.7	15.8	903.9			Present	5.1
1006	9/23/2008	44.376667	-122.001667	3017.3	919.7	6.5	913.2			Present	5.3
1007	9/23/2008	44.376883	-122.001350	3017.3	919.7	4.6	915.1			Present	5.5
1008	9/23/2008	44.377100	-122.001067	3017.3	919.7	2.3	917.4			Present	5.6
1009	9/23/2008	44.376733	-122.001183	3017.3	919.7	14.5	905.2			Present	5.7
1010	9/23/2008	44.376133	-122.001417	3017.3	919.7	12.5	907.2			Present	5.7
1011	9/23/2008	44.376083	-122.001433	3017.3	919.7	10.4	909.3			Present	5.7
1012	9/23/2008	44.375800	-122.001533	3017.3	919.7	2.8	916.9			Present	5.2
1013	9/23/2008	44.375933	-122.001283	3017.3	919.7	7.8	911.9			Present	4.9
1014	9/23/2008	44.376133	-122.001100	3017.3	919.7	13.3	906.4			Present	4.8
1015	9/23/2008	44.376233	-122.001017	3017.3	919.7	13.5	906.2			Present	4.9
1016	9/23/2008	44.376483	-122.000783	3017.3	919.7	11.0	908.7			Present	5.1
1017	9/23/2008	44.376683	-122.000550	3017.3	919.7	9.5	910.2			Present	5.3
1018	9/23/2008	44.376867	-122.000367	3017.3	919.7	10.2	909.5			Present	5.3
1019	9/23/2008	44.377117	-122.000167	3017.3	919.7	13.4	906.3			Present	5.3
1020	9/23/2008	44.377317	-122.000350	3017.3	919.7	11.7	908.0			Present	5.2
1021	9/23/2008	44.377433	-122.000617	3017.3	919.7	8.1	911.6			Present	5.1
1022	9/23/2008	44.377617	-122.000700	3017.3	919.7	4.9	914.8			Present	5.3
1023	9/23/2008	44.377667	-122.000517	3017.3	919.7	7.2	912.5			Present	5.7
1024	9/23/2008	44.377633	-122.000333	3017.3	919.7	9.2	910.5			Present	5.8

Note: USGS gage 14158500 is located at the Clear Lake outlet (see Fig. 2b); USGS gage elevation determined by taking averaging gage height over the period out on the lake (maximum range: 0.02 ft) and adding this value to the gage datum (3015.32 ft above sea level). The water temperature is of the top 30 cm of the lake.

TABLE A3. BATHYMETRIC DATA AND OBSERVATIONS FOR CLEAR LAKE

Waypoint	Collection date	Latitude	Longitude	USGS gage elevation (ft)	USGS gage elevation (m)	Depth (m)	Elevation (m)	Tree top depth (m)	Tree height (m)	Whiteline	Water temperature (°C)
1025	9/23/2008	44.377733	-122.000100	3017.3	919.7	9.6	910.1			Present	5.7
1026	9/23/2008	44.377917	-121.999817	3017.3	919.7	8.8	910.9			Present	5.7
1027	9/23/2008	44.378067	-121.999683	3017.3	919.7	8.4	911.3			Present	5.6
1028	9/23/2008	44.378183	-121.999667	3017.3	919.7	1.9	917.8			Absent	5.4
1029	9/23/2008	44.378000	-121.999483	3017.3	919.7	9.7	910.0			Present	4.1
1030	9/23/2008	44.377817	-121.999433	3017.3	919.7	4.5	915.2			Present	4.9
1031	9/23/2008	44.377750	-121.999400	3017.3	919.7	2.3	917.4			Present	4.8
1032	9/23/2008	44.377567	-121.999517	3017.3	919.7	10.9	908.8			Present	4.7
1033	9/23/2008	44.377417	-121.999633	3017.3	919.7	14.3	905.4			Present	4.6
1034	9/23/2008	44.377233	-121.999733	3017.3	919.7	16.7	903.0			Present	4.5
1035	9/23/2008	44.377067	-121.999817	3017.3	919.7	18.5	901.2			Present	4.6
1036	9/23/2008	44.376883	-121.999883	3017.3	919.7	16.6	903.1			Present	4.8
1037	9/23/2008	44.376667	-121.999950	3017.3	919.7	15.1	904.6			Present	4.9
1038	9/23/2008	44.376500	-122.000017	3017.3	919.7	12.8	906.9			Present	5.1
1039	9/23/2008	44.376267	-122.000117	3017.3	919.7	11.9	907.8			Present	5.3
1040	9/23/2008	44.376083	-122.000183	3017.3	919.7	11.2	908.5			Present	5.4
1041	9/23/2008	44.375950	-122.000217	3017.3	919.7	10.6	909.1			Present	5.5
1042	9/23/2008	44.375783	-122.000150	3017.3	919.7	4.0	915.7			Present	5.2
1043	9/23/2008	44.375883	-121.999883	3017.3	919.7	9.0	910.7			Present	4.9
1044	9/23/2008	44.375983	-121.999633	3017.3	919.7	9.4	910.3			Present	5.0
1045	9/23/2008	44.376150	-121.999317	3017.3	919.7	9.9	909.8			Present	5.3
1046	9/23/2008	44.376233	-121.999133	3017.3	919.7	11.0	908.7			Present	5.4
1047	9/23/2008	44.376333	-121.998933	3017.3	919.7	12.6	907.1			Present	5.2
1048	9/23/2008	44.376367	-121.998733	3017.3	919.7	14.1	905.6			Present	4.9
1049	9/23/2008	44.376450	-121.998533	3017.3	919.7	14.7	905.0			Flow edge	4.6
1050	9/23/2008	44.376633	-121.998400	3017.3	919.7	8.9	910.8			Present (definitively lava flow)	4.0
1051	9/23/2008	44.376550	-121.998333	3017.3	919.7	4.9	914.8			Present	3.8
1052	9/23/2008	44.376500	-121.998350	3017.3	919.7	9.8	909.9			Present	3.8
1053	9/23/2008	44.376450	-121.998367	3017.3	919.7	14.5	905.2			Present	3.7
1054	9/23/2008	44.376317	-121.998467	3017.3	919.7	13.0	906.7			Present	3.6
1055	9/23/2008	44.376150	-121.998617	3017.3	919.7	14.2	905.5			Present	3.6
1056	9/23/2008	44.376067	-121.998717	3017.3	919.7	11.0	908.7			Present	3.5
1057	9/23/2008	44.375967	-121.998883	3017.3	919.7	9.8	909.9			Present	3.5
1058	9/23/2008	44.375833	-121.999017	3017.3	919.7	5.7	914.0			Present	3.5
1059	9/23/2008	44.375683	-121.998633	3017.3	919.7	9.4	910.3			Present	4.0
1060	9/23/2008	44.375567	-121.998517	3017.3	919.7	7.3	912.4			Present	4.1
1061	9/23/2008	44.375467	-121.998367	3017.3	919.7	6.2	913.5			Absent	4.3
1062	9/23/2008	44.375367	-121.998167	3017.3	919.7	5.5	914.2			Absent	4.4
1063	9/23/2008	44.375267	-121.998067	3017.3	919.7	4.5	915.2			Absent	4.4
1064	9/23/2008	44.374833	-121.998017	3017.3	919.7	2.4	917.3			Absent	4.8
1065	9/23/2008	44.374750	-121.997700	3017.3	919.7	6.3	913.4			Absent	4.9
1066	9/23/2008	44.374483	-121.997567	3017.3	919.7	7.8	911.9			Absent	5.0
1067	9/23/2008	44.374350	-121.997400	3017.3	919.7	5.5	914.2			Present	5.0

Note: USGS gage 14158500 is located at the Clear Lake outlet (see Fig. 2b); USGS gage elevation determined by taking averaging gage height over the period out on the lake (maximum range: 0.02 ft) and adding this value to the gage datum (3015.32 ft above sea level). The water temperature is of the top 30 cm of the lake.

TABLE A3. BATHYMETRIC DATA AND OBSERVATIONS FOR CLEAR LAKE

Waypoint	Collection date	Latitude	Longitude	USGS gage elevation (ft)	USGS gage elevation (m)	Depth (m)	Elevation (m)	Tree top depth (m)	Tree height (m)	Whiteline	Water temperature (°C)
1068	9/23/2008	44.374233	-121.997400	3017.3	919.7	9.1	910.6			Present	5.0
1069	9/23/2008	44.374050	-121.997450	3017.3	919.7	9.1	910.6			Present	5.0
1070	9/23/2008	44.373883	-121.997467	3017.3	919.7	7.8	911.9			Barely present	4.9
1071	9/23/2008	44.373733	-121.997433	3017.3	919.7	8.7	911.0			Absent	5.2
1072	9/23/2008	44.373633	-121.997283	3017.3	919.7	8.5	911.2			Present	6.1
1073	9/23/2008	44.373600	-121.997150	3017.3	919.7	5.1	914.6			Present	6.5
1074	9/23/2008	44.373567	-121.996967	3017.3	919.7	4.3	915.4			Barely present	6.8
1075	9/23/2008	44.373467	-121.996817	3017.3	919.7	3.5	916.2			Barely present	7.1
1076	9/23/2008	44.373433	-121.996667	3017.3	919.7	2.3	917.4			Barely present	7.4
1077	9/23/2008	44.373350	-121.996550	3017.3	919.7	3.0	916.7			Barely present	7.5
1078	9/23/2008	44.373250	-121.996333	3017.3	919.7	3.7	916.0			Barely present	7.6
1079	9/23/2008	44.373167	-121.996250	3017.3	919.7	3.1	916.6			Barely present	7.7
1080	9/23/2008	44.373050	-121.996083	3017.3	919.7	3.8	915.9			Barely present	7.8
1081	9/23/2008	44.372983	-121.995917	3017.3	919.7	5.2	914.5			Present	7.9
1082	9/23/2008	44.372883	-121.995750	3017.3	919.7	7.2	912.5			Barely present	8.0
1083	9/23/2008	44.372783	-121.995583	3017.3	919.7	8.4	911.3			Present	7.9
1084	9/23/2008	44.372550	-121.995750	3017.3	919.7	13.9	905.8			Flow edge	7.6
1085	9/23/2008	44.372400	-121.995867	3017.3	919.7	25.0	894.7			Present	7.2
1086	9/23/2008	44.372350	-121.995567	3017.3	919.7	17.7	902.0			Present	7.0
1087	9/23/2008	44.372300	-121.995317	3017.3	919.7	16.9	902.8			Present	6.9
1088	9/23/2008	44.372233	-121.995117	3017.3	919.7	19.5	900.2			Present	6.9
1089	9/23/2008	44.372217	-121.994967	3017.3	919.7	17.5	902.2			Flow edge	6.9
1090	9/23/2008	44.372183	-121.994700	3017.3	919.7	11.6	908.1			Present	6.9
1091	9/23/2008	44.372117	-121.994533	3017.3	919.7	11.1	908.6			Present	6.9
1092	9/23/2008	44.372050	-121.994333	3017.3	919.7	5.9	913.8			Present	7.0
1093	9/23/2008	44.372067	-121.994117	3017.3	919.7	3.1	916.6			Barely present	6.9
1094	9/23/2008	44.372100	-121.993867	3017.3	919.7	0.5	919.2			Absent	6.8
1095	9/23/2008	44.371983	-121.993883	3017.3	919.7	1.4	918.3			Barely present	6.7
1096	9/23/2008	44.371983	-121.994050	3017.3	919.7	2.7	917.0			Present	6.7
1097	9/23/2008	44.372017	-121.994483	3017.3	919.7	10.0	909.7			Present	6.5
1098	9/23/2008	44.372017	-121.994650	3017.3	919.7	14.3	905.4			Barely present	6.6
1099	9/23/2008	44.372000	-121.994817	3017.3	919.7	18.4	901.3			Absent	6.7
1100	9/23/2008	44.372117	-121.995117	3017.3	919.7	20.4	899.3			Barely present	6.9
1101	9/23/2008	44.372467	-121.995817	3017.3	919.7	18.9	900.8			Barely present	6.7
1102	9/23/2008	44.372550	-121.995933	3017.3	919.7	18.8	900.9			Flow edge	6.6
1103	9/23/2008	44.372733	-121.996200	3017.3	919.7	18.1	901.6			Absent	6.5
1104	9/23/2008	44.372817	-121.996417	3017.3	919.7	15.1	904.6			Present	6.4
1105	9/23/2008	44.372900	-121.996633	3017.3	919.7	11.6	908.1			Present	6.4
1106	9/23/2008	44.373050	-121.996983	3017.3	919.7	14.2	905.5			Present	6.6
1107	9/23/2008	44.373250	-121.997417	3017.3	919.7	6.6	913.1			Present	6.8
1108	9/23/2008	44.373317	-121.997600	3017.3	919.7	4.7	915.0			Present	6.9
1109	9/23/2008	44.372833	-121.997933	3017.3	919.7	6.8	912.9			Present	7.4
1110	9/23/2008	44.372567	-121.998017	3017.3	919.7	6.8	912.9			Present	7.4

Note: USGS gage 14158500 is located at the Clear Lake outlet (see Fig. 2b); USGS gage elevation determined by taking averaging gage height over the period out on the lake (maximum range: 0.02 ft) and adding this value to the gage datum (3015.32 ft above sea level). The water temperature is of the top 30 cm of the lake.

TABLE A3. BATHYMETRIC DATA AND OBSERVATIONS FOR CLEAR LAKE

Waypoint	Collection date	Latitude	Longitude	USGS gage elevation (ft)	USGS gage elevation (m)	Depth (m)	Elevation (m)	Tree top depth (m)	Tree height (m)	Whiteline	Water temperature (°C)
1111	9/23/2008	44.372283	-121.997917	3017.3	919.7	7.6	912.1			Absent	7.4
1112	9/23/2008	44.372083	-121.997833	3017.3	919.7	6.1	913.6			Absent	7.3
1113	9/23/2008	44.371933	-121.997750	3017.3	919.7	4.6	915.1			Absent	7.1
1114	9/23/2008	44.371800	-121.997650	3017.3	919.7	2.8	916.9			Present	7.0
1115	9/23/2008	44.371700	-121.997517	3017.3	919.7	4.5	915.2			Present	6.8
1116	9/23/2008	44.371617	-121.997367	3017.3	919.7	7.3	912.4			Present	6.5
1117	9/23/2008	44.371617	-121.996917	3017.3	919.7	26.8	892.9			Barely present	6.3
1118	9/23/2008	44.371617	-121.996650	3017.3	919.7	27.8	891.9			Absent	6.3
1119	9/23/2008	44.371617	-121.996467	3017.3	919.7	28.4	891.3			Barely present	6.3
1120	9/23/2008	44.371617	-121.996200	3017.3	919.7	28.4	891.3			Barely present	6.3
1121	9/23/2008	44.371633	-121.995950	3017.3	919.7	30.2	889.5			Absent	6.4
1122	9/23/2008	44.371633	-121.995750	3017.3	919.7	29.5	890.2			Barely present	6.3
1123	9/23/2008	44.371667	-121.995467	3017.3	919.7	30.0	889.7			Barely present	6.3
1124	9/23/2008	44.371700	-121.995250	3017.3	919.7	29.2	890.5			Barely present	6.3
1125	9/23/2008	44.371767	-121.994900	3017.3	919.7	27.4	892.3			Absent	6.4
1126	9/23/2008	44.371817	-121.994767	3017.3	919.7	24.0	895.7			Absent	6.5
1127	9/23/2008	44.371867	-121.994667	3017.3	919.7	20.2	899.5			Flow edge	6.5
1128	9/23/2008	44.371950	-121.994533	3017.3	919.7	12.2	907.5			Present	6.6
1129	9/23/2008	44.371833	-121.994483	3017.3	919.7	14.5	905.2			Present	6.7
1130	9/23/2008	44.371767	-121.994450	3017.3	919.7	18.0	901.7			Flow edge	6.7
1131	9/23/2008	44.371700	-121.994317	3017.3	919.7	16.1	903.6			Barely present	6.8
1132	9/23/2008	44.371583	-121.994250	3017.3	919.7	15.0	904.7			Absent	6.8
1133	9/23/2008	44.371500	-121.994217	3017.3	919.7	15.0	904.7			Absent	6.9
1134	9/23/2008	44.371467	-121.994183	3017.3	919.7	14.5	905.2			Present	6.9
1135	9/23/2008	44.371367	-121.994133	3017.3	919.7	11.3	908.4			Present (definitively lava flow)	7.0
1136	9/23/2008	44.371233	-121.994100	3017.3	919.7	16.2	903.5			Present (definitively lava flow)	7.0
1137	9/23/2008	44.371117	-121.994050	3017.3	919.7	18.3	901.4			Flow edge	7.1
1138	9/23/2008	44.371283	-121.994250	3017.3	919.7	19.0	900.7			Present	7.2
1139	9/23/2008	44.371333	-121.994417	3017.3	919.7	23.5	896.2			Present	7.2
1140	9/23/2008	44.371417	-121.994667	3017.3	919.7	30.7	889.0			Barely present	7.1
1141	9/23/2008	44.371333	-121.994717	3017.3	919.7	30.7	889.0			Absent	6.9
1142	9/23/2008	44.371200	-121.994583	3017.3	919.7	29.6	890.1			Absent	6.9
1143	9/23/2008	44.371083	-121.994483	3017.3	919.7	29.5	890.2			Absent	6.8
1144	9/23/2008	44.370933	-121.994350	3017.3	919.7	23.3	896.4			Absent	6.8
1145	9/23/2008	44.370917	-121.994183	3017.3	919.7	19.9	899.8			Absent	6.7
1146	9/23/2008	44.370933	-121.994067	3017.3	919.7	21.3	898.4			Absent	6.7
1147	9/23/2008	44.370917	-121.993883	3017.3	919.7	18.3	901.4			Absent	6.8
1148	9/23/2008	44.370933	-121.993700	3017.3	919.7	10.9	908.8			Present (definitively lava flow)	6.9
1149	9/23/2008	44.371050	-121.993517	3017.3	919.7	3.6	916.1			Barely present	7.0
1150	9/23/2008	44.371133	-121.993650	3017.3	919.7	7.3	912.4			Flow edge	7.1
1151	9/23/2008	44.371183	-121.993717	3017.3	919.7	6.6	913.1			Flow edge	6.9
1152	9/23/2008	44.370833	-121.993733	3017.3	919.7	9.3	910.4			Present (definitively lava flow)	7.0
1153	9/23/2008	44.370717	-121.993683	3017.3	919.7	3.1	916.6			Present	7.1

Note: USGS gage 14158500 is located at the Clear Lake outlet (see Fig. 2b); USGS gage elevation determined by taking averaging gage height over the period out on the lake (maximum range: 0.02 ft) and adding this value to the gage datum (3015.32 ft above sea level). The water temperature is of the top 30 cm of the lake.

TABLE A3. BATHYMETRIC DATA AND OBSERVATIONS FOR CLEAR LAKE

Waypoint	Collection date	Latitude	Longitude	USGS gage elevation (ft)	USGS gage elevation (m)	Depth (m)	Elevation (m)	Tree top depth (m)	Tree height (m)	Whiteline	Water temperature (°C)
1154	9/23/2008	44.370583	-121.993600	3017.3	919.7	5.7	914.0			Present (definitively lava flow)	7.2
1155	9/23/2008	44.370483	-121.993567	3017.3	919.7	10.2	909.5			Present (definitively lava flow)	7.3
1156	9/23/2008	44.370333	-121.993567	3017.3	919.7	17.5	902.2			Present (definitively lava flow)	7.3
1157	9/23/2008	44.370217	-121.993583	3017.3	919.7	21.7	898.0			Absent	7.4
1158	9/23/2008	44.370117	-121.993583	3017.3	919.7	22.2	897.5			Absent	7.4
1159	9/23/2008	44.369983	-121.993583	3017.3	919.7	18.9	900.8			Present (definitively lava flow)	7.5
1160	9/23/2008	44.369850	-121.993600	3017.3	919.7	18.9	900.8			Present (definitively lava flow)	7.5
1161	9/23/2008	44.369717	-121.993567	3017.3	919.7	18.0	901.7			Flow edge	7.6
1162	9/23/2008	44.369567	-121.993567	3017.3	919.7	19.7	900.0			Absent	7.6
1163	9/23/2008	44.369467	-121.993533	3017.3	919.7	24.7	895.0			Absent	7.5
1164	9/23/2008	44.369467	-121.993500	3017.3	919.7	22.4	897.3			Flow edge	7.5
1165	9/23/2008	44.369367	-121.993317	3017.3	919.7	14.3	905.4			Present (definitively lava flow)	7.3
1166	9/23/2008	44.369467	-121.993400	3017.3	919.7	14.1	905.6			Present (definitively lava flow)	7.1
1167	9/23/2008	44.369450	-121.993383	3017.3	919.7	15.6	904.1			Present (definitively lava flow)	7.1
1168	9/23/2008	44.369283	-121.993133	3017.3	919.7	11.9	907.8			Present (definitively lava flow)	7.0
1169	9/23/2008	44.369100	-121.993467	3017.3	919.7	30.7	889.0			Flow edge	7.0
1170	9/23/2008	44.368950	-121.993800	3017.3	919.7	40.8	878.9			Absent	6.9
1171	9/23/2008	44.368733	-121.993933	3017.3	919.7	42.7	877.0			Barely present	6.3
1172	9/23/2008	44.368800	-121.993700	3017.3	919.7	42.8	876.9			Barely present	6.3
1173	9/23/2008	44.368883	-121.993500	3017.3	919.7	41.5	878.2			Barely present	6.3
1174	9/23/2008	44.368983	-121.993350	3017.3	919.7	39.8	879.9			Barely present	6.3
1175	9/23/2008	44.369033	-121.993250	3017.3	919.7	31.4	888.3			Barely present	6.3
1176	9/23/2008	44.369117	-121.993150	3017.3	919.7	24.0	895.7			Present	6.3
1177	9/23/2008	44.369150	-121.993100	3017.3	919.7	18.4	901.3			Present (definitively lava flow)	6.2
1178	9/23/2008	44.369133	-121.992900	3017.3	919.7	11.9	907.8			Present (definitively lava flow)	6.4
1179	9/23/2008	44.369100	-121.992750	3017.3	919.7	11.5	908.2			Present (definitively lava flow)	6.5
1180	9/23/2008	44.369050	-121.992567	3017.3	919.7	12.4	907.3			Present (definitively lava flow)	6.5
1181	9/23/2008	44.369000	-121.992283	3017.3	919.7	14.1	905.6			Present (definitively lava flow)	6.5
1182	9/23/2008	44.368950	-121.992000	3017.3	919.7	13.7	906.0			Present	6.6
1183	9/23/2008	44.368867	-121.992117	3017.3	919.7	19.1	900.6			Barely present	6.6
1184	9/23/2008	44.368833	-121.992250	3017.3	919.7	24.0	895.7			Barely present	6.6
1185	9/23/2008	44.368800	-121.992417	3017.3	919.7	26.6	893.1			Absent	6.6
1186	9/23/2008	44.368750	-121.992583	3017.3	919.7	29.4	890.3			Absent	6.6
1187	9/23/2008	44.368683	-121.992767	3017.3	919.7	31.5	888.2			Absent	6.6
1188	9/23/2008	44.368617	-121.992917	3017.3	919.7	37.0	882.7			Absent	6.5
1189	9/23/2008	44.368567	-121.993050	3017.3	919.7	39.8	879.9			Absent	6.5
1190	9/23/2008	44.368517	-121.993217	3017.3	919.7	42.5	877.2			Absent	6.4
1191	9/23/2008	44.368400	-121.993350	3017.3	919.7	44.4	875.3			Barely present	6.3
1192	9/23/2008	44.368267	-121.993333	3017.3	919.7	43.9	875.8			Barely present	6.3
1193	9/23/2008	44.368117	-121.993333	3017.3	919.7	43.5	876.2			Barely present	6.3
1194	9/23/2008	44.367967	-121.993317	3017.3	919.7	43.5	876.2			Barely present	6.3
1195	9/23/2008	44.367850	-121.993317	3017.3	919.7	43.7	876.0			Barely present	6.2
1196	9/23/2008	44.367700	-121.993333	3017.3	919.7	45.2	874.5			Barely present	6.2

Note: USGS gage 14158500 is located at the Clear Lake outlet (see Fig. 2b); USGS gage elevation determined by taking averaging gage height over the period out on the lake (maximum range: 0.02 ft) and adding this value to the gage datum (3015.32 ft above sea level). The water temperature is of the top 30 cm of the lake.

TABLE A3. BATHYMETRIC DATA AND OBSERVATIONS FOR CLEAR LAKE

Waypoint	Collection date	Latitude	Longitude	USGS gage elevation (ft)	USGS gage elevation (m)	Depth (m)	Elevation (m)	Tree top depth (m)	Tree height (m)	Whiteline	Water temperature (°C)
1197	9/23/2008	44.367500	-121.993333	3017.3	919.7	46.7	873.0			Barely present	6.2
1198	9/23/2008	44.367417	-121.993217	3017.3	919.7	47.7	872.0			Barely present	6.2
1199	9/23/2008	44.367400	-121.993033	3017.3	919.7	47.9	871.8			Barely present	6.2
1200	9/23/2008	44.367417	-121.992767	3017.3	919.7	46.7	873.0			Barely present	6.2
1201	9/23/2008	44.367433	-121.992550	3017.3	919.7	45.5	874.2			Absent	6.2
1202	9/23/2008	44.367400	-121.992350	3017.3	919.7	42.2	877.5			Barely present	6.2
1203	9/23/2008	44.367383	-121.992217	3017.3	919.7	43.2	876.5			Barely present	6.2
1204	9/23/2008	44.367367	-121.992000	3017.3	919.7	35.0	884.7			Barely present	6.2
1205	9/23/2008	44.367367	-121.991867	3017.3	919.7	31.4	888.3			Barely present	6.2
1206	9/23/2008	44.367350	-121.991767	3017.3	919.7	27.1	892.6			Flow edge	6.2
1207	9/23/2008	44.367400	-121.991533	3017.3	919.7	14.7	905.0			Present (definitively lava flow)	6.3
1208	9/23/2008	44.367383	-121.991417	3017.3	919.7	10.0	909.7			Present (definitively lava flow)	6.3
1209	9/23/2008	44.367300	-121.991167	3017.3	919.7	2.7	917.0			Present (definitively lava flow)	6.7
1210	9/23/2008	44.367100	-121.991067	3017.3	919.7	7.0	912.7			Present	7.0
1211	9/23/2008	44.366950	-121.991050	3017.3	919.7	8.6	911.1			Absent	7.0
1212	9/23/2008	44.366800	-121.990983	3017.3	919.7	6.0	913.7			Barely present	6.9
1213	9/23/2008	44.366633	-121.990983	3017.3	919.7	4.9	914.8			Absent	6.9
1214	9/23/2008	44.366617	-121.991233	3017.3	919.7	14.3	905.4			Present	7.0
1215	9/23/2008	44.366600	-121.991550	3017.3	919.7	28.1	891.6			Barely present	6.9
1216	9/23/2008	44.366583	-121.991783	3017.3	919.7	37.5	882.2			Absent	6.8
1217	9/23/2008	44.366583	-121.992100	3017.3	919.7	51.6	868.1			Present	6.7
1218	9/23/2008	44.366550	-121.992317	3017.3	919.7	51.6	868.1			Present	6.7
1219	9/23/2008	44.366500	-121.992500	3017.3	919.7	51.6	868.1			Present	6.6
1220	9/23/2008	44.366467	-121.992667	3017.3	919.7	53.0	866.7			Present	6.6
1221	9/23/2008	44.366417	-121.992867	3017.3	919.7	53.2	866.5			Present	6.6
1222	9/23/2008	44.366333	-121.993117	3017.3	919.7	52.4	867.3			Present	6.5
1223	9/23/2008	44.366067	-121.993100	3017.3	919.7	53.2	866.5			Present	6.5
1224	9/23/2008	44.365833	-121.993083	3017.3	919.7	53.7	866.0			Present	6.4
1225	9/23/2008	44.365467	-121.993133	3017.3	919.7	53.9	865.8			Present	6.4
1226	9/23/2008	44.365283	-121.993183	3017.3	919.7	54.1	865.6			Present	6.4
1227	9/23/2008	44.365067	-121.993233	3017.3	919.7	53.0	866.7			Present	6.4
1228	9/23/2008	44.364900	-121.993300	3017.3	919.7	53.2	866.5			Present	6.4
1229	9/23/2008	44.364700	-121.993300	3017.3	919.7	53.7	866.0			Present	6.4
1230	9/23/2008	44.364533	-121.993350	3017.3	919.7	54.1	865.6			Present	6.4
1231	9/23/2008	44.364433	-121.993400	3017.3	919.7	51.1	868.6			Present	6.4
1232	9/23/2008	44.364283	-121.993500	3017.3	919.7	45.7	874.0			Present	6.4
1233	9/23/2008	44.364150	-121.993650	3017.3	919.7	47.9	871.8			Present	6.4
1234	9/23/2008	44.364000	-121.993767	3017.3	919.7	49.1	870.6			Present	6.5
1235	9/23/2008	44.363883	-121.993900	3017.3	919.7	51.4	868.3			Present	6.5
1236	9/23/2008	44.363800	-121.994000	3017.3	919.7	48.5	871.2			Present	6.5
1237	9/23/2008	44.363617	-121.994100	3017.3	919.7	43.2	876.5			Present	6.5
1238	9/23/2008	44.363483	-121.994167	3017.3	919.7	38.9	880.8			Present	6.5
1239	9/23/2008	44.363350	-121.994283	3017.3	919.7	30.3	889.4			Present	6.5

Note: USGS gage 14158500 is located at the Clear Lake outlet (see Fig. 2b); USGS gage elevation determined by taking averaging gage height over the period out on the lake (maximum range: 0.02 ft) and adding this value to the gage datum (3015.32 ft above sea level). The water temperature is of the top 30 cm of the lake.

TABLE A3. BATHYMETRIC DATA AND OBSERVATIONS FOR CLEAR LAKE

Waypoint	Collection date	Latitude	Longitude	USGS gage elevation (ft)	USGS gage elevation (m)	Depth (m)	Elevation (m)	Tree top depth (m)	Tree height (m)	Whiteline	Water temperature (°C)
1240	9/23/2008	44.363117	-121.994417	3017.3	919.7	24.4	895.3			Present	6.5
1241	9/23/2008	44.362883	-121.994550	3017.3	919.7	16.0	903.7			Barely present	6.6
1242	9/23/2008	44.362600	-121.994633	3017.3	919.7	9.8	909.9			Present	6.9
1243	9/23/2008	44.362350	-121.994700	3017.3	919.7	7.1	912.6			Present	7.1
1244	9/23/2008	44.362100	-121.994700	3017.3	919.7	4.6	915.1			Barely present	7.2
1245	9/23/2008	44.361917	-121.994567	3017.3	919.7	4.5	915.2			Present	7.2
1246	9/23/2008	44.361733	-121.994333	3017.3	919.7	2.1	917.6			Present	7.0
1247	9/23/2008	44.361917	-121.994117	3017.3	919.7	5.4	914.3			Present	6.7
1248	9/23/2008	44.361883	-121.993867	3017.3	919.7	2.0	917.7			Present	6.7
1249	9/23/2008	44.361867	-121.993567	3017.3	919.7	4.8	914.9			Barely present	6.6
1250	9/23/2008	44.361867	-121.993300	3017.3	919.7	5.3	914.4			Absent	6.7
1251	9/23/2008	44.361850	-121.993033	3017.3	919.7	4.2	915.5			Present	6.8
1252	9/23/2008	44.361850	-121.992783	3017.3	919.7	6.7	913.0			Present	6.9
1253	9/23/2008	44.361833	-121.992550	3017.3	919.7	9.9	909.8				6.9
1254	9/23/2008	44.361833	-121.992250	3017.3	919.7	10.0	909.7			Present	7.0
1255	9/23/2008	44.361833	-121.991967	3017.3	919.7	6.3	913.4			Barely present	7.0
1256	9/23/2008	44.361850	-121.991600	3017.3	919.7	10.5	909.2				7.0
1257	9/23/2008	44.361917	-121.991417	3017.3	919.7	8.6	911.1				7.0
1258	9/23/2008	44.362050	-121.991167	3017.3	919.7	6.0	913.7			Present	7.0
1259	9/23/2008	44.362183	-121.990883	3017.3	919.7	5.9	913.8			Present	7.0
1260	9/23/2008	44.362350	-121.990517	3017.3	919.7	5.1	914.6			Present	7.1
1261	9/23/2008	44.362517	-121.990283	3017.3	919.7	5.6	914.1			Present	7.2
1262	9/23/2008	44.362683	-121.990117	3017.3	919.7	5.8	913.9			Present	7.3
1263	9/23/2008	44.363017	-121.989883	3017.3	919.7	5.7	914.0			Present	7.3
1264	9/23/2008	44.363167	-121.990033	3017.3	919.7	6.4	913.3			Present	7.4
1265	9/23/2008	44.363150	-121.990267	3017.3	919.7	7.2	912.5			Present	7.4
1266	9/23/2008	44.363150	-121.990550	3017.3	919.7	7.6	912.1			Present	7.3
1267	9/23/2008	44.363167	-121.990800	3017.3	919.7	9.2	910.5			Present	7.6
1268	9/23/2008	44.363183	-121.991083	3017.3	919.7	12.4	907.3			Present	7.5
1269	9/23/2008	44.363183	-121.991433	3017.3	919.7	11.1	908.6			Present	7.4
1270	9/23/2008	44.363217	-121.991700	3017.3	919.7	11.1	908.6			Present	7.3
1271	9/23/2008	44.363233	-121.992050	3017.3	919.7	12.5	907.2			Present	7.2
1272	9/23/2008	44.363250	-121.992300	3017.3	919.7	13.3	906.4			Present	7.1
1273	9/23/2008	44.363300	-121.992533	3017.3	919.7	14.7	905.0			Present	7.1
1274	9/23/2008	44.363367	-121.992783	3017.3	919.7	15.7	904.0			Present	7.0
1275	9/23/2008	44.363417	-121.993017	3017.3	919.7	18.9	900.8			Present	7.0
1276	9/23/2008	44.363467	-121.993233	3017.3	919.7	19.9	899.8			Present	6.9
1277	9/23/2008	44.363517	-121.993417	3017.3	919.7	24.1	895.6			Present	6.9
1278	9/23/2008	44.363550	-121.993617	3017.3	919.7	31.1	888.6			Present	6.8
1279	9/23/2008	44.363617	-121.993900	3017.3	919.7	44.5	875.2			Present	6.7
1280	9/23/2008	44.363617	-121.994433	3017.3	919.7	30.9	888.8			Present	6.7
1281	9/23/2008	44.363633	-121.994717	3017.3	919.7	20.5	899.2			Absent	6.7
1282	9/23/2008	44.363650	-121.994983	3017.3	919.7	9.3	910.4			Absent	6.7

Note: USGS gage 14158500 is located at the Clear Lake outlet (see Fig. 2b); USGS gage elevation determined by taking averaging gage height over the period out on the lake (maximum range: 0.02 ft) and adding this value to the gage datum (3015.32 ft above sea level). The water temperature is of the top 30 cm of the lake.

TABLE A3. BATHYMETRIC DATA AND OBSERVATIONS FOR CLEAR LAKE

Waypoint	Collection date	Latitude	Longitude	USGS gage elevation (ft)	USGS gage elevation (m)	Depth (m)	Elevation (m)	Tree top depth (m)	Tree height (m)	Whiteline	Water temperature (°C)
1283	9/23/2008	44.363700	-121.995067	3017.3	919.7	5.1	914.6			Barely present	7.0
1284	9/23/2008	44.363733	-121.994717	3017.3	919.7	17.9	901.8			Present	7.1
1285	9/23/2008	44.363767	-121.994317	3017.3	919.7	32.1	887.6			Present	7.0
1286	9/23/2008	44.363850	-121.993783	3017.3	919.7	50.2	869.5			Present	6.9
1287	9/23/2008	44.363900	-121.993533	3017.3	919.7	45.5	874.2			Present	6.8
1288	9/23/2008	44.363933	-121.993283	3017.3	919.7	35.8	883.9			Present	6.7
1289	9/23/2008	44.363983	-121.993017	3017.3	919.7	35.0	884.7			Present	6.7
1290	9/23/2008	44.364033	-121.992800	3017.3	919.7	22.7	897.0			Present	6.7
1291	9/23/2008	44.364067	-121.992567	3017.3	919.7	18.8	900.9			Present	6.7
1292	9/23/2008	44.364150	-121.992317	3017.3	919.7	18.1	901.6			Present	6.6
1293	9/23/2008	44.364217	-121.992050	3017.3	919.7	17.7	902.0			Present	6.5
1294	9/23/2008	44.364250	-121.991783	3017.3	919.7	20.1	899.6			Present	6.5
1295	9/23/2008	44.364300	-121.991567	3017.3	919.7	23.5	896.2			Present	6.6
1296	9/23/2008	44.364350	-121.991350	3017.3	919.7	21.5	898.2			Present	6.6
1297	9/23/2008	44.364383	-121.991100	3017.3	919.7	18.6	901.1			Barely present	6.5
1298	9/23/2008	44.364417	-121.990833	3017.3	919.7	20.0	899.7			Present	6.5
1299	9/23/2008	44.364417	-121.990600	3017.3	919.7	17.7	902.0			Barely present	6.5
1300	9/23/2008	44.364400	-121.990433	3017.3	919.7	14.3	905.4			Barely present	6.6
1301	9/23/2008	44.364367	-121.990167	3017.3	919.7	3.8	915.9			Barely present	6.8
1302	9/23/2008	44.364567	-121.990350	3017.3	919.7	8.4	911.3			Present	7.2
1303	9/23/2008	44.364600	-121.990650	3017.3	919.7	18.7	901.0			Barely present	7.3
1304	9/23/2008	44.364617	-121.990933	3017.3	919.7	25.9	893.8			Barely present	7.3
1305	9/23/2008	44.364667	-121.991183	3017.3	919.7	26.5	893.2			Present	7.2
1306	9/23/2008	44.364700	-121.991417	3017.3	919.7	30.4	889.3			Barely present	7.2
1307	9/23/2008	44.364750	-121.991700	3017.3	919.7	39.3	880.4			Present	7.1
1308	9/23/2008	44.364800	-121.991967	3017.3	919.7	43.2	876.5			Barely present	7.0
1309	9/23/2008	44.364800	-121.992183	3017.3	919.7	40.3	879.4			Present	6.9
1310	9/23/2008	44.364850	-121.992417	3017.3	919.7	41.6	878.1			Present	6.9
1311	9/23/2008	44.364900	-121.992633	3017.3	919.7	46.7	873.0			Present	6.8
1312	9/23/2008	44.364933	-121.992817	3017.3	919.7	48.9	870.8			Present	6.8
1313	9/23/2008	44.364967	-121.993050	3017.3	919.7	50.0	869.7			Present	6.7
1314	9/23/2008	44.364967	-121.993417	3017.3	919.7	53.4	866.3			Present	6.7
1315	9/23/2008	44.364983	-121.993633	3017.3	919.7	53.9	865.8			Present	6.6
1316	9/23/2008	44.365017	-121.993800	3017.3	919.7	54.1	865.6			Present	6.6
1317	9/23/2008	44.365050	-121.994067	3017.3	919.7	54.0	865.7			Present	6.6
1318	9/23/2008	44.365100	-121.994533	3017.3	919.7	44.8	874.9			Present	6.6
1319	9/23/2008	44.365133	-121.994783	3017.3	919.7	36.5	883.2			Present	6.6
1320	9/23/2008	44.365150	-121.995067	3017.3	919.7	26.1	893.6			Present	6.7
1321	9/23/2008	44.365217	-121.995450	3017.3	919.7	14.3	905.4			Present	6.9
1322	9/23/2008	44.365400	-121.995800	3017.3	919.7	4.0	915.7			Absent	7.1
1323	9/23/2008	44.365433	-121.995483	3017.3	919.7	13.3	906.4			Present	7.0
1324	9/23/2008	44.365467	-121.995233	3017.3	919.7	19.6	900.1			Present	7.0
1325	9/23/2008	44.365483	-121.994967	3017.3	919.7	28.2	891.5			Present	7.2

Note: USGS gage 14158500 is located at the Clear Lake outlet (see Fig. 2b); USGS gage elevation determined by taking averaging gage height over the period out on the lake (maximum range: 0.02 ft) and adding this value to the gage datum (3015.32 ft above sea level). The water temperature is of the top 30 cm of the lake.

TABLE A3. BATHYMETRIC DATA AND OBSERVATIONS FOR CLEAR LAKE

Waypoint	Collection date	Latitude	Longitude	USGS gage elevation (ft)	USGS gage elevation (m)	Depth (m)	Elevation (m)	Tree top depth (m)	Tree height (m)	Whiteline	Water temperature (°C)
1326	9/23/2008	44.365517	-121.994717	3017.3	919.7	34.7	885.0			Present	7.3
1327	9/23/2008	44.365567	-121.994333	3017.3	919.7	46.3	873.4			Present	7.3
1328	9/23/2008	44.365617	-121.994017	3017.3	919.7	53.9	865.8			Present	7.2
1329	9/23/2008	44.365650	-121.993717	3017.3	919.7	53.7	866.0			Present	7.1
1330	9/23/2008	44.365667	-121.993500	3017.3	919.7	53.4	866.3			Present	7.0
1331	9/23/2008	44.365733	-121.993250	3017.3	919.7	53.7	866.0			Present	7.0
1332	9/23/2008	44.365750	-121.993067	3017.3	919.7	53.7	866.0			Present	6.9
1333	9/23/2008	44.365850	-121.992850	3017.3	919.7	53.8	865.9			Present	6.9
1334	9/23/2008	44.365933	-121.992633	3017.3	919.7	53.8	865.9			Present	6.8
1335	9/23/2008	44.366017	-121.992433	3017.3	919.7	53.7	866.0			Present	6.7
1336	9/23/2008	44.366067	-121.992183	3017.3	919.7	53.2	866.5			Present	6.7
1337	9/23/2008	44.366117	-121.991900	3017.3	919.7	52.2	867.5			Present	6.6
1338	9/23/2008	44.366183	-121.991683	3017.3	919.7	48.5	871.2			Present	6.6
1339	9/23/2008	44.366233	-121.991567	3017.3	919.7	38.3	881.4			Present	6.6
1340	9/23/2008	44.366183	-121.991617	3017.3	919.7	44.8	874.9			Present	6.5
1341	9/23/2008	44.366150	-121.991617	3017.3	919.7	35.2	884.5			Present	6.5
1342	9/23/2008	44.366150	-121.991617	3017.3	919.7	43.6	876.1			Present	6.5
1343	9/23/2008	44.366167	-121.991450	3017.3	919.7	34.8	884.9			Present	6.4
1344	9/23/2008	44.366383	-121.991517	3017.3	919.7	31.1	888.6			Present	6.5
1345	9/23/2008	44.366317	-121.991567	3017.3	919.7	37.9	881.8			Present	6.5
1346	9/23/2008	44.366200	-121.991333	3017.3	919.7	23.8	895.9			Present	6.4
1347	9/23/2008	44.366350	-121.991133	3017.3	919.7	19.7	900.0			Barely present	6.5
1348	9/23/2008	44.366317	-121.990917	3017.3	919.7	7.4	912.3			Barely present	6.5
1349	9/23/2008	44.366650	-121.990750	3017.3	919.7	2.3	917.4			Absent	6.9
1350	9/23/2008	44.366900	-121.990800	3017.3	919.7	2.6	917.1			Present	7.3
1351	9/23/2008	44.367117	-121.991233	3017.3	919.7	14.9	904.8			Present	7.5
1352	9/23/2008	44.367150	-121.991383	3017.3	919.7	20.8	898.9			Absent	7.4
1353	9/23/2008	44.367150	-121.991617	3017.3	919.7	29.9	889.8			Absent	7.3
1354	9/23/2008	44.367150	-121.991850	3017.3	919.7	37.4	882.3			Absent	7.3
1355	9/23/2008	44.367150	-121.992050	3017.3	919.7	44.2	875.5			Barely present	7.2
1356	9/23/2008	44.367150	-121.992267	3017.3	919.7	47.7	872.0			Present	7.1
1357	9/23/2008	44.367150	-121.992500	3017.3	919.7	48.9	870.8			Present	7.0
1358	9/23/2008	44.367167	-121.992683	3017.3	919.7	48.9	870.8			Present	7.0
1359	9/23/2008	44.367167	-121.993017	3017.3	919.7	49.8	869.9			Present	6.9
1360	9/23/2008	44.367183	-121.993283	3017.3	919.7	49.6	870.1			Present	6.9
1361	9/23/2008	44.367183	-121.993483	3017.3	919.7	49.8	869.9			Present	6.9
1362	9/23/2008	44.367150	-121.993717	3017.3	919.7	50.0	869.7			Present	6.8
1363	9/23/2008	44.367150	-121.993983	3017.3	919.7	47.7	872.0			Present	6.8
1364	9/23/2008	44.367167	-121.994250	3017.3	919.7	47.9	871.8			Present	6.8
1365	9/23/2008	44.367133	-121.994483	3017.3	919.7	49.6	870.1			Present	6.9
1366	9/23/2008	44.367083	-121.994667	3017.3	919.7	50.0	869.7			Present	7.0
1367	9/23/2008	44.367017	-121.994867	3017.3	919.7	42.0	877.7			Present	7.1
1368	9/23/2008	44.366983	-121.995083	3017.3	919.7	31.6	888.1			Present	7.2

Note: USGS gage 14158500 is located at the Clear Lake outlet (see Fig. 2b); USGS gage elevation determined by taking averaging gage height over the period out on the lake (maximum range: 0.02 ft) and adding this value to the gage datum (3015.32 ft above sea level). The water temperature is of the top 30 cm of the lake.

TABLE A3. BATHYMETRIC DATA AND OBSERVATIONS FOR CLEAR LAKE

Waypoint	Collection date	Latitude	Longitude	USGS gage elevation (ft)	USGS gage elevation (m)	Depth (m)	Elevation (m)	Tree top depth (m)	Tree height (m)	Whiteline	Water temperature (°C)
1369	9/23/2008	44.366917	-121.995300	3017.3	919.7	21.7	898.0			Present	7.3
1370	9/23/2008	44.366883	-121.995633	3017.3	919.7	11.8	907.9			Present	7.4
1371	9/23/2008	44.366883	-121.995883	3017.3	919.7	5.6	914.1			Barely present	7.4
1372	9/23/2008	44.367083	-121.995900	3017.3	919.7	5.2	914.5			Barely present	7.1
1373	9/23/2008	44.367317	-121.995750	3017.3	919.7	9.7	910.0			Present	7.0
1374	9/23/2008	44.367533	-121.995600	3017.3	919.7	14.3	905.4			Present	6.9
1375	9/23/2008	44.367750	-121.995450	3017.3	919.7	21.0	898.7			Present	6.9
1376	9/23/2008	44.367950	-121.995267	3017.3	919.7	28.7	891.0			Present	7.0
1377	9/23/2008	44.368133	-121.995133	3017.3	919.7	34.8	884.9			Present	7.1
1378	9/23/2008	44.368300	-121.995083	3017.3	919.7	41.1	878.6			Present	7.2
1379	9/23/2008	44.368517	-121.995017	3017.3	919.7	47.1	872.6			Present	7.3
1380	9/23/2008	44.368767	-121.995000	3017.3	919.7	45.5	874.2			Present	7.4
1381	9/23/2008	44.369033	-121.994983	3017.3	919.7	43.8	875.9			Present	7.4
1382	9/23/2008	44.369283	-121.995017	3017.3	919.7	44.0	875.7			Present	7.5
1383	9/23/2008	44.369533	-121.995067	3017.3	919.7	42.2	877.5			Present	7.5
1384	9/23/2008	44.369800	-121.995100	3017.3	919.7	40.1	879.6			Present	7.6
1385	9/23/2008	44.370050	-121.995133	3017.3	919.7	40.3	879.4			Present	7.6
1386	9/23/2008	44.370267	-121.995200	3017.3	919.7	38.5	881.2			Present	7.6
1387	9/23/2008	44.370533	-121.995267	3017.3	919.7	36.9	882.8			Present	7.6
1388	9/23/2008	44.370767	-121.995350	3017.3	919.7	34.5	885.2			Present	7.6
1389	9/23/2008	44.370983	-121.995417	3017.3	919.7	33.7	886.0			Present	7.6
1390	9/23/2008	44.371250	-121.995600	3017.3	919.7	32.1	887.6			Present	7.7
1391	9/23/2008	44.371517	-121.995750	3017.3	919.7	30.9	888.8			Present	7.7
1392	9/23/2008	44.371833	-121.995917	3017.3	919.7	30.0	889.7			Present	7.7
1393	9/23/2008	44.372000	-121.996067	3017.3	919.7	28.5	891.2			Present	7.7
1394	9/23/2008	44.372183	-121.996217	3017.3	919.7	25.7	894.0			Present	7.7
1395	9/23/2008	44.372417	-121.996300	3017.3	919.7	25.4	894.3			Present	7.7
1396	9/23/2008	44.372600	-121.996417	3017.3	919.7	24.7	895.0			Present	7.7
1397	9/23/2008	44.372783	-121.996550	3017.3	919.7	19.7	900.0			Present	7.6
1398	9/23/2008	44.373050	-121.996717	3017.3	919.7	7.8	911.9			Present	7.6
1399	9/23/2008	44.373250	-121.996850	3017.3	919.7	5.0	914.7			Present	7.6
1400	9/23/2008	44.373383	-121.997017	3017.3	919.7	6.6	913.1			Present	7.6
1401	9/23/2008	44.373533	-121.997150	3017.3	919.7	8.0	911.7			Present	7.6
1402	9/23/2008	44.374633	-121.997717	3017.3	919.7	5.7	914.0			Present	7.9
1403	6/23/2009	44.373317	-121.996917	3017.8	919.8	5.1	914.7				10.4
1406	6/23/2009	44.373317	-121.996617	3017.8	919.8	3.4	916.4	1.3	2.1		9.7
1407	6/23/2009	44.372733	-121.995333	3017.8	919.8	6.7	913.1				8.7
1408	6/23/2009	44.372700	-121.995017	3017.8	919.8	7.3	912.5				8.6
1409	6/23/2009	44.372633	-121.994683	3017.8	919.8	8.3	911.5				8.5
1410	6/23/2009	44.372517	-121.994483	3017.8	919.8	5.5	914.3				8.5
1411	6/23/2009	44.372617	-121.994217	3017.8	919.8	2.1	917.7	1.2	0.9		9.2
1412	6/23/2009	44.372283	-121.994317	3017.8	919.8	5.4	914.4				9.8
1413	6/23/2009	44.372150	-121.993983	3017.8	919.8	2.8	917.0				9.5

Note: USGS gage 14158500 is located at the Clear Lake outlet (see Fig. 2b); USGS gage elevation determined by taking averaging gage height over the period out on the lake (maximum range: 0.02 ft) and adding this value to the gage datum (3015.32 ft above sea level). The water temperature is of the top 30 cm of the lake.

TABLE A3. BATHYMETRIC DATA AND OBSERVATIONS FOR CLEAR LAKE

Waypoint	Collection date	Latitude	Longitude	USGS gage elevation (ft)	USGS gage elevation (m)	Depth (m)	Elevation (m)	Tree top depth (m)	Tree height (m)	Whiteline	Water temperature (°C)
1415	6/23/2009	44.371633	-121.995083	3017.8	919.8	30.3	889.5				8.4
1416	6/23/2009	44.371033	-121.995900	3017.8	919.8	33.0	886.8				8.3
1417	6/23/2009	44.370817	-121.996183	3017.8	919.8	32.1	887.7				8.3
1418	6/23/2009	44.370633	-121.996483	3017.8	919.8	35.6	884.2				8.4
1419	6/23/2009	44.370450	-121.996667	3017.8	919.8	31.8	888.0	20.1	11.7		8.6
1420	6/23/2009	44.370100	-121.997117	3017.8	919.8	9.3	910.5	0.1	9.2		10.2
1421	6/23/2009	44.370117	-121.996833	3017.8	919.8	18.3	901.5				10.4
1422	6/23/2009	44.370267	-121.996933	3017.8	919.8	18.6	901.2	0.8	17.8		10.5
1423	6/23/2009	44.370400	-121.997033	3017.8	919.8	19.5	900.3	0.8	18.7		10.6
1424	6/23/2009	44.370267	-121.996933	3017.8	919.8	18.4	901.4	10.0	8.4		10.6
1425	6/23/2009	44.369900	-121.996617	3017.8	919.8	15.6	904.2				10.6
1426	6/23/2009	44.369733	-121.996500	3017.8	919.8	15.0	904.8				10.6
1427	6/23/2009	44.369517	-121.996350	3017.8	919.8	14.0	905.8				10.7
1428	6/23/2009	44.369333	-121.996267	3017.8	919.8	13.2	906.6				10.7
1429	6/23/2009	44.369133	-121.996117	3017.8	919.8	15.0	904.8				10.6
1430	6/23/2009	44.368867	-121.995933	3017.8	919.8	16.7	903.1				10.5
1431	6/23/2009	44.368783	-121.996117	3017.8	919.8	10.0	909.8				10.6
1432	6/23/2009	44.368683	-121.996417	3017.8	919.8	3.9	915.9				10.9
1435	6/23/2009	44.367800	-121.994850	3017.8	919.8	38.1	881.7	26.8	11.3		10.2
1436	6/23/2009	44.366883	-121.994317	3017.8	919.8	49.9	869.9				10.2
1437	6/23/2009	44.366550	-121.994317	3017.8	919.8	52.3	867.5				10.3
1438	6/23/2009	44.366433	-121.994417	3017.8	919.8	52.4	867.4				10.3
1439	6/23/2009	44.366233	-121.994583	3017.8	919.8	48.4	871.4				10.4
1440	6/23/2009	44.366133	-121.994683	3017.8	919.8	41.3	878.5	20.3	21.0		
1441	6/23/2009	44.366000	-121.995067	3017.8	919.8	25.5	894.3				
1442	6/23/2009	44.366083	-121.995000	3017.8	919.8	28.2	891.6	0.5	27.7		9.5
1443	6/23/2009	44.366000	-121.995067	3017.8	919.8	26.8	893.0	0.5	26.3		10.2
1444	6/23/2009	44.364950	-121.995317	3017.8	919.8	16.8	903.0				11.5
1445	6/23/2009	44.365033	-121.995400	3017.8	919.8	12.8	907.0	7.2	5.6		11.5
1446	6/23/2009	44.364983	-121.995467	3017.8	919.8	11.2	908.6	7.6	3.6		11.6
1447	6/23/2009	44.364983	-121.995400	3017.8	919.8	13.9	905.9	3.0	10.9		10.0
1448	6/23/2009	44.364917	-121.995267	3017.8	919.8	16.6	903.2	4.1	12.5		10.7
1449	6/23/2009	44.364717	-121.994883	3017.8	919.8	25.2	894.6				10.9
1450	6/23/2009	44.364483	-121.994767	3017.8	919.8	26.2	893.6				11.2
1451	6/23/2009	44.364283	-121.994683	3017.8	919.8	25.9	893.9				11.2
1452	6/23/2009	44.364117	-121.994850	3017.8	919.8	18.6	901.2				10.9
1453	6/23/2009	44.363817	-121.995033	3017.8	919.8	8.1	911.7	0.8	7.3		11.0
1454	6/23/2009	44.363700	-121.994800	3017.8	919.8	14.6	905.2	0.8	13.8		10.8
1455	6/23/2009	44.363650	-121.994917	3017.8	919.8	9.8	910.0	1.6	8.2		11.2
1456	6/23/2009	44.363483	-121.994733	3017.8	919.8	14.2	905.6				11.5
1457	6/23/2009	44.363350	-121.994433	3017.8	919.8	21.4	898.4	1.6	19.8		11.5
1458	6/23/2009	44.363333	-121.993917	3017.8	919.8	40.0	879.8				11.3
1459	6/23/2009	44.363083	-121.993533	3017.8	919.8	24.4	895.4				11.1

Note: USGS gage 14158500 is located at the Clear Lake outlet (see Fig. 2b); USGS gage elevation determined by taking averaging gage height over the period out on the lake (maximum range: 0.02 ft) and adding this value to the gage datum (3015.32 ft above sea level). The water temperature is of the top 30 cm of the lake.

TABLE A3. BATHYMETRIC DATA AND OBSERVATIONS FOR CLEAR LAKE

Waypoint	Collection date	Latitude	Longitude	USGS gage elevation (ft)	USGS gage elevation (m)	Depth (m)	Elevation (m)	Tree top depth (m)	Tree height (m)	Whiteline	Water temperature (°C)
1460	6/23/2009	44.362933	-121.993150	3017.8	919.8	20.7	899.1				10.9
1461	6/23/2009	44.362733	-121.992750	3017.8	919.8	14.7	905.1				10.6
1462	6/23/2009	44.362650	-121.992400	3017.8	919.8	14.2	905.6				10.5
1463	6/23/2009	44.362650	-121.991983	3017.8	919.8	12.7	907.1				10.3
1464	6/23/2009	44.362683	-121.991533	3017.8	919.8	9.8	910.0				10.1
1465	6/23/2009	44.362733	-121.991200	3017.8	919.8	9.7	910.1				9.9
1466	6/23/2009	44.363883	-121.990433	3017.8	919.8	3.4	916.4	0.9	2.5		9.7
1467	6/23/2009	44.363867	-121.990550	3017.8	919.8	7.2	912.6	0.7	6.5		10.3
1468	6/23/2009	44.364167	-121.990783	3017.8	919.8	16.9	902.9				9.3
1469	6/23/2009	44.365050	-121.991067	3017.8	919.8	39.5	880.3				9.5
1470	6/23/2009	44.365517	-121.991367	3017.8	919.8	41.7	878.1				9.2
1471	6/23/2009	44.365850	-121.991650	3017.8	919.8	31.4	888.4				9.1
1472	6/23/2009	44.365967	-121.991800	3017.8	919.8	39.4	880.4	13.7	25.7		9.0
1473	6/23/2009	44.366433	-121.992117	3017.8	919.8	52.4	867.4				9.2
1474	6/23/2009	44.366900	-121.992317	3017.8	919.8	51.0	868.8				9.0
1475	6/23/2009	44.367750	-121.992750	3017.8	919.8	38.6	881.2				8.6
1476	6/23/2009	44.368233	-121.992867	3017.8	919.8	39.6	880.2				8.7
1477	6/23/2009	44.368517	-121.992917	3017.8	919.8	35.0	884.8				9.1
1478	6/23/2009	44.368900	-121.993067	3017.8	919.8	37.6	882.2				9.1
1479	6/23/2009	44.369850	-121.993950	3017.8	919.8	29.6	890.2				9.7
1480	6/23/2009	44.370117	-121.994167	3017.8	919.8	34.2	885.6				9.8
1481	6/23/2009	44.370400	-121.994400	3017.8	919.8	35.5	884.3				9.9
1482	6/23/2009	44.370650	-121.994550	3017.8	919.8	30.9	888.9				10.0
1483	6/23/2009	44.370983	-121.994717	3017.8	919.8	24.4	895.4				9.9
1484	6/23/2009	44.371233	-121.994950	3017.8	919.8	33.8	886.0				9.9
1485	6/23/2009	44.371400	-121.995217	3017.8	919.8	34.3	885.5				10.0
1486	6/23/2009	44.371600	-121.995517	3017.8	919.8	32.0	887.8				9.9
1487	6/23/2009	44.372800	-121.996850	3017.8	919.8	21.7	898.1				10.4
1488	6/23/2009	44.373883	-121.997617	3017.8	919.8	5.8	914.0				10.1
1489	6/23/2009	44.374083	-121.997683	3017.8	919.8	5.2	914.6	3.1	2.1		9.9
1500	6/24/2009	44.364617	-121.992800	3017.8	919.8	47.7	872.1				8.4
1501	6/24/2009	44.364417	-121.992733	3017.8	919.8	36.0	883.8				8.4
1502	6/24/2009	44.364283	-121.992750	3017.8	919.8	24.0	895.8				8.4
1503	6/24/2009	44.363983	-121.994167	3017.8	919.8	43.1	876.7				8.4
1504	6/24/2009	44.364017	-121.994467	3017.8	919.8	32.8	887.0				8.4
1505	6/24/2009	44.363217	-121.994633	3017.8	919.8	9.0	910.8				8.8
1506	6/24/2009	44.362750	-121.994250	3017.8	919.8	24.1	895.7				8.5
1507	6/24/2009	44.362667	-121.994033	3017.8	919.8	26.7	893.1				8.5
1508	6/24/2009	44.362483	-121.993783	3017.8	919.8	21.1	898.7				8.5
1509	6/24/2009	44.362217	-121.993683	3017.8	919.8	12.2	907.6				8.3
1510	6/24/2009	44.361800	-121.991333	3017.8	919.8	9.7	910.1				8.4
1511	6/24/2009	44.361633	-121.991283	3017.8	919.8	8.4	911.4				8.2
1512	6/24/2009	44.361433	-121.991117	3017.8	919.8	5.0	914.8				8.1

Note: USGS gage 14158500 is located at the Clear Lake outlet (see Fig. 2b); USGS gage elevation determined by taking averaging gage height over the period out on the lake (maximum range: 0.02 ft) and adding this value to the gage datum (3015.32 ft above sea level). The water temperature is of the top 30 cm of the lake.

TABLE A3. BATHYMETRIC DATA AND OBSERVATIONS FOR CLEAR LAKE

Waypoint	Collection date	Latitude	Longitude	USGS gage elevation (ft)	USGS gage elevation (m)	Depth (m)	Elevation (m)	Tree top depth (m)	Tree height (m)	Whiteline	Water temperature (°C)
1513	6/24/2009	44.361300	-121.990933	3017.8	919.8	5.0	914.8				8.2
1514	6/24/2009	44.361283	-121.990767	3017.8	919.8	3.4	916.4	1.7	1.7		8.5
1515	6/24/2009	44.361550	-121.990783	3017.8	919.8	4.9	914.9				8.4
1516	6/24/2009	44.361767	-121.990600	3017.8	919.8	1.5	918.3				8.3
1517	6/24/2009	44.362017	-121.990633	3017.8	919.8	1.0	918.8				8.2
1518	6/24/2009	44.362267	-121.990183	3017.8	919.8	2.3	917.5				9.1
1519	6/24/2009	44.362617	-121.989967	3017.8	919.8	5.2	914.6				8.9
1520	6/24/2009	44.362883	-121.989800	3017.8	919.8	5.1	914.7				8.6
1521	6/24/2009	44.363067	-121.989800	3017.8	919.8	4.3	915.5	1.1	3.2		8.1
1522	6/24/2009	44.363450	-121.990433	3017.8	919.8	6.7	913.1				7.7
1523	6/24/2009	44.363750	-121.990617	3017.8	919.8	4.7	915.1				7.8
1524	6/24/2009	44.363900	-121.990550	3017.8	919.8	2.9	916.9	0.8	2.1		7.4
1525	6/24/2009	44.364883	-121.990533	3017.8	919.8	10.5	909.3				7.6
1526	6/24/2009	44.365500	-121.990717	3017.8	919.8	10.3	909.5				7.7
1527	6/24/2009	44.365867	-121.990950	3017.8	919.8	8.1	911.7				7.7
1528	6/24/2009	44.366550	-121.990883	3017.8	919.8	5.6	914.2				7.8
1529	6/24/2009	44.367900	-121.991667	3017.8	919.8	10.0	909.8				8.0
1530	6/24/2009	44.368217	-121.991667	3017.8	919.8	5.1	914.7				8.1
1531	6/24/2009	44.368317	-121.991750	3017.8	919.8	6.3	913.5	0.4	5.9		8.1
1532	6/24/2009	44.368483	-121.992000	3017.8	919.8	16.5	903.3				8.1
1533	6/24/2009	44.368683	-121.992283	3017.8	919.8	24.4	895.4				8.1
1534	6/24/2009	44.369050	-121.992283	3017.8	919.8	14.2	905.6	0.8	13.4		8.1
1535	6/24/2009	44.368583	-121.994067	3017.8	919.8	42.1	877.7				7.6
1536	6/24/2009	44.368517	-121.994183	3017.8	919.8	41.5	878.3				7.3
1537	6/24/2009	44.368450	-121.994417	3017.8	919.8	45.9	873.9				7.1
1538	6/24/2009	44.368133	-121.995617	3017.8	919.8	19.9	899.9				6.8
1539	6/24/2009	44.368133	-121.995867	3017.8	919.8	11.4	908.4				6.9
1540	6/24/2009	44.368083	-121.996283	3017.8	919.8	2.0	917.8				8.5
1541	6/24/2009	44.369150	-121.996517	3017.8	919.8	5.5	914.3				8.5
1542	6/24/2009	44.369433	-121.996633	3017.8	919.8	6.2	913.6				8.4
1543	6/24/2009	44.369633	-121.996783	3017.8	919.8	5.1	914.7				8.3
1544	6/24/2009	44.369867	-121.996933	3017.8	919.8	7.3	912.5				8.1
1545	6/24/2009	44.370400	-121.997267	3017.8	919.8	10.1	909.7				7.8
1546	6/24/2009	44.370683	-121.997317	3017.8	919.8	6.3	913.5				7.6
1547	6/24/2009	44.370883	-121.997283	3017.8	919.8	4.7	915.1				7.5
1548	6/24/2009	44.371133	-121.997333	3017.8	919.8	7.5	912.3				7.3
1549	6/24/2009	44.371533	-121.997467	3017.8	919.8	3.7	916.1				7.3
1550	6/24/2009	44.372583	-121.997833	3017.8	919.8	10.8	909.0				7.1
1551	6/24/2009	44.373183	-121.997733	3017.8	919.8	3.8	916.0				7.0
1552	6/24/2009	44.373583	-121.997533	3017.8	919.8	7.7	912.1				7.0
1553	6/24/2009	44.375017	-121.997783	3017.8	919.8	6.4	913.4				5.1
1554	6/24/2009	44.377133	-122.000950	3017.8	919.8	6.4	913.4	1.2	5.2		5.1
1555	6/24/2009	44.377083	-122.001033	3017.8	919.8	4.9	914.9	2.2	2.7		6.1

Note: USGS gage 14158500 is located at the Clear Lake outlet (see Fig. 2b); USGS gage elevation determined by taking averaging gage height over the period out on the lake (maximum range: 0.02 ft) and adding this value to the gage datum (3015.32 ft above sea level). The water temperature is of the top 30 cm of the lake.

TABLE A3. BATHYMETRIC DATA AND OBSERVATIONS FOR CLEAR LAKE

Waypoint	Collection date	Latitude	Longitude	USGS gage elevation (ft)	USGS gage elevation (m)	Depth (m)	Elevation (m)	Tree top depth (m)	Tree height (m)	Whiteline	Water temperature (°C)
1556	6/24/2009	44.376900	-122.000817	3017.8	919.8	8.7	911.1	1.5	7.2		5.9
1557	6/24/2009	44.376883	-122.000917	3017.8	919.8	8.2	911.6	3.9	4.3		6.0
1558	6/24/2009	44.376833	-122.001050	3017.8	919.8	10.3	909.5				6.0
1559	6/24/2009	44.376333	-122.001683	3017.8	919.8	12.9	906.9				6.2
1561	6/24/2009	44.375883	-122.000417	3017.8	919.8	5.9	913.9				6.7
1562	6/24/2009	44.376117	-121.999967	3017.8	919.8	11.7	908.1				6.0
1563	6/24/2009	44.375950	-121.999450	3017.8	919.8	7.3	912.5				5.4
1564	6/24/2009	44.375817	-121.999317	3017.8	919.8	4.9	914.9				5.2
1565	6/24/2009	44.375700	-121.999233	3017.8	919.8	4.2	915.6				5.1
1566	6/24/2009	44.375633	-121.998967	3017.8	919.8	4.1	915.7				4.9
1567	6/24/2009	44.375500	-121.998983	3017.8	919.8	3.4	916.4	0.5	2.9		4.0
1568	6/24/2009	44.375450	-121.998883	3017.8	919.8	3.2	916.6	0.5	2.7		3.9
1569	6/24/2009	44.375583	-121.998650	3017.8	919.8	5.4	914.4	1.9	3.5		3.8
1570	6/24/2009	44.375517	-121.998683	3017.8	919.8	3.7	916.1	1.4	2.3		3.8
1571	6/24/2009	44.375417	-121.998483	3017.8	919.8	3.7	916.1	0.4	3.3		3.8
1572	6/24/2009	44.375483	-121.998417	3017.8	919.8	5.7	914.1	0.5	5.2		3.8
1573	6/24/2009	44.375483	-121.998267	3017.8	919.8	6.8	913.0	1.0	5.8		3.7
1574	6/24/2009	44.374950	-121.998150	3017.8	919.8	1.6	918.2				3.9

Note: USGS gage 14158500 is located at the Clear Lake outlet (see Fig. 2b); USGS gage elevation determined by taking averaging gage height over the period out on the lake (maximum range: 0.02 ft) and adding this value to the gage datum (3015.32 ft above sea level). The water temperature is of the top 30 cm of the lake.

REFERENCES CITED

CHAPTER II

Amidon, W.H., and Farley, K.A., 2011, Cosmogenic ^{3}He dating of apatite, zircon and pyroxene from Bonneville flood erosional surfaces: Quaternary Geochronology, v. 6, p. 10–21.

Arculus, R.J., 2003, Use and abuse of the terms calcalkaline and calcalkaic: Journal of Petrology, v. 44, 929–935.

Benson, G.T., 1965, The Age of Clear Lake, Oregon: Ore Bin, v. 27, p. 37–40.

Cashman, K.V., Deligne, N.I., Gannett, M.W., Grant, G.E., and Jefferson, A., 2009, Fire and water: Volcanology, geomorphology, and hydrogeology of the Cascade Range, central Oregon, *in* O'Connor, J.E., Dorsey, R.J., and Madin, I.P., eds., Volcanoes to Vineyards: Geologic Field Trips through the Dynamic Landscape of the Pacific Northwest: Geological Society of America Field Guide 15, p. 539–582, doi: 10.1130/2009.fl d015(26).

Champion, D.E., 1980, Holocene geomagnetic secular variation in the western United States: U.S. Geological Survey Open-File Report 80-824.

Chatters, R.M., 1968, Washington State University Natural Radiocarbon Measurements I: Radiocarbon, v. 10, p. 479–498.

Deardorff, N.D., Cashman, K.V., in revision, Emplacement conditions of the c.1600 ybp Collier Cone lava flow, Oregon: a lidar investigation: Bulletin of Volcanology.

Desilets, D., Zreda, M., Prabu, T., 2006, Extended scaling factors for in situ cosmogenic nuclides: New measurements at low latitude: Earth and Planetary Science Letters, v. 246, p. 265–276.

Gill, J.B., 1981, Orogenic andesites and plate tectonics: Berlin, Germany, Springer-Verlag, 336 p.

Hagstrum, J.T., and D.E. Champion, 2002, A Holocene paleosecular variation record from ^{14}C-dated volcanic rocks in western United States: Journal of Geophysical Research, v. 107, JB000524.

Harmon, M.E., Franklin, J.F., Swanson, F.J., Sollins, P., Gregory, S.V., Lattin, J.D., Anderson, N.H., S.P. CLINE, Cline, S.P., Aumen, N.G., Sedell, J.R., Lienkaemper, G.W., Cromack, K., Jr., Cummins, K.W., 1986, Ecology of coarse woody debris in temperate ecosystems: Advances in Ecological Research, v. 15, p. 133–302.

Hildreth, W., 2007, Quaternary magmatism in the Cascades: Geologic perspectives: U.S. Geological Survey Professional Paper 1744, 136 p.

Jefferson, A., Grant, G., and Rose, T., 2006, Influence of volcanic history on groundwater patterns on the west slope of the Oregon High Cascades: Water Resources Research, v. 42, W12411, 15 p. doi: 10.1029/2005WR004812.

Johnson, D.M., Peterson, R.R., Lycan, D.R., Sweet, J.W., Neuhaus, M.E., and Schaedel, A.L., 1985, Atlas of Oregon Lakes: Corvallis, Oregon, Oregon State University Press, 317 p.

Licciardi, J.M., Kurz, M.D., Clark, P.U., and Brook, E.J., 1999, Calibration of cosmogenic ^{3}He production rates from Holocene lava flows in Oregon, USA, and effects of the Earth's magnetic field: Earth and Planetary Science Letters, v. 172, p. 261–271.

Loy, W.G., Allan, S., Buckley, A. and Meacham, J., 2001, Atlas of Oregon, 2nd edition: Eugene, Oregon, University of Oregon Press, 320 p.

McCaffrey, R., Qamar, A.I., King, R.W., Wells, R., Khazaradze, G., Williams, C.A., Stevens, C.W., Vollick, J.J., and Zwick, P.C., Fault locking, block rotation and crustal deformation in the Pacific Northwest: Geophysical Journal International, v. 169, p. 1315–1340.

McElhinny, M.W., 1973, Paleomagnetism and Plate Tectonics: Cambridge, UK, Cambridge University Press, 368p.

Mckay, D., 2012, Recent mafic eruptions at Newberry Volcano and in the central Oregon Cascades: Physical volcanology and implications for hazards [Ph.D. thesis]: University of Oregon, 146 p.

Mckay, D., Donnelly-Nolan, J.M., Jenson, R.A., and Champion, D.E., 2009, The post-Mazama northwest rift zone eruption at Newberry Volcano, Oregon, *in* O'Connor, J.E., Dorsey, R.J., and Madin, I.P., eds., Volcanoes to Vineyards: Geologic Field Trips through the Dynamic Landscape of the Pacific Northwest: Geological Society of America Field Guide 15, p. 91–110, doi: 10.1130/2009.fld015(05).

Pearce, J.A., and Parkinson, I.J., 1993, Trace element models for mantle melting: application to volcanic arc petrogenesis: Geological Society, London, Special Publications, v. 76, p. 373–403.

Reimer, P.J., Baillie, M.G.L., Bard, E., Bayliss, A., Beck, J.W., Bertrand, C.J.H., Blackwell, P.G., Buck, C.E., Burr, G.S., Cutler, K.B., Damon, P.E., Edwards, R.L., Fairbanks, R.G., Friedrich, M., Guilderson, T.P., Hogg, A.G., Hughen, K.A., Kromer, B., McCormac, F.G., Manning, S.W., Ramsey, C.B., Reimer, R.W., Remmele, S., Southon, J.R., Stuiver, M., Talamo, S., Taylor, F.W., van der Plicht, J., and Weyhenmeyer, C.E., 2004, IntCal04 Terrestrial radiocarbon age calibration, 26 - 0 ka BP: Radiocarbon, v. 46, p. 1029–1058.

Scott, W.E., Iverson, R.M, Schilling, S.P., and Fisher, B.J., 1999, Volcano hazards in the Three Sisters Region, Oregon: U.S. Geological Survey Open-File Report 99-437.

Sherrod, D.R., and Smith, J.G., 1990, Quaternary extrusion rates of the Cascade Range, northwestern United States and southern British Columbia: Journal of Geophysical Research, v. 95, p. 465–474.

Sherrod, D.R., Taylor, E.M., Ferns, M.L., Scott, W.E., Conrey, R.M., and Smith, G.A., 2004, Geologic map of the Bend 30- by 60-minute quadrangle, central Oregon: U.S. Geological Survey Miscellaneous Investigations Map I-2683, scale 1:100 000, 2 sheets.

Sibson, R., 1981, A brief description of natural neighbor interpolation, *in* Barnett, V., Interpolating multivariate data: New York, New York, John Wiley & Sons, p. 21–36.

Stearns, H.T., 1929, Geology and water resources of the Upper McKenzie Valley, Oregon: U.S. Geological Survey Water-Supply Paper 597-D, p. 171–188.

Stuiver, M., Reimer, P.J., and Braziunas, T.F., 1998, High-precision radiocarbon age calibration for terrestrial and marine samples: Radiocarbon, v. 40, p. 1127–1151.

Stuiver, M., Reimer, P.J., and Reimer, R.W., 2005, CALIB 5.0. [http://calib.qub.ac.uk/calib/].

Tague, C., and Grant, G.E., 2004, A geological framework for interpreting the low flow regimes of Cascade streams, Willamette River Basin, Oregon: Water Resources Research, v. 40, no. W04303, doi: 10.1029/2003WR002629.

Taylor, E.M., 1965, Recent volcanism between Three Fingered Jack and North Sister: Oregon Cascade Range: Ore Bin, v. 27, p. 121–147.

Taylor, E.M., 1968, Roadside Geology, Santiam and McKenzie Pass Highways, Oregon, *in* Dole, H.M., ed., Andesite Conference Guidebook: Portland, Oregon, Department of Geology and Mineral Industries, p. 3–33.

Taylor, E.M, 1990, Volcanic history and tectonic development of the central High Cascade Range, Oregon: Journal of Geophysical Research, v. 95, p. 19,611–19,622.

Taylor, G. H., and Hannan, C., 1999, The Climate of Oregon: From Rain Forest to Desert: Corvallis, Oregon, Oregon State University Press, 211 p.

Walker, G.W., and MacLeod, N.S., 1991, Geologic map of Oregon: U.S. Geological Survey, scale 1:100 000, 2 sheets.

Wells, R.E, Weaver, C.S., and Blakely, R.J., 1998, Fore-arc migration in Cascadia and its neotectonic significance: Geology, v. 26, p. 759–762.

Williams, H., 1957, A geologic map of the Bend quadrangle, and a reconnaissance geologic map of the central portion of the High Cascade Mountains: Oregon Department of Geology and Mineral Industries, scale 1:125 000 and 1:250 000, 2 sheets.

CHAPTER III

Aplet, G.H., Hughes, R.F. & Vitousek, P.M. 1998. Ecosystem development on Hawaiian lava flows: biomass and species composition. *Journal of Vegetation Science* 9: 17-26.

Bashan, Y., Li, C.Y., Lebsky, V.K., Moreno, M. & de-Bashan, L.E. 2002. Primany colonization of volcanic rocks by plants in arid Baja California, Mexico. *Plant Biology* 4: 392-402.

Bernhardt, K.G. 1986. Mosaic vegetation characteristics of the prehistoric lava fields of the Hekla area near Galtaleakur, Iceland. *Folia Geobotanica* 21: 243-248.

Boudreau, J., Nelson, R.F., Margolis, H.A., Beaudoin, A., Guindon, L. & Kimes, D.S. 2008. Regional aboveground forest biomass using airborne and spaceborne LiDAR in Québec. *Remote Sensing of Environment* 112: 3876-3890.

Brady, P.V., Dorn, R.I., Brazel, A.J., Clark, J., Moore, R.B. & Glidewell, T. 1999. Direct measurement of the combined effects of lichen, rainfall, and temperature on silicate weathering. *Geochimica et Cosmochimica Acta* 63: 3293-3300.

Cashman K.V., Deligne, N.I., Gannett, M.W., Grant, G.E. & Jefferson, A. 2009. Fire and water: Volcanology, geomorphology, and hydrogeology of the Cascades Range, central Oregon. In: O'Connor, J.E., Dorsey, R.I. & Madin, I.P. (eds.) *Volcanoes to Vineyards: Geologic Field Trips through the Dynamic Landscape of the Pacific Northwest: Field Guide 15,* pp. 539-582. Geological Society of America, Boulder, CO, US.

Cashman, K.V., Soule, S.A., Mackey, B., Deligne, N.I., Deardorff, N.D. & Dietterich, H.R. in press. How lava flows: New insights from applications of lidar technologies to lava flow studies. *Geosphere*.

Chadwick, O.A., Derry, L.A., Vitousek, P.M., Huebert, B.J. & Hedin, L.O. 1999. Changing sources of nutrients during four million years of ecosystem development. *Nature* 397: 491-497.

Chadwick, O.A., Gavenda, R.T., Kelly, E.F., Ziegler, K., Olson, C.G., Elliott, W.C. & Hendricks D.M. 2003. The impact of climate on the biogeochemical functioning of volcanic soils. *Chemical Geology* 202: 195-223.

Clarkson, B.D. 1990. A review of vegetation development following recent (<450 years) volcanic disturbance in North Island, New Zealand. *New Zealand Journal of Ecology* 14: 59-71.

Cutler, N.A., Belyea, L.R. & Dugmore, A.J. 2008. Spatial patterns of microsite colonisation on two young lava flows on Mount Hekla, Iceland. *Journal of Vegetation Science* 19: 277-286.

Deardorff, N. 2011. *Eruptive processes of mafic arc volcanoes - subaerial and submarine perspectives*. Ph.D. thesis, University of Oregon, Eugene, OR, US.

del Moral, R. & Wood, D.M. 1993. Early primary succession on the volcano Mount St. Helens. *Journal of Vegetation Science* 4: 223-234.

Drake, D.R. 1992. Seed dispersal of *Metrosideros polymorpha* (Myrtaceae): a pioneer tree of Hawaiian lava flows. *American Journal of Botany* 79: 1224-1228.

Drake, D.R. & Mueller-Dombois, D. 1993. Population development of rain forest trees on a chronosequence of Hawaiian lava flows. *Ecology* 74: 1012-1019.

Egli, M., Nater, M., Mirabella, A., Raimondi, S., Plötze, M. & Alioth L. 2008. Clay minerals, oxyhydroxide formation, element leaching and humus development in volcanic soils. *Geoderma* 143: 101-114.

Franklin, J.F. & Dyrness, C.T. 1992. *Natural vegetation of Oregon and Washington*. Oregon State University Press, Corvallis, OR, US.

Fridriksson, S. 1987. Colonization of a Volcanic Island, Surtsey, Iceland. *Arctic and Alpine Research* 19: 425-431.

Gannett, M.W., Lite, K.E., Jr., Morgan, D.S. & Collins, C.A. 2001. *Ground-water hydrology of the upper Deschutes Basin, Oregon*. United States Geologic Survey [USGS Water-Resources Investigations Report 00-4162], Reston, VA, US.

Gannett, M.W. & Lite, K.E., Jr. 2004. *Simulation of regional ground-water flow in the upper Deschutes Basin, Oregon*. United States Geologic Survey [USGS Water-Resources Investigations Report 03-4195], Reston, VA, US.

Gordon, S.J. 2005. Effect of environmental factors on the chemical weathering of plagioclase in Hawaiian basalt. *Physical Geography* 26: 69-84.

Griffiths, R.W. 2000. The dynamics of lava flows. *Annual Review of Fluid Mechanics* 32: 477-518.

Grishin, S.Y., del Moral, R., Krestov, P.V. & Verkhola, V.P. 1996. Succession following the catastrophic eruption of Ksudash volcano (Kamchatka, 1907). *Plant Ecology* 127: 129-153.

Hildreth, W. 2007. *Quaternary magmatism in the Cascades: Geologic perspectives*. United States Geologic Survey [USGS Professional Paper 1744], Reston, VA, US.

Jackson, T.A. & Keller, W.D. 1970. A comparative study of the role of lichens and "inorganic" processes in the chemical weathering of recent Hawaiian lava flows. *American Journal of Science* 269: 446-466.

Kilsgaard, C. 1999. *OR Land cover type descriptions: Oregon gap analysis 1998 land cover for Oregon*. Oregon Natural Heritage Program, Portland.

Kitayama, K., Mueller-Dombois, D. & Vitousek, P.M. 1995. Primary succession of Hawaiian montane rain forest on a chronosequence of eight lava flows. *Journal of Vegetation Science* 6: 211-222.

Kurina, L.M. & Vitousek, P.M. 1999. Controls over the accumulation and decline of a nitrogen-fixing lichen, *Stereocaulon vulcani*, on young Hawaiian lava flows. *Journal of Ecology* 87: 784-799.

Kurtz, A.C., Derry, L.A. & Chadwick, O.A. 2001. Accretion of Asian dust to Hawaiian soils: Isotopic, elemental, and mineral mass balances. *Geochemica et Cosmochimica Acta*, 65: 1971-1983.

Lefsky, M.A., Cohen, W.B, Acker, S.A., Parker, G.G., Spies, T.A. & Harding, D. 1999. Lidar remote sensing of the canopy structure and biophysical properties of Douglas-Fir Western Hemlock forests. *Remote Sensing of Environment* 70: 339-361.

Lim, K., Treitz, P., Wulder, M., St-Onge, B. & Flood, M. 2003. LiDAR remote sensing of forest structure. *Progress in Physical Geography* 27: 88-106.

Lindig-Cisnerosa, R., Galindo-Vallejoa, S. & Lara-Cabrera, S. 2006. Vegetation of tephra deposits 50 years after the end of the eruption of the Paricutín Volcano, Mexico. *The Southwest Naturalist* 51: 445-461.

Marler, T.E. & del Moral, R. 2011. Primary succession along an elevation gradient 15 years after the eruption of Mount Pinatubo, Luzon, Philippines. *Pacific Science* 65: 157-173.

Means, J.E., Acker, S.A., Harding, D.J., Blair, J.B., Lefsky, M.A., Cohen, W.B., Harmon, M.E. & McKee, W.A. 1999. Use of large-footprint scanning airborne Lidar to estimate forest stand characteristics in the western Cascades of Oregon. *Remote Sensing of Environment* 67: 298-308.

Næsset, E. 2002. Predicting forest stand characteristics with airborne scanning laser using a practical two-stage procedure and field data. *Remote Sensing of Environment* 80: 88-99.

Nelson, R., Krabill, W. & Tonelli, J. 1988. Estimating forest biomass and volume using airborne laser data. *Remote Sensing of Environment* 24: 247-267.

O'Connor, J.E., Hardison, J.H., III & Costa, J.E. 2001. *Debris flows from failures of neoglacial – age moraine dams in the Three Sisters and Mount Jefferson Wilderness Areas, Oregon*. United States Geologic Survey [USGS Professional Paper 1606], Reston, VA, US.

Porder, S., Hilley, G.E. & Chadwick, O.A. 2007. Chemical weathering, mass loss, and dust inputs across a climate by time matrix in the Hawaiian Islands. *Earth and Planetary Sciences Letters* 258: 414-427.

Pyle, D.M. & Elliott, J.R. 2006. Quantitative morphology, recent evolution, and future activity of the Kameni Islands volcano, Santorini, Greece. *Geosphere* 2: 252-268.

Rasmussen, C., Dahlgren, R.A. & Southard, R.J. 2010. Basalt weathering and pedogenesis across an environmental gradient in the southern Cascade Range, California, USA. *Geoderma* 154: 473-485.

Rea, D.K. 1994. The paleoclimatic record provided by Eolian deposition in the deep sea: the geologic history of wind. *Reviews of Geophysics* 32: 159-195.

Roach A.W. 1952. Phytosociology of the Nash Crater lava flows, Linn County, Oregon. *Ecological Monographs* 22: 169-193.

Schick, J.D. 1994. *Origin of the compositional variability of the lavas at Collier Cone, High Cascades, Oregon*. M.S. thesis, University of Oregon, Eugene, OR, US.

Sherrod, D.R., Gannett, M.W. & Lite, K.E., Jr. 2002. Hydrogeology of the upper Deschutes Basin, Central Oregon – A young basin adjacent to the Cascade volcanic arc. In: Moore, G.E. (ed.) *Field Guide to Geologic Processes in Cascadia*, pp. 109-144. Oregon Department of Geology and Mineral Industries [Special Paper 36], Portland, OR, US.

Sherrod, D.R., Taylor, E.M., Ferns, M.L., Scott, W.E., Conrey, R.M. & Smith, G.A. 2004. *Geologic map of the Bend 30- x 60- minute quadrangle, central Oregon*. United States Geologic Survey [Geologic Investigation Series I-2683], Reston, VA, US.

Sparks, R.S.J., Pinkerton, H. & Hulme, G. 1976. Classification and formation of lava levees on Mount Etna, Sicily. *Geology* 4: 269-271.

Taylor, B.W. 1957. Plant succession on recent volcanoes in Papua. *Journal of Ecology* 45: 223-243.

Tewksbury, J.J. & Lloyd, J.D. 2001. Positive interactions under nurse-plants: spatial scale, stress gradients and benefactor size. *Oecologia* 127: 425-434.

Tsuyuzaki, S. & Hase, A. 2005. Plant community dynamics on the volcano Mount Koma, Northern Japan, after the 1996 eruption. *Folia Geobotanica* 40: 319-330.

Vaughan, K.L. & McDaniel, P.A. 2009. Organic soils on basaltic lava flows in a cool, arid environment. *Soil Science Society of America Journal* 73: 1510-1518.

Vaughan, K.L., McDaniel, P.A. & Phillips, W.M. 2011. Episodic soil succession on basaltic lava fields in a cool, dry environment. *Soil Science Society of America Journal* 75: 1462-1470.

Walker, L.R. & del Moral, R. 2003. *Primary Succession and Ecosystem Rehabilitation*. Cambridge University Press, Cambridge, UK.

Wells, S.G., Dohrenwend, J.C., McFadden, L.D., Turrin, B.R. & Mahrer, K.D. 1985. Late Cenozoic landscape evolution on lava flow surfaces of the Cima volcanic field, Mojave Desert, California. *Geological Society of America Bulletin* 96: 1518-1529.

Whittaker, R.J., Bush, M.B., Partomihardjo, T., Asquith N.M & Richards, K. 1992. Ecological aspects of plant colonisation of the Krakatau Islands. *GeoJournal* 28: 201-211.

Zimble, D.A., Evans, D.L., Carlson, G.C., Parker, R.C., Grado, S.C. & Gerard, P.D. 2003. Characterizing vertical forest structure using small-footprint airborne LiDAR. *Remote Sensing of Environment* 87: 171-182.

CHAPTER IV

Aiuppa, A., Allard, P., D'Alessandro, W., Michel, A., Parello, F., Treuil, M., Valenza, M., 2000. Mobility and fluxes of major, minor and trace metals during basalt weathering and groundwater transport at Mt. Etna volcano (Sicily). Geochimica et Cosmochimica Acta 64: 1827-1841.

Aplet, G.H., Hughes, R.F., Vitousek, P.M., 1998. Ecosystem development on Hawaiian lava flows: biomass and species composition. Journal of Vegetation Science 9: 17-26.

Bashan, Y., Li, C.Y., Lebsky, V.K., Moreno, M., de-Bashan, L.E., 2002. Primany colonization of volcanic rocks by plants in arid Baja California, Mexico. Plant Biology 4: 392-402.

Benson, G.T., 1965. The Age of Clear Lake, Oregon. Ore Bin 27: 37-40.

Bernhardt, K.G., 1986. Mosaic vegetation characteristics of the prehistoric lava fields of the Hekla area near Galtaleakur, Iceland. Folia Geobotanica 21: 243-248.

Burt, R. 2009. Soil survey field and laboratory methods manual. Soil Survey Investigations Report 51, version 1.0. USDA-NRCS, National Soil Survey Center, Lincoln, NE, USA>

Chadwick, O.A., Derry, L.A., Vitousek, P.M., Huebert, B.J., Hedin, L.O., 1999. Changing sources of nutrients during four million years of ecosystem development. Nature 397: 491-497.

Chadwick, O.A., Gavenda, R.T., Kelly, E.F., Ziegler, K., Olson, C.G., Elliott, W.C., Hendricks, D.M., 2003. The impact of climate on the biogeochemical functioning of volcanic soils. Chemical Geology 202: 195-223.

Champion, D.E., 1980. Holocene geomagnetic secular variation in the western United States. U.S. Geological Survey Open-File Report 80-824. 314 pp.

Clarkson, B.D., 1990. A review of vegetation development following recent (<450 years) volcanic disturbance in North Island, New Zealand. *New Zealand Journal of Ecology* 14: 59-71.

Cutler, N.A., Belyea, L.R., Dugmore, A.J., 2008. Spatial patterns of microsite colonisation on two young lava flows on Mount Hekla, Iceland. Journal of Vegetation Science 19: 277-286.

Dale, V.H., Swanson, F.J., Crisafulli, C.M. (eds), 2005. Ecological Responses to the 1980 Eruption of Mount St. Helens. Springer, United States of America.

Das., A, Krishnaswami, S., Sarin, M.M., Pande, K., 2005. Chemical weathering in the Krishna Basin and Western Ghats of the Deccan Traps, India: Rates of basalt weathering and their controls. Geochimica et Cosmochimica Acta 69: 2067-2084.

Dean, W.E., 1974. Determination of carbonate and organic matter in calcareous sediments and sedimentary rocks by loss on ignition; comparison with other methods. Journal of Sedimentary Research 44: 242-248.

Deardorff, N., Cashman, K., in revision. Emplacement conditions of the c.1600 ybp Collier Cone lava flow, Oregon: a lidar investigation. Bulletin of Volcanology.

del Moral, R., Wood, D.M., 1993. Early primary succession on the volcano Mount St. Helens. Journal of Vegetation Science 4: 223-234.

Dessert, C., Dupréa, B., Gaillardet, J., François, L.M., Allègre, C.J., 2003. Basalt weathering laws and the impact of basalt weathering on the global carbon cycle. Chemical Geology 202: 257-273.

Drake, D.R., 1992. Seed dispersal of Metrosideros polymorpha (Myrtaceae): a pioneer tree of Hawaiian lava flows. American Journal of Botany 79: 1224-1228.

Drake, D.R., Mueller-Dombois, D., 1993. Population development of rain forest trees on a chronosequence of Hawaiian lava flows. Ecology 74: 1012-1019.

Eggleton, R.A., Foudoulis, C., Varkevisser, D., 1987. Weathering of basalt: changes in chemistry and mineralogy. Clays and Clay Minerals 35: 161-169.

Erlund, E.J., Cashman, K.V., Wallace, P.J., Pioli, L., Rosi, M., Johnson, E., Delgado Granados, H., 2010. Compositional evolution of magma from Parícutin Volcano, Mexico: The tephra record. Journal of Volcanology and Geothermal Research 197: 167–187.

Ferrier, K.L., Kirchner, J.W., Finkel, R.C., 2011. Estimating millennial-scale rates of dust incorporation into eroding hillslope regolith using cosmogenic nuclides and immobile weathering tracers. Journal of Geophysical Research 116: F03022.

Franklin, J.F., Dyrness, C.T., 1992. Natural vegetation of Oregon and Washington. Oregon State University Press, Corvallis, OR, USA.

Fridriksson, S., 1987. Colonization of a Volcanic Island, Surtsey, Iceland. Arctic and Alpine Research 19: 425-431.

Gadow, H., 1930. Jorullo: The history of the volcano of Jorullo and the reclamation of the devastated district of animals and plants. Cambridge University Press, London, UK.

Gislason, S.R., Oelkers, E.H., 2003. Mechanism, rates, and consequences of basaltic glass dissolution: II. An experimental study of the dissolution rates of basaltic glass as a function of pH and temperature. Geochimica et Cosmochimica Acta 67: 3817-3832.

Grishin, S.Y., del Moral, R., Krestov, P.V., Verkhola, V.P., 1996. Succession following the catastrophic eruption of Ksudash volcano (Kamchatka, 1907). Plant Ecology 127: 129-153.

Grissino-Mayer, H.D., 2001. Evaluating Crossdating Accuracy: A Manual and Tutorial for the Computer Program COFECHA. Tree-Ring Research 57: 205-221.

Halpern, C.B., Frenzen, P.M., Means, J.E., Franklin, J.F., 1990. Plant succession in areas of scorched and blown-down forest after the 1980 eruption of Mount St. Helens, Washington. Journal of Vegetation Science 1: 181-194.

Hansen, H.P., 1942. Post-Mount Mazama Forest Succession on the East Slope of the Central Cascades of Oregon. American Midland Naturalist 27: 523-534.

Heath, J.P., 1967. Primary Conifer Succession, Lassen Volcanic National Park. Ecology 48: 270-275.

Heiri, O., Lotter, A.F., Lemcke, G., 2001. Loss on ignition as a method for estimating organic and carbonate content in sediments: reproducibility and comparability of results. Journal of Paleolimnology 25: 101-110.

Hildreth, W., 2007. Quaternary magmatism in the Cascades: Geologic perspectives. U.S. Geological Survey Professional Paper 1744. 136 pp.

Hopson, R.E., 1960. Collier Glacier - A Photographic Record. Mazama 42: 15-26.

Jefferson, A., Grant, G., Rose, T., 2006. Influence of volcanic history on groundwater patters on the west slope of the Oregon High Cascades. Water Resources Research 42: W12411.

Jenny, H., 1941. Factors of soil formation: A system of quantitative pedology. McGraw-Hill, Dover, Mineola, NY.

Kilsgaard, C., 1999. OR Land cover type descriptions: Oregon gap analysis 1998 land cover for Oregon. Oregon Natural Heritage Program, Portland.

Kitayama, K., Mueller-Dombois, D., Vitousek, P.M., 1995. Primary succession of Hawaiian montane rain forest on a chronosequence of eight lava flows. Journal of Vegetation Science 6: 211-222.

Kroh, G.C., White, J.D., Heath, S.K., Pinder III, J.E., 2000. Colonization of a Volcanic Mudflow by an Upper Montane Coniferous Forest at Lassen Volcanic National Park, California. The American Midland Naturalist 143: 126-140.

Kroh, G.C., McNew, K., Pinder III, J.E., 2008. Conifer colonization of a 350-year old rock fall at Lassen Volcanic National Park in northern California. Plant Ecology 199: 281-294.

Kurtz, A.C., Derry, L.A., Chadwick, O.A., Alfano, M.J., 2000. Refractory element mobility in volcanic soils. Geology 28: 683-868.

Kurtz, A.C., Derry, L.A., Chadwick, O.A., 2001. Accretion of Asian dust to Hawaiian soils: Isotopic, elemental, and mineral mass balances. Geochemica et Cosmochimica Acta, 65: 1971-1983.

Licciardi, J.M., Kurz, M.D., Clarka, P.U., Brook, E.J., 1999. Calibration of cosmogenic ^{3}He production rates from Holocene lava flows in Oregon, USA, and effects of the Earth's magnetic field. Earth and Planetary Science Letters 172: 261-271.

Lindig-Cisnerosa, R., Galindo-Vallejoa, S., Lara-Cabrera, S., 2006. Vegetation of tephra deposits 50 years after the end of the eruption of the Paricutín Volcano, Mexico. The Southwest Naturalist 51: 445-461.

Louvat, P., Allègre C.J., 1997. Present denudation rates on the island of Réunion determined by river geochemistry: Basalt weathering and mass budget between chemical and mechanical erosions. Geochimica et Cosmochimica Acta 61: 3645-3669.

Luhr, J.F., Simkin, T., 1993. Paricutín: The Volcano Born in a Mexican Cornfield. Geoscience Press, Inc., Phoenix, Arizona, USA.

Marler, T.E., del Moral, R., 2011. Primary succession along an elevation gradient 15 years after the eruption of Mount Pinatubo, Luzon, Philippines. Pacific Science 65: 157-173.

Mckay, D., 2012. Recent mafic eruptions at Newberry Volcano and in the central Oregon Cascades: Physical volcanology and implications for hazards. Ph.D. Thesis, University of Oregon, Eugene, Oregon, USA.

Navarre-Sitchler, A., Brantley, S., 2007. Basalt weathering across scales. Earth and Planetary Science Letters 261: 321-334.

Oelkers, E.H., Gislason, S.R., 2001. The mechanism, rates and consequences of basaltic glass dissolution: I. An experimental study of the dissolution rates of basaltic glass as a function of aqueous Al, Si and oxalic acid concentration at 25°C and pH = 3 and 11. Geochimica et Cosmochimica Acta 65: 3671-3681.

O'Connor, J.E., Hardison, J.H., III, Costa, J.E., 2001. Debris flows from failures of neoglacial – age moraine dams in the Three Sisters and Mount Jefferson Wilderness Areas, Oregon. U.S. Geological Survey Professional Paper 1606. 93 pp.

Ort, M.H., Elson, M.D., Champion, D.E., 2002. A paleomagnetic dating study of Sunset Crater Volcano. Technical Report No. 2002-16, Desert Archaeology, Tucson, Arizona, USA, 16 p.

Ort, M.H., Elson, M.D., Anderson, K.C., Duffield, W.A., Hooten, J.A., Champion, D.E., Waring, G., 2008. Effects of scoria-cone eruptions upon nearby human communities. Geological Society of America Bulletin 120: 476-486.

Phipps, R.L., 1985. Collecting, Preparing, Crossdating, and Measuring Tree Increment Cores. U.S. Geological Survey Water-Resources Investigations Report 85-4148. 48 p.

Porder, S., Hilley, G.E., Chadwick, O.A., 2007. Chemical weathering, mass loss, and dust inputs across a climate by time matrix in the Hawaiian Islands. Earth and Planetary Sciences Letters 258: 414-427.

Rasmussen, C., Dahlgren, R.A., Southard, R.J., 2010. Basalt weathering and pedogenesis across an environmental gradient in the southern Cascade Range, California, USA. Geoderma 154: 473-485.

Rejmánek, M., Haagerová, R., Haager, J., 1982. Progress of Plant Succession on the Parícutin Volcano: 25 Years after Activity Ceased. American Midland Naturalist 108: 194-198.

Roach, A.W., 1952. Phytosociology of the Nash Crater lava flows, Linn County, Oregon. Ecological Monographs 22: 169-193.

Rowland, S.K., Jurado-Chichay, Z., Ernst, G., Walker, G.P.L., 2009. Pyroclastic deposits and lava flows from the 1759–1774 eruption of El Jorullo, México: aspects of 'violent Strombolian' activity and comparison with Parícutin. In: Thordarson, T., Self, S., Larsen, G., Rowland, S.K., Hoskuldsson, A. (Eds), Studies in Volcanology: The Legacy of George Walker. Special Publications of IAVCEI 2, Geological Society, London, pp. 105-128.

Schick, J.D., 1994. Origin of the compositional variability of the lavas at Collier Cone, High Cascades, Oregon. M.S. thesis, University of Oregon, Eugene, OR, USA.

Sibson, R., 1981. A Brief Description of Natural Neighbor Interpolation. Chapter 2 in Interpolating multivariate data. John Wiley & Sons, New York, pp. 21-36.

Stearns, H.T., 1929. Geology and Water Resources of the Upper McKenzie Valley, Oregon. U.S. Geological Survey Water-Supply Paper 597-D. 20 pp.

Sherrod, D.R., Gannett, M.W., Lite, K.E., Jr., 2002. Hydrogeology of the upper Deschutes Basin, central Oregon—A young basin adjacent to the Cascade volcanic arc. In: Moore, G.E. (Ed.), Field Guide to Geologic Processes in Cascadia. Oregon Department of Geology and Mineral Industries Special Paper 36, p. 109–144.

Sherrod, D.R., Taylor, E.M., Ferns, M.L., Scott, W.E., Conrey, R.M., Smith, G.A., 2004. Geologic map of the Bend 30- x 60- minute quadrangle, central Oregon. U.S. Geologic Survey Geologic Investigation Series I-2683.

Taylor, B.W., 1957. Plant succession on recent volcanoes in Papua. Journal of Ecology 45: 223-243.

Tsuyuzaki, S., Hase, A., 2005. Plant community dynamics on the volcano Mount Koma, Northern Japan, after the 1996 eruption. Folia Geobotanica 40: 319-330.

USDA Forest Service, 2010. Willamette National Forest Soil Resource Inventory. Springfield, Oregon, USA.

Vaughan, K.L., McDaniel, P.A., 2009. Organic soils on basaltic lava flows in a cool, arid environment. Soil Science Society of America Journal 73: 1510-1518.

Vaughan, K.L., McDaniel, P.A., Phillips, W.M., 2011. Episodic soil succession on basaltic lava fields in a cool, dry environment. Soil Science Society of America Journal 75:1462-147.

Wells, S.G., Dohrenwend, J.C., McFadden, L.D., Turrin, B.R., Mahrer, K.D., 1985. Late Cenozoic landscape evolution on lava flow surfaces of the Cima volcanic field, Mojave Desert, California. Geological Society of America Bulletin 96: 1518-1529.

Whittaker, R.J., Bush, M.B., Partomihardjo, T., Asquith N.M, Richards, K., 1992. Ecological aspects of plant colonisation of the Krakatau Islands. GeoJournal 28: 201-211.

Wolman, M.G., 1954. A Method of Sampling Coarse River-Bed Material. Transactions of the American Geophysical Union 35: 951-956.